The photocatalytic abatement of nitrogen oxides

Jordan, Philip Henry

Award date:
1995

Awarding institution:
University of Bath

THE PHOTOCATALYTIC ABATEMENT OF NITROGEN OXIDES.

Submitted by Philip Henry Jordan

for the degree of PhD

of the University of Bath

1995.

Copyright.

ProQuest LLC
789 East Eisenhower Parkway
P.O. Box 1346
Ann Arbor, MI 48106-1346

SUMMARY.

Work has been undertaken to investigate the photocatalytic reactions of oxides of nitrogen (NOx) on near-UV irradiated titanium dioxide in an annular photoreactor.

An initial review of literature work has shown that a small body of work on the photocatalytic reactions of NOx have been previously undertaken, however, all of this work has been undertaken at the small scale chemistry level. The work outlined in this thesis was therefore directed at the chemical engineering aspects of the process.

Both nitrogen dioxide (NO_2) and nitric oxide (NO) were examined at levels of 4000ppm, in nitrogen or helium as the bulk gas. These levels were similar to those in the discharge from a nitric acid production plant.

Both NO_2 and NO were seen to undergo photocatalytic reactions to form nitrous oxide (N_2O) and ozone, however, reduction of NOx to nitrogen and oxygen was not seen.

Several reactor parameters such as flowrate, UV intensity, temperature and others were experimentally examined and their effect on the photocatalytic reactions assessed.

Rate data obtained from the experimental work was used to estimate the rate-limiting step in the photocatalytic reaction of NO on titanium dioxide.

Several catalyst materials were compared with each other and the best photocatalyst determine. The physical and chemical properties of these materials were investigated and correlations suggested between these properties and their relative performance.

ACKNOWLEDGEMENTS.

The research work outlined in this thesis could not have been completed without the assistance of several other people who deserve a mention.

First on the list is my partner Helen, whose constant nagging, intimidation and cups of coffee kept me going through my long and painful write-up. Also to my step-kids, Paul and Carly, for putting up with me constantly spending evenings typing at the computer.

To my parents, for believing, most of the time, that I would eventually finish this tome of high learning and allow my father to hassle somebody else for a change. Also to the rest of my family for their continuous support and encouragement.

To my initial supervisor at the University of Bath, Dr Po Lok Yue, who saw me through the experimental work. He also coped with having a very sarcastic student with the experiences of industry behind him, who always asked the difficult questions. To Dr Robert Field, for taking on the job of supervisor during my write-up time, who suffered the task of reading this thesis with no complaints. Also to Dr Roger Bickley at the University of Bradford who gave me his frank opinions on the quality of the chemistry put forward by a chemical engineer. Finally to the Revered Barry Chapman of the University of Bath for his help with the Scanning Electron Microscope.

To all my student colleges at the university throughout my time there. In particular, John, Rob, Susan, Shunji, Omar, Jan-Luca, Dave, Arife, Sabiha and all the others to numerous to mention, who kept me happy when times got difficult.

Finally, to all the support staff in the School of Chemical Engineering, in the workshop and school office, but particularly Tom for making life so hard and therefore allowing me to appreciate what I have finally achieved.

"All that is gold does not glitter,
Not all those who wander are lost;
The old that is strong does not wither,
Deep roots are not reached by the frost.
From the ashes a fire shall be woken,
A light from the shadows shall spring;
Renewed shall be blade that was broken,
The crownless again shall be king."

From Book One, The Fellowship of the Ring, THE LORD OF THE RINGS,
by J R R Tolkien. Published by Unwin Paperbacks, 1978.

CONTENTS.

CHAPTER 1.

CHAPTER 2.

CHAPTER 5.

CHAPTER 6.

CHAPTER 7.

CHAPTER 8.

CHAPTER 9.

TABLES.

CHAPTER 1.

1.0 OBJECTIVES OF THE PROJECT.

The purpose of this research project was to develop the basis for a novel catalytic process for the abatement of nitrogen oxides (NO_X). The abatement process was achieved by light-induced reactions using three photocatalysts: titanium dioxide, size modified titanium dioxide and iron doped titanium dioxide. The advantages of using an annular fluidised gas/solid reactor were to be exploited. However, this was found to be impractical, due to the kinetics of the reaction and the experiments were finally carried out in an annular fixed bed reactor. The surface chemistry and reaction kinetics of the process were studied to allow basic modelling of the reactor system to be achieved.

1.1 Current Legislation.

Recently built nitric acid production plants have been designed with greater efficiencies in response to pressures from government and recently introduced legislation under the Environmental Protection Act 1990 Part 1.

Under the Environmental Protection Act 1990 Part 1, the concept of Integrated Pollution Control (IPC) has been identified. IPC is a new system of pollution control intended to apply to the most potentially polluting or technologically complex industrial and other processes throughout England and Wales. The enforcing (and authorising) authority is Her Majesty's Inspectorate of Pollution (HMIP) and HMIP has been responsible for introducing IPC since 1st April 1991.

IPC is concerned with the control of releases to all three environmental media - air, water and land. The Regulations list the substances which are most potentially harmful or polluting when released to the environment. These "prescribed substances" are subject to special requirements to ensure that BATNEEC (**B**est **A**vailable **T**echnologies **N**ot **E**ntailing **E**xcessive **C**ost) is used to prevent their release to specified environmental media or (if that is not practicable) to minimise such releases. All substances which might cause harm if released into any medium are additionally subject to the use of BATNEEC to render them harmless. There are three separate lists of prescribed substances according to whether the substance is to be controlled in relation to air, water or land releases.

Under the regulations for IPC, "nitrogen and other nitrogen compounds" is identified as a prescribed substance under the heading of substances being released to the air. Therefore, greater consideration most be given by all industries that emit NO_X into the air.

The current permissible discharges' limits are stated as:

" For new plant the emission of nitrogen oxides, namely nitric oxide and nitrogen dioxide taken together, shall not in normal operation exceed a concentration of 200 parts per million by volume. For existing nitric acid plants, where practicable and by dates to be agreed, the emission of nitrogen oxides shall not in normal operation exceed 1000 parts per million by volume. Emission concentrations shall be measured before admixture of the plant tail gases with air or other gases. For nitric acid plants, the final emission to air shall in normal operation be substantially colourless, to the satisfaction of the inspector." [19].

The discharge limits set in England and Wales for the discharge of NO_X are among the most severe restrictions that exist in the world. In relation, the discharge limits in the United States of America, are set at 1.5Kg NO_X per tonne of product acid, which corresponds to a tail gas concentration of about 230 vppm and in Japan, where the limit is set at 200 vppm.

The Environmental Protection Act 1990 Part 1, Integrated Pollution Control and BATNEEC therefore present a significant body of legislation which imparts a great incentive, and legal obligation, to the nitric acid industry to develop new, better and more energy efficient treatment systems for the reduction of NO_X discharges to the air.

1.2 Basis for the Research Work.

Nitric acid became a major industrial chemical with the development of the explosives and dyestuffs industries at the end of the nineteenth century. This early growth was dwarfed by the growth after World War II, when the enormous expansion in the use of synthetic fertilisers increased demand for nitric acid to an extent that placed its annual rate of production among the ten largest chemicals produced in the United States.

The earliest description of a method for making nitric acid generally is attributed to eighth-century Arabian sources which described the distillation of a mixture of Cyprus vitriol, saltpetre, and alum to yield a liquor with "high solvent action", later called *aqua fortis*. In 1798, Milner reported the successful oxidation of ammonia vapour over red hot manganese dioxide to yield nitrogen oxides and acid. In 1824, Henry demonstrated that ammonia reacts directly with oxygen at elevated temperatures in the presence of spongy platinum. During the nineteenth and early twentieth centuries, hundreds of catalysts were tested for use in the latter reaction which was to become the foundation of the modern nitric acid industry. In 1784, Cavendish synthesised the acid by action of electric sparks in humid air, and in 1816 Gay-Lussac and Berthollet established the acids composition.

Until 1900, nitric acid was produced commercially from potassium nitrate and then, with the development of the Chile saltpetre deposits in South America, from sodium nitrate by reaction with sulphuric acid. The latter process was supplanted in 1903 with the

operation in Norway of the first successful plant to produce nitric acid directly from nitrogen and oxygen in an electric arc furnace. More than a dozen electric arc plants were installed in Norway where inexpensive electricity was available.

The catalytic oxidation of ammonia in air in the presence of a platinum catalyst was studied in detail by Ostwald starting in about 1901, and by 1908 a commercial plant was built near Bochum, Germany, which produced 3 t/d of nitric acid. With the demonstration of the Haber-Bosch ammonia synthesis process at Oppau, Germany, in 1913, the future of ammonia oxidation was assured, and additional nitric acid plants were installed in Germany.

Variations in plant design since the 1920's have mainly been in the areas of increasing the capacity of the plants and the pressure at which they are operated; modern plants typically produce 1000 t/d in single trains operating at 1MPa (10 atm).

The typical levels of discharge from a nitric acid production plant are given in Table 1.1:-

Table 1.1 Typical Levels of NOx Discharge from a Nitric Acid Production Plant. (Data obtained from ICI Billingham.)

Component	Concentration
nitrogen oxides	0.40%
oxygen	1.31%
water vapour	1.04%
carbon dioxide	0.03%
nitrogen	balance

1.3 Production of Nitric Acid.

In the majority of existing nitric acid production plants, the acid is produced via a set of ammonia oxidation reactions. The process has three main stages, in the first stage ammonia is oxidised to nitric oxide with air over a rhodium/platinum catalyst. The resultant nitric oxide is then oxidised further with air to nitrogen dioxide and then absorbed in water to form nitric acid.

1.31 Oxidation of Ammonia.

In the first stage, the overall oxidation reaction is:-

$$4NH_3 + 5O_2 \longrightarrow 4NO + 6H_2O \quad \Delta H_{298K} = -226kJ/mol \qquad (1.1)$$

and this takes place over a rhodium/platinum gauze catalyst and yields about 95% or more conversion rate when a 10% v/v ammonia/air mixture preheated to 250°C is passed over it.

The oxidation of ammonia with air to nitric acid is one of the most efficient catalytic reactions known. Virtually every ammonia molecule that strikes the catalyst surface is oxidised to nitric oxide, in a reaction time of approximately 10^{-11} seconds. With such a brief reaction time the rate controlling factor is the supply of ammonia and oxygen to the catalyst surface. The diffusion rate of ammonia is faster than that of oxygen, but is still slower than the reaction rate. Diffusion processes of this type are affected by such factors as temperature and pressure.

The stoichiometric gas composition for the reaction corresponds to 14.2 volume % of ammonia in air. However, this composition is within the explosive range of ammonia-air mixtures and it is therefore usual to operate with lower ammonia concentrations. The explosive limit falls at high pressures and as a consequence in a high pressure plant the gas

mixture does not exceed 11% NH_3 compared with 13.5% NH_3 at atmospheric pressure. One result of the lower ammonia concentration is that it is necessary to preheat the gas mixture in a high pressure plant in order to achieve the gauze temperature (900 - 950°C) required for economic operation.

Other variables, including linear, space and mass velocities; reactor design; and particularly, freedom from impurities, appear to have greater significance than pressure in determining actual efficiencies. The advantage of higher temperatures in improving yields has been demonstrated but, to some extent, this advantage is offset by a rapid increase in the loss of the precious-metal catalyst.

1.32 Oxidation of Nitric Oxide.

Nitric oxide undergoes a slow homogeneous reaction with oxygen to yield nitrogen dioxide:

$$2\,NO + O_2 \longleftrightarrow 2\,NO_2 \qquad (1.2)$$

The equilibrium constant for the reaction strongly favours the production of NO_2 at lower temperatures, so that below 150°C almost all nitric oxide combines with any oxygen that is present if sufficient residence time is allowed. The reaction rate is slow and the rate constant decreases with increasing temperature. The plant operating conditions generally are sufficiently far from equilibrium so that the reverse reaction can be neglected.

Nitrogen dioxide dimerises almost instantaneously to an equilibrium mixture with dinitrogen tetroxide

$$2NO_2 \longleftrightarrow N_2O_4 \qquad (1.3)$$

Lower temperatures and increasing pressures shift the reaction to the production of the tetroxide.

1.33 Absorption of Nitrogen Oxides.

In the absorption of nitrogen oxides in water, there are uncertainties about the reaction mechanism, and complexities resulting from mass diffusion in a vapour and in a liquid phase are involved. The overall reaction usually is shown as if only the nitrogen dioxide that is present in the gas reacts with liquid water:

$$3NO_2(g) + H_2O(l) \longleftrightarrow 2HNO_3(aq) + NO(g) \quad (1.4)$$

Extensive measurements of the reaction equilibrium have been made at various temperatures and acid concentrations. Theories that were formulated regarding the possible mechanisms of absorption were based on gas-phase reaction or liquid-phase reaction and control by gas-film diffusion or liquid-film diffusion as well as upon the various molecular species present, e.g., NO_2, N_2O_4 and N_2O_5. Ten possible mechanisms for absorption have been compared and it was concluded that, at high concentrations of nitrogen oxide in the vapour, the controlling mechanism is the solution of N_2O_4 and its hydrolysis to HNO_2 plus HNO_3; whereas, at low concentration, the control is either diffusion of NO_2 through the liquid film or absorption of HNO_2. The basics of equipment design can be deduced from equation 1.4 above and the available equilibrium data. Equipment sizes can be calculated to produce a given amount and concentration of acid, or more of a higher concentration of acid can be produced by making the following changes: reduce operating temperatures, increase operating pressures, increase the proportion of NO_2/NO in the feed gas, and increase the reaction volume after vapour-liquid contact to permit reoxidation of released NO.

1.4 Consideration of the Treatment Options for the "Tail Gas" from a Nitric Acid Production Plant.

Because of the complexities of the reaction of NO_2 with water, incomplete absorption of the NO_2 results. The resultant gases emitted from the exit of the absorption towers have still therefore, a relatively high concentration of NO_2 present. Under the current Environmental Protection Act Part 2, these gases are at to high a concentration to be emitted to the atmosphere. Therefore some method of treating the "tail gases" is required before final discharge may take place.

A second absorption tower may be added to the system, however, the economics of such a decision are not particularly attractive to an industrial operation. The added cost of a second absorption tower, capable of removing the residual NO_2 would incur an unacceptable increase in the cost of the final product.

Several techniques for removal of the tail gas NO_2 are currently in use around the world. These techniques are outlined below and a final analysis of their relative advantages and disadvantages is supplied.

1.41 Platinum group catalysts.

Several precious metal catalysts, mainly based on combinations with platinum, are used in the catalytic reduction of the oxides of nitrogen to nitrogen and water. In such processes, a reducing fuel e.g., hydrogen, carbon monoxide and gaseous or liquid hydrocarbons, are injected into the tail gas and reacted with the oxides of nitrogen in the stream. The reaction takes place over a gauze or monolith, impregnated with a precious metal mixture. When the fuel exceeds the nitrogen oxides and oxygen stoichometrically and the temperature of the gauze/monolith is above that of the ignition temperature of the gas, the nitrogen oxides are reduced to low levels.

Several different types of catalysts and catalyst configurations are used in the various processes available. The chemical nature of the material may be platinum, rhodium or palladium, as the main element present in any mixture, with trace quantities of other materials added. From a physical criteria, ceramic or metal honeycombs/monoliths are commonly used, possibly with the addition of small quantities of other elements e.g. Zirconia or thoria, as a strengthening agent for the monolith. However, despite the variations in the specifics of the process, the basic concepts are the same.

1.42 Other metal catalysts

Several other metals can be used, utilising a similar basic chemistry approach as with the platinum group metals, that of a fixed catalyst with a reducing fuel at an elevated temperature. Supported zinc, nickel or copper can be used with ammonia as the fuel or silver/copper with carbon monoxide.

1.43 Sorption techniques - adsorbents, oxidation and adsorption, others

Adsorbents.

Several different materials may be used in the adsorption of oxides of nitrogen from gas streams. Most are in the form of fine powders or impregnated monoliths, through which the gas is passed and undergoes one of two main processes; (i) chemical reaction with the solid or (ii) physical adsorption onto the surface of the material.

In (i) materials such as sodium carbonate, iron sulphate and calcium oxide are used in a granular form or impregnated onto molecular sieves. The materials then undergo chemical reactions with the oxides of nitrogen to form nitrogen based salts. The adsorbate material may be regenerated by heating or by the use of an air/oxygen purge to displace the

adsorbant from the adsorbate. However, the action of regenerating may, in turn, lead to the production of some amount of NOx and other gaseous species.

(ii) With the physical adsorbent materials, such as activated carbon, silica gel, molecular sieve or silica, the contaminated gas is again passed through a bed of granular powder, in which it is adsorbed onto the powder's surface. The adsorbate is usually regenerated by heating to several hundred degrees Celsius, which causes the oxides of nitrogen to be desorbed. This technique however, does not ultimately remove the problem, it merely concentrates the gas up and allows for easier adsorption in a standard gas adsorption tower.

1.44 Oxidation and adsorption.

Gaseous oxides of nitrogen, may be adsorbed onto materials exhibiting low surface activity, such as charcoal, peat, lignite coke or other organic materials from the destructive distillation of coal. After being adsorbed onto the materials surface, the oxides of nitrogen are oxidised to higher valence states, e.g. $NO \longrightarrow NO_2$, due to the presence of free oxygen or air being present on the materials surface. Alternatively, the oxygen can be present in the gas stream itself, and will therefore give a continuous supply of oxygen to the surface. If water is also present in the gas stream, then the NO_2 produced by oxidation will combine with the water present to form HNO_3, further enhancing the effectiveness of the material.

An alternative system using ferric oxide/sodium oxide, called an "oxsorbent", may be used to turn residual nitric oxide directly into nitrogen bearing salts. Nitric oxide, which normally forms a large part of tail gas emissions, is directly converted to nitrates/nitrites without previous oxidation to nitrogen dioxide. However, with a proper choice of catalyst, the NO can be transformed exclusively into nitrates to the exclusion of nitrites. This reaction is performed at several hundred degrees Celsius, and the material may be regenerated by heating the catalyst/salt mass to in excess of $700^{o}C$. The remaining material

may then be reused for further reaction.

Other, more exotic processes do exist, using molten baths of carbonate salts, potassium/sodium hydroxide or liquid fluorocarbons. However, these find limited usage in industry.

1.45 Liquid scrubber processes - nitric acid processes, coke oven gas, others

Several systems exist for the liquid scrubbing of nitrogen oxides, in standard liquid-gas contacting equipment. The only notable differences between the various liquid scrubber processes being the chemical composition of the scrubber liquid feed and the chemical composition of the salts produced after the reaction of the scrubber feed with the NOx gas. The engineering details of the liquid scrubber processes are, in the main, the same. Typical systems are;

(i) aqueous suspensions of magnesium hydroxide/carbonate, giving rise to a solution of magnesium nitrite. The nitrite is then heated to cause decomposition of the nitrite to nitrate.

(ii) aqueous calcium carbonate solutions, which when reacted with oxides of nitrogen, give rise to nitrite and nitrate salts.

(iii) aqueous solutions of ammonium sulphite and bisulphite used under atmospheric conditions of temperature and pressure, and producing, on reaction, ammonium sulphate. The reaction is rather complex, as it involves free oxygen that may be present in the gas stream with the oxides of nitrogen. Care most be taken with this system to have excess sulphite/bisulphite present at all times, to prevent the formation of solutions of nitrite/nitrate.

(iv) solutions of slightly acidic urea will react with oxides of nitrogen by absorption of the oxides of nitrogen in the solution to initially form nitrous acid, which then reacts

with the urea to form nitrogen, carbon dioxide and water. Conventional acidic compounds are used, such as nitric acid, sulphuric acid, hydrochloric acid or acetic acid.

(v) a widely used technique for the removal of oxides of nitrogen, is absorption into a solution of sodium hydroxide. This system is particularly effective for those processes producing significantly more nitric oxide in the outlet stream than the other oxides of nitrogen. The main requirement of the process is that NO and NO_2 are present in the gas in roughly equimolar concentrations, such that sodium nitrite is the main product. An excess of nitrogen dioxide in the gas stream, would cause preferential reaction of the nitrogen dioxide, thus leaving the nitric oxide in the stream.

Comparison table for the advantages and disadvantages of the various processes for Tail Gas treatment.

Process	Advantages	Disadvantages	Cost
Platinum group catalysts	Excellent NOx removal	Expensive catalyst, fuel required, high temperature required	High
Other metal catalysts	Excellent NOx removal	Fuel required, high temperature required	High
Sorption techniques: adsorbents	Moderate to excellent NOx removal	Adsorbent required, regeneration required, salts produced/gases desorbed	Medium
Sorption techniques: adsorption and oxidation	Moderate to excellent NOx removal, useful products may be formed	Adsorbent required, oxygen/air required, high temperature required	High
Liquid scrubber processes	Moderate to excellent NOx removal, useful products may be formed	Scrubber solution required, additional absorption tower required	Medium
Combustion and oxidation		Adsorbent required, high temperature required, fuel required	High

1.5 Proposed System.

It is envisaged that a photocatalytic NO_X abatement process would yield substantial savings in terms of energy and material costs. The proposed process will require little or no preheat and would in fact allow further recovery of heat from the nitric acid tail gas. Thus

allowing a better recovery of energy which could then be used to preheat the nitric acid inlet gases. The relative costs of the catalysts in the proposed system and a typical abatement process are significantly different, allowing for further cost cutting, not withstanding the difference in catalyst quantities used. Also, whereas typical abatement processes use a fuel in the process, the proposed system uses no fuel except possibly for the occasional regeneration of the catalyst with an air purge (no significant cost), an oxygen purge (low cost) or possibly an acid wash with dilute acid (low cost). Overall therefore, this process is of great potential to the nitric acid industry and possibly to wider areas as well.

CHAPTER 2.

2.0 PHOTOCHEMICAL PRINCIPLES.

2.1 The Basis of Photocatalysis.

Photocatalytic reactions taking place on n-type semiconductor materials are based on the following phenomenon. A photon of electromagnetic radiation, whose energy is equal to or greater than the band gap for the n-type material, excites an electron from the valence band to the conductance band, thus leaving a positive hole in the valence band. In the presence of electrophilic compounds, the solid surface is covered by negative adsorbed species A^-. Therefore, the photoproduced hole is attracted to the surface by the electrical field thus created. Under these conditions the semiconductor becomes capable of separating the photoproduced charges and can behave as a photocatalyst. Maintenance of the electrical neutrality may be achieved either by direct charge recombination of the hole and electron or by an equilibrium between the holes reacting with oxidizable negative species and the electrons captured by reducible species.

2.11 Quantum Yield.

A concept of great value in photochemistry is that of the quantum yield, π. As originally understood, it was "the number of molecules of reactant consumed for each photon of light absorbed". In this form the quantum yield reflects without distinction both the efficiencies of the primary photochemical process in bringing about chemical change, and also the extent of secondary reaction. A quantum yield greater than unity suggests the

occurrence of secondary reactions, since the Stark-Einstein law indicates that not more than one molecule can be decomposed in the primary step (a quantum yield of greater than two, points to the operation of a chain reaction mechanism). However, it can be shown that the chemical change is not the only consequence of absorption of radiation; physical quenching on the reactor wall, luminescence or intramolecular energy transfer, radical production etc. may be occurring. Thus a chain reaction may be taking place in a photochemical reaction, due to the presence of radicals, even though the overall quantum yield is less than unity.

The determination of overall quantum yields for chemical change requires measurement of the numbers of molecules of reactant consumed, or of product formed, and of the number of quanta of radiation absorbed. The former measurement just involves the use of suitable analytical techniques, while the latter requires a method for measuring absolute numbers of photons. These techniques are outlined later in this chapter through the use of actinometers.

2.12 The Beer-Lambert Law.

The fraction of light transmitted through an absorbing system is very frequently found to be represented by the relationship

$$\frac{I_t}{I_o} = 10^{(-\varepsilon C d)} \qquad (2.1)$$

I_t, and I_0 are the transmitted and incident light intensities, C is the concentration of the absorber, and d is the depth of absorber through which the light beam has passed. ε is a constant of proportionality known as the extinction coefficient; it is dependent on the wavelength of the radiation and may vary with C. The law outlined in equation (2.1) was originally known as Lamberts Law; a second law, Beers Law, stated that if C and d were

altered but the product Cd was constant, then the fraction of light transmitted remained the same. Since the latter law follows in any case from Lamberts Law, the equation (2.1) is now known as the Beer-Lambert Law.

A proof of the Beer-Lambert Law may be derived if it is assumed that the rate of loss of photons is proportional to the rate of bimolecular collisions between photons and the absorbing species. The decrease, -dI, in intensity I at any point x in the system (see Figure 2.1) for a small increase in x, dx, is given by

$$-dI = \alpha ICdx$$

where α is a constant of proportionality. Integration, with the boundary conditions $I=I_0$ at $x=0$, $I=I_t$ at $x=d$, yields the result

$$\frac{I_t}{I_o} = e^{-\alpha Cd} \qquad (2.2)$$

which is the same as Equation (2.1) with $\alpha = 2.303\varepsilon$

The intensity of radiation absorbed, I_{abs}, is of course, $I_0 - I_t$, so that the fraction of absorbed radiation is given by

$$\frac{I_{abs}}{I_o} = 1 - \exp\left(-\alpha Cd\right) \qquad (2.3)$$

More than one absorber may be present in the system, therefore the rate of bimolecular collisions between photons and each species is dependent on the intensity and the concentration of each species. Therefore, the right hand side of equation (2.2) must have terms for the other components added on. Integration will now yield the result

$$\frac{It}{Io} = e^{-(\alpha_{1Cd}+\alpha_{2Cd}....)} \qquad (2.4)$$

This form of the equation may be used as a basis for the modelling of photochemical reactors.

2.2 Types of Photochemical Reactors.

Among a wide range of possible reactor-lamp-reflector configurations, those most widely studied in the literature are the annular reactor, the cylindrical reactor with elliptical reflector, and the cylindrical reactor with parabolic reflector; these are described briefly below. Other types of configurations can be used in commercial applications, however, they arise from different combinations of the three mentioned above, i.e. pseudo-annular; multi lamp, single reactor; multi lamp, multi reactor.

2.21 Annular Reactor.

Annular photoreactors are an excellent approach to what is perhaps the most practical type of photochemical reactor to be used for commercial purposes. The utilisation of energy can be the maximum expected and, moreover, they represent the common case of a reaction vessel with a tubular lamp placed at its axis by means of an immersion well in the case of liquid systems.

Figure 2.2 shows the main features of the annular reactor system. The reacting stream is contained in the annular space (R) that surrounds the lamp (L). If the reactor vessel is separated from the lamp, the annular space between them can be used to cool the lamp and/or control the operating temperature of the reactor. However, it most be noted that the requirement of light transmission introduces some limitations in the heat transfer possibilities because at least the inner reactor wall must be made of quartz. In the case of a large cooling load being present, the inner wall of the reactor may actually be a water

jacket, where gas cooling would not suffice. Since light transparency is not required in the outer reactor wall, it provides much more freedom for design purposes, such as cooling, reflection of unabsorbed light, etc. Hence if one requires to improve the absorption efficiency of the reactor, a reflective surface covering can be used on the outer reactor wall.

2.22 Cylindrical Reactor with Elliptical Reflector.

This system consists of a reactor made with a cylindrical tube (R) placed at one of the focuses of a cylindrical reflector of elliptical cross section. A tubular radiation source (L) is placed at the other focus (Figure 2.3).

The possibility of using cylindrical tubular reactors with a small cross sectional area, together with the generally accepted concept of the existence of a uniform irradiation from outside has resulted in a rather extensive application of this reactor for laboratory and bench scale research work. However, since the incidence efficiency of this type of reactor, defined as the capacity of concentrating the energy within the reactor boundaries, is not very high, this is not an advisable device for commercial-scale operation unless other thermodynamic considerations compel its use.

2.23 Cylindrical Reactor with Parabolic Reflector.

Another possibility of isolating the reaction system from the radiation source consists of the use of a cylindrical reactor (R) irradiated from the bottom by a tubular source (L) located at the focal axis of a cylindrical reflector of parabolic cross section (Figure 2.4). Since the cylindrical reactor may be a perfectly stirred tank reactor, this device is especially appropriate to carry out liquid or liquid/gas reactions where vigorous stirring is required.

2.3 Photochemical Measuring Techniques.

Photochemical processes may lead to chemical changes. The nature of the products, and the rates of their formation may be determined by standard chemical techniques. The techniques for studying the particular system under consideration in this paper are outlined later.

Measurement of absorbed light intensities are essential to determinations of quantum yields, which in themselves are a measure of the efficiency of the primary photochemical processes. Quantum yields are usually determined under steady state illumination, however a technique called flash photolysis may also be used.

Ideally a photochemical experiment employs the use of monochromatic light, since the nature of the primary processes, and their quantum efficiencies, may be wavelength dependent. The use of monochromatic radiation also simplifies the measurement of absolute light intensities. Since most light sources are polychromatic, some technique must therefore be used to isolate a narrow wavelength band, if this is required for the particular application. Colour filters are the usual method of reducing the wavelength band. These may be liquid solutions or glass filters of substances which strongly absorb the light of unwanted wavelengths.

The three most commonly used techniques of radiation detection are the thermopile, the photocell and chemical actinometry.

The use of the thermopile (see Figure 2.5) is a well established but less frequently used technique. Since light is a form of energy it may be degraded to heat, and if the light falls on a blackened surface the temperature of that surface will rise. The temperature rise can be measured by a thermopile, this is an assembly of thermocouples, connected in series, whose front junctions are blackened.

2.31 Photocells.

The sensing of UV light can be under taken by using a photocell, which works on the principle of photodetection. Photodetection is usually related to three phenomena. These are photoemmisive, photoconductive and photovoltaic actions. Photocells are made from solid-state materials and hence work on the latter two principles. In photoconduction, the incident light on a photosensitive material causes the material to alter its conduction. In photovoltaic action, the incident light generates a voltage when it strikes the photosensitive material.

2.32 Photoconduction.

Operation through photoconduction involves a change in the resistance of the photosensitive material. A wafer of photoconductive material is placed underneath a glass window to protect it from exposure (Figure 2.6). The photoconductive material is tied to a load resistance and a power source. The clear glass window allows light radiation to strike the photoconductive material, freeing valence electrons. The resistance of the photoconductive material decreases, causing current through the load to increase. The resistance of the photoconductive material may change from several million Ohms to several hundred, depending on the current demand of the device.

2.33 Photovoltaic.

Operation of a photovoltaic cell involves the use of dissimilar metals to generate an electromotive force in response to radiated light. In Figure 2.7 a light sensitive material is placed beneath a thin layer of transparent metal and next to a dissimilar metal. The light sensitive material is exposed to radiation through the thin transparent metal, which acts as a

filter. When exposed, free electrons are removed from the light sensitive material, causing electrons to flow to the dissimilar metal. This creates current flow and a difference of potential between the two terminals connected to the load.

2.34 Actinometry.

Chemical actinometers are photochemical systems, inorganic or organic, used for the measuring of light intensity. The intensity of light absorbed in an actinometer can be determined by a simple experimental method, which is then used to evaluate the following equation:

$$V_o \frac{dA}{dt} = -V_R \sum_{\lambda} \phi_\lambda Q_\lambda \qquad (2.5)$$

Where V_O = Total volume of solution in the reactor (m^3)

V_r = Radiation volume of reactor (m^3)

dA/dt = Rate of disappearance of species A per unit time (mol m^{-3} sec^{-1})

Q_λ = Light absorption rate at wavelength λ (einstein m^{-3} sec^{-1})

ϕ_λ = Quantum yield at wavelength λ for the actinometer (mole $einstein^{-1}$)

There are two general types of actinometer,

(i) Optically dense actinometers, which totally absorb all incident light and

(ii) Optically dilute actinometers, where the transmitance of the actinometer cell approaches 100%.

In the project concerned, the reactions take place in the gas phase, in the wavelength ~360 nm. No suitable gas phase actinometers for this wavelength range have been reported in the literature. Therefore, a liquid actinometer has been used to measure the light intensity in the reactor. This figure did not exactly represent the actual intensity in a reactor containing catalyst, however, in the absence of a suitable gas phase antinometer, it afforded the best possible estimate of total energy emitted by the light source.

CHAPTER 3.

3.0 FLUIDISATION.

3.1 Introduction

It was initially the intention of this research work to utilise the phenomenon of fluidisation, to aid in the transfer of light through the reactor catalyst bed. It was felt that the circulation of particles in a fluidised bed would help in the reaction, in that, particles would enter the illuminate zones at the inside of the bed, be "charged up" with energy by the incident UV-light and then return into the bulk of the gas flow to undergo reaction with the reactant gases. By using this fluidised bed set-up a larger quantum yield would be obtained than for fixed beds. Therefore, the basic theories behind the phenomenon of fluidisation were investigated and these are outlined in this chapter. The experimental results obtained to supply some of the data required to assess these theories for practical application to this work are detailed in Chapter 7.

3.2 The Phenomenon of Fluidisation.

The passage of a fluid upward through a bed of fine particles is shown in Figure 3.1. At a low flowrate, the fluid simply percolates through the void spaces between the stationary particles. This is a "fixed bed".

With an increase in flowrate, particles move apart and a few are seen to vibrate and move about in restricted regions. This is an "expanded bed".

At a still higher velocity, a point is reached when the particles are all just suspended in the upward flowing fluid. At this point the frictional force between a particle and the fluid offsets the weight of the particle, the vertical component of the compressive force between adjacent particles disappears and the pressure drop through any section of the bed about equals the weight of fluid and particles in that section. The bed is considered to be just fluidised and is referred to as a bed at "minimum fluidisation".

With an increase in flowrate beyond minimum fluidisation, gas-solid beds show large instabilities with bubbling and channelling of the gas being observed. At higher flowrates the agitation becomes more violent and the movement of solids more vigorous. In addition, the bed does not expand much beyond its volume at minimum fluidisation. Such a bed is called a "aggregative fluidised bed" or a "bubbling fluidised bed".

Both gas and liquid fluidised beds are considered to be dense-phase fluidised beds as long as there is a fairly well defined upper limit or surface to the bed. However, at a sufficiently high fluid flowrate the terminal velocity of the solids is exceeded, the upper surface of the bed disappears entrainment becomes appreciable and solids are carried out of the bed with the fluid stream. Under these conditions we have a "dilute" or "lean-phase fluidised bed".

3.3 Pressure drop - Velocity behaviour.

Ideal Behaviour:- If a fluid is passed vertically upwards through a bed of particles, the pressure drop δp, will initially rise as the velocity, U, is increased (Figure 3.2). The relationship between pressure drop and velocity will be that which is applicable to a fixed bed, and for fine particles the Carmen-Kozeny equation will hold and a linear relationship will exist. When the velocity has reached a value such that the pressure drop is equal to the buoyant weight per unit area of the particles, any further increase in the velocity must

result in a slight upward movement of the particles. The particles will become rearranged so that the resistance to the fluid flow is reduced and, in general, the voidage of the bed will increase and in an ideal system the pressure drop will remain constant. Further increases in velocity will result in continued expansion of the bed until any further separation of the particles will only be possible if they become physically separated from one another and are free to move within the fluid. At this stage the bed is just fluidised, and is said to be at the point of "incipient fluidisation". As the fluid velocity is further increased, the pressure drop over the bed remains constant. If the fluid velocity is now slowly reduced, the pressure remains constant until the point of "incipient fluidisation" is reached and it is at this point on the downward pressure curve that the "minimum fluidisation velocity", U_{mf}, can be determined. Further decreases in fluid velocity are accompanied by an incremental decrease in pressure drop, however the pressure drop-velocity curve will generally be lower than that obtained when the velocity was being increased, since due to the absence of vibration, the bed voidage will remain at approximately the value, e_{mf}, corresponding to the bed at the point of incipient fluidisation.

Deviations from Ideal Behaviour:- The behaviour described above is an idealised one which is virtually never experienced in practise. The principal deviations from ideal behaviour are;

(i) As the velocity approaches the minimum fluidisation velocity, some bed expansion will normally occur before the pressure drop has reached the buoyant weight per unit area of the bed. This effect will be most marked when the bed is initially highly consolidated.

(ii) Because of the tendency of particles to interlock with one another, partial bridging can occur, particularly in beds of a small diameter, with the result that frictional forces are exerted by the walls of the container on the bed. It is possible for pressure drops

in excess of the theoretical value to be obtained and the curve will pass through a point of maximum pressure drop, hence giving rise to a small characteristic "hump", as shown in Figure 3.3.

(iii) Non-uniformity in the structure of the bed will result in preferential flow of fluid in particular areas, with the result of fixed and fluidised areas co-existing in the same bed. The bed may appear to be well fluidised, but part of the weight of the bed may still be borne by the bed distributor, with the result that the pressure drop is below the expected value. The minimum velocity at which the bed weight is fully supported by the fluid (U_{fs}) is shown in Figure 3.4.

(iv) Circulation patterns will be set up within the bed, with the result that a net frictional force is exerted by the walls in the opposite direction to that in which the bed is moving at the walls. This effect can give rise to anomalous pressure drops.

(v) Severe channelling may occur within the bed, with the result that a high proportion of the fluid may flow through the channels, with the remainder of the bed possibly remaining unfluidised.

(vi) When the flowrate is progressively reduced below the minimum fluidising velocity, the bed may well not remain at its voidage at the point of incipient fluidisation because of the effects of vibration.

(vii) If the distributor at the base of the bed does not give an even distribution of fluid, the formation of channels may be induced by the distributor.

The form of the pressure drop vs velocity curve for the fixed and fluidised bed does therefore give a considerable amount of information about the structure of the bed. Rarely is the ideal behaviour obtained and most of the deviations are attributable to inter particle forces and to maldistribution of fluid in the bed. For practical purposes, the minimum fluidising velocity is defined as shown in Figure 3.4, as the point of intersection of the

pressure drop lines for the fluidised and fixed regions (preferably determined with decreasing flow).

3.4 Minimum Fluidising Velocity.

The onset of fluidisation occurs at the minimum fluidising velocity, when

$$\{\text{Drag force by upward moving fluid}\} = \{\text{Weight of particles}\} \qquad (3.1)$$

or

$$\begin{Bmatrix}\text{Pressure drop}\\ \text{across bed}\end{Bmatrix}\begin{Bmatrix}\text{Cross sectional}\\ \text{area of bed}\end{Bmatrix} = \begin{Bmatrix}\text{Volume}\\ \text{of bed}\end{Bmatrix}\begin{Bmatrix}\text{Fraction}\\ \text{of solids}\end{Bmatrix}\begin{Bmatrix}\text{Specific weight}\\ \text{of solids}\end{Bmatrix} \qquad (3.2)$$

From these basic equations numerous authors have derived relationships for the dependence of U_{mf} on various factors, e.g.;

Correlation	Units/Definitio	Author
$_{mf} = 0.00081g\frac{\rho_p \ \rho_f \ d_p^2}{\mu}$	All units in SI	Davidson and Harrison (Ref. 21)

$U_{mf} = \frac{0.0093 \; d_p^{1.82} \left(\rho_p - \rho_f\right)^{0.94}}{\mu^{0.88} \; \rho_f^{0.06}}$	All units in SI	Leva (Ref. 22).

Prediction 1, by Harrison and Davidson, is based on several assumptions which need to be stated:

(i) the theory is based upon the idea of flow through an inclined pipe having the same flow resistance as a packed bed.

(ii) that the particles in the bed, at the point of minimum fluidisation, set themselves in the loosest possible arrangement of packing and give the theoretical bed voidage value of 0.476 for spheres.

(iii) the basic equations above, (Eq 3.1 and 3.2), apply to a packed bed at the point of minimum fluidisation.

(iv) a relationship between the force on a single sphere in a regular array of particles acted upon by an upwardly moving fluid and a direct correlation of this force with that encountered at minimum fluidisation.

Prediction 2, by Leva is also based on several assumptions as stated below:

(i) the theory is based upon the idea of flow through an inclined pipe having the same flow resistance as a packed bed.

(ii) empirical data was used to generate some of the dimensionless constants used in the derivation of the final equation for U_{mf}.

(iii) the particles in the fluidised bed are assumed to be spherical in nature and are taken as smooth glass beads.

(iv) the basic equations above, (Eq 3.1 and 3.2), apply to a packed bed at the point of minimum fluidisation.

3.5 The Geldart Classification for Gas Fluidisation.

The behaviour of solids fluidised by gases falls into four clearly recognisable groups, characterised by density difference $\rho_s - \rho_f$ and mean particle size (Figure 7.19 & [29]).

Group A:- Materials having a small mean size and/or a low particle density (<1.4 g/cm^3) generally exhibit the type of behaviour described below.

Beds of powders in this group expand considerably before bubbling commences. When the gas is suddenly cut off the bed collapses slowly, typically at a rate of 0.3-0.6 cm/s, this being similar to the superficial velocity of the gas in the dense phase. Gross circulation of powder occurs even when few bubbles are present, providing rapid mixing but this is usually due to poor distribution of the gas in the reactor. Bubbles in a two-dimensional bed appear to split and recoalesce very frequently. Considerable back-mixing of gas in the dense phase occurs and gas exchange between bubble and dense phase is generally high. When the superficial velocity is sufficiently high to produce slugging conditions, the slugs produced are axi-symmetric; as the superficial gas velocity is further increased slug flow breaks down into a turbulent region with "tongues of fluid darting zigzag fashion up the bed". The velocity at which this occurs appears to decrease with particle size.

Group B:- Group B contains most materials in the mean size and density ranges of $40\mu m < d_{sv} < 500\mu m$, and $4g/cm^3 > \rho_s > 1.4g/cm^3$.

In contrast with Group A powders, naturally occurring bubbles start to form in this type of powder at or only slightly above the minimum fluidisation velocity. Bed expansion before bubbling is small and the bed collapses very rapidly when the gas supply is cut off. There is little or no powder circulation in the absence of bubbles and bubbles burst at the surface of the bed as discrete entities. Most bubbles rise more quickly than the interstitial gas velocity and bubble size increases linearly with both bed height and excess gas velocity. Back mixing of the dense phase gas is relatively low as is gas exchange between bubbles and dense phase. When the gas velocity is so high that slugging commences, the slugs are initially axi-symmetric, but with further increase in gas velocity an increasing proportion become asymmetric, moving up the wall with an enhanced velocity rather than up the tube axis. There is no evidence of the breakdown of slugging into turbulent flow.

Group C:- Powders which are in any way cohesive belong in this category. "Normal" fluidisation of such powders is extremely difficult; the powder lifts as a plug in small diameter tubes, or channels badly. This difficulty arises because the interparticle forces are greater than those which the fluid can exert on the particle, and these are generally the result of very fine particle size, strong electrostatic charges or the presence in the bed of very wet or sticky materials. Particle mixing and consequently heat transfer between a surface and the bed is much poorer than with powders of groups A and B.

Group D:- The justification for this class of powders is not as strong for those in the other three groups. The general note is that the bed/particles can be spouted.

Certainly all but the largest bubbles rise more slowly than the interstitial fluidising gas, so that gas flows into the base of the bubble and out of the top, providing a mode of gas exchange and by-passing different from those observed with group A and B powders.

The gas velocity in the dense phase is high, solids mixing relatively poorly, consequently backmixing of the dense phase gas is small.

CHAPTER 4.

4.0 TITANIUM DIOXIDE CATALYST.

4.1 Introduction.

Titanium is a relatively common element which has been known for over 170 years. It is the ninth most abundant element in the earth's crust, the average titanium content of the lithosphere being 0.63% by weight. However, it is only in this century, that the element has developed any industrial potential, partly because of the difficulties associated with its refinement.

Titanium was discovered in 1791 by William Gregor, an English clergyman and amateur chemist. He identified it in a black sand (now known as ilmenite), which had been sent to him for analysis from the Menacchan valley in Cornwall. Four years later, the famous German chemist Klaproth rediscovered the element in the ore rutile, one of the forms of titanium dioxide. He gave it the name titanium after the Titans who in Greek mythology were the sons of the Earth.

Titanium is widely distributed on the Earth's surface, and also occurs in the sun and in meteorites. In the Earth's crust, the principal ores are ilmenite ($FeTiO_3$) and rutile (TiO_2).

The main use of titanium is as the oxide in the form of the dioxide (TiO_2). Titanium dioxide is industrially important as a white pigment for paints on account of its high opacity, its relative chemical inertness and the comparative abundance (and hence cheapness) of titanium ores suitable for its manufacture. In the case of Degussa P-25, a product manufactured by Degussa in Germany, the added bonus of a relatively high surface

area, low bulk density and low particle size, give it the added bonus of a high covering power, resulting in a lower loading requirement of TiO_2 per square metre. The dioxide also possesses a wide range of semi-conductor and dielectric properties, which are highly dependent on the density of point defects. Indeed much physical and photochemical research has been carried out on this oxide.

Titanium dioxide exists in three crystalline modifications, anatase, brookite and rutile, (see Figures 4.1 and 4.2 and Table 4.1 below) all of which have been prepared synthetically. These crystals are substantially pure titanium dioxide but usually contain small amounts of impurities, eg. iron, chromium, or vanadium, which darkens them.

Table 4.1. X-Ray data on TiO_2 modifications.

	Cell Parameters (Å)			Ti-O (Å)[a]
	a	b	c	
Anatase (tetragonal)	5.36	9.53	-	1.91(2), 1.95(4)
Brookite (orthorhombic)	9.15	5.44	5.14	1.84 - 2.03
Rutile (tetragonal)	4.59	2.96	-	1.944(4), 1.988(2)

[a] The numbers in parentheses refer to the number of equivalent oxygen atoms at the stated distance from a titanium atom.

4.2 Industrial Preparation.

Titanium dioxide is manufactured by two main processes,

(i) In the sulphate process, ilmenite ($FeTiO_3$) is digested with sulphuric acid at 150-200^{o}C with air agitation. The iron and titanium sulphates thus produced are then

leached from the reaction mass and the iron crystallised out as the salt $FeSO_4.7H_2O$. Concentration of the solution over a period of some six hours precipitates hydrated titanium dioxide. This product is then filtered, washed and calcined at 900-950^{o}C. The dioxide is in the form of anatase unless seed-rutile crystals are added to the liquor in the hydrolysis tank and a rutilising agent is added to the precipitated dioxide prior to the calcining. However, due to the high calcining temperature ~900^{o}C, compared with the anatase to rutile phase transition temperature of ~650^{o}C, some rutile will exist in the product, the exact percentage depending on the duration of calcination.

(ii) The second method involves the vapour-phase oxidation of the tetrachloride, the latter being prepared from the rutile ore. A mixture of dry oxygen and the tetrachloride vapour is passed along a silica tube at 650-750^{o}C, and the following reactions takes place to produce anatase:-

$$TiCl_4 + O_2 \longrightarrow TiO_2 + 2\,Cl_2$$

Before cooling the deposit, a current of pure oxygen is passed along the tube to remove traces of the tetrachloride. When the oxidation is carried out in the presence of a few percent of water, silicon tetrachloride or aluminium tetrachloride, the oxide is deposited in the rutile modification. Again, as with the sulphate process, due to the operating temperatures, a small amount of rutile will be produced, because of the anatase to rutile phase change.

Rutile ore is not used for the sulphate process because it does not dissolve readily in H_2SO_4. Ilmenite is not used for the chloride process because much ferric chloride would be produced during the chlorination step and this has little commercial use and merely wastes chlorine.

CHAPTER 5.

5.0 PREVIOUS WORK.

Previous work in the area investigated in this thesis is discussed in this chapter under four main headings, (i) Photolysis of NO_X and Other Gases, Relevant to this Area of Research; (ii) General Photocatalysis; (iii) Action of NO_X on Illuminated Semiconductors; (iv) Photocatalysts other than Titanium Dioxide.

These categories are further subdivided within these sections to give a substantial outline of previous research work in these areas.

5.1 Photolysis of NO_X and Other Gases, Relevant to this Area of Research.

5.12 Absorption spectra for NO_X.

Several studies have been performed on determining the absorption spectra of NO_2 and NO (Ref. 15,29,32,34). These papers give details of the absorption spectra in the visible and near UV range of the spectrum. The experimentally determined absorption spectra are shown in Figure 5.1 (Ref. 15 and 29) for NO_2 and Figure 5.2 (Ref. 15) for NO. Various photolysis reactions result from the absorption of visible and near UV radiation and these are outlined below.

5.13 Photolysis of NO_2, NO and N_2O.

The photolysis of nitrogen oxides, i.e. the interaction of electromagnetic radiation with a single molecule of material, has been studied by several authors (14, 15, 30, 31, 32, 33, 34, 35, 36, 38, 40, 41, 78).

5.131 Nitrogen Dioxide (NO_2).

Several papers (14, 15, 30, 32, 33, 34, 35, 36, 38, 40, 41, 78) detail the photolytic reactions of nitrogen dioxide. The primary reaction is as stated below:

$$NO_2 + hv \longrightarrow NO + O \qquad (5.1)$$

Since the thermodynamic dissociation energy of NO_2 is 71-72 kcal/mole, then it is reasonable that irradiation below 4000 Å should result in dissociation as indicated by reaction (5.1).

In the mm pressure range for NO_2, virtually complete dissociation of NO_2 into NO and O atoms was seen at 3130 and 3660 Å and partial dissociation at 3800 and 4047 Å. There was essentially no dissociation noted at 4358 Å. The O atoms produced in the initial photolytic reaction react as stated in (5.2) and form O_2 molecules.

$$O + NO_2 \longrightarrow NO + O_2 \qquad (5.2)$$

The quantum yield of oxygen seen in this literature work approached unity between 3000 - 3600 Å and a full set of results are shown in Table 5.1 (14). The information on the wavelength effect on dissociation is shown in Figure 5.3 (14) and therefore predicts that at the wavelengths to be used in the photoreactor, dissociation of NO_2 should be seen, as the incident radiation will be in the main at 3550 Å.

Table 5.1. Quantum yields of oxygen as a function of temperature at two wavelengths.

Temperature (^{o}C)	Φ_{O2} 3600Å	Φ_{O2} 4047Å
23	0.95	0.36
23	0.92	0.35
71	1.02	0.41
71	0.95	0.42
133	0.99	0.50
133	0.97	0.52
223	1.00	0.70
223	b	0.71
293	b	0.90
293	b	0.92

b - Not determined

The effect of temperature on the overall photolysis reaction is discussed and it is shown that an increase in temperature produces an increase in the quantum yield of O_2. Therefore, this might infer, that the initial dissociation reaction is enhanced by an increase in reactor temperature. However, it should be noted that the temperature coefficients of most photolytic processes are exceptionally small and therefore the overall thermal influence is more likely to arise from the reaction step (5.2) which is not photolytic. In any case however, the increase in O_2 quantum yield is not major over the temperature ranges that are used in the present study, i.e. 20 - 70^{o}C. The observed increase in O_2 quantum yield is seen as only approximately 5% over this range.

A complex set of 13 possible reactions result from the initiation reaction. Several of these reactions result in the production of O_2, as mentioned previously. This oxygen can then react with further O atoms to produce ozone as indicated in (5.3):

$$O + O_2 + M \longrightarrow O_3 + M \qquad (5.3)$$

The component, M, in the above equation is some substance capable of absorbing the excess energy from the combination of the O atom and O_2 molecule. This substance M, could be the surface of the reactor, water vapour or any inert gas present in the gas stream. With the proposed design of reactor system for the present study, the factor M is present in various forms and therefore it is expected that ozone production will occur.

When NO_2 is photolysed in the presence of a large excess of air, reaction (5.2) has to compete with reaction (5.3). Literature (13) cites that in air at 300K the rates of removal of O atoms by reactions (5.2) and (5.3) are equal at an NO_2 concentration of $1.8 * 10^{16}$ molecules cm^{-3}. Thus when the concentration of NO_2 is less than this value, which corresponds to approximately 7000 ppm, then reaction (5.3) will predominate over reaction (5.2), and NO_2 photolysis will lead to the formation of ozone.

Further work (41) shows that when N_2 is added to the system, where NO_2 is present in the mmHg pressure range, then the quantum yield for NO_2 dissociation is reduced. From zero N_2 pressure where $\Phi NO_2 = 2$, the value drops to $\Phi NO_2 = 1.47$ at PN_2 = 760 mm Hg. Therefore in the proposed experimental photoreactor, photolysis of NO_2 will still occur but at a reduced level due to the presence of N_2 in the inlet stream, in contrast to a system with only NO_2 present.

Experiments (41) with N_2 or CO_2 as the predominant gas have been carried out. The resultant dissociation of NO_2 with these two gases is approximately the same. This implies that the "third body efficiencies" of N_2 and CO_2 are approximately the same. The "third body efficiency" is a measure of the capability of the gas to absorb the excess energy generated in the molecules and atoms of the dissociation reactions of NO_2 (Equation 5.3). The third body efficiency of helium is not known under the proposed system conditions.

5.132 Nitric Oxide (NO).

Photolysis of NO at wavelengths above 2300 Å does not occur. Just below this value, NO has two significant absorption bands at 2144 and 2265 Å. In a pure NO system the following reactions occur at these wavelengths:

$$NO + hv \longrightarrow NO(A^2\Sigma) \qquad (5.4)$$

$$NO(A^2\Sigma) + NO \longrightarrow N_2 + O_2 \qquad (5.5)$$

$$\longrightarrow N_2O + O \qquad (5.6)$$

Other dissociative reactions take place at wavelengths below these two absorption bands and at wavelengths less than 1343 Å, photoionisation takes place yielding NO^+ and e^-.

5.133 Nitrous Oxide (N_2O).

Pure N_2O absorbs at all wavelengths below about 2050 Å. At all of these wavelengths, N_2O exhibits photodissociative reactions, shown below:

$$N_2O + hv \longrightarrow N_2 + O \qquad (5.7)$$

$$\longrightarrow N + NO \qquad (5.8)$$

These two initial reactions initiate a complex series of reactions, similar to those found with the photodissociation of NO_2, as discussed previously.

The information presented previously indicates that no photolysis of N_2O will occur at the wavelengths of irradiation encountered in the photoreactor system to be used in this project.

5.14 Photolysis of Other Relevant Gases. (Ozone, Nitrogen, Oxygen, Carbon Dioxide and Water).

5.141 Ozone (O_3).

The ozone produced by the photolysis of NO_2 itself undergoes several possible reactions. Ozone is itself photolysed in reaction (5.9).

$$O_3 + hv \longrightarrow O_2 + O \qquad (5.9)$$

by radiation across a wide spectrum in the visible, near and far UV range. Reaction (5.9) does not have a significant effect on the ozone concentration in a system where NO_2 is present because of reaction 5.3, which dominates, however it does serve to augment the concentration of O atoms.

Reaction 5.5, also serves as an alternative route for the removal of O atoms:

$$O + O_3 \longrightarrow 2O_2 \qquad (5.10)$$

However, it has been shown (32) that this reaction is unimportant in comparison with reaction (5.3) in air at atmospheric pressures.

Ozone reacts slowly with NO_2 to yield the unstable NO_3 radical, by reaction (5.11):

$$NO_2 + O_3 \longrightarrow NO_3 + O_2 \qquad (5.11)$$

NO_3 in turn reacts with NO and NO_2 to produce various molecules, one of which is N_2O_5. This molecule however is not stable and dissociates into NO_3 and NO_2. Therefore, even

though NO_3 and N_2O_5 are produced in the photolysis reaction of NO_2, it is not expected that either of these two gases would be detected in the outlet stream from the photoreactor, due to their unstable nature.

5.142 Nitrogen (N_2).

Pure N_2 does not absorb significantly at wavelengths greater than 1000 Å, except for some minor dissociation at 1100 and 1450 Å. At wavelengths less than 1000 Å dissociation occurs and at wavelengths less than 795.8 Å, ionisation occurs.

This information infers that no photodissociation of N_2 should occur in the photoreactor to be used in this system.

5.143 Oxygen (O_2).

Pure O_2 absorbs radiation below a wavelength limit of approximately 2420 Å. At wavelengths less than 1027 Å, ionisation of the molecular O_2 occurs.

This information infers that O_2 will not photodissociate in the proposed photoreactor system.

5.144 Carbon Dioxide (CO_2).

Pure CO_2 absorbs radiation at wavelengths less than 1800 Å, and at wavelengths less than 986 Å, CO_2 photoionises. Between these two limits, photodissociation occurs.

The above information infers that if any CO_2 is present in the inlet stream to the photoreactor being considered in this system, then no photodissociation will occur.

5.145 Water (H_2O).

Water vapour will undergo photoionisation when irradiated with radiation of a wavelength of less than 984 Å. Above the ionisation limit, up to approximately 1850 Å, water vapour undergoes photodissociation.

The information above indicates that any water present in the inlet stream of the system to be considered, would not be expected to undergo photodissociation.

5.2 General Photocatalysis.

A large body of information is in existence, covering the subject of photocatalysis (Ref. 1, 3, 4, 5, 7, 9, 10, 11, 13, 17, 39, 42, 82, 83, 84, 85, 86, 87.) Some of the major researchers in the area are; Bickley, Cunningham, Gerisher, Grätzel, Matthews, Ollis, Pichat, Rizzuti, Serpone, Tanaka, Teichner, Yue; these people and others have contributed to a large body of work in the area of photocatalysis.

The general work carried out by these people has provided a good base to the subject. The main areas covered in the general references are as follows:

(a) Fundamentals of photocatalysis (Ref. 1, 39, 87, 89, 92)

The primary reaction in photocatalysis, is the reaction between a photon of UV-light and the surface of the TiO_2. In order for this reaction to take place, the absorption spectra of the TiO_2 to be used has to match part of the output spectra of the UV-light source. The diffuse reflectance spectra of TiO_2 (89) indicates that UV irradiation of wavelengths shorter than ~400nm are required to excite the surface of the TiO_2. This interaction results in the production of a free electron and a "hole", i.e. a positively charged TiO_2 site as outlined in Reference 92:

$$TiO_2 + hv \longrightarrow e^- + h^+ \qquad (5.12a)$$

$$h^+ + e^- \longrightarrow \text{heat} \quad \text{(in the volume)} \qquad (5.12b)$$

$$h^+ + e^- \longrightarrow \text{heat} \quad \text{(at the surface)} \qquad (5.12c)$$

These free electrons and holes are then available to react with electron donors and acceptors on the surface of the catalysts, which lead to the following reactions:

$$h^+ + D \longrightarrow D^+ \quad \text{(at the surface)(5.12d)}$$

$$e^- + A \longrightarrow A^- \quad \text{(at the surface)(5.12e)}$$

If the TiO_2 is in an aqueous system then production of hydroxyl radicals results, due to a surface reaction between the water and any dissolved oxygen that is present. If however, the system is gaseous, then the resultant reaction depends on the gases present. The interaction of photocatalytic reaction of NO_x with irradiated TiO_2 is discussed in Section 5.3.

(b) Oxidation of organics through photocatalysis (Ref. 1, 4, 82, 85, 87)

A considerable body of work has been performed on the photocatalytic destruction of organic molecules, both in the liquid and the gaseous phases. Reaction systems covering the oxidation of ethane, propene, isobutane, ethanol, trichloroethylene, several pesticides and herbicides and numerous other compounds have been studied. While these systems are interesting in their own right, they are not of great relevance to the system covered in this thesis. The basic photocatalytic theories are the same, however the reaction kinetics, reactor design and general engineering concepts are different.

(c) Doping of photocatalysts to improve efficiency (Ref. 10, 11, 17, 83, 84, 86)

Ref. 10 examined the effects of adding small amounts of platinum (Pt^o) onto the surface of Degussa P-25 TiO_2. The TiO_2 was suspended in a solution containing the required weight percent of H_2PtCl_6 solution. The particle size of the Pt^o deposited on the

TiO_2 surface ranged from 1 - 4 nm with an average of ~ 2 nm. The samples showed a decrease in the amount of O_2 photoadsorbed under illumination, these decreases being very significant even for 0.5% Pt^0 on TiO_2: 0.366 (0-Pt); 0.134 (0.5-Pt); 0.025 (5-Pt); 0.018 (10-Pt) where the numbers indicate the amounts of photoadsorbed oxygen in molecules/nm^2. This result, in correspondence with conductivity and photoconductivity measurements under vacuum, indicates that the presence of Pt^0 particles on the TiO_2 causes a decrease in the free electron density of the TiO_2. These results were consistent with an electron transfer from the semiconductor to the metal.

Isotropic exchange (IE) between gaseous O_2 and surface O atoms occurred on TiO_2 in the absence of Pt^0 deposits. At low Pt^0 concentrations (0.5 wt%), this was seen to have a beneficial effect on the IE, which was progressively reduced for higher concentrations. The phenomenon cannot arise from shading of the photosensitive TiO_2 surface since, for 10 wt% Pt^0 on TiO_2, measurements indicated that only 6% of the surface is masked by Pt^0 particles, which is much less than the variations observed. An explanation based on a variation in Pt^0 particle size is also excluded since the mean size did not vary appreciably.

Ref. 11 examined the effects of chromium doping on the photocatalytic properties of powdered TiO_2. It was found that Cr-doped TiO_2 (~ 0.85 %) absorbs in the visible light region, however it becomes a photoconductor only through band-gap illumination, and the doping causes a considerable decrease in the photoconductance. Its activity for oxidations (propene, 2-propanol) and for oxygen IE was found to be nil under visible illumination and 25-1000 times reduced under UV light as compared with pure TiO_2. The decrease in activity was attributed to an increase in charge recombination, enhanced at the chromium ion sites.

Ref. 17 examines the use of Fe^{3+} doped TiO_2 in a flow reactor for dinitrogen fixation. The results presented showed that where as Fe^{3+} doping of TiO_2 had little effect

on the wavelength absorption properties of TiO_2, it apparently did have a beneficial effect on the diffusion length of the charge carriers. This leads to an improved separation between electrons and holes, therefore improving the photocatalytic properties of the material. The optimum Fe^{3+} concentration was found to be 0.4-0.5 % , since this corresponded to the formation of a solid solution and not a separate Fe_2TiO_5 phase.

(d) Nitrogen fixation/water splitting/ammonia production (Ref. 13, 17, 42)

Some work has been done in the area of ammonia production from water/N_2 mixtures. This work was carried out using doped ion-exchange material as the catalyst. TiO_2 or doped TiO_2 was supported or exchanged onto γ-alumina or 3A, 4A and 5A zeolites.

The mechanism of the reaction consisted firstly of the cleavage of water molecules present on the catalyst surface. The hydrogen radicals produced from this reaction, subsequently reacted with nitrogen in the gas stream, to produce ammonia.

Literature (13,17,42) reports the basic results found from this reaction system, some reaction kinetics and basic reactor design information. However, this information is of limited relevance to the present system.

5.3 Action of NO_x on Illuminated Semiconductors.

Various authors (3,5,7,9,39) have studied the interaction of NO_x and semiconductors under the influence of UV irradiation.

As early as 1970 Cunningham et al.(Ref. 5) and Tanaka et al.(Ref. 9) were studying the effects of using ferric or zinc oxide on the photocatalytic reactions of nitrous oxide

under UV illumination. Cunningham showed that gaseous nitrous oxide dissociated when contacted at 20°C with the illuminated surfaces of powered zinc or ferric oxides. The quantum efficiency of the photodissociated reaction of N_2O over pure zinc oxide was small, over the range of conditions covered by Cunningham, at ~ 10^{-5}. These yields were obtained at pressures of N_2O up to 500 Torr and with photons of energy >3.2 eV, the band gap of ZnO. At photon energies of <3.2 eV the quantum yield was reduced to ~ 10^{-6} and with photons of <2.0 eV, no detectable photoassisted dissociation was observed. This reduction in yield was not explained by Cunningham. However, it may result from bi-photon collisions at 3.2 - 2.0 eV still producing enough energy to cause a shift in the valency state, whereas at photon energies of <2.0 eV, multi-photon collisions, with a greatly reduced probability of occurrence, would be required in order for a detectable yield to be observed.

Cunningham reiterated the widely accepted mechanism for the heterogeneously catalysed dissociation of nitrous oxide in the dark at 20°C (steps Ia to Ic) and presented a case for the mechanism under irradiation (steps Ia to Ie).

Weak chemisorption

$$MO(s) + N_2O(g) \longrightarrow \{N_2O(abs)....MO(s)\}$$

Localisation of an electron from the conduction band of the oxide

$$\{N_2O(abs)....MO(s)\} \longrightarrow \{N_2O^-(abs)....(MO)^+(s)\}$$

Dissociation of N_2O-(abs)

$$\{N_2O^-(abs)....(MO)^+(s)\} \longrightarrow N_2(g) + \{O^-(abs)....(MO)^+(s)\}$$

Neutralisation of surface charge by hole transfer

$\{O^-(abs)....(MO)^+(s)\} \longrightarrow \{O(abs)....MO(s)\}$

Desorption of oxygen

$2\{O(abs)....MO(s)\} \longrightarrow \{O_2(abs)....MO(s)\}$

$\{O_2(abs)...MO(s)\} \longrightarrow O_2(g) + MO(s)$

These results may apply to the illumination of N_2O over titanium dioxide semiconductor material, and will therefore be of interest in this current project.

Tanaka [9] studied the photocatalytic decomposition of nitrous oxide over zinc oxide and compared it with the thermal catalytic decomposition. The two types of reaction were studied in the same temperature range, 371 - 431 ^oC, and at pressures of 19 - 160 mm Hg of N_2O. The research determined that the thermal catalytic decomposition of N_2O was first order with respect to N_2O pressure over the range studied. The observed photocatalytic reaction however was seen to be a combination of a photocatalytic reaction and a thermal reaction. With increasing N_2O pressure, the photocatalytic reaction rate was seen to decrease, until at higher pressures the rate of the combined reaction approached that of the thermal reaction. These results show that at higher N_2O pressures, the reaction rate becomes zero-order w.r.t. N_2O pressure. This would seem to imply that the reaction of N_2O is possibly surface coverage limited. Tanaka proposes a model for the setting up of rate equations in the system, involving the transfer of electrons from the valence to conduction bands of the ZnO (See Figure 5.4). While the electronic structure of the surface is presumably complicated by non-uniformities, Tanaka simplifies the approach by considering the surface in terms of the band gap model in Figure 5.4. When the oxide is exposed to band gap illumination, electrons are excited into the conductance band from the valence band, process 1. Electrons excited into the conductance band are repelled from the surface by the potential barrier α at the surface. When the only surface acceptor is nitrous

oxide, which is known to be an efficient electron scavenger, electron transfer between the ZnO and N_2O and/or N_2O^- will be established. Assuming that direct electron transfer from the valence band to N_2O molecules rarely occurs at the experimental conditions, the electron transfer processes established on the surface are described by processes 2,2',3 and 3'. When two types of electron acceptors are on the surface, oxygen and nitrous oxide, a similar set of processes will occurs for the second acceptor, 4,4',5 and 5'.

In 1982 Pichat et al. (7) examined the photocatalytic oxidation of various compounds over illuminated TiO_2 and various other semiconductors. In particular they examined the interaction of NO and TiO_2 in the gas phase.

They showed that on introduction of NO to an illuminated sample of TiO_2, previously evacuated at 423K and then illuminated at room temperature for 7 hours, there was an instantaneously measured large decrease in the photoconductance θ of the TiO_2, with an equilibrium value being obtained within one hour. From variations in θ, as a function of NO pressure, information was obtained about the nature of the absorbed species arising from the gases. In the case of reactions on TiO_2, a log-log plot of θ vs partial pressure of NO yielded a straight line with a slope of -1 and from this plot it was interpreted that an NO^- species was involved in the interaction between gaseous NO and the free electrons.

In 1984 Courbon and Pichat (3) published further and more detailed work on the interaction of NO with illuminated TiO_2. Tests were done over preoxidised (OX) and prereduced (RED) samples of anatase TiO_2 powder. The OX samples had been treated by heating to 723K under $1.33 * 10^4$ Pa of O_2 and maintained at that temperature for 3 hours, then cooled to 423K and evacuated for 1 hour and finally cooled to room temperature while pumping. The PRE samples were obtained by heating at 723K under $1.33 * 10^4$ Pa of H_2 for 5 hours and evacuated while being cooled to room temperature. This paper showed that

under UV illumination, NO is photoabsorbed on the TiO_2, each molecule capturing one semiconductor free electron from the conduction band as inferred from photoconductance measurements. The NO is then partially transformed into N_2 and N_2O, no NO_2 was detected, and it is also capable of oxidising primary and secondary alcohols, such as butanols, to the corresponding aldehyde or ketone. To give a better indication of the interactions of NO and UV illuminated TiO_2, $N^{18}O$ isotopes were used. The purpose being to follow the isotopic exchange (IE) of $N^{18}O$ with oxygen atoms supplied by the semiconductor, and to determine whether the IE and alcohol oxidation were competing reactions.

The experiments were carried out in a static cell, 5 cm in diameter. The TiO_2 was spread as a thin layer on the lower optical window of the cell. The catalyst was illuminated by a 125W UV lamp coupled with a 300 - 410 nm filter, giving a radiant flux of ~3.85 mW cm^{-2}. The TiO_2 used was Degussa P-25, with a measured surface area of ~50 m^2 g^{-1}. 100 mg of catalyst was in the cell; all experiments were carried out at an NO partial pressure of 495 Pa and at a temperature of 295K. The analysis of the result gases was carried out using a mass spectrometer.

Under the experimental conditions used, the formation of N_2O plus N_2 corresponded to ~15% (RED sample) or ~20% (OX sample) of the decrease in gaseous NO gas phase concentration for illumination times of 1 - 30 min. The remainder of the decrease in NO gas phase concentration can be accounted for by considering the surface adsorption of the NO. The results showed an immediate appearance of N_2 on illumination but this attained a limit within ~ 2 min. The variation of the ratio $N_2/(N_2 + N_2O)$ indicated a greater initial formation of N_2, particularly over the RED sample. It infers from the results that the production of N_2 is favoured by an oxygen deficient surface.

In the presence of butan-2-ol (pressure ratio NO/alcohol ~ 1) the absorbed alcohol eliminated the isotopic exchange of $N^{18}O$. Simultaneously, a decrease in the number of

gaseous molecules of $N^{18}O$ and of butan-2-ol, as well as the appearance of gaseous butanone and N_2O was observed.

Pichat also noted that TiO_2 is relatively inactive for the thermal decomposition of NO.

As recently as 1992, Cant and Cole (39), have looked at the photocatalytic reaction between ammonia and nitric oxide on TiO_2 surfaces. A section of their work examined the photocatalytic decomposition of NO. This work showed that when low pressures of NO, approximately 10 Torr, were irradiated with UV light in the presence of a TiO_2 surface, N_2 and N_2O was produced. Normally one would also expect to see evidence of O_2 production, but none was reported. It was suggested that any O_2 produced was desorbed from the catalyst surface, into the bulk gas, where it reacted with NO to produce NO_2. The NO_2 produced would then be readsorbed on the catalyst surface and result in the production of nitrate species. The type of nitrates likely to be formed was not suggested.

It was noted that when NH_3 was introduced into this system, the rate of N_2O production was increased by a factor of 6. However, it was seen that the added NH_3 did not enter into the reaction producing the N_2O, but it did enter into the reaction producing the N_2. By using ^{14}NO and $^{15}NH_3$, it was possible to deduce that in the reaction, the N_2 formed had one atom from the ^{14}NO and the second atom from the $^{15}NH_3$, in 97 +/- 2% of cases. The remaining 3% of the N_2 formed, had both atoms derived from the NO. The N_2O formed in the reaction had all of it's N atoms from the NO in all cases.

A mechanism for the photocatalytic decomposition of NO on irradiated TiO_2 is suggested. The first four steps of the reaction have already been proposed by Courbon (3).

$$TiO_2 + hv \longrightarrow p^+ + e^-$$

$$O^{2-}(cus) + p^+ \longrightarrow O^-(cus)$$

$$NO(ads) + e^- \longrightarrow NO^-(ads)$$

$$NO^-(ads) + O^-(cus) \longrightarrow N(ads) + O(ads) + O^{2-}(cus)$$

The authors then suggest the following reactions for the formation of N_2 and N_2O.

$$N(ads) + N(ads) \longrightarrow N_2(ads) \longrightarrow N_2(gas)$$
$$N(ads) + NO(ads) \longrightarrow N_2O(ads) \longrightarrow N_2O(gas)$$

The presence of nitrates on the catalyst surface were noted through infrared adsorption techniques. The production of these nitrates could arise from the following reaction:

$$NO(ads) + O(ads) \longrightarrow NO_2(ads) \longrightarrow \text{nitrates}$$

or by a combination of O atoms, desorption of the O_2 produced, oxidation of NO in the gas phase and adsorption of the resultant NO_2 back onto the catalyst surface via the reactions below:

$$O(ads) + O(ads) \longrightarrow O_2(ads) \longrightarrow O_2(gas)$$
$$2NO(gas) + O_2(gas) \longrightarrow 2NO_2(gas)$$
$$NO_2(gas) \longrightarrow NO_2(ads) \longrightarrow \text{nitrates}$$

No explanation of the chemical composition of the nitrates present on the TiO_2 surface was given however.

5.4 Photocatalysts other than Titanium Dioxide.

Various catalyst mixtures and modifications have been used for the decomposition of NO_x and other substances under illuminated and non-illuminated conditions. The general information is outlined in Table 5.2.

Table 5.2. References on previous work with photocatalytic materials.

Reference	Material(s)	Application
Ref 4.	TiO_2, ZrO_2, V_2O_5, ZnO, SnO_2, Sb_2O_4, CeO_2, WO_3, and a mixed oxide Sn-O-Sb.	A comparison of the efficiency and selectivity of the photocatalytic oxidation of propene over various oxides at 320K.
Ref 5.	ZnO and Fe_2O_3.	Photocatalytic decomposition of N_2O
Ref 7.	TiO_2, ZrO_2, V_2O_5, ZnO, SnO_2, Sb_2O_4, CeO_2, WO_3, and a mixed oxide Sn-O-Sb.	O_2 isotopic exchange, oxidation by O_2 of various alcohols and hydrocarbons, NO decomposition and oxidation of butanols by NO.
Ref 9.	ZnO.	Decomposition of N_2O.

The work covered by Refs. 3, 5, 7 and 9, has been discussed in a previous section, this work being mainly with unmodified TiO_2, ZnO and Fe_2O_3.

Ref. 4 gives a comparison of the photoactivities of various catalysts. V_2O_5 was the only catalyst from the group examined which was found to be photocatalytically inactive.

All of the other oxides considered showed some photocatalytic activity, however in the absence of illumination no activity was noted for any sample. The quantum yields differed greatly as a function of the catalyst and even according to the particular sample. Amongst the samples examined, only one TiO_2 sample had a quantum yield sufficient for possible practical uses, this sample had a surface area of 70 m^2g^{-1} and a corresponding quantum yield of 0.1. As the other samples examined are of no practical interest, their performance will not be discussed further.

CHAPTER 6.

6.1 EXPERIMENTAL RIG LAYOUT.

The experimental rig has four main parts (see Figure 6.1):

(a) The gas supply system.

The supply gases are fed from standard calibration gas cylinders. In the experiments mixtures of 4000 ppm nitric oxide (NO) in nitrogen or helium, and 4000 ppm nitrogen dioxide (NO_2) in nitrogen or helium were used, to access the effects of the reaction on the individual gases. The feed to the reactor, either pure purge gas or NO_X mixture, entered into the feed control system via two separate on/off valves. The flow is then split as required via a 3-way valve to either the high or low flow rotameters, capable of delivering 0-2000, or 0-100 ml/min. The gas passes out via a T-piece, where a thermocouple measures the inlet temperature. Then through a gas sampling point, fitted with a septum and into the reactor.

(b) The annular photoreactor (see Figure 6.2).

The reactor is designed to exploit the efficient usage of the UV-light, this being inherent in an annular reactor.

Two reactors were used in the work presented here; a low power reactor, using an 8-watt, black-light-blue UV source and air cooling; and a 250-watt, medium pressure mercury arc lamp, requiring water cooling to obtain satisfactory temperature control. Due

to the different reactor cooling requirements, the two reactors are of different design, within the broad description of annular rectors.

The 8-watt reactor consists of three main parts:

a dished end inlet section, made of Pyrex glass, through which the reactant gas enters into the outer annulus of the reactor, and the coolant gas (nitrogen or air) enters through the central quartz tube to cool the UV light;

a straight concentric tube reaction section consisting of an inner tube of quartz glass and an outer tube of Pyrex glass. The ultra-violet (UV source) lamp is mounted centrally within the quartz sleeve, with its electrical supply wires entering and exiting via opposite gas coolant ports. The UV source is an 8-watt black-light-blue fluorescent tube, with an output in the range 310-410nm, as shown in Figure 6.3 (97), having 0.8 watts of output at a wavelength of <400nm. The nature of the black-light-blue lamp means that almost all of the visible light emitted by the source is changed into useful output by the nature of the dye coating the UV-source surface;

and a dished end outlet section through which the product gases and the coolant gas leave the reactor.

The three sections of the reactor are held together by two sets of brass rings, with threaded studs in them (Figure 6.4). These are fitted over the flanges on the ends of the three parts of the reactor, with "O"-rings between the rings and the flanges to prevent breakage of the reactor and to assist in reactor sealing. The whole reactor is then tightened up using "wing" nuts on the ends of the threaded studs. Between the inlet section and the reaction section is placed a flat annulus of porous plastic, through which the reactant gases are dispersed.

The 250-watt reactor has 4 main sections (Figure 6.5);

(i) a dished end inlet section made of Pyrex glass, through which the reactant gas enters into the outer annulus of the reactor. At the point, the inlet section comprises the whole of the outer annulus.

(ii & iii) a straight concentric tube reaction section, consisting of an outer Pyrex glass tube and an inner quartz glass cooling jacket. The inner quartz glass cooling jacket consists of an annular cylinder of glass of ~3mm internal thickness, with inlet/outlet ports at each end. At two positions on the outer walls of the cooling jacket are raised rings of quartz glass. These provide gripping points on which to support the sealing viton "O"-rings and pass fully around the cooling jacket. The outer Pyrex tube is tapered out at the ends, to allow for the increase in the cooling jacket diameter, due to the raised quartz support rings.

The UV source was mounted centrally within the quartz cooling jacket, the output from the UV source being detailed in Figure 6.7.

(iv) a dished end outlet section made of Pyrex glass, making up the whole outer annulus and allowing the outlet gas to pass from the reactor.

The separate sections of the reactor are held together using two sets of brass rings, fitted with threaded studs and tightened with "wing" nuts. Polypropylene "o"-rings are used to protect the glass from damage by the brass rings and to give a better distribution of the forces. Between the top of the inlet section and the bottom of the central Pyrex section/raised gripping ring on the quartz cooing jacket is a porous plastic plate, through which the reactants gases are distributed.

(c) The outlet gas clean up system.

The gas leaves the reactor, passes through a glass sampling point and on to a T-piece, where the temperature is measured and then through an on/off valve into the

caustic scrubber. This consists of a gas scrubber with a liquid caustic feed (see Figure 6.6). The product gas from the reactor may still contain some NO_X. Therefore an additional method of treatment has been installed to ensure the reduction/absorption of NO_X to a safe level before discharging the gas to the high toxicity ventilation system. The reactor outlet gases pass counter currently to a stream of sodium hydroxide solution. The contacting takes place on glass rashig rings of ~5mm OD. The liquid stream is run from a batch supply and is doped with pH indicator to show when the caustic needs replenishing.

(d) The gas chromatography analysis system.

The analysis of the inlet and outlet gases from the reactor was achieved using gas chromatography. The analysis was undertaken using a Pye 204 Series Gas Chromatograph with a thermal conductivity detector. The separation of the gases was performed on Poropak-Q and Molecular Sieve 5A columns.

In the set of experiments where the bulk gas used with the NOx was nitrogen, the gas chromatograph was set-up as follows:

The Poropak Q column was 3m long with an internal diameter of 1/8 inch, and made of stainless steel. NO_X, N_2O, O_3 and H_2O may be separated on this column, with a carrier gas flowrate of 27 ml/min of nitrogen at an inlet pressure of 25 psig.

An unpacked reference column was used to balance the Wheatstone Bridge in the thermal conductivity detector. This reference column was run at 26 ml/min of nitrogen at 4psig and consisted of an unpacked 1/4 inch stainless steel tube of approximately 30cm in length.

The 5A molecular sieve column was 3m long and had an internal diameter of ¼ inch, and was made of glass. N_2 and O_2 was separated on this column, with a carrier gas flow of 12 ml/min of helium, at an inlet pressure of 10 psig.

The 204 chromatograph was run with; Inlet temperature = 200^{o}C; Column temperature = 105^{o}C; Detector temperature = 250^{o}C. A sensitivity of 3 was used at an attenuation setting of 4.

The data produced by the gas chromatography equipment was exported to a Hewlett Packard Integrator for printout and integration.

Two integration methods were used for processing the different sets of data from the Poropac Q and Molecular 5A columns. Program 1, used for the Poropac Q work was as follows:

Run Parameters.

zero = 10

attenuation = 2^4

chart speed = 1 cm/min

peak width = 0.04

threshold = 4

area reject = 0

Time Table.

0.00 Start

1.15 Zero = 40

1.20 Attenuation = 2^{-2}

1.20 threshold = -1

2.50 zero = 20

2.50 attenuation = 2^{-1}

2.50 peak width = 0.08

2.50 threshold = 2

4.00 Stop

Program 2, used for the Molecular 5A work was as follows:

Run Parameters:

Zero = 10

attenuation = 2^{7}

Chart speed = 0.5cm/min

peak width = 0.04

threshold = 0

area reject = 1800

Time Table.

0.00 Start

4.00 Stop

These two sets of programs ensured that the correct parameters were used at all points in the integration program. This gave the correct integration of the eluted peaks on the chromatogram.

CHAPTER 7.

7.0 NON CATALYTIC EXPERIMENTAL WORK.

7.1 Gas Analysis.

The experimental conditions for gas analysis using gas chromatography (GC) were determined and were outlined in Chapter 6.

Two main methods of introducing a gas sample into a GC exist; valve injection or syringe injection. Initially valve injection was tried, as this tends to give a more reproducible injection volume and injection style. However, it is important in valve injection for the GC carrier gas and the sample gas to be at about the some pressure. In the case of this experimental work the sample gas was at atmospheric pressure and the carrier gas at 25 psig and this led to a significant "pressure trough" being produced on the chromatogram. This pressure trough did not allow the baseline of the chromatograph to return to the zero level before the NOx peak was emitted from the GC. This caused very poor reproducibility in the results obtained for the test mixtures hence valve injection was not used. In syringe injection, a set volume of gas (100 μl) is introduced through a septum into the carrier gas flow. This technique was shown to give good reproducibility in experiments with the test gases and these results are shown below in Table 7.1.

Table 7.1. Test Injections for a Gas Injection System.

Injection Number	1	2	3	4	5	6	7	8	9	10	Average
Area Units Result	2166	2141	2141	2118	2309	2118	2197	2241	2105	2341	+/- 7.2%

From the above results a mean of 2188 and a standard deviation of 79.1 was obtained. This gives a variation of +/- 7.2% around the mean value if we consider that 99% of the results fall within two standard deviations of the mean value. In terms of GC analysis a result of +/- 5% is considered to be a good error value for the injection of liquid samples, however, no reference is given for gas samples. It is therefore considered that the levels of error detected in this test set of samples are acceptable.

A number of gases were tested for their residence time on the columns and the following data obtained as shown in Table 7.2:

Table 7.2. Residence Time Data for Various Gases.

Gas	Residence Time (mins) (molecular sieve)	Residence Time (mins) (Poropak Q)
Hydrogen	not determined	0.68
Oxygen	1.70	0.80
Nitrogen	2.13	0.80
Nitric Oxide	not determined	0.80
Nitrogen Dioxide	not eluted	0.80
Carbon Monoxide	not determined	0.81
Carbon Dioxide	not eluted	1.32
Ozone	not eluted	1.37
Nitrous Oxide	not eluted	1.51
Ammonia	not determined	1.93
Water	not eluted	2.61
Ethanol	not determined	10.05

Hydrogen, carbon monoxide, ammonia and ethanol were not determined for their residence time on the molecular sieve for various reasons. Initially, ethanol was to be used as a sacrificial molecule in the NOx system, however this was not followed up due to the results of work undertaken at Bradford University. The Bradford University work showed that ethanol was not being photocatalytically oxidised as the NOx was being reduced, therefore, no benefit in using ethanol as a sacrificial molecule was seen. The three other gases not determined were thought to be possible products of water cleavage but none were seen in the experiments when Poropak Q was used (See Chapter 9) hence the gases were not tested for on the molecular sieve.

All of the other gases were thought to be possible products of the photolytic/photocatalytic reactions of NOx, or NOx itself, or other compounds present in the NOx such as water.

The information on residence times gained allowed the integrator for the gas chromatograph to be programmed with the optimum time table. This permitted both the large peak for the NOx and the smaller peaks for the ozone and nitrous oxide to be well resolved. Also it highlighted that if the GC column was run below 100°C, then a long residence time for water would be encountered, approximately 10 minutes. Therefore the column was run at 105°C to shorten the residence time of water to approximately 2.6 minutes, hence increasing the frequency with which samples could be analysed.

7.2 Catalyst Preparation.

Several types of titanium dioxide catalyst have been tested for their attrition resistant properties. None of the standard catalysts are in a suitable form for use in a fluidised bed reactor due to their attrition rates and the very fine nature of the particles, hence leading to a significant loss of catalyst from the reactor and poor fluidising properties. Experiments have been undertaken to increase the size and strength of the catalysts particles by heat treatment to produce Size Modified Degussa P-25 (SM Degussa P-25).

Initial samples of Degussa P-25 were mixed into a paste with a small quantity of demineralised water, to ensure that no other species were introduced into the catalyst. Approximately twice the mass of water as compared with the Degussa P-25 was added, such that the resultant material formed into a thick, but fully wetted, paste. The resultant material was then split into batches and heated in a muffle furnace for 1 hour under an air atmosphere at a range of temperatures, 300, 400, 500, 600 and 700°C.

The catalysts prepared have been examined for their physical and chemical properties, to see if any significant change has occurred. The phase of the samples was determined, after treatment, by x-ray diffraction and compared with the original material (See Section 7.4 for details of this technique). No phase change was observed below 600^{o}C, the ratio of anatase/rutile being the same as the initial value of 80/20, however the sample heated at 700^{o}C showed a ratio of 50/50. Therefore, the sample fired at 700^{o}C would not be suitable for use as a comparison material with Degussa P-25 since the crystalline composition as well as the physical properties are different.

Another technique for the preparation of catalysts involves dispersing an active component(s) on a "support" material. Normally the carrier matrix is impregnated with a solution of a soluble compound of the catalyst, this is then converted to the desired catalyst by oxidation, reduction or thermal decomposition etc.

This general principle is used in the preparation of iron doped titanium dioxide (Fe^{3+}-P-25). However, in the case of normal impregnation the "support" material is inert, whereas in Fe^{3+} P-25, the addition of the iron effects the already catalytically active titanium dioxide. The reasons for doping TiO_2 with Fe^{3+} are outlined fully in Ref. 89. It is noted that one of the main drawbacks of photocatalysis are the relatively low overall quantum efficiencies. These are as a result of the combined effects of the inherently slow photocatalytic processes themselves and the requirement to use near UV light for activation of the photocatalyst. Impregnation with Fe^{3+} partly solves one of these problems, in that the band gap of the pure TiO_2, usually 3.2 eV is moved to ~3.0 eV which is partly in the range of visible light. Therefore, this shift of the band gap allows for the use of less expensive irradiation sources or even natural sunlight itself.

The Fe^{3+} doped Degussa P-25 was made as outlined in Ref. 89, a solution of ferric nitrate in ultra-pure water being added to the commercial Degussa P-25. The mixture was then allowed to stand for 48 hours at room temperature and then the liquid phase was

evaporated off at 120°C for 24 hours. After this, the resultant solid material was fired at 300°C for 24 hours.

The best condition for production of the catalyst and the loading of Fe^{3+} on the TiO_2 were decided upon through consultation with Dr Roger Bickley at Bradford University and through examination of Ref. 89. It was decided that a 0.5 atom% loading of Fe^{3+} on TiO_2 would be the best for the current application.

For a 0.5 atom% Fe^{3+} doping of TiO_2:

ferric nitrate: $Fe(NO_3)_3.9H_2O$ mw = 404.00

titanium dioxide: TiO_2 mw = 79.899

Therefore, since both chemicals have one atom of Fe and Ti present, a 0.5 atom% mixture requires:-

1*404.00 grams of ferric nitrate per 200*79.899 grams of TiO_2

= 404.00 g ferric nitrate per 15,979.76 g TiO_2

= 2.528 g ferric nitrate per 100 g TiO_2 (to 4 sig. figs.)

Therefore 2.528 g of ferric nitrate was mixed with a few mls of ultra-pure water and then added to 100 g TiO_2. More ultra-pure water was then added until the whole mass became a paste. The whole mixture was then thoroughly stirred to obtained a homogeneous mixture.

The firing temperature for the catalyst was chosen as 500°C, as this would cause the formation of a physically stable catalyst. Also, firing at this temperature would not change the initial anatase/rutile ratio in the Degussa P-25 since it is below the phase change temperature for anatase to rutile.

These materials were tested for their reactivity against the original Degussa P-25 in later experiments detailed in Chapter 9.

7.3 Surface Area Measurements.

The surface areas of various catalysts have been measured by a nitrogen adsorption technique, and BET analysis of the results has been undertaken. The surface area determination involved admitting an adsorbing gas, nitrogen in this case, to a sample of material of known weight. The sample had been previously dried, weighed and freed of adsorbed gases and vapours from the atmosphere, by heating the sample under vacuum. The gas was then admitted in incremental steps, and adsorption of the nitrogen onto the solid surface resulted. The nitrogen pressure over the sample was monitored before and after each increment of nitrogen was introduced. The nature of the change in equilibrium pressures for adsorption and desorption gave an indication as to whether the material was of a porous nature or not.

A set of data results from the surface area determinations that can then be interpreted using the theories of Brunauer, Emmett and Teller (BET Method). The BET equations are based on the principle of having a monolayer coverage of the surface of a material by the adsorbing gas, nitrogen in our case. The relevant theories and assumptions produce an equation of the form:

$$\frac{p}{V\left(p_o - p\right)} = \frac{1}{V_m c} + \frac{(c-1)}{V_m c}\,\frac{p}{p_o} \qquad (7.1)$$

Where p = mean total pressure

p_o = vapour pressure of adsorbed phase

V = volume of fluid

V_m = equivalent gas volume of gas in a complete monolayer

c = constant

On examination of equation 7.1, it can be seen that a plot of $p/V(p_o-p)$ versus p/p_o will give a straight line with the following parameters:

slope = $(c-1)/V_m c$ and intercept = $1/V_m c$

A BET surface area analyser from Micromeritics Ltd, was used for surface area determination, as well as independent analysis by collaborators at the University of Bradford. The surface area of various materials was measured in this way, the plots for Degussa P-25 and SM Degussa P-25 being shown in Figure 7.1 and 7.2. A full set of results for all the catalyst materials used are shown in Table 7.3.

Table 7.3. The surface areas of various forms of titanium dioxide.

Material	Surface Area (m^2/g) (average)
SCM TiO_2	6.0[a]
Tioxide TiO_2	7.0[a]
BDH TiO_2	20.5[a]
Degussa P-25	53.02[b]
SM Degussa P-25	52.10[b]
Fe^{3+} Doped Degussa P-25	50.8[a]

a - Determined at the University of Bradford.

b - Determined at the University of Bath.

It should be noted that there is only a small reduction in the surface area of SM and Fe^{3+} Doped Degussa P-25 as compared with that of the original Degussa P-25. This could be explained by the fact that the particles in Degussa P-25 are only slightly touching in the SM Degussa P-25 and Fe^{3+} Doped Degussa P-25 materials. This would mean that the only surface area lost would be at the points of contact between particles. In theory, the surface

area lost in contact would be insignificant if all of the particles were perfect spheres, however in practice, the particles are not spherical (See 7.8 for confirmation). Therefore, some small percentage of the surface area would be lost in the production process for SM and Fe^{3+} Doped Degussa P-25 and this is reflected in the loss of surface area as noted in the results above.

Several other TiO_2 materials from various manufacturers were measured for their surface area and the results are shown above. It should be noted that all of these materials had surface areas below that of Degussa P-25, SM Degussa P-25 and Fe^{3+} Doped Degussa P-25. These materials were tested under standard conditions by other researchers(90) and shown to have no significant photocatalytic activity. The fact that their surface areas were less than that of Degussa P-25, SM Degussa P-25 and Fe^{3+} Doped Degussa P-25, may partly explain the lack of photocatalytic activity, but is unlikely to be the only factor influencing this result.

7.31 Adsorption Isotherms.

Adsorption isotherms for Degussa P-25 and SM Degussa P-25 were also obtained (Figures 7.3 and 7.4). The isotherms are both of the type typical for non-porous solids(91). Fe^{3+} Doped Degussa P-25 was also indicated to be of a non-porous nature by tests carried out at the University of Bradford. The non-porous nature of the materials indicates that only the surface of the materials will be available in any catalytic reaction. This negates any factors due to pore diffusion in the modelling of the reaction kinetics as there is no delay in the reactants reaching the active sites of the catalyst due to pore diffusion effects.

One notable difference does exist however, between the two absorption isotherms in Figures 7.3 & 7.4, the fact that the final volume adsorbed is greater for SM Degussa P-25 than for Degussa P-25. The nature of the agglomerations of particles in SM Degussa P-

25 (See Section 7.8 for SEM picture confirmation), creates the apparent effect of the material having macropores.

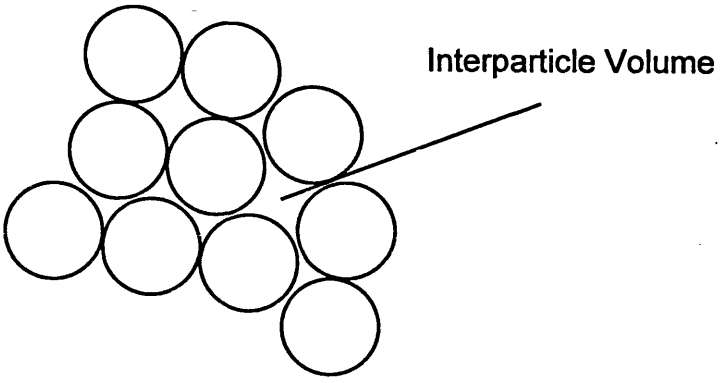

As the space between the particles fill up, the volume of gas adsorbed onto each particle is apparently greater that for the single particles on their own. The interparticle spaces fill up and because of the compact nature of the spaces, the gas molecules are more easily held than in a single particle situation, resulting in a greater volume of gas being held by the particles per unit mass. This may or may not lead to an increase in the reactivity of the SM Degussa P-25 relative to that of the Degussa P-25 and this will be proved or disproved later in Chapter 9.

7.4 X-ray Diffraction (XRD) Phase Measurements.

Introduction.

When an x-ray beam passes through matter, a small fraction of it is scattered by the electrons of each atom. One portion is scattered with a change of wavelength and the other without a change of wavelength. It is the portion scattered without a change in wavelength, the coherent portion, that is of concern in XRD. The phase relations between rays scattered by different atoms result in the destructive interference in certain directions and

reinforcement in others and the resulting pattern of diffracted rays depends on the spatial arrangement of the atoms as well as the wavelength of the x-rays.

From the positions and relative intensities of the diffracted x-ray beams, it is often possible to deduce the distribution of electron density within a crystal and thus to arrive at a very complete knowledge of its chemical structure. Each atom is a spherical concentration of electron density, the total number of electrons in a particular spherical concentration identifies the atom, while the position of the maximum electron density pinpoints its centre.

As noted previously, titanium dioxide exists mainly in two structural phases, anatase and rutile. Literature reports show, that both of these phases are useful in the photocatalytic activity of TiO_2, with anatase generally accepted as the more active phase. There is therefore a requirement to know the relative phase distribution of the materials used in the study, in order to access there contribution to the activity of the catalyst.

Phase measurements were undertaken in the School of Physics, with the assistance of Rev. B F Chapman, who performed the analysis. Figures 7.5 to 7.9, show the diffraction patterns for five common forms of TiO_2. The peaks of greatest significance occur at approximately 27.5^{o} for rutile and 26.0^{o} for anatase.

A set of standard mixtures were measured, allowing greater measurement accuracy to be obtained. This involved mixing set proportions of anatase and rutile together and measuring the relative responses of the 27.5 and 26.0^{o} peaks. An error in the measured ratio of anatase:rutile of +/- 2.5% was shown to exist.

The SM Degussa P-25 was assessed by the use of x-ray diffraction techniques to ensure that the temperature used in it's production did not significantly change the anatase:rutile ratio in the new material. As noted in Section 7.2 above, if a temperature of $600^{o}C$ or below was used in the preparation of the SM Degussa P-25 then no significant phase modification was evident. At a temperature of $700^{o}C$ however, a significant change

in the anatase:rutile ratio from 80:20 to 50:50 was evident using x-ray diffraction techniques. It was upon this evidence that the SM Degussa P-25 material made at 600°C was used in the experimental program as a photocatalyst since, (i) the material was of the same phase ratio as the original Degussa P-25 and (ii) the material produced at 600°C was expected to give better fluidising properties than materials produced at other temperatures, however this was not confirmed.

7.5 Fluidising Properties.

Two potential TiO_2 catalysts (from Degussa and Tioxide), one possible catalyst support material (γ-alumina) and two manufactured catalysts were tested for their fluidising properties.

The experimental apparatus used in the tests is shown in Figure 7.10, the differential pressure across the bed being measured by a water manometer.

The gas distributor was made from a porous plastic material called Vyon D. The plate was 3.2mm thick and had an average pore size of 30 microns. The pressure drop over the plate on it's own is shown in Figure 7.11.

The results obtained for pressure drop versus gas flowrate are shown in Figures 7.12 to 7.18. A summary of the measured variables are given in Table 7.4 below.

Table 7.4. Summary of the fluidisation conditions and properties of various photocatalysts and support materials.

Material	Size Range (μm)	Geldart Group Classification.	Minimum Fluidisation Velocity (m/sec).
Degussa P-25	150 - 250	B	0.021
Tioxide TiO_2	150 - 180	B	0.035
Tioxide TiO_2	180 - 212	B	0.041
Tioxide TiO_2	212 - 250	B	0.051
Size-modified P-25	150 - 250	B	0.110
½ atom% Fe^{3+} P 25	150 - 250	B	0.111
γ-alumina	150 - 250	B	0.112

All of the materials examined showed "Group B" characteristics as proposed by Geldart[2] (Figure 7.19). Group B contains most materials in the mean size range and density ranges of 40 μm < d_S < 500 μm, 4 g/cm^3 > ρ_S > 1.4 g/cm^3 respectively. Naturally occurring bubbles start to form in this type of powder at or slightly above the minimum fluidisation velocity. Bed expansion is small and the bed collapses very rapidly when the gas supply is cut off. There is little or no circulation in the absence of bubbles. All of these observations were noted with the powders used.

7.6 Comparison of Measured U_{mf} and Correlated U_{mf}.

Values of the parameters:

$g = 9.81$ m/s2 (acceleration due to gravity)

$\rho_P = 3900$ Kg/m^3 (density of TiO_2), 800 Kg/m^3 (density of γ-alumina)

$\rho_f = 1.24$ Kg/m^3 (density of nitrogen at 20°C)

μ = 1.74 E-05 newton.sec/m^2 (viscosity of N_2 at 20°C) (0.0174 centipoise)

dp = average value for the size range indicated in the material column of Table 7.5 below.

The correlations outlined in Chapter 3 have been compared with the measured values obtained for the various materials used. The results of these comparisons are outlined in Table 7.5.

Table 7.5. Values of U_{mf} from measurements and correlations for various materials.

Material	Measured value of U_{mf} (m/s)	Davidson and Harrison	Leva
Degussa P-25 150 - 250 μm	0.021	0.0883 (+320%)	0.0623 (+300%)
Tioxide 150 - 180 μm	0.035	0.0580 (+65%)	0.0439 (+25%)
Tioxide 180 - 212 μm	0.041	0.0848 (+105%)	0.0601 (+45%)
Tioxide 212 - 250 μm	0.051	0.118 (+130%)	0.0810 (+60%)
Size-modified P-25 150 - 250 μm	0.110	0.0883 (-25%)	0.0623 (-75%)
½ atom% Fe^{3+} P-25 150 - 250 μm	0.111	0.0883 (-25%)	0.0623 (-80%)
γ - Alumina 150 - 250 μm	0.112	0.181 (+60%)	0.0140 (-90%)

The correlations show the following results:-

(i) None of the correlations used were shown to be suitable for predicting the value of U_{mf} for Degussa P-25. The poor fit of correlation results is probably in the main due to the fact that the particles of P-25 are actually agglomerations of much smaller particles. These particles are of a sub-micron size, however, if the primary particle size of ~20nm was used in the correlation a predictive value of less than that measured would be found. Therefore, the actual value for the size of the particles of P-25 to be used in the correlation is some figure between the primary particle size and that of the agglomerates.

(ii) The correlation results for Tioxide became worse as the particle size was increased. This may be due to a similar reason as that for P-25 above, since the Tioxide material is also made up of agglomerations. However, the constituent particles of the Tioxide material are of the order of tens of microns rather than tens of nanometres.

(iii) The correlation results for the SM P-25 and Fe SM P-25 were seen to give a reasonable fit. This may well be due to the fact that the particle size used in the correlation is actually that of the particles, since these particles are not made up of loosely held together agglomerates. The particles are effectively solid lumps of the titanium dioxide material, however, the particles do have a significant amount of porosity (See Section 7.32) which may account for the slight miss match of the correlations.

(iv) The correlations for γ-alumina were seen to vary greatly, this in the main, resulted from two significant factors: (i) That the γ-alumina particles were not spheres and therefore did not fit the criteria for either of the two correlations examined in this work; (ii) That the bulk density used in the correlations was not truly representative of the actual density of the γ-alumina particles due to the materials high porosity.

(v) Overall it was seen that neither of the two correlations considered gave suitable results when used to estimate the minimum fluidising velocity of Degussa P-25. The correlation by Leva was seen to be best when applied to the Tioxide material. The correlation by Davidson and Harrison was seen to be best for the size-modified materials. Neither correlation was seen to be suitable for the estimation of the minimum fluidising velocity for the γ-alumina support material.

7.7 Catalyst Attrition.

A range of experiments have been carried out on a series of photocatalysts, to assess the potential problem of catalyst attrition in the photoreactor.

The experimental set-up was the same as that used in the determination of the fluidising properties above (Figure 7.10). The materials to be tested were first sieved into their component fractions, and the ratio of the fractions noted. These fractions were then recombined in the same manner, but by adding together known masses of the material fractions. The made up samples were then tested and the size distribution after the attrition experiments compared with the original.

Some of the catalysts examined showed a significant amount of attrition after seven hours fluidisation at approximately three times their minimum fluidising velocity (Figures 7.20 to 7.22). The material from Tioxide showed an ~20% change in it's size distribution after fluidisation and Degussa P-25 showed an ~40% change. However, Size Modified Degussa P-25 only showed an ~5% change in it's size distribution profile.

This attrition was not thought to be due to action of the particles on the distribution plate, since the plate was a porous plastic plate. However, it should be noted that high velocities would be expected at the surface of the perforated plate and would therefore possibly lead to attrition taking place in the vicinity of the plate. The main cause of particle

attrition would have been due to the action of the particles on each other in the bulk of the catalyst bed.

The percentage change in the size distribution for the various materials shows a significant enhancement in stability for SM Degussa P-25 over the initial Degussa P-25 and the Tioxide material. Therefore, from the point purely of physical stability SM Degussa P-25 is seen to be a much more suitable material to use as a photocatalyst in a fluidised bed reactor.

7.8 Scanning Electron Microscopy.

The Figures used in this Section are a representative selection from several dozen photographs that were actually taken and are detailed in Table 7.6.

Table 7.6. A Listing of the SEM and TEM Pictures taken of Degussa P-25, SM Degussa P-25 and Fe^{3+} Doped Degussa P-25.

Picture Number and type.	Material	Magnification	Nature of View
(7.23)EM4047 - TEM	Degussa P-25	*100K	particles
(7.24)EM4050 - TEM	Degussa P-25	*100K	particles
(7.25)SM0018 - SEM	Degussa P-25	*200K	Fine particles
(7.26)SM0021 - SEM	Degussa P-25	*200K	Fine particles
(7.27)020445 - SEM	Degussa P-25	*20K	surface
(7.28)020446 - SEM	Degussa P-25	*350	particle
(7.29)SM0024 - SEM	SM Degussa P-25	*200K	Surface view
(7.30)020449 - SEM	SM Degussa P-25	*20K	edge of particle
(7.31)020451 - SEM	SM Degussa P-25	*350	particle
(7.32)SM0026 - SEM	Fe^{3+} Doped P-25	*200K	Surface view
(7.33)020454 - SEM	Fe^{3+} Doped P-25	*20K	edge of particle
(7.34)020455 - SEM	Fe^{3+} Doped P-25	*350	particle

7.81 Introduction.

Microscopy is the science of the interpretative use and applications of the microscope. Microscopy involves the co-ordinated use of the microscope, the eye and the brain. The microscope permits seeing and interpreting structures which are to close together to be resolved by the normal unaided eye.

Electron microscopy becomes desirable whenever the relevant structure is too fine to be depicted in any other way. The limit of resolution of the light microscope is reached with particles whose size is comparable to the wavelength of the light used. In chemical technology, the borderline of usefulness between light microscopes includes all pigments, because their light scattering efficiency is at a maximum when the diameters of the acting particles are of the order of the wavelengths of the light. Titanium Dioxide is a standard paint pigment due to it's light scattering properties, therefore electron microscopy was used to examine the TiO_2 catalyst material.

The main problem with the electron microscope is preserving the material to be looked at in the high vacuum conditions required in the machine. This is particularly difficult when gaseous, liquid or low melting point materials are to be examined. However, with solid materials this is not a problem, as the material can be chemically/physically anchored to a large substrate, which can then be examined.

The main difference between the light microscope on the electron microscope is that a beam of electrons is used rather than a beam of light. The image produced in an electron microscope is based on differences in electron scattering power, which is a function of atomic number. Thus the electron microscope can frequently show structures which are not perceptible on the basis of refraction, absorption or reflection of light.

Degussa P-25, size modified Degussa P-25 and iron doped Degussa P-25 were all examined using a Scanning Electron Microscope (SEM) and the Degussa P-25 was also examined using a Transmission Electron Microscope (TEM).

7.82 Degussa P-25.

TEM was used to determine the primary particle size of Degussa P-25. Degussa P-25 is made up of primary particles of the order of 10-50nm, which then agglomerate into

particles of the order of 10-250μm. TEM pictures were taken of Degussa P-25 to confirm the manufactures information on the size of the primary particles.

Figures 7.23 and 7.24 (Pictures EM4047 and EM4050), TEM photographs, show Degussa P-25 powder and indicate that the primary particle size of Degussa P-25 is as reported, i.e. of the order of 10-50nm. These observations are confirmed by the SEM photographs of Degussa P-25 powder shown in Figures 7.25 (Picture SM0018) and 7.26 (Picture SM0021).

Figure 7.27 (Picture 020445) shows a close-up of a secondary Degussa P-25 agglomeration. The picture shows the agglomeration of the nanometre size particles seen in Figure 7.23 and 7.24 to form the basis of the micrometre size particles.

Figure 7.28 (Picture 020446) shows a general view of the Degussa P-25 agglomerations. Several particles of the order of 10-20μm can be seen in this Figure, however, particles up to 250μm also exist, these particles simply being larger agglomerations of the primary particles.

The combination of the TEM and SEM pictures for Degussa P-25 confirms that the material is not macroporous in the order of the nm scale, however the primary particles are of the nm size. The resulting agglomerations formed from the primary Degussa P-25 particles form secondary particles of the order of 10-250μm. This explains the surface area measurements obtained earlier by BET measurements and helps to explain the poor fluidising properties of Degussa P-25 due to the extremely small primary particle size.

7.83 Size Modified (SM) Degussa P-25.

SEM pictures of SM Degussa P-25 were taken to aid in explaining the limited change in surface area of the material when compared with the original Degussa P-25.

Figure 7.29 (Picture SM0024) shows that the same primary particle size seen in the photographs of the original Degussa P-25 material can again be seen. This indicates that

the Degussa P-25 has not lost it's physical integrity during the process to produce the SM Degussa P-25. This photographic evidence supports the surface area theories postulated in Section 7.32.

Figure 7.30 (Picture 020449) shows that the primary particles in SM Degussa P-25 are held together in larger agglomerations as in the case of the original Degussa P-25. However, it should be noted that a much more dense structure is evident in Figure 7.30 for the SM Degussa P-25 than in Figure 7.27 for the original Degussa P-25. This observation may explain the added strength of the SM Degussa P-25, as shown in the attrition experiments outlined in Section 7.7. The denser SM Degussa P-25 would have greater strength than the original Degussa P-25, due to greater interparticle forces holding the material together. Also, some degree of sintering may have taken place due to the heating process used to make the SM Degussa P-25.

Figure 7.31 (Picture 020451) shows a single particle of SM Degussa P-25.

7.84 Fe^{3+} Doped Degussa P-25.

SEM photographs of the Fe^{3+} doped Degussa P-25 were taken (Figures 7.32, 7.33 and 7.34) and compared with those taken for SM Degussa P-25. The photographs show that a similar physical structure existed for the Fe3+ doped Degussa P-25 as that for the SM Degussa P-25. This confirms the surface area data seen for Fe3+ doped Degussa P-25 shown above in Section 7.31.

7.9 Conclusions.

The non-catalytic experimental work described in this chapter has shown the following points:-

(a) The inlet and expected outlet gases for the reactor systems to be examined in later chapters, can be analysed for using gas chromatography and the conditions for this analysis have been determined.

(b) Experimental work has been undertaken to produce catalysts with physical properties which have advantages for use in a fluidised or fixed bed reactor systems. Both physical and chemical modifications of Degussa P-25 titanium dioxide have been undertaken.

(c) Surface areas for all catalysts to be used in the reactor systems described in this work have been determined by nitrogen adsorption techniques (BET).

(d) Nitrogen gas adsorption isotherms have been determined for Degussa P-25, SM Degussa P-26 and Fe^{3+} Doped Degussa P-25. All of these isotherms have shown that the materials are of a non-porous nature, therefore pore diffusion effects need not be considered in reaction pathway modelling outlined in Chapter 10.

(e) X-ray diffraction data for SM Degussa P-25 manufacture at different temperatures showed that heating of the initial Degussa P-25 above 600°C resulted in a phase change taking place within the original material. Therefore, it was possible to set the preparation temperature such that only the physical properties of the Degussa P-25 changed and the crystalline structure remained the same as the original material.

(f) Determination of the Geldart Group classification and minimum fluidisation velocity of several potential photocatalysts and support materials were undertaken. The results obtained allowed some of the operating parameters for the photocatalytic reactor systems examined in Chapter 9 to be set.

(g) Literature correlations for the fluidising properties of some particulate materials, were investigated for their applicability to the catalysts and support materials used in later chapters. It was shown that the fluidising properties of Degussa P-25 were not possible to

estimate using the correlations considered, however, the size modified (SM) materials did fit the correlations considerably better.

(h) Degree of attrition was examined for several of the potential catalyst materials to be used in later work. It was shown that the size modified (SM) materials manufactured by myself, were significantly more resistant to attrition than the original Degussa P-25 material.

(i) The physical nature of Degussa P-25, SM Degussa P-25 and Fe^{3+} Doped Degussa P-25 was examined using electron microscopy. These observations showed the primary particles of Degussa P-25 and their appearance when combined to form SM Degussa P-25 and Fe^{3+} Doped Degussa P-25.

CHAPTER 8.

8.1 BASIS FOR THE PHOTOLYSIS WORK.

The first thing to decide upon in starting the experimental work on the photoassisted reactions was to decide on the concentrations and compositions of the inlet gases to be examined.

Figures were taken from Ref. 79 which indicated that approximately 4000ppm of NOx was a typical value for the tail gas exiting the primary stage of a nitric acid production process. This tail gas would then go forward to subsequent abatement equipment and it would therefore be at this point that any new abatement system would be sited.

Due to the complex nature of the tail gas exiting the plant, it was thought impractical to attempt to use the full tail gas specification in the laboratory work. Analysis problems could well occur due to the ongoing reactions that would be taking place in such a complex gas mixture, particularly between the NOx and O_2. Therefore it was decided to simplify the experimental gases to two compositions, (i) 4000ppm NO_2 in nitrogen and (ii) 4000ppm NO in nitrogen. Oxygen was specifically excluded from the inlet gas, as the fast reaction rates of NO with O_2 would give rise to difficulties in knowing the exact inlet concentrations at any given time. It was also decided that any residual water present in the standard gases purchased would not be removed as the actual plant gas contained water.

8.2 Initial Photolysis Experiments.

Photolysis is a process by which direct interaction of a photon of energy with a molecule results in a change of that molecule. Therefore, before the photocatalytic reactions of NO and NO_2 were examined, it was decided to establish whether any direct photolysis reactions were taking place in the gases to be investigated. It was known from literature (14,15,29,30,31,32,33,34,35,36,37,38,40,41,78) that all of the gases to be used in the photocatalysis experiments would undergo photolysis at certain wavelengths, except for helium. Therefore, tests were done on the reactant gases in the presence of the UV light, with no catalyst present.

The results from these "blank" experiments are outlined below. The standard experiment involved several steps which were undertaken in a set sequence: (i) the reactor was physically set-up as outlined in Chapter 6; (ii) the analysis system was calibrated; (iii) the reactor was purged with a set sequence of gases, this might initially involve purging with an inert gas such as nitrogen to remove the atmospheric gases initially in the reactor, followed by purging with the reaction gas itself; (iv) when it was seen that the outlet gas composition was the same as the inlet gas composition, through determination by analysis, the experiment was started by turning on the UV light source; (v) the experiment was timed, samples were analysed every four minutes, the reactor temperature was monitored, the flowrate of inlet gas was monitored; (vi) the results obtained were immediately displayed on a computer graphics package, which allowed the optimum end time for the experiment to be determined.

8.21 Nitrogen.

Nitrogen was examined as it was the bulk gas present in the reactor inlet gas at approximately some 99.6%. An experiment was undertaken where pure nitrogen was

introduced to the reactor with no catalyst present. A flow of 17 ml/min of nitrogen, the lowest measurable with the available flowmeters, was introduced into the reactor while being irradiated by an 8 watt black-light-blue. No detectable reaction was seen to take place between the nitrogen and the UV light, as expected from information in literature (15). No other gaseous species were detected in the reactor outlet and this was taken as an indication that there were no leaks into the reactor from the external atmosphere.

8.22 Oxygen.

Oxygen was examined, as it was expected to be seen as a product from the photolysis of NO_2. Also, ozone, O_3, was also expected to be produced from the photolysis of NO_2, therefore it was required to test whether any O_3 that might be detected in the photolysis of NO_2 came from the O_2 produced by photolysis of the NO_2 or by some other method.

An experiment was undertaken at a flowrate of 18.5 ml/min of pure oxygen, which was fed to the reactor containing an 8 watt black-light-blue. The reactor did not contain any catalyst, therefore any reaction seen would have been purely due to photolysis of the oxygen.

No reaction was seen, as expected, since oxygen does not absorb energy of the wavelengths emitted by the black-light-blue source(15). No appearance of unidentified gaseous species was noted in the outlet from the reactor, therefore indicating that no nitrogen, carbon dioxide or other gases from the atmosphere were leaking into the reactor.

8.23 Nitric oxide.

Two experiments were undertaken with a 4000ppm NO/bulk N_2 mixture as the inlet gas. Both experiments were undertaken at a flowrate of 18.5 ml/min of NO/N_2

mixture, which was fed to the reactor containing an 8 watt black-light-blue. The reactor did not contain any catalyst, therefore any reaction seen would have been purely due to photolysis of the NO. No photolysis of the NO was seen to occur as expected from Section 5.132, and no photolysis of the nitrogen was detected either as expected from Section 5.142, and as shown in Section 8.21. This result was fully as expected having considered the adsorption spectra for NO as shown previously in Figure 5.2.

8.24 Nitrogen Dioxide.

Several runs were undertaken with NO_2/bulk N_2 in a reactor containing an 8 watt black-light-blue UV light source with no catalyst present. A summary of the operating conditions for the experiments are shown in Table 8.1 and a brief summary of the results is presented in Table 8.2.

Several conclusions can be drawn from the experimental photolysis work done on NO_2 as follows:

(i) When the reactor is initially purged with N_2, then N_2/NO_2 mixture and subsequently irradiated with the 8W black-light-blue, photolysis occurs as expected. This is presumably by the reaction sequence outlined in Ref. 15:-

$$NO_2 + h\nu \longrightarrow NO + O \qquad (8.1)$$

$$O + O_2 (+M) \longrightarrow O_3 (+M) \qquad (8.2)$$

$$O_3 + NO \longrightarrow NO_2 + O_2 \qquad (8.3)$$

Because of the fact that in the gas chromatography (GC) analysis used, O_2, NO_2 and NO all exit the separation column together, independent determination of the presence of all of these species was not possible.

(ii) As a result of the photolysis of NO_2, ozone is produced and is detected in the exit gas from the reactor. The O_3 gas exits the GC analysis column at a significantly different residence time to the other outlet gases from the reactor and can therefore be determined. O_3 was seen in the photolysis experiments as expected, at levels up to 620ppm.

N_2O may be present but in very small quantities on the limit of detection capable of the G.C.

(iii) Increasing the flowrate of the N_2/NO_2 mixture through the reactor (i.e. reducing the residence time) decreases the average quantity of ozone in the outlet (Figure 8.13). The graph shows a logarithmic rise in the concentration of ozone in the outlet with respect to an increase in residence time. This can be explained by considering the equilibrium (Reactions 8.1 - 3) that exists between NO_2, NO and O_3/O_2 in the reactor. A maximum value for the concentration of ozone will exist even at infinite residence time, i.e. a batch reactor system, since any O_3 produced reacts with the NO and forms NO_2.

(iv) The production of ozone was seen to definitely be photolytically caused. This was seen in two experiments 1B and 2B (Figures 8.1 and 8.2), where at various times into the experiment, the UV source was turned off and a decline in the level of ozone in the outlet gas was seen to occur.

Also there seemed to be a thermal effect in the production of ozone, when in Experiment 10B (Figure 8.10), the quantity of ozone in the outlet from the reactor reduced when the UV lamp cooling was turned on. This would indicate that an Arrhenius type equation might be deduced for the rate constant of the photolytic reaction of NO_2. However, it was not possible to control the temperature of the reactor system used in the

experimental work to a precise enough extent to be able to examine the Arrhenius relationship, due to the unavailability of suitable temperature control equipment.

(v) In runs where both N_2 and N_2/NO_2 purges were used, the value of the NOx/O_2 peak in the outlet gas was consistently at or above that for the inlet. Due to the fact that O_3 was being formed in the reaction, it would be expected that a reduction in the value of the NOx peak would be seen. However, a reaction in the NOx peak was not seen and this may well be due to the formation of NO and O_2 from the NO_2 via the reaction:

$$NO_2 + h\nu \longrightarrow NO + \tfrac{1}{2}O_2$$

This would lead to an increase in the total size of the peak due to the two gases being present concurrently. This is due to the principles by which the thermal conductivity detector in the gas chromatograph works; when a sample passes the detector a change in voltage across the Wheatstone Bridge in the detector produces a peak on the plotter, the larger the difference in the thermal conductivity between the carrier gas (i.e. helium) and the sample, the larger the peak will be. Therefore since the thermal conductivity for helium at 150°C, the temperature of the detector head, is 0.1968 W/m°C and for NO_2 and NO are 0.01852 and 0.01656 W/m°C respectively (Ref. 81), then the value of the peak on the plotter would be greater for a mixture of 50/50 NO_2/NO than for pure NO_2 only. Hence the increase seen in the height of the peak on the plotter can be explained by the presence of NO in the outlet gas as expected.

This assumption indicates the main problem in the quantification of the reaction products in this work, the fact that the analysis equipment available was not able to distinguish between all of the reaction products.

(vi) Production of N_2O photolytically from N_2/NO_2 is not seen to any significant degree, although some formation of N_2O at the limit of detection of the GC is possible. However, in Experiments 1B and 2B, where residual O_2 was present in the reactor due either to an oxygen purge before the run started or a purge only with N_2, N_2O production was seen (Figures 8.1 and 8.2).

The presence of N_2O in the outlet can be explained by considering the initial reaction of NO_2 with the UV irradiation. The cycle of reactions set up by this initial reaction is as shown:

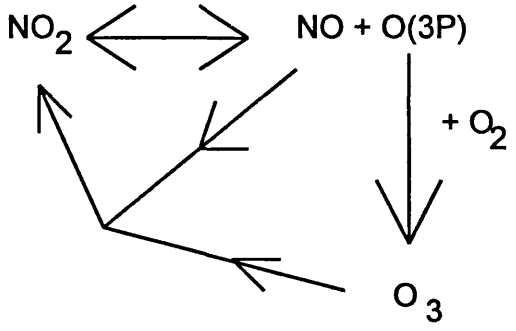

The cycle of these reactions can be represented concisely, but not in balance, as:

$$NO_2 \xrightleftharpoons{h\nu + O_2} NO + O_3$$

Therefore, when an excess of O_2 is present in the reactor, as in Experiments 1B and 2B, the equilibrium is pushed towards the right and more NO is produced.

Under the normal conditions of irradiation from a black-light-blue, NO would undergo no further photolysis at the wavelengths emitted, i.e. >300nm. However, from evidence supplied by the lamp manufacturer (Fig 6.3), it was shown that approximately 1/35th of the wattage of the irradiation emitted at 355nm was emitted at 254nm from the black-light-blue being used. This is close to the longwave absorption bands for NO at

227nm and 214nm. It is therefore possible that if these longwave bands were also present with the 254nm band, then the following reaction may occur:

$$NO + h\nu \longrightarrow NO(A^2\Sigma)$$

It is then possible (although unconfirmed due to my lack of knowledge of the complex science of molecular vibrational states and transitions) that the excited $NO(A^2\Sigma)$ could react with the excess O_2 present and cause quenching of the vibrational energy to form NO molecules. These NO molecules could then react with excited $NO(A^2\Sigma)$ molecules by the following reaction:

$$NO(A^2\Sigma) + NO \longrightarrow N_2O + O$$

This reaction would account for the presence of N_2O in the outlet stream, but only when excess O_2 was present to quench the excess vibrational energy of the $NO(A^2\Sigma)$.

8.3 Conclusions.

The photolysis experimental work described in this chapter has shown the following points:-

(a) Nitrogen, oxygen and nitric oxide do not undergo photolysis under UV irradiation from an 8 watt black-light-blue in an annular flow reactor.

(b) Nitrogen dioxide undergoes photolysis when irradiated by an 8 watt black-light-blue in an annular flow reactor. The photolysis yields a mixture of NO_2, NO and O_3 as

product gases, also when O_2 is present in the inlet gas to the reactor N_2O may be seen in the outlet.

(c) The production of O_3 by photolysis of NO_2 has been shown to be dependant on the flowrate at which the gas is introduced into the reactor, this results from the increased residence time within the reactor at lower flowrates.

(d) The production of O_3 from the photolysis of NO_2, has been seen to be due to the irradiation by UV light of the NO_2 and has also been shown to be dependant in some way to the temperature at which the reactions occur.

(e) The production of N_2O from the photolysis of NO_2 was not able to be confirmed, as any N_2O was at the limit of detection of the analysis equipment used and hence the results were unreliable.

Table 8.1 Photolysis Experiments on Nitrogen Dioxide/Nitrogen Mixtures.

Run Number and Figure.	Conditions
1B - Fig 8.1	NO_2(14ml/min) + UV + O_2 purge
2B - Fig 8.2	NO_2(17ml/min) + UV + N_2 purge
3B - Fig 8.3	NO_2(17ml/min) + UV + N_2 & NO_2/N_2 purge
4B - Fig 8.4	NO_2(14ml/min) + UV + N_2 & NO_2/N_2 purge
5B - Fig 8.5	NO_2(18.5ml/min) + UV + N_2 & NO_2/N_2 purge
6B - Fig 8.6	NO_2(18.5ml/min) + UV + N_2 & NO_2/N_2 purge
7B - No Figure	NO_2(18.5ml/min) + UV + N_2 & NO_2/N_2 purge, Aborted.
8B - Fig 8.8	NO_2(18.5ml/min) + UV + N_2 & NO_2/N_2 purge
9B - Fig 8.9	NO_2(10ml/min) + UV + N_2 & NO_2/N_2 purge
10B - Fig 8.10	NO_2(25ml/min) + UV + N_2 & NO_2/N_2 purge
11B - Fig 8.11	NO_2(51ml/min) + UV + N_2 & NO_2/N_2 purge
12B - Fig 8.12	NO_2(32ml/min) + UV + N_2 & NO_2/N_2 purge

Table 8.2 Data Obtained from Nitrogen Dioxide/Nitrogen Mixture Photolysis Experiments.

Run Number	Outlet gases present	Average Ozone level (ppm)
1B	O_3 and N_2O	620
2B	O_3 and N_2O	370
3B	O_3	620
4B	O_3	270
5B	O_3	400
6B	O_3	210
7B	Run aborted	-
8B	O_3	300
9B	O_3	300
10B	O_3	220
11B	O_3	140
12B	O_3	140

CHAPTER 9.

9.0 PHOTOCATALYSIS EXPERIMENTS.

Numerous experiments were undertaken on several different inlet gas streams. The two reaction gases examined were NO_2 and NO at a concentration of 4000vppm, in either nitrogen or helium as the bulk gas. The use of nitrogen as the bulk gas was determined from the specification for the nitric acid plant NOx discharge composition as detailed in Table 1.1. The use of helium as a bulk gas was in order to assist in the analysis of the outlet gases from the reaction system, since nitrogen, if used, might mask the production of any small amounts of nitrogen from the photocatalytic reactions under investigation.

The first point to note in the photocatalysis work is that due to the fact that NO_2 undergoes photolysis, as shown in Section 8.24, we must consider what fraction of the reaction we see in the photocatalysis reaction of NO_2 is due to photolysis. In order to estimate the fraction of photolysis in the photocatalysis reaction, we are required to estimate the depth to which the UV light penetrates into the catalyst bed. Previous work (93,94) has shown that catalyst densities of >60mg/l for a liquid system and 0.15mg/cm^2 for a deposited solid film system, are enough to absorb all the incident light from a UV source. If we take the density of TiO_2 as 3.9 g/cm^3 (Section 7.6) then previous work (93,94) yields figures of 60μg/cm^3 for the required bulk density of TiO_2 or a slab of solid TiO_2 of thickness 3.9 E-5 cm, being required to absorb all of the incident UV light from a low power UV source.

The reactor used in the photocatalytic reactions of NOx is approximately 160cm^3 volume and contains approximately 10g of catalyst. This yields a bulk density of 63mg/cm^3 of TiO_2 in the reactor, i.e. ~100 times greater a density than required as

indicated in literature (93,94), to absorb all of the incident irradiation from a low power UV source. Alternatively, by comparing the bulk density in the reactor with the density of a solid TiO_2 slab the thickness of TiO_2 in the reactor which would absorb all of the incident UV irradiation would be
3.9E-5 * (3.9/63E-3) = 0.0024cm = 0.024mm. The actual thickness of the annulus of the reactor containing the catalyst is 5mm, ~200 greater than that required.

From consideration of the bulk density and the annulus thickness in the previous paragraph, it has been shown that all of the UV light from the source used in the photocatalysis experiments, will be almost totally absorbed in the surface layer of catalyst closest to the UV source. Therefore, no bulk gas phase photolytic reaction is expected to take place as no UV irradiation will penetrate into the bulk of the reactor.

9.1 Photocatalysis in a Fluidised Bed System.

The initial work on the photocatalysis reactions involving NO and NO_2 were due to take place in a fluidised bed reactor, therefore experimental work was undertaken at these conditions.

Several experiments involving NO_2 in bulk N_2 and NO in bulk N_2 showed no evidence of any reaction at or above the minimum fluidisation velocity for Degussa P-25, approximately 0.21 m/s (Table 7.4). Also it should be noted that no photolysis was seen either at these conditions and this can be explained by examination of Figure 8.13. It was therefore evident that the residence times allowed in the fluidised bed system did not give enough time for the photocatalysis reactions to take place with the set-up used and all of the subsequent experimental work was undertaken in a fixed bed system.

9.2 Nitrogen Dioxide Photocatalysis, in a Fixed Bed Reactor, with Nitrogen as the Bulk Gas.

It was initially decided to look at NO_2 in N_2 as the feed to the photoreactor. A standard consisting of 4000ppm NO_2 in N_2 was used in several experiments and fed to the reactor at the conditions outlined in Table 9.1

Initially, the experiments were conducted in the following way:

Step 1. The reactor was cleaned from the previous run and the catalyst replaced with a weighed amount of new catalyst material.

Step 2. The reactor was connected to the rig set-up (Figure 6.2) and purged with nitrogen gas at a flow below the fluidisation velocity. The reactor was purged until the inlet and outlet gas compositions were the same.

Step 3. The experiment was started at time zero by turning on the UV light source and switching from the nitrogen purge gas to the inlet reaction gas.

Step 4. The gas outlet was sampled at regular intervals, usually every four minutes and analysed; the gas inlet at 60 minute intervals; the temperature every four minutes and the gas flowrate continuously monitored.

Step 5. The experiment was terminated by turning off the reaction gas and UV light source at a time dependant upon the experiment being undertaken and the progress of that experiment.

Miscellaneous operations. On occasion, the operating conditions of the experiment being investigated were modified during the run. Operations such as reducing the flow of inlet gas "Gas Down", turning the inlet gas flow off "Gas Off", turning the UV source off "UV Off" and other operations, are indicated on the individual graphs representing the particular experiments in question.

The main modification to the above operations was that in runs 4C and 5C, when an oxygen purge was used on the catalyst prior to the start of the experiment rather than a nitrogen purge and in runs 6C - 12C both a nitrogen and a nitrogen dioxide purges were undertaken prior to the start of the experiment.

Table 9.1. The "C" Series of Experiments, NO_2 Photocatalysis with N_2 as the bulk gas.

Run Number and Figure Number.	Conditions
1C - 9.1	NO_2(200ml/min) + UV + N_2 purge +TiO_2(10.53g) + water saturator
2C - 9.2	NO_2(270 & 200ml/min) + UV + N_2 purge + TiO_2(11.2g)
3C - 9.3	NO_2(200,80 & 35ml/min) + UV + N_2 purge + TiO_2(10.62g)
4C - 9.4	NO_2(35ml/min) + UV + O_2 purge + TiO_2(10.87g)
5C - 9.5	NO_2(67ml/min) + UV + O_2 purge + TiO_2(10.91g)
6C - 9.6	NO_2(45ml/min) + UV + N_2 & NO_2 purges + TiO_2(10.5g)
7C - 9.7	NO_2(45ml/min) + UV + N_2 & NO_2 purges + TiO_2(10.64g)
8C - 9.8	NO_2(45ml/min) + UV + N_2 & NO_2 purges + TiO_2(11.02g)
9C - 9.9	NO_2(50ml/min) + UV + N_2 & NO_2 purges + TiO_2(10.69g)
10C - 9.10	NO_2(30ml/min) + UV + N_2 & NO_2 purges + TiO_2(10.41g)
11C - 9.11	NO_2(80ml/min) + UV + N_2 & NO_2 purges + TiO_2(10.58g)
12C - No Figure	NO_2(25ml/min) + UV + N_2 & NO_2 purges + TiO_2(10.58g), Run Aborted

The main point to note from the "C" Series of experiments is that nitrous oxide and ozone are produced from the reaction of NO_2 on the surface of a titanium dioxide catalyst under UV irradiation, under certain experimental conditions. The effect of numerous reactor operating parameters are detailed in the following sections:-

9.21 Effect of a Water Saturator.

Run 1C was undertaken with a water saturator in the feed line to the reactor. This was done to make the inlet gas more representative of the typical discharge levels from a nitric acid production plant as outlined in Table 1.1. The main problem with introducing water to the feed gas was that the catalyst retained a significant amount of water and the whole reactor system became damp and eventually water logged. It was therefore decided to omit the water saturator from the system and only have the water initially in the NO_2 standard, which was not entirely dry, in the feed to the photocatalytic reactor. In any case, it was seen in later experiments, when they are compared with the results of experiment 1C, that the presence of water up to the dew point of the gas, does not appear to affect the photocatalytic reaction of NO_2.

9.22 Effect of the Composition of the Initial Purge Gas.

The start up procedure for the experiments as outlined in Section 9.2 was modified in several ways during the "C" Series of experiments. Initially (Runs 1 - 3C), the start up procedure was undertaken as outlined, with the reactor being purged with N_2 and at time zero the NO_2/N_2 mixture was introduced to the reactor. In Runs 4C and 5C, N_2 was replaced with O_2 as the purge gas and again the NO_2/N_2 mixture introduced at time zero.

In subsequent Runs, 6 - 13C, the reactor was purged with N_2 and then with the NO_2/N_2 mixture, resulting in the NO_2/N_2 mixture being fully present in the reactor at time zero.

In the cases where N_2 or O_2 was the initial purge gas (Fig's 9.1 - 9.5), it can be seen that O_3 is seen in the reactor outlet before any N_2O is detected. This is thought to be due to the presence of residual O_2 in the reactor at the start of the experiment, in the case of an O_2 purge then obviously there will be residual O_2 present in the reactor at time zero. However, it should be noted that with an N_2 purge, residual O_2 is still present due to the presence of O_2 contamination in the N_2 bulk, at about 0.1%, much less than for pure O_2 but still significant. The residual O_2 present in the reactor combines with the O molecules produced in the reaction to form O_3 (See Section 9.27) and this reaction is enhanced due to the presence of the O_2.

In the case where NO_2/N_2 was the final gas purge at time zero (Fig's 9.6 - 9.11), it can be seen that in the experiments where both N_2O and O_3 were formed, that the N_2O was always seen in the outlet from the reactor before the O_3. The reaction of the O molecules to give O_3 is greatly reduced due to the absence of the residual O_2 as compared with Figures 9.1 - 9.5, and therefore the O_3 is produced by the reaction of three O molecules (See Section 9.27). The reaction of the three O atoms results in an increase in the time by which the O_3 is detected in the outlet from the reactor to a time after the N_2O is detected in the outlet.

In addition to the change in the order of appearance of O_3 and N_2O from the reactor outlet, there is another significant observation to be noted from the examination of the effect of the purge gas. As shown in Figure 9.12 and discussed in Section 9.23, the effect of increasing the residence time of the reaction gas in the reactor is to increase the amounts of O_3 and N_2O seen in the reactor outlet. If the results examined in Figure 9.12, which are only those for the experiments 6C - 12C, are compared with the experiments 1C

- 5C, where residual oxygen was present, it can be seen that an enhanced production of both O_3 and N_2O occurs when residual O_2 is present over the equivalent experiments where no residual O_2 is present at the same residence times. Therefore, it has been shown that having residual O_2 present in the reactor increases the photocatalytic production of both N_2O and O_3 from NO_2.

9.23 Effect of Flowrate of the Reaction Gas.

In Figure 9.12, a plot of residence time vs. production percentage of N_2O and O_3 with regards to the inlet concentrations, is shown. The experimental data is indicated by the data points and a power curve fit of the data is indicated by the lines. It can be seen from the curve fits, that the production of N_2O and O_3 increases as the residence time in the reactor increases, this is as expected. It should also be noted that the increase in production of N_2O is estimated to reach a plateau at a residence time of about 16 - 20 minutes, whereas the maximum production of O_3 is estimated to peak at a longer residence time of perhaps 25 - 30 minutes. The difference in the maximum conversions and the residence time at which a constant conversion is reached are effects of the reaction pathways in the photocatalytic reaction and these are discussed in Section 9.27.

9.24 Effect of UV-light Irradiation on the Progress of the Reaction.

Several blank experiments were undertaken in which the UV light source was not switched on at time zero and as expected , these experiments showed no change in the gas composition across the reactor as expected. During experiment 5C (Figure 9.5), as part of the experiment, the UV light source was turned off during the reaction and the production of N_2O and O_3 was still monitored. When the UV light source was turned off two significant events can be seen to occur:

(9.241) Production of N_2O still takes place, but it drops off slowly,

(9.242) Production of O_3 drops off, but significantly quicker than the decay in the rate of N_2O production.

The UV light source was then switched on again and two further significant events occurred:

(9.243) The production of N_2O increases slowly back to it's original level,

(9.244) The production of O_3 increases rapidly, also back to it's original level.

These four events, 9.241 - 9.244, indicate that the reaction producing N_2O and O_3 from the NO_2/N_2 inlet gas is a photocatalytic reaction and that it would not take place if UV irradiation was not present. Also, it might be inferred that, due to the relative rates of decay of the production of N_2O and O_3 that the production of O_3 is a faster reaction than the production of the N_2O. The difference in the rates of decay might be due to a difference in the reaction rate constants for the two reactions, or a difference in the length of the reaction pathways, or a difference in the mass transfer mechanics of the two reactions i.e. the rates of desorption of the two gases from the catalyst surface.

The facts presented in this section are examined in 9.27 were the possible reaction pathway is examined and also in Chapter 10.

9.25 Effect of Reactor Cooling and Temperature on the Progress of the Reaction.

It is a commonly known fact in reaction kinetics, that the reaction rate constant for a particular reaction varies with varying temperature in the general form outlined by the Arrhenius Equation:

$$k(T) = A e^{-E/RT} \qquad (9.1)$$

Therefore, a test to determine whether the photocatalytic reaction of NO_2 on TiO_2 was temperature dependant was undertaken. Figure 9.13 shows the effect of cooling the reactor in Experiment 6C, by using a purge of nitrogen gas passed over the UV light in the inner annulus of the reactor.

The temperature of the inner annulus of the reactor at time 120 minutes was ~102°C. Then the reactor cooling was turned on and the temperature fell to ~35°C by 126 minutes. The temperature stayed at ~35°C until 160 minutes at which time the reactor cooling was turned off. The temperature then increased from ~35°C to ~100°C by 190 minutes into the experiment.

The effect on the production of N_2O and O_3 due to the temperature changes detailed in the previous paragraph were as detailed as follows:- (i) At the temperature of ~102°C at a time before 120 minutes, the production of N_2O was ~600 area units and O_3 ~400 area units; (ii) between 120 and 140 minutes, when the reactor temperature decreased from ~102 - 35°C, the values for both N_2O and O_3 reduced to ~180 area units; (iii) At 140 minutes the gas flow to the reactor was turned off, such that if any N_2O or O_3 was formed in the reactor then it would remain there and be detected more easily; (iv) at 150 minutes the gas feed to the reactor was turned back on, in order to flush out any N_2O or O_3, however, samples taken between 150 and 160 minutes showed no indication of any formation of N_2O or O_3; (v) at 160 minutes the reactor cooling was turned off and the reactor temperature increased and by 168 minutes production of N_2O had restarted, production of O_3 restarting by 176 minutes. It should be noted however, that the rate of increase of O_3 was greater than the rate for N_2O when the reactor cooling was turned off and the temperature of the reactor increased back to it's initial level.

These observations show that a significant temperature dependence of the photocatalytic reaction of NO_2 exists, however, due to the practical problems of keeping the 8 watt reactor at a constant temperature, it was not possible to determine the magnitude of the temperature effect.

An additional factor to consider is the temperature of the reactor at the time the first O_3 is seen in the outlet from the reactor. By reference to Table 9.2, it can be seen that the temperature of first detection of O_3 various greatly, even between experiments of almost identical operating parameters, shown by reference to experiments 6C - 8C. These observations further underline the great variability of the NO_2/N_2 photocatalytic system in terms of the repeatability of the experiments as outlined next in Section 9.26

9.26 General Comments on the Repeatability of the NO_2 Photocatalytic Reactions.

Examination of the average values for N_2O and O_3 production in experiments 6C, 7C and 8C give an indication of the difficulties of repeating experiments in the NO_2/N_2 system. N_2O production varied from 10 vol% to 0 vol% to 0 vol% over three experiments at the same experimental conditions and the production of O_3 varied from 10 vol% to 19.2 vol% to 0 vol% over the same conditions. Even taking into consideration the experimental error involved in the analysis of the gas concentrations, as outlined in Chapter 7, i.e. +/- 7%, this does not fully account for the differences seen in Experiments 6 - 8C. In any case, it would not be expected that no reaction at all was observed, as was the case in Experiment 8C. It should therefore be noted that the experimental work on the NO_2/N_2 system is qualitative in nature rather than quantitative.

However, it should be noted that if we look at the sum of N_2O and O_3 production, results given in Table 9.2, for experiments 6C - 11C then there is some consistency in this parameter. Except for experiment 8C where, as discussed previously, there was no reaction evident, the sum of N_2O and O_3 production is fairly consistent when compared with the residence time of the reaction gas in the reactor. It is unclear as to the reason for this, since the production of N_2O and O_3 are different reactions, i.e. reduction and oxidation respectively, however, it may be due to the two reactions occurring on different sites on the

catalyst. Therefore, the same amount of catalyst surface maybe available but the split of reduction and oxidation sites may vary from catalyst batch to catalyst batch.

The reasons behind the poor repeatability of the NO_2/N_2 system are unknown as the experimental procedure was consistently adhered to and did not vary enough to account for the large differences seen in the experimental results.

9.27 Postulated Mechanism for the Photocatalytic Destruction of NO_2.

From the experimental observations noted in this set of work and literature information outlined in Chapter 5, an examination of the potential reaction mechanism has been undertaken.

From the experimental observations in Section 9.2, the following general, unbalanced reaction was observed:

$$NO_2 \text{ ----------> } N_2O + O_3$$

This reaction is postulated to take place via several intermediates, the reactions being:

9.271 The adsorption of the NO_2 gas onto the catalyst surface:

$$NO_2(g) \xrightarrow{TiO_2} NO_2(ads)$$

The generally accepted theory in photocatalytic reactions is that the reactions taking place do so on the surface of the catalyst and do not propagate into the bulk gas or liquid phase (95). Therefore, the assumption that the reaction involves the adsorption of a gaseous molecule onto the catalyst surface is valid and the adsorption of NO_2 onto the catalysts surface is confirmed in literature (96)

The assumption that the catalyst reaction is a surface phenomenon was not examined for the NO_2/N_2 system due to the inconsistency of the results. However, this theory is examined for the NO/He system later in this chapter.

9.272 The activation of the adsorbed NO_2 gas:

$$NO_2(ads) + hv \xrightarrow{TiO_2} NO_2(ads)^*$$

The energy for the reaction is supplied via the photons of UV light interacting with the catalyst surface, as outlined in Chapter 2 and Chapter 5. This interaction will, most likely, lead to a charged intermediate by reaction of an electron or hole leading to an NO_2 molecule with either a positive or negative charge. A decision as to whether the adsorbed intermediate is positively or negatively charged is not possible from the experimental work undertaken in this thesis and no literature work is available to support step 9.272. However, other work (3, 5, 7, 9, 39) has shown that charged intermediates of NO and N_2O are formed in photocatalytic reactions by the formation of negatively charged intermediates, therefore, it might follow that the intermediate formed in the case of NO_2 is $NO_2^-(ads)$, however, the confirmation of this hypothesis is beyond the scope of this thesis.

9.273 The dissociation of the excited intermediate to products:

$$NO_2(ads)^* \longrightarrow NO(ads) + O(ads)^*$$

The presence of O_3 in the outlet from the reactor indicates that it is produced in the reaction mechanism. The presence of O_2 in the initial reactor purge, in Experiments 4C and 5C, showed an enhancement in the amount of O_3 exiting the reactor. As show in Section 9.277 of this chapter, the formation of O_3 may occur from the interaction of O

with themselves or with O_2 molecules. The possible reactions outlined in 9.277 are only possible if O atoms are formed, and the production of O atoms by the reactions outlined in this section therefore seems appropriate.

It should also be noted, that if the NO_2(ads)* species has a negative charge, as suggested in Section 9.272, then O atoms produced by the reaction outlined in this section would therefore have a negative charge. The postulation of O atoms being negative charge carriers has also been put forward in literature papers (5, 39) and is therefore a reasonably sound proposition.

When the formation of NO(ads) is considered, direct experimental confirmation was not available due to the inability of the available analytical equipment to determine if NO(g) was present or not. However, the presence of N_2O as a reaction product, from the reaction outlined in Section 9.277 and supported by literature work (3, 39) suggests that the reaction outlined in this section is broadly valid.

9.274 The release of the NO(ads) from the catalyst surface or the further reaction of the NO(ads):

$$NO(ads) \longrightarrow NO(g) \qquad \text{or} \qquad NO(ads) + h\nu \xrightarrow{TiO_2} NO(ads)^*$$

As noted in Section 9.273, the direct determination of NO(g) was not possible due to the appropriate analytical equipment not being available, however, information put forward by S. White (96), indicates that NO(g) is formed in the photocatalytic reaction of NO_2 on TiO_2.

9.275 The dissociation of the excited intermediates to further products:

$$NO(ads)^* \longrightarrow N(ads)^* + O(ads)$$

or NO(ads)* ---------> O(ads)* + N(ads)

Direct analysis for O and N atoms was not possible, however, the further products from the reactions outlined in this section were. The further interaction of N and O atoms with other molecules, as outlined in Section 9.277, would appear to indicate that the reactions outlined in this section as feasible.

The reactions outlined in this section are also supported by other literature work (3, 5, 39), indicating the formation of N and O atoms in the photocatalytic reactions of NOx on TiO_2.

9.276 The interaction of adsorbed atoms to form gaseous molecular products:

$2N(ads) \text{ ---------> } N_2(ads) \text{ ---------> } N_2(g)$

$2O(ads) \text{ ---------> } O_2(ads) \text{ ---------> } O_2(g)$

During the "C" Series of experiments, $N_2(g)$ and $O_2(g)$ were not detected in the outlet from the reactor. The main factors responsible for not being able to detect the gases were the unavailability of the correct analysis equipment and the fact that, in the case of $N_2(g)$, the gas was already present in a large excess (99.6%) in the inlet feed to the reactor. Any $N_2(g)$ formed from the NO_2 in the reactor feed (0.4%) would therefore have been swamped by the bulk gas phase and made any photocatalytically formed $N_2(g)$ undetectable. The inability to detect any changes in the N_2 content of the outlet gas, compared with the inlet gas, when a N_2 bulk gas was used, was one of the main reasons for undertaking further work on the NO_2 system with helium as the bulk gas. It was hoped that having no great excess of N_2 present in the reactor inlet feed would make it possible to detect photocatalytically produced $N_2(g)$ in the reactor outlet.

9.277 The further interaction of adsorbed surface atoms with adsorbed surface molecules:

$N(ads)^* + NO(ads) \text{ ---------> } N_2O(ads)^*$

and

$O(ads)^* + O_2(ads) \text{ ---------> } O_3(ads)^*$

The formation of N_2O via the reaction outlined in this section is postulated by another author in literature (39). The detection of N_2O in the outlet gas was definite and the interaction of a molecule of NO with an adsorbed N atom seems a possible method.

Formation of O_3 can be from either $O_2(ads)$ on the surface of the catalyst as a result of $O_2(g)$ in the bulk phase or from $O_2(ads)$ photocatalytically formed on the surface of the catalyst as outlined in Section 9.276.

9.278 The desorption of adsorbed products:

$N_2O(ads)^* \text{ --------> } N_2O(g) + \text{energy}$

and

$O_3(ads)^* \text{ ---------> } O_3(g) + \text{energy}$

The desorption of N_2O and O_3 was evident, due to the presence of these gases in the outlet from the reactor.

Table 9.28 Summery Table for Photocatalytic Reaction of Nitrogen Dioxide with Nitrogen as the Bulk Gas.

Reaction Step	Literature Suggests	Experimental Comment
9.271 $NO_2(g)$ -----> $NO_2(ads)$	Surface based reaction	Not confirmed in this work
9.272 $NO_2(ads)$ + hv ----> $NO_2(ads)^*$	Literature does not address the nature of the intermediate species	Beyond the scope of this work to confirm this fact
9.273 $NO_2(ads)^*$ ---------> NO(ads) + O(ads)*	Production of NO as an intermediate suggested by literature. Literature suggests the production of $O(ads)^-$ species	Independent analysis of NO not possible. Evidence of O_3 seen as a confirmation of $O(ads)^-$ intermediate
9.274 NO(ads) -----> NO(g) or NO(ads) + hv --> NO(ads)*	Production of NO seen in literature. Production of NO(ads)* intermediate suggested	Independent analysis of NO not possible.
9.275 NO(ads)* -----> N(ads)* + O(ads) or NO(ads)* -----> O(ads)* + N(ads)	Literature suggests N and O atoms as intermediates	Conformation of the formation of N and O atoms beyond the scope of this work, however, formation of N_2O and O_3 suggests their formation

9.276 $2N(ads) \rightarrow N_2(ads) \rightarrow N_2(g)$ $2O(ads) \rightarrow O_2(ads) \rightarrow O_2(g)$	Literature shows the formation of N_2 and O_2	N_2 production masked by N_2 bulk gas. O_2 production masked by O_2 contamination in N_2 bulk gas.
9.277 $N(ads)^* + NO(ads) \rightarrow N_2O(ads)^*$ $O(ads)^* + O_2(ads) \rightarrow O_3(ads)^*$	Literature suggests this pathway	Experimental confirmation of activated intermediates not possible, but de-activated molecules detected experimentally
9.278 $N_2O(ads)^* \rightarrow N_2O(g) +$ energy $O_3(ads)^* \rightarrow O_3(g) +$ energy	Literature suggests these products	Experimental data confirms the production of these products

Table 9.2. A Summery of Data from the "C" Series of Experiments, NO_2 Photocatalysis with N_2 as the Bulk Gas.

Run Number and purges	Flowrate (ml/min)	Max N_2O (% of inlet)/average	Max O_3 (% of inlet/average	Sum of av N_2O and av O_3	Temp of 1st O_3 Production (^oC)
1C - N_2	200 & zero	0.0/0.0 17.0/0.0	9.0/9.0 80.0/9.0	9 9	n/a
2C - N_2	270 & 200	0.0/0.0 6.5/0.0	3.5/1.9 6.9/5.8	1.9 5.8	n/a
3C - N_2	220 & 33 & 14	2.1/1.0 6.7/4.2 21+/21+	2.5/1.2 8.3/6.3 18+/18+	2.2 10.5 39+	n/a
4C - O_2	14	38.9/7.4	57.4/24.6	32.0	n/a
5C - O_2	28	10.9/5.0	14.3/11.3	16.3	n/a
6C - N_2 & NO_2	18	20.0/10.0	20.0/10.0	20	102
7C - N_2 & NO_2	18	0.0/0.0	57.7/19.2	19.2	37
8C - N_2 & NO_2	18	0.0/0.0	0.0/0.0	0	n/a
9C - N_2 & NO_2	21	20.7/6.2	31.0/10.3	16.5	48
10C - N_2 & NO_2	12	16.1/10.0	17.9/15.0	25	69
11C - N_2 & NO_2	34	12.1/6.9	13.8/6.9	13.8	64
12C - N_2 & NO_2	Aborted				n/a

9.3 Nitric Oxide Photocatalysis, in a Fixed Bed Reactor, with Nitrogen as the Bulk Gas.

As outlined in Section 9.2, it was not possible to assess whether the photocatalytic reaction of NO_2 went any further than the production of N_2O and O_3 due to the presence of the bulk nitrogen in the inlet gas. It should also be noted, that the postulated mechanism of NO_2 photocatalysis showed the production of NO as an intermediate in the reaction and the subsequent production of N_2O and O_3 as a result. Due to these facts, it was decided not to undertake experiments with nitric oxide in bulk nitrogen, as any nitrogen produced in the reaction would still not be detectable and the same questions concerning the reaction mechanism would remain.

9.4 Nitrogen Dioxide Photocatalysis, in a Fixed Bed Reactor, with Helium as the Bulk Gas.

Due to the inability to detect any small traces of nitrogen produced in the photocatalysis experiments with nitrogen as a bulk gas as noted in Sections 9.2 and 9.3, it was decided to use helium as an alternative bulk gas.

The choice of helium as a bulk gas was for two main reasons; (i) Helium is a common carrier gas in gas chromatography, therefore if it was used as the bulk gas it would not interfere with the detection of any gases formed in the reaction and (ii) Helium is generally considered as a non-adsorbing gas at atmospheric conditions and was therefore not expected to compete with the NOx for adsorption sites on the catalyst surface. This observation is noted from surface area measurement techniques, such as the classic Brunauer, Emmett and Teller method (BET Method), outlined in Chapter 7.

A new reactor gas feed of 4000vppm NO_2 in helium was therefore purchased and used in further experiments. The experiments carried out are outlined below in Table 9.3.

Table 9.3. The "F" Series of Experiments, NO_2 Photocatalysis with He as the bulk gas.

Run Number and Figure Number.	Conditions
1F - 9.18	NO_2(17ml/min) + UV + He & NO_2 purges + TiO_2(10.62g) Bed height=180mm
2F - 9.19	NO_2(30ml/min) + UV + He & NO_2 purges + TiO_2(10.60g) Bed height=200mm
3F - 9.20	NO_2(18ml/min) + UV + He & NO2 purges + TiO2(10.90g) Bed height=200mm
4F - 9.21	NO2(200 & 100ml/min) + UV(250W) + He & NO_2 purges + TiO_2(10.09g) Bed height=180mm, Water Bath=22^oC
5F - 9.22	NO_2(52 & 30ml/min) + UV(250W) + He & NO_2 purges + TiO_2(10.06g) Bed height=180mm, Water Bath=22^oC
6F - 9.23	NO_2(30ml/min) + UV(250W) + He & NO_2 purges + TiO_2(9.98g) Bed height=180mm, Water Bath=43^oC
7F - 9.24	NO_2(30ml/min) + UV(250W) + He & NO_2 purges + TiO_2(10.03g) Bed height=185mm, Water Bath=45 & 65^oC
8F - 9.25	NO_2(30ml/min) + UV(250W) + He & NO_2 purges + TiO_2(10.05g) Bed height=180mm, Water Bath=40 & 60^oC
9F - No Figure	NO_2(38ml/min) + UV(250W) + He & NO_2 purges + TiO_2(9.94g) Bed height=175mm, Water Bath=45^oC, RUN ABORTED.

The main points to note from the "F" Series of experiments are; that ozone was seen to be produced from the reaction of NO_2 on the surface of a titanium dioxide catalyst

under UV irradiation, under certain experimental conditions; and that nitrous oxide (N_2O) was not seen to be produced from the reaction of NO_2, which is different from the experimental observations outlined in section 9.2. The only significant change in the experimental set-up between in the experiments in section 9.2 and those outlined in this section, is the change in the bulk carrier gas used in the experiments, nitrogen was used in section 9.2 experiments and helium in section 9.4 experiments.

It should also be noted that no N_2 or O_2 was detected in the outlet from the reactor under any of the experimental conditions examined in this section. The explanation for this will be detailed later in Section 9.48.

As in section 9.2, various reactor parameters have been varied and the effect of these are outlined in the following sections:-

9.41 Effect of the Composition of the Initial Purge Gas.

In section 9.2, the initial gas with which the reactor was purged was varied between nitrogen, oxygen and NO_2/N_2 mixtures. In this section no such variation was made due to the fact that the use of any purge gas, other than pure helium before the introduction of the reaction gas, might interfere with the subsequent analysis of the outlet gases from the reactor. For example, if nitrogen or oxygen was used as a purge gas, any residual purge gas would potentially effect the subsequently observed outlet gases from the reactor and since the helium gas in the reaction mixture was specifically introduced in order to allow any N_2 or O_2 produced in the reaction to be analysed, then this would defeat the object of this section. Therefore, the experiments in this section were undertaken as outlined in section 9.201 - 9.205, except that in sections 9.202 and 9.203, the purge gas was helium and not nitrogen.

9.42 Effect of Using Helium as the Bulk Gas.

In section 9.2, nitrogen was used as the bulk gas fed to the photocatalytic reactor, however, this was changed to helium for the reasons outlined previously.

The "F" Series of experiments, shown by Figures 9.18 - 9.25, indicated no significant levels of N_2O production when helium was used as the bulk inlet gas. The experimental conditions; flowrate, catalyst loading, reactor temperature, reactor design etc; used in the "F" Series were the same as those used in the "C" Series, and in the case of UV source power a more powerful source was used in 4F - 9F. Therefore, the only major change in reactor conditions was the use of helium over that of nitrogen and this must have contributed to the dramatic reduction in the production of N_2O in the "F" Series experiments.

The explanation for the reduction in O_3 production is suggested from literature (14) detailed previously in Section 5.131 and shown in Equation 5.3. It is shown that a substance "M" is required to aid in the production of ozone, by absorbing the excess energy released in reaction 5.3. It is detailed in literature that this substance "M" can be the surface of the reactor, water vapour or any inert gas present in the gas stream and obviously the nitrogen present in the gas inlet in the "C" Series could be the substance "M".

It is also suggested that the photocatalytic reactions which produced N_2O in the "C" Series may consist of a step involving the participation of an energy sump or "M" type substance. Again, this is due to the almost complete absence of N_2O production in the "F" Series as compared with the "C" Series. The step involving "M" may be those considered in Section 9.277 or 9.278 for the "C" Series of experiments. "M" could be the energy sump for the energy (or charge) that the N_2O molecule in step 9.278 requires to loose;

$$N_2O(ads)^* \text{ --------> } N_2O(g) + \text{energy}$$

Or, the step in 9.278 may be incorrect and the excess energy present in step 9.277 may be lost at the same time as the formation of the N_2O(ads) as follows:-

$$N(ads)^* + NO(ads) \text{ ---------> } N_2O(ads) + \text{energy}$$

From photocatalytic work done in aqueous solution (Photocatalytic Purification and Treatment of Water and Air. Conference Proceedings 1992) by J Cunningham and M Fox (98) it has been shown that photocatalytic reactions involving hydroxyl radicals take place on the surface of the catalyst and not in the bulk aqueous phase. If we extend this hypothesis to the gas phase work detailed in this thesis, then the substance "M" required for energy transfer would be required to be present on the surface of the catalyst. As outlined previously in Section 9.4, helium is generally recognised as a non-adsorbing gas and would therefore not be present on the catalyst surface and thus not be able to assist in the energy transfer reaction with the excited intermediates. However, nitrogen, as an adsorbing gas, would be present on the catalyst surface in the "C" Series of experiments and would therefore be able to enter into the energy transfer reactions. This is therefore suggested as a possible explanation for the difference in the nature of the photocatalytic reactions seen in the two systems with nitrogen and helium as the bulk reaction gas.

9.43 Effect of Flowrate of the Reaction Gas.

The effect of increasing the flowrate of gas into the reactor is to reduce the amount of ozone seen in the outlet gas (Figures 9.26 and 9.27) and this is the same observation as seen in Section 9.23. This observation is again as expected, the increase in the residence time of the reaction gases in the reactor allowing more of the inlet gas to react and form more ozone. It should be noted that in experiments 2F - 9F, no N_2O formation was observed, however, when the residence time was reduced to the lowest possible that could

be measured with the available equipment (a residence time of approximately 9 minutes), traces of N_2O were observed. The detection of the presence of N_2O suggests that the same reactions as in Section 9.2 were taking place but at a much reduced level in the "F" Series.

It should be noted that the change from an 8 watt light source, which was used in 1F - 3F, to a 250 watt light source, used in 4F - 9F, changed the total amount of O_3 produced at various residence times. The reasons for the change in the amount of O_3 produced at the same residence times is discussed in Section 9.44, however, the same form of relationship exists for the 8 and 250 watt systems, in that an increase in the residence time produces an increase in the total amount of O_3 produced.

9.44 Effect of UV-light Irradiation on the Progress of the Reaction.

Section 9.24 showed that in the NO_2/N_2 system, when the UV source was turned off an immediate reduction in the outlet concentration of O_3 occurred. Similarly, in this section when the UV source was turned off in experiment 6F (Figure 9.23) at 120 minutes, the outlet concentration of O_3 decreased. However, it should be noted that the rate of reduction in O_3 concentration in the two experiments 6F and 5C was not the same. If we express the rate of reduction of O_3 concentration in the outlet as a percentage of the value of O_3 concentration at the time which the UV source was turned off, then the rate of reduction in 6F was 1.4%/min and that for 5C was 5.6%/min.

The different rates of drop off in O_3 production can be partly explained if we consider the difference in the flowrates of the two experiments. Normalising the two experiments to the same flowrate gives values of 1.4%/min and 2.5%/min for 6F and 5C respectively, still leaving however, a significant difference between the two experimental systems. This may well be due to experimental variation, since it has been shown in Section 9.26 that there was a large variation in the experimental results in Section 9.2 as a whole and the variability of the NO_2/He system is discussed in Section 9.47. However,

there may well be an alternative reason for the difference in the rate of drop off of O_3 production between 6F and 5C, that of the percentage coverage of the TiO_2 catalyst.

Nitrogen is an adsorbing gas and as such is used to determine the surface area of catalysts via the BET Method (91), helium however, is a non-adsorbing gas and is used in the same surface area technique (91) specifically for it's non-adsorbing properties. Therefore, in the NO_2/N_2 system of Section 9.2 a competitive adsorption process between NO_2 and N_2 onto the TiO_2 catalyst surface will have been taking place during the experiments, resulting in N_2 being present on some of the sites which could have been used for NO_2 adsorption. In the NO_2/He system however, the helium will not have been competing for the reaction sites with NO_2, thus allowing a much greater coverage of the TiO_2 catalyst by the NO_2. The difference in the surface coverage of NO_2 in the N_2 and He systems could therefore lead to a difference in the total time required to purge the catalyst of the O_3 reaction product. In the case of 6F, the experiment with the higher NO_2 coverage percentage, the O_3 would take a longer time to fully purge off the catalyst than in 5C where the surface coverage was less.

9.45 Effect of UV-light Intensity on the Photocatalytic Reaction of NO_2.

In experiments 1F - 3F an 8 watt black-light-blue was used as the UV source in the reactor and in experiments 4F - 9F a 250 watt medium pressure mercury lamp was used. The relative wavelength output distributions of these two UV sources (97) are shown in Figure 9.28 and 9.29. As can be seen from the wavelength distributions, the amount of useful UV irradiation from the two sources (i.e. those wavelengths below the band gap of TiO_2, approximately <355nm) are approximately 0.56 and 9.0 watts respectfully. It can therefore be seen that the useful UV output power from the 250 watt UV source is almost 16 times that of the 8 watt UV source.

Therefore, if a straight line relationship existed between the intensity of the UV irradiation and the degree of photocatalytic reaction detected, then a significant difference between the levels of O_3 produced in the experiments in the "F" Series would be expected. Upon examining Figures 9.26 and 9.27, showing the results of O_3 production for the 8 and 250 watt systems respectively, it can be seen that an increase in O_3 production is evident, however it is of the order of a 1.5 times not 16 times.

There is obviously no simple relationship between the intensity of the UV irradiation and the degree of photocatalytic reaction detected. However, there is no simple system here, as say in a conventional chemical reaction where first, second, third or similar order kinetic equations can be derived for the reaction w.r.t. a single component in the reaction mechanism. If we consider the UV irradiation as a source of energy, as it obviously is, and compare this to the chemical system where a substance would have a concentration which is similar to the intensity of the UV source. In the chemical system a doubling of the concentration of a substance with first order kinetics would result in a doubling of the reaction products seen. In a photocatalytic system a doubling of the "concentration" or intensity of the UV irradiation in a system with first order reaction kinetics may well produce a less than first order increase in the reaction products seen. This observation in general, and specifically shown in this section, may occur and is in the main due to the geometry of the photocatalytic system and the degree to which the surface of the photocatalyst is activated.

The intensity of the UV irradiation from the source may well be increased by 16 times, but the percentage of the increased UV irradiation that is usefully presented to the photocatalyst may be much less than the 16 times factor. However, in the case of the physical geometry of the 8 and 250 watt reactors, there is little significant physical difference between then as can be seen from Figures 6.2 and 6.5. There is a difference in total reactor length, length of reactor irradiated and the length of the UV arc, however,

these are not sufficient to account for a lack of increase in the photocatalytic reaction seen with the 250 watt system.

We should therefore consider the degree of activation of the photocatalyst surface in the two systems and how much this could be increased by the increase in UV intensity from the 8 to 250 watt systems. It has been shown by other researchers (99) that at low levels of UV intensity, a proportional relationship exists between the intensity of the UV and the degree of photocatalytic reaction detected. This proportional relationship is seen to be only valid however, upto intensities corresponding to one sun or less, i.e. ~35 W/m^2 (99, 100) and at intensities greater than this a square root dependence prevails. This relationship is shown in Figure 9.30 for a hypothetical photocatalytic reaction.

Therefore, how do the 8 and 250 watt reactor systems compare with the "one sun" point on the graph.

The UV intensity for the 8 watt reactor is:-

Intensity = power output/irradiation area

= 0.8 watts / $2\pi rh$

= $0.8 / 2*\pi*1.5*29$

= 29 W/m^2 (i.e. less than one sun)

and for the 250 watt reactor is:-

Intensity = $9.0/2*\pi*2.0*20$

= 360 W/m^2 (approximately 10 times one sun)

Therefore, if we compare the expected degree of reaction for the 8 and 250 watt systems from Figure 9.30 we see that these are 85% and 320%, i.e. the reaction seen in the 250 system, purely considering the intensity relationship should be approximately 3.7 times that of the 8 watt system. The value of 3.7 is closer to the observed increase of 1.5

and is therefore more in line with the predicted theories (99,100), however, it is still significantly different.

A further consideration is the fact that the correlation outline in Figure 9.30 is for a well mixed, aqueous based system. The experimental set-up used in the work outlined in this thesis was undertaken in a gas phase system which, in terms of the catalyst, was very poorly mixed, as the catalyst was in the reactor in the form of a fixed bed.

The fact that the relationship in Figure 9.30 is for an aqueous system rather than a gaseous system should not impact on the relevance of the relationship with respect to the gaseous system. The catalytic reason for the relationship in Figure 9.30 is due to the activation of the catalyst surface. At intensities less than one sun, the UV light is effectively used by the catalyst to generate electron/hole pairs as detailed in Chapter 2, however, at intensities greater than one sun, the increase in the surface density of the electron/hole pairs means that more of the incident UV light produce electron/hole pairs that recombine before reacting further. The recombination of the electron/hole pairs results mainly in the production of heat and is thus a wasteful use of the incident UV energy. Therefore, the relationship outlined in Figure 9.30 is as a result of the properties of the catalyst itself rather than of the system in which the catalyst is, i.e. aqueous or gaseous. However, the hydrodynamics of the system are significant.

In an aqueous system, or a gaseous system where the catalyst forms a fluidised bed, the particles of catalyst are frequently circulated towards and away from the UV source. This allows the particles to become charged when at the closest point to the UV source and then as the particles move into the less well irradiated parts of the system they are still reacting with the reactant mixture, be it an aqueous or gaseous system. In a static, fixed bed system however, the particles have no significant movement, therefore, those closest to the UV source will become highly charged and excess energy will be wasted as heat. Those

particles further from the UV source will not be charged to their full potential and will therefore not be as photocatalytically effective as possible.

The theory detailed in the previous paragraphs would therefore lead to the degree of reaction, as shown in Figure 9.30, being further reduced from the expected value of 3.7 for the difference between the 8 and 250 watt reactors, to a value further approaching that of the 1.5 times experimentally observed.

9.46 Effect of Reactor Cooling and Temperature on the Progress of the Reaction.

It can be seen from Figure 9.31 that the temperature of the photocatalytic reactor again has an effect on the production of O_3, as was shown for the NO_2/N_2 system in Section 9.25. In experiment 2F, the nitrogen cooling gas to the reactor was turned on 62 minutes into the experiment with a resultant drop in reactor temperature from 54 to 35°C being seen over the following 10 minutes. A drop in the outlet concentration of O_3 accompanied this temperature drop until the outlet concentration of O_3 reached zero approximately 21 minutes after the cooling gas was turned on. The subsequent turning off of the cooling gas 92 minutes into the experiment resulted in an increase in the reactor temperature and a corresponding raise in the outlet O_3 concentration.

The observations from experiment 2F again hints towards the Arrhenius nature of the rate constant for the photocatalytic reaction of NO_2 on irradiated TiO_2. Again however, due to the nature of the experimental equipment available for use with the 8 watt photoreactor, it was not possible to control the temperature precisely enough to be able to experimentally determine the rate constants for the Arrhenius relationship.

A common factor in both the "C" and "F" Series of experiments was the production of O_3 from the photocatalytic reaction. Therefore, the temperature of the reactor at the point at which the first O_3 is seen to exit the reactor may be of some use in the analysis of

the Arrhenius relationship. If we examine Table 9.4, this shows that experiments 1F - 3F indicate a temperature of first O_3 production of 31 - 45°C. This compares with results from the "C" Series which indicate O_3 production onset temperatures ranging from 37 - 102°C, however, as previously noted in Section 9.25 the experiments in the "C" Series showed a great variability in the results obtained. It is therefore thought that the temperature indicated by experiments 1F - 3F gives a better indication of the temperatures required for the production of O_3 to take place, i.e. in the range ~30 - 50°C.

Experiments 4F - 9F were undertaken using a 250 watt medium pressure mercury lamp and due to the heat output of this lamp, water cooling of the reactor was required. The detail of the construction of the 250 watt reactor is given in Chapter 6 and shows that the reactor is cooled via a water supply from a thermostatically temperature controlled water bath. Therefore, in experiments 4F - 9F it was possible to further reinforce the assumption outlined in the previous paragraph, in that the temperature range required for O_3 production was ~30 - 50°C. By reference to Table 9.4, it can be seen that the onset temperatures for first O_3 production when using the 250 watt reactor was in the range ~20 - 50°C. This range differs slightly from the range for the 8 watt reactor, however this is not surprising when the increase in UV radiation between the 8 and 250 watt reactors is considered. As outlined in Section 9.45, the increase in intensity between the 8 and 250 watt reactors is of the order of 16 times and as outlined later in Chapter 10, the rate constant for a photocatalytic reaction is also dependent on the photon flux of the system as well as the relationships involved in the standard Arrhenius type relationship. Therefore, the increase in photon flux between the 8 and 250 watt reactors can explain the reduction in the temperature at which the first O_3 production was detected in the 250 watt reactor as compared with the 8 watt system.

9.47 General Comments on the Repeatability of the NO_2 Photocatalytic Reactions.

It has been noted previously in Section 9.26, that photocatalytic reactions on a NO_2/N_2 mixture gave large variations in the results obtained. It is again the case with the NO_2/He system and as detailed previously, the results in Section 9.4 should only be considered as qualitative and not fully quantitative.

9.48 Postulated Mechanism for the Photocatalytic Destruction of NO_2.

The postulated mechanism for the photocatalytic reaction of NO_2/He on TiO_2 is generally the same as that outlined for NO_2/N_2 in Section 9.27. The main suggested difference is as outlined in Section 9.42, where the role of surface adsorbed N_2 is discussed as taking place in the "C" Series of experiments and this effect not taking place in the "F" Series of experiments due to the use of He instead of N_2.

In addition, it was the intention of Section 9.4 to determine if N_2 and O_2 were produced in the photocatalytic reaction of NO_2. As noted previously, the use of He as an alternative to N_2 has resulted in the absence of N_2O production, however the production of O_3 was still seen. This has been attributed to the participation of the N_2 in the absorption of excess energy as outlined in Section 9.42. In addition, due to the absence of N_2 and O_2 in the reactor outlet, the reactions noted in Section 9.276 are obviously absent. Therefore, it would appear that the reactions generating N and O atoms, those outlined in 9.275 are also absent. Therefore, a much reduced reaction pathway would appear to be on going in the NO_2/He system as compared with the NO_2/N_2 system.

Table 9.49. Summery Table for Photocatalytic Reaction of Nitrogen Dioxide with Helium as the Bulk Gas.

Reaction Step	Literature Suggests	Experimental Comment
9.491 $NO_2(g)$ -----> $NO_2(ads)$	Surface based reaction	Not confirmed in this work
9.492 $NO_2(ads)$ + hv ----> $NO_2(ads)$*	Literature does not address the nature of the intermediate species	Beyond the scope of this work to confirm this fact
9.493 $NO_2(ads)$* --------> NO(ads) + O(ads)*	Production of NO as an intermediate suggested by literature. Literature suggests the production of $O(ads)^-$ species	Independent analysis of NO not possible. Evidence of O3 seen as a confirmation of $O(ads)^-$ intermediate
9.494 NO(ads) -----> NO(g) or NO(ads) + hv --> NO(ads)*	Production of NO seen in literature. Production of NO(ads)* intermediate suggested	Independent analysis of NO not possible.
9.495 O(ads)* + $O_2(ads)$ --> $O_3(ads)$*	Literature suggests this pathway	Experimental confirmation of activated intermediates not possible, but de-activated molecules detected experimentally

9.496 $O_3(ads)^*$ ---> $O_3(g)$ + energy	Literature suggests these products	Experimental data confirms the production of this product

Table 9.4. A Summery of Data from the "F" Series of Experiments, NO_2 Photocatalysis with He as the Bulk Gas.

Run Number	Flowrate (ml/min)	Max/average N_2O % of inlet	Max/average O_3 % of inlet	Temp of 1st O_3 Production (^oC)
1F	17	0.013/0.01	0.029/0.029	45
2F	30	none/none	0.019/0.016	45
3F	18	none/none	0.037/0.031	31
4F	200 & 100	none/none none/none	0.011/0.008 0.017/0.014	22
5F	52 & 30	none/none none/none	none/none 0.018/0.015	23
6F	30	none/none	0.14/0.058	42
7F	30	none/none	0.035/0.023	51
8F	30	none/none	0.024/0.013	45
9F	38	Run aborted		

9.5 Nitric Oxide Photocatalysis, in a Fixed Bed Reactor with Helium as the Bulk Gas.

Photocatalytic reactions involving NO/N_2 mixtures were not undertaken for the reasons outlined in Section 9.3. However, photocatalytic experiments involving NO/He mixtures were thought to be of significant value since, as outlined in Sections 9.2 and 9.4, NO was postulated as an intermediate in the photocatalytic reaction of NO_2 with either N_2 or He as the bulk gas, on irradiated TiO_2.

Table 9.5 outlines the "G" Series of experiments carried out on the NO/He system.

Table 9.5. The "G" Series of Experiments, NO Photocatalysis with He as the bulk gas.

Run Number and Figure Number.	Conditions
1G - 9.32	NO(14,26,38&55ml/min) + UV + He & NO purges + TiO_2(10.0g) Bed height=195mm
2G - 9.33	NO(14ml/min) + UV + He & NO purges + TiO_2(10.0g) Bed height=190mm
3G - 9.34	NO(14ml/min) + UV + He & NO purges + TiO_2(4.99g) Bed height=90mm
4G - 9.35	NO(14ml/min) + UV + He & NO purges + TiO_2(7.48g) Bed height=145mm
5G - 9.36	NO(14ml/min) + UV(250W) + He & NO purges + TiO_2(10.01g) Bed height=200mm, Water Bath=40^oC
6G - 9.37	NO(26ml/min) + UV(250W) + He & NO purges + TiO_2(9.96g) Bed height=195mm, Water Bath=40^oC

The main point to note from the "G" Series of experiments is that nitrous oxide and ozone are produced from the reaction of NO on the surface of a titanium dioxide catalyst under UV irradiation, under certain experimental conditions. The effect of numerous reactor operating parameters are detailed in the following sections:-

9.51 Effect of Using Helium as the Bulk Gas.

It was not possible to assess the effect of using helium as compared with nitrogen since, for the reasons outlined in Section 9.3, photocatalytic reactions of NO/N_2 mixtures over TiO_2 were not carried out. However, if the hypothesis outlined in Section 9.27 and 9.48 for the reaction of NO_2 with bulk N_2 or He are valid, then it is postulated that the use of N_2 as a bulk gas would have increased the photocatalytic reaction seen in this section.

9.52 Effect of the Composition of the Initial Purge Gas.

Helium and NO/He purges only, were used in the "G" Series of experiments. This was mainly due to the consideration that using an oxygen purge would result in a change to the inlet gas composition, through the reaction of $NO + ½O_2$ -------> NO_2 which would not allow the actual inlet gas composition to be correctly assessed. Also, if an oxygen or nitrogen purge was used, then it would not be able to accurately assess the photocatalytic production of any oxygen or nitrogen from the reaction of NO.

9.53 Effect of Flowrate of the Reaction Gas.

It can be seen from the results detailed in Figure 9.32, Experiment 1G, there is a variation between the amount of N_2O seen in the outlet from the reactor and the residence time of the reaction gas in the reactor. Figure 9.41 shows the relationship that results from

1G and shows the relationship between N_2O outlet concentration and residence time. The relationship is seen to be approximately of a straight line nature, at least over the residence times covered in 1G. It should be noted again, that the minimum residence time used in 1G, i.e. ~3 mins, is still more than the residence time that would result if the system were run as a fluidised bed. Therefore, it was still not possible to run the photocatalytic system in a fluidised bed set-up, since no appreciable reaction would be detected at the required flowrates.

9.54 Effect of UV-light Irradiation on the Progress of the Reaction.

In previous Sections 9.24 and 9.44, it has been shown that the production of O_3 from NO_2 is photocatalytic in nature. However, it has not yet been shown conclusively as to whether the production of N_2O is fully photocatalytic in nature. In Section 9.24 it was shown that the production of N_2O was photocatalytic in nature, however, due to the fact that no significant N_2O production was detected in Section 9.44, it was not possible to say categorically that the production of N_2O from NO_2 was photocatalytic.

In this section we examine whether the reaction of NO to give N_2O and O_3 is photocatalytic. Considering the previously noted fact that NO is suggested as an intermediate of the photocatalytic reactions of NO_2, then it should be possible to see the photocatalytic production of N_2O and O_3 from NO in greater detail.

If we examine Figure 9.39, experiment 1G, it should be noted that at ~252mins into the experiment, the 8 watt UV source was switched off and the progress of the reaction monitored. It can be seen that over the 15 minutes following the turning off of the UV source, the concentration of both the N_2O and O_3 in the outlet from the reactor both declined sharply. This would seem to indicate that both the N_2O and O_3 are produced as a result of the interaction of the UV irradiation with the TiO_2 photocatalyst. This reinforces the view put forward in Sections 9.27 and 9.48, that NO is an intermediate of the

photocatalytic reaction of NO_2 on TiO_2, as the same products, i.e. N_2O and O_3, are seen from both NO_2 and NO.

9.55 Effect of Reactor Cooling and Temperature on the Progress of the Reaction.

If we examine Figure 9.40 (a detailed examination of part of Figure 9.37) then we can see that at 184 minutes into the reaction, at which point the production of N_2O and O_3 were approximately constant, cooling of the reactor was undertaken. There was then a reduction in the concentration of both N_2O and O_3 in the outlet from the reactor and when the cooling was turned off at 208 minutes into the experiments, the levels of N_2O and O_3 production returned to the constant level. This again indicates that an Arhenius Equation type relationship exists for the photocatalytic reactions of NOx over TiO_2.

9.56 The Effect of Catalyst Bed Height on the Degree of Photocatalytic Reaction.

As outlined later in Section 9.57, the photocatalytic reaction of NO/He over irradiated TiO_2 was seen to be particularly reproducible and it was therefore decided to use this system to determine some additional reactor parameters, as compared with Sections 9.2, 9.3 and 9.4 previously.

A significant consideration in reactor design is, does the reaction take place linearly along the length of the reactor? If this is the case, then it will probable be possible to arrange a set of reactors in series to obtain the required degree of reaction.

A set of experiments was therefore undertaken, 2G - 4G, in which various loadings of the photocatalytic reactor were used. These are detailed specifically in Table 9.6:-

Table 9.6 Effect of Bed Height/Catalyst Mass on the Degree of Photocatalytic Reaction of NO/He Mixtures.

Experiment Number and Figure Number.	Bed Height (mm)	Catalyst Mass (g)	Max N_2O/ Av N_2O
2G - 9.33	190	10.0	675/620
3G - 9.34	90	4.99	480/335
4G - 9.35	145	7.48	515/480

These results are summarised in Figure 9.41, where we can see that there is a straight line relationship between the bed height of the catalyst and the concentration of N_2O in the outlet gas.

It is not possible however, to state a relationship between the bed height of catalyst and the concentration of O_3 in the outlet from the reactor. This is due to the fact that the production of O_3 in the NO/He system is seen to slowly increase over almost the whole of the experimental runs in the "G" Series of experiments. This is a different observation compared to the NO_2/He system, where the O_3 production is fast and will be considered later in Section 9.57

9.57 General Comments on the Repeatability of the NO Photocatalytic Reactions.

In general, the experiments undertaken on the NO/He system were much more repeatable than those undertaken with NO_2/N_2 or NO_2/He. This is illustrated by the fact that the work outlined in Figures 9.38 and 9.41 gave such consistent relationships between the factors considered in the work. This is compared with the work on the NO_2 systems,

outlined in Figures 9.11 - 9.17 and 9.27, where the relationships were far less consistent. An explanation for the more consistent results from the NO system as compared with the NO_2 system may originate from the chemical state of the catalyst surface. It may be that NO adsorbs onto the TiO_2 more consistently than NO_2 and is not as sensitive to changes in the catalyst surface. The presence of trace quantities of impurities in the reactor feed may block the active sites for NO_2 photocatalysis easier than the sites for NO photocatalysis. The validation of this theory is however beyond the scope of this work as a chemical engineering project and would require detailed examination at a pure chemistry level.

9.58 Postulated Mechanism for the Photocatalytic Destruction of NO.

From the experimental observations outlined in this section and from literature information (3,5,7), the following reaction pathway for the photocatalytic reaction of NO on irradiated TiO_2 is presented.

The general equation is of the following form:

$$2NO \text{ ----------> } N_2O + 1/3\ O_3$$

9.581 The adsorption of the NO gas onto the catalyst surface:

$$NO(g) \xrightarrow{TiO_2} NO(ads)$$

As outlined previously in Section 9.271, in literature (95) and in complimentary work at the University of Bradford (96), NO is shown to adsorb onto the surface of a TiO_2 catalyst.

9.582 The interaction of the NO(ads), via the TiO_2 catalyst, with a photon of UV light:

$$NO(ads) + hv \xrightarrow{TiO_2} NO(ads)^-$$

Literature (7,39) has shown that under detailed chemical examination, the species formed on the surface of TiO_2 when adsorbed NO gas is present are NO^- ions.

9.583 Reaction of the $NO(ads)^-$:

$$NO(ads)^- \longrightarrow N(ads)^- + O(g)$$

or $$NO(ads)^- \longrightarrow O(ads)^- + N(g)$$

Due to the potential for oxygen to be a negative charge carrier, the second reaction noted in this section is possibly significant. This theory is also backed up by other literature work (5,39) which indicate the strong potential that oxygen has to be a negative charge carrier in the photocatalytic reaction of NO.

The feasibility of nitrogen to be a negative charge carrier is not known. However, the reactions outlined later in Section 9.586, yielding N_2O would appear to indicate that nitrogen can accept electrons and obtain a negative charge as indicated in this section.

9.584 The interaction of gaseous atoms to form molecular products:

$$2N(ads) \longrightarrow N_2(ads) \longrightarrow N_2(g)$$

$$2O(ads) \longrightarrow O_2(ads) \longrightarrow O_2(g)$$

The independent formation of N_2 and O_2 was again not seen, despite the use of He as the bulk gas, in order to allow the easier detection of these two gases in the outlet from the reactor.

9.585 The further interaction of adsorbed surface atoms with adsorbed surface molecules:

$$N(ads)^- + NO(ads) \text{ ---------> } N_2O(ads)^-$$

and

$$O(ads)^- + O_2(ads) \text{ ---------> } O_3(ads)^-$$

The photocatalytic formation of N_2O has been shown to occur during the experimental work outlined in Section 9.5. Therefore, formation of N_2O must occur from NO via some intermediate reaction. Literature (39) has indicated the possible formation of N_2O from NO via the addition of an adsorbed N atom to an adsorbed NO molecule and this hypothesis is backed up by the experimental observations of this section.

The photocatalytic formation of O_3 from NO has however, never been seen before in reported literature work. This may well be as a result of the detection methods used which, in the main, has been mass spectrometry. O_3 is impossible to detect using standard mass spec. techniques and therefore any O_3 produced would appear to be as a result of O_2 or the fragments from NOx. $O_3(g)$ was detected in the work outlined in this thesis as shown previously and its photocatalytic formation via adsorbed oxygen seems a possible route.

9.586 The desorption of adsorbed products:

$$N_2O(ads)^- \text{ --------> } N_2O(g) + \text{energy}$$

and

$O_3(ads)^-$ ---------> $O_3(g)$ + energy

The detection of the formation of N_2O and O_3 shows that they are photocatalytically produced from the reaction of NO.

9.59 Summery Table for Photocatalytic Reaction of Nitric Oxide with Helium as the Bulk Gas.

Reaction Step	Literature Suggests	Experimental Comment
9.581 NO(g) ----------> NO(ads)	Literature confirms this reaction	Beyond the scope of this work
9.582 NO(ads) + hv -----> $NO(ads)^-$	Production of $NO(ads)^-$ intermediate suggested	Analysis of $NO(ads)^-$ not possible.
9.583 $NO(ads)^-$ -----> $N(ads)^-$ + O(ads) or $NO(ads)^-$ -----> $O(ads)^-$ + N(ads)	Literature suggests N and O atoms as intermediates	Confirmation of the formation of N and O atoms beyond the scope of this work, however, formation of N_2O and O_3 suggests their formation
9.584 2N(ads) ---> $N_2(ads)$ ---> $N_2(g)$ 2O(ads) ---> $O_2(ads)$ ---> $O_2(g)$	Literature shows the formation of N_2 and O_2	Evidence of N_2 and O_2 production not seen.

9.585 $N(ads)^- + NO(ads) \rightarrow N_2O(ads)^-$ $O(ads)^- + O_2(ads) \rightarrow O_3(ads)^-$	Literature suggests this pathway	Experimental confirmation of activated intermediates not possible, but de-activated molecules detected experimentally
9.586 $N_2O(ads)^- \rightarrow N_2O(g) +$ energy $O_3(ads)^- \rightarrow O_3(g) +$ energy	Literature suggests these products	Experimental data confirms the production of these products

Table 9.7. A Summery of Data from the "G" Series of Experiments, NO Photocatalysis with He as the Bulk Gas.

Run Number	Flowrate (ml/min)	Max N2O/ average (ppm)/ initial rate (ppm/min)
1G	14	895/835//70
	26	610
	38	400
	55	240
2G	14	675/620//42
3G	14	480/335//24
4G	14	515/480//22
5G	14	830/650//53
6G	26	1695/1265//212

9.6 Nitric Oxide Photocatalysis, in a Fixed Bed Reactor with Helium as the Bulk Gas: Miscellaneous Experimental Work.

As outlined previously in Section 9.5, a set of experimental work was undertaken to determine some of the primary factors involved in the photocatalytic reaction of an NO/He mixture over TiO_2. Several other sets of experimental work were also undertaken. These were mainly to determine physical rather than chemical parameters of the reaction and are outlined in this section.

9.61 Catalyst Nature.

In the work detailed in Section 9.5, the only catalyst used was Degussa P-25 TiO_2. P-25 is the most commonly used photocatalyst as it is commercially available in large quantities at a relatively cheap cost. However, due to the physical nature of P-25, as detailed in Chapter 4, there are significant operational problems with handling P-25. Therefore, a material called Size Modified Degussa P-25 (SM Degussa P-25) was made as detailed in Chapter 7 and examined in the "H" Series of experiments.

In addition to enhancing the physical properties of P-25, it is also possible to enhance the radiation absorbence band for the catalyst so that light in the visible wavelengths can be used by the photocatalyst. As detailed in literature (13,17) TiO_2 doped with iron has a band gap that is moved slightly into the visible range. The catalyst was prepared as detailed earlier in Chapter 7 and was tested against the other catalysts used in this section.

A further TiO_2 based catalyst, WDB TiO_2 made by SCM Chemicals, had been shown to give better degradation results, in the aqueous phase, than Degussa P-25. This was shown by work undertaken by others at the University of Bath and is not published information. However, it was therefore decided to test this material to compare it with Degussa P-25 also.

As a baseline experiment by which to compare the performance of the various catalysts, I have used experiment 1G as shown in Figure 9.32.

Table 9.8. The "H" Series of Experiments, NO Photocatalysis with He as the bulk gas.

Run Number and Figure Number.	Conditions
1H - 9.42	NO(26ml/min) + UV + He & NO purges + ½ a/o Fe^{3+} on TiO_2 P-25 (105.6g) Particle size 150 - 250 μm. Bed height=208mm
2H - 9.43	NO(26ml/min) + UV + He & NO purges + WDB TiO_2 from SCM(10.0g) Bed height=200mm
3H - 9.44	NO(26ml/min) + UV + He & NO purges + TiO_2-modified (87.86g) 150-250μm Bed height=200mm
4H - 9.45	NO(26ml/min) + UV + He & NO purges + TiO_2-modified (83.65g) 75-150μm Bed height=205mm
5H - 9.46	NO(26ml/min) + UV + He & NO purges + TiO_2-modified (70.63g) <75μm Bed height=200mm
1G - 9.32 - For comparison	NO(26ml/min) + UV + He & NO purges + TiO_2 (10.0g) Bed height=195mm

9.611 Fe^{3+} Doped Degussa P-25.

As indicated previously in Section 9.61 and in literature (13,17), the doping of TiO_2 with Fe^{3+} results in a change in the band-gap of the photocatalyst. Therefore, Fe^{3+} doped TiO_2 was investigated. If we examine Figure 9.42 and compare this with Figure 9.32 for pure TiO_2, and in addition consult Table 9.9 for the quantitative results we can see the relative performances of the two catalysts.

Qualitatively, it can be seen that both N_2O and O_3 are produced on both of the catalysts, however in significantly different ratios. The main component produced on the P-

25 is N_2O with very little O_3 production being evident. This compares with the slight production of N_2O on the Fe^{3+} doped catalyst, with a comparable production of O_3 being evident.

Quantitatively, it can be seen from Table 9.9 that Fe^{3+} doped catalyst does not compare well with P-25 either from a production per unit mass or per unit surface area, P-25 being ~60 and ~61 times better than Fe^{3+} doped catalyst respectively.

9.612 SCM WDB TiO_2.

As indicated in Section 9.61, SCM WDB TiO_2 had been identified by the Photocatalysis Research Group at the University of Bath as a superior catalyst to P-25 for aqueous based photocatalysis. It was therefore decided to compare it's performance against P-25 for gaseous applications also.

Qualitatively, both N_2O and O_3 were seen to be produced from the SCM TiO_2 (Figure 9.43) as was the case with the P-25 catalyst, therefore, the same photocatalytic reaction was seen to take place in both systems. However, as was seen with the Fe^{3+} doped catalyst in Section 9.611 it was seen with the SCM TiO_2 that the ratio of production of O_3:N_2O increased. This was due to a reduction in the quantity of N_2O produced and an increase in the relative quantity of O_3 produced.

Quantitatively, it can be seen form Table 9.9 that on a production per unit mass basis, that P-25 performed ~7 times better than the SCM TiO_2. However, due to the low surface area of SCM TiO_2, 6.0 m^2/g, as compared with the surface area of P-25, 53.2 m^2/g, the SCM TiO_2 actually out performs the P-25 by ~1.3 times on a per unit surface area basis.

9.613 Size Modified Degussa P-25 (SM P-25).

As noted previously in Chapter 7, the physical properties of P-25 are such that bulk handling of the power would be difficult, hence the production and examination of SM P-25.

Qualitative comparison of the performance of P-25 and SM P-25 show that both catalysts produce N_2O and O_3 photocatalytically from NO. However, as seen with other catalysts in Sections 9.611 and 9.612, the ratio of O_3:N_2O increased, resulting in a greater production of O_3 than that seen for P-25.

Quantitatively, the production of N_2O on SM P-25 varied with both mass of catalyst present and surface area present in the reactor. The production of N_2O was seen to be greater for the larger size fractions of the SM P-25. However the reasons for this are unclear but may be due to the looser packing of the larger size fractions allowing the UV irradiation to penetrate deeper into the annular bed and hence utilise more of the catalyst.

In comparison with the P-25 TiO_2, the SM P-25 was seen to produce significantly less N_2O, the P-25 being ~14 or ~20 or ~19.5 times more effective than the SM P-25 depending on the particular particle size of the SM P-25 being examined. However, we must consider that even though the surface areas of P-25 and SM P-25 are similar, 53.2 and 51.3 m^2/g respectively, the effective surface area of SM P-25 is significantly lower than this. As outlined in Chapter 7, Section 7.32, it is postulated that a significant percentage of the surface area of SM P-25 is internal to the particle agglomerates, this being backed up by SEM photographs examined in Section 7.8. Therefore, the actual surface area exposed to the UV irradiation and hence available to be photocatalytically activated is significantly less than the 51.3 m^2/g measured as the actual surface area. Thus, due to the internal surface area not being photocatalytically activated, the observed production of N_2O was seen to be significantly less.

Table 9.9 A Summery of Data from the "H" Series of Experiments, NO Photocatalysis with He as the Bulk Gas.

Run Number	Flowrate (ml/min)	Max N_2O/ average (ppm)/ initial rate (ppm/min)	Average N_2O Production (ppm) per 1000m^2 of Catalyst Surface	Average N_2O Production (ppm) per 100g of Catalyst
1H - Fe	26	200/100//11	18.7	95
2H - SCM	26	130/90//12	1500	900
3H - SM	26	570/360//37	83.6	429
4H - SM	26	370/245//29	57.1	293
5H - SM	26	375/215//31	59.2	304
1G - For comparison	26	--/610/--	1150	6100

9.62 Concentration Dependence of the Photocatalytic Reaction.

To aid in the determination of the rate limiting step of the photocatalytic reaction of NO over irradiated TiO_2, detailed later in Chapter 10, the "J" Series of experiments was undertaken. The "J" Series involved running an NO photocatalysis experiment at four different concentrations and determining the initial rate of N_2O production in the first few minutes of the experiment, after the switching on of the UV source. From this initial rate data, it will be shown in Chapter 10, how the rate limiting step for the reaction can be determined.

If we examine Figures 9.47 - 9.50, we can see that the four experiments were run at 25, 50, 75 and 100% concentration, this corresponded to approximately 1000, 2000, 3000 and 4000ppm NO in bulk helium as the inlet gas to the reactor. In all four experiments, it can be seen that the photocatalysis of NO produced N_2O and O_3 as expected and also that the 100% experiment produced a higher level of outlet concentration of N_2O than the other experiments as expected.

If we measure the initial rate of N_2O production for the four experiments we obtain the data presented in Table 9.10

Table 9.10 A Summery of Data from the "J" Series of Experiments, NO Photocatalysis with He as the Bulk Gas.

Run Number and Figure Number	Conditions	Initial Rate of N_2O Production (ppm/min)
1J - 9.47	NO(26ml/min) + UV + He & NO purges + TiO_2 (9.91g) Bed height=190mm	12.3
2J - 9.48	NO(26ml/min) + UV + He & NO purges + TiO_2 (10.06g) Bed height=195mm	15.8
3J - 9.49	NO(26ml/min) + UV + He & NO purges + TiO_2 (9.91g) Bed height=190mm	17.8
4J - 9.50	NO(26ml/min) + UV + He & NO purges + TiO_2 (10.03g) Bed height=192mm	28.6

The results presented in Table 9.10 are shown in Figure 9.51 and 9.52.

Figure 9.51 shows the relationship between the initial rate of photocatalytic production of N_2O from NO versus the concentration of NO. It can be seen from Figure 9.51 that a first order relationship is shown for this reaction with respect to the concentration of NO and thus the following equation can be written:-

$$r_{N2O} = kC_{NO}fn(a,b,c,etc)$$

The items "a,b,c,etc" refer to other parameters that influence the production rate of N_2O, such as; the intensity of UV irradiation, the mass of catalyst in the reactor, the length of the reactor etc. These factors will all be considered in Chapter 10, where the modelling of the photocatalytic reaction of NO is considered.

Figure 9.52 shows a plot of initial reaction rate versus total system pressure. Due to the physical nature of the experimental set-up used in this project, it was not possible to vary the total system pressure. However, the information presented will be used in the determination of the rate-limiting step for the photocatalytic reaction of NO as outlined in Chapter 10

9.7 Conclusions.

The photocatalysis experimental work described in this chapter has shown the following points:-

(a) Photocatalysis reactions of NOx in a fluidised bed reactor system were not observed. It was assumed that this was due, in the main, to the short residence times of the reactant gases in the reactor when flows, large enough to fluidise the catalyst, were used.

For $NO_2 + N_2$ reacting on UV irradiated titanium dioxide:

(b) NO_2 reacts on a UV irradiated TiO_2 catalyst surface to produce N_2O and O_3 in the gas phase. NO is presumably produced but it was not possible to detect any due to the analysis system used.

(c) In a system containing $NO_2 + N_2$ bulk, N_2O was seen in the exit stream from the reactor first, with O_3 seen second. When an oxygen purge was used or residual oxygen was present on the catalyst surface then O_3 was seen first in the reactor exit stream followed by N_2O.

(d) The photocatalytic reaction of NO_2 to give $N_2O + O_3$ was seen to be erratic and depends on the pre-treatment of the catalyst surface, i.e. had the catalyst been purged for significant periods of time and was residual O_2 present on the catalyst surface. It was therefore impossible to give any definite correlations between the degree of reaction and quantitative parameters such as flowrate, bed height, UV intensity etc.

(e) Qualitative results for the photocatalytic reaction of NO_2 show that; an increase in the flowrate of the inlet gases gives a decrease in the degree of photocatalytic reaction seen; the photocatalytic reaction was confirmed as UV-light initiated, since when the UV source was turned off the photocatalytic reaction was seen to stop; a relationship between the temperature of the reactor and the degree of photocatalytic reaction seen was noted.

(f) Postulated reaction mechanisms for the photocatalytic reaction of NO_2 on irradiated titanium dioxide have been suggested.

For $NO + N_2$ reacting on UV irradiated titanium dioxide:

(g) The system of nitric oxide and nitrogen as the inlet gas to a photocatalytic system was not investigated, due to the fact that it would have been impossible to determine if any nitrogen was formed from the NO itself.

For NO_2 + helium reacting on UV irradiated titanium dioxide:

(h) NO_2 reacts on a UV irradiated TiO_2 catalyst surface to produce O_3 in the gas phase when helium was present as the bulk inlet gas. No N_2 or O_2 was detected as outlet gases from the reactor.

(i) When helium was used as the bulk gas with NO_2, it was seen that only O_3 was seen in the outlet from the reactor, as compared with using nitrogen as the bulk gas when both N_2O and O_3 were observed in the reactor outlet.

(j) An increase in inlet gas flowrate resulted in a reduction in the levels of O_3 in the outlet from the reactor.

(k) The reaction of NO_2 on irradiated TiO_2 was shown to be photocatalytic in nature, due to the fact that when the UV source was switched off, the reaction was seen to stop.

(l) Increasing the intensity of the incident UV light used in the reactor in which the photocatalytic reaction of NO_2 + helium was performed, showed that an increase in the outlet concentration of O_3 resulted.

(m) A relationship between the degree of photocatalytic reaction seen at the outlet from the reactor and the temperature of the reactor was seen, however it was not possible to quantify this relationship with the experimental equipment available.

(n) Postulated reaction mechanisms for the reaction of NO_2 + helium on irradiated TiO_2 are presented.

For NO + helium reacting on UV irradiated titanium dioxide:

(o) NO reacts on a UV irradiated TiO_2 catalyst surface to produce N_2O and O_3 in the gas phase.

(p) An increase in the flowrate of the reaction gas into the reactor resulted in a decrease in the degree of photocatalytic reaction observed.

(q) The reaction of NO + helium was shown to photocatalytic due to the fact that upon switching off of the UV light source, the reaction was seen to stop.

(r) The photocatalytic reaction of NO + helium was seen to have a temperature dependence, resulting in an increased temperature leading to an increased degree of photocatalytic reaction being observed.

(s) It was seen that increasing the depth of the photocatalyst bed in the reactor, resulted in a proportional increase in the degree of photocatalytic reaction seen across the reactor.

(t) Postulated mechanisms for the photocatalytic reaction of NO + helium on irradiated TiO_2 were put forward.

For NO + helium reacting on UV irradiated titanium dioxide, miscellaneous experimental work:

(u) An examination of several photocatalytic materials was undertaken. It was determined that Degussa P-25 was the best photocatalyst material from those examined in this work.

(v) The effect of NO concentration in the photocatalytic system, with helium as the bulk gas, was examined. It was seen that a first order relationship between NO concentration and the rate of N_2O production existed.

CHAPTER 10.

10.0 INTRODUCTION.

Primary concerns in chemical engineering are what are the rate limiting factors involved in a chemical reaction and how will the chemistry be scaled-up to a commercial process? This chapter tries to address some of the points that arise in trying to answer these questions.

10.1 Basic Kinetic Principles.

Some of the basic reactions and kinetics of photocatalytic processes, which may be applied to the TiO_2/NO_X system, have been studied. From several papers in literature (8, 12, 48, 50, 54, 65, 92, 95, 96) the following basic approach for modelling the photocatalytic reactor has been agreed upon:-

(i) Reaction Kinetics:- The amount of a selected component, A, being converted or produced per unit time per unit quantity of a reference variable, y, in a chemically reacting system, is defined as the rate of reaction r_A.

$$r_A = \frac{1}{y}\frac{dN_A}{d\theta} \qquad (10.1)$$

For many purposes it is permissible to use a single apparent or overall volumetric rate constant, k, hence giving;

$$r_A = \frac{1}{y}\frac{dN_A}{d\theta} = k\,C_A^n \qquad (10.2)$$

where n is the order of the reaction and C_A is the local bulk concentration of gaseous reactant A. However, in a heterogeneous photocatalytic system several steps are involved in the overall reaction mechanism. Hence an overall rate constant such as that outlined in

Equation 10.2 is not appropriate to this system. The rate equations for the reaction of NO on illuminated titanium dioxide are discussed in more detail later in this chapter.

In addition to having a non-simplistic rate equation, photocatalytic reactions also have the added complication of an added factor dependant on the rate of light photon absorption, Q.

The resultant rate equation for a photocatalytic reaction is therefore of the general form:

$$-r_A = fn(Q)fn(C_A) \qquad (10.3)$$

The light absorption rate is proportional to the light intensity, I_O, in the reactor, which is proportional to the light energy emitted from the UV source, E_O.

$$Q_\lambda = A\frac{I_{o\lambda}q_\lambda}{V_r} \qquad (10.4)$$

Where Q_λ is the light absorption rate at wavelength λ, A is the average area of the reactor, $I_{O\lambda}$ is the light intensity at wavelength λ, V_r is the reactor volume and q_λ is the fraction of light absorbed in the reactor. q_λ is a function of the weight of solids in the reactor, the particle diameter and the hydrodynamics of the system.

Substituting for Q_λ from 10.4 into 10.3, yields an equation of the form;

$$r_A = k\left(A\frac{I_{o\lambda}q_\lambda}{V_r}\right)^m fn(C_A) \qquad (10.5)$$

In order therefore, for us to be able to formulate a basic model for the photocatalytic system, we will initially examine the relationship between the concentration of the substrate and the rate of reaction.

10.2 Rate Limiting Factor for a Catalytic Reaction.

We shall examine the data for the photocatalytic reaction of NO/He on TiO_2, (Section 9.62), since this was the most consistent data available from Chapter 9. It is then possible to write a general reaction pathway as:

$$6NO \text{ ----------> } 3N_2O + O_3 \qquad (10.6)$$

In addition to this general reaction equation, we consider the photocatalytic reaction to take place via the general physical pathway outlined in the following steps A - D.

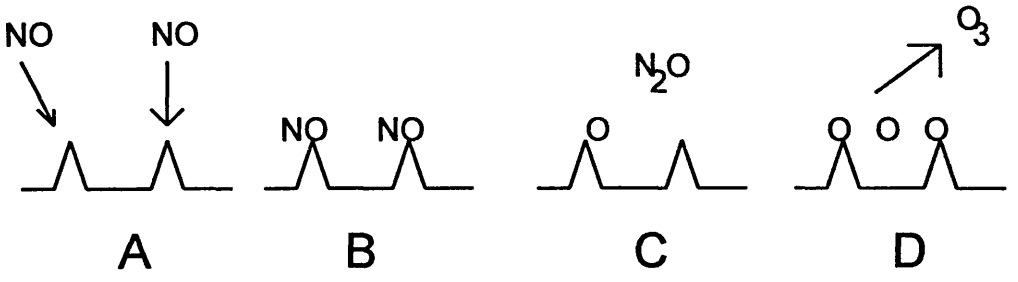

Step A to B shows the adsorption of NO on the surface of the catalyst; step B to C shows the surface reaction of NO to give N_2O (and it's subsequent desorption) and O due to the interaction of the incident UV-light with the catalyst surface; step C to D shows the combination of three O atoms (or equally the combination of an O atom with an O_2 molecule) to give a molecule of O_3;

It should be noted that from the observations in Chapter 9, it seems that the above simplified mechanism is reasonable since the N_2O is seen almost immediately upon commencement of the reaction, whereas O_3 is only seen to appear slowly in the outlet gas stream. Also, the reaction does not take place in the absence of the catalyst material and therefore a surface interaction must be involved as well as a surface reaction.

The reaction sequence can therefore be represented by three basic equations:

$$NO + \text{surface(S)} \underset{k_{-A}}{\overset{k_A}{<\!\!-\!\!-\!\!-\!\!-\!\!-\!\!-\!\!-\!\!-\!\!-\!\!-\!\!>}} NO^*S \qquad (10.7)$$

$$2NO^*S \underset{k_{-S}}{\overset{k_S}{<\!\!-\!\!-\!\!-\!\!-\!\!-\!\!-\!\!-\!\!-\!\!-\!\!-\!\!-\!\!-\!\!-\!\!->}} N_2O + O^*S \qquad (10.8)$$

$$3O^*S \underset{k_{-D}}{\overset{k_D}{<\!\!-\!\!-\!\!-\!\!-\!\!-\!\!-\!\!-\!\!-\!\!-\!\!-\!\!-\!\!-\!\!-\!\!->}} O_3 \qquad (10.9)$$

k_A, k_S and k_D being the rate constants for the forward reactions and k_{-A}, k_{-S} and k_{-D} being the rate constants for the reverse reactions.

From consideration of the data in Sections 9.5 and 9.6, where NO was used with helium as the bulk gas, it can be assumed that helium, being a none adsorbing gas at room temperature and pressure, does not interact with the surface of the catalyst. Therefore, the helium will not occupy any of the reaction sites on the catalyst surface, hence the presence of any inhibitor, helium in this case, to the NO reaction need not be considered.

The rate expression for the adsorption of NO as indicated in (10.7) is:

$$r_{AD} = k_A P_{NO} C_v - k_{-A} C_{NO^*S}$$

$$r_{AD} = k_A \left(P_{NO} C_v - \frac{C_{NO^*S}}{K_A} \right) \qquad (10.10)$$

If r_{AD} has units of mol/g(cat)*sec and C_{NO^*S} has units of mol/g(cat), then typical units of k_A, k_{-A} and K_A would be:

$k_A = (atm^*sec)^{-1}$

$k_{-A} = sec^{-1}$

$K_A = k_A/k_{-A} = atm^{-1}$

The rate law for the surface reaction step producing absorbed O atoms and N_2O in the gas phase by reaction (10.8) gives:

$$r_S = k_S C_{NO*S} - k_{-S} P_{N2O} C_{O*S}$$

$$r_S = k_S \left(C_{NO*S} - \frac{P_{N2O} C_{O*S}}{K_S} \right) \qquad (10.11)$$

with the surface reaction equilibrium constant being $K_S = k_S/k_{-S}$, and typical units being:

$k_S = s^{-1}$

$k_{-S} = (s.atm)^{-1}$

$K_S = atm$

If we consider that N_2O is negligibly adsorbed onto the surface of the catalyst due to its immediate appearance in the outlet gas then $C_{N2O*S} = 0$. Therefore the rate of ozone desorption is given by

$$r_D = k_D C_{O*S} - k_{-D} P_O C_v$$

$$r_D = k_D \left(C_{O*S} - \frac{P_O C_v}{K_D} \right) \qquad (10.12)$$

Typical units are:

$k_D = s^{-1}$

$k_{-D} = (s.atm)^{-1}$

$K_D = atm$

To determine if the general reaction outlined above in (10.6) and the postulated mechanism suggested for that reaction is valid we need to determine the rate-limiting step for the reaction. This is done by assuming that one of the steps in the reaction, i.e. adsorption, surface reaction or desorption, is indeed rate-limiting. By then determining the initial rate equations for the three steps and their variation with the initial system pressure, it will be possible to determine if the assumed mechanism and rate-limiting step are correct.

10.21 Is the Adsorption of NO Rate Limiting?

So, the first question we will ask is, "Is the adsorption of NO rate limiting?"

To answer this question we shall assume that the adsorption of NO is indeed rate limiting, derive the corresponding rate law, and then check to see if it is consistent with experimental observation. By assuming that this (or any other) step is rate limiting, we are considering that the reaction rate constant of this step (in this case k_A) is small with respect to the specific rates of the other steps (in this case k_S and k_D). The rate of adsorption is

$$-r'_{NO} = r_{AD} = k_A\left(P_{NO}C_v - \frac{C_{NO*S}}{K_A}\right) \qquad (10.10)$$

Since we cannot measure either C_V or C_{NO*S}, we must replace these variables in the rate equation with measurable quantities for the equation to be meaningful.

For steady state operation we have

$$-r'_{NO} = r_{AD} = r_S = r_D = r_{N2O} \qquad (10.13)$$

For adsorption limited reactions, k_A is small and k_S and k_D are large. Consequently, the ratios r_S/k_S and r_D/k_D are very small (approximately zero), whereas the ratio r_A/k_A is relatively large. The surface reaction expression is

$$r_S = k_S\left(C_{NO*S} - \frac{C_{O*S}P_{N2O}}{K_S}\right) \qquad (10.14)$$

For adsorption limited reactions the surface specific reaction rate k_S is large by comparison and we can set:

$$\frac{r_S}{k_S} \approx 0$$

and solve equation (10.14) for C_{NO*S}

$$C_{NO*S} = \frac{C_{O*S}\ P_{N2O}}{K_S} \qquad (10.15)$$

To be able to express C_{NO*S} solely in terms of the partial pressures of the species present, we must evaluate C_{O*S}. The rate of desorption is:

$$r_D = k_D\left(C_{O*S} - \frac{P_O C_v}{K_D}\right) \qquad (10.12)$$

However, for adsorption limited reactions, k_D is large by comparison and we can set

$$\frac{r_D}{k_D} \approx 0$$

and then solve equation (10.12) for C_{O*S}:

$$C_{O*S} = \frac{P_O\ C_v}{K_D} \qquad (10.16)$$

After combining equations (10.15) and (10.16), we have

$$C_{NO*S} = \frac{P_O\ P_{N2O}}{K_D\ K_S}\ C_v \qquad (10.17)$$

Replacing C_{C*S} in the rate equation (10.10) by equation (10.17), and then factoring C_V, we obtain

$$r_{AD} = k_A \left(P_{NO} - \frac{P_O \; P_{N2O}}{K_S \; K_D \; K_A} \right) C_v$$
$$= k_A \left(P_{NO} - \frac{P_O \; P_{N2O}}{K_e} \right) C_v \qquad (10.18)$$

Observe that by setting $r_{AD}=0$, the product $K_S K_D K_A$ is simply the overall equilibrium constant K_e for the reaction

$$NO \; <=====> \; N_2O + O$$

$$K_A \; K_S \; K_D = K_e \qquad (10.19)$$

The concentration of vacant sites, C_V, can now be eliminated from equation (10.18) by utilising the equation to give the total concentration of sites, C_t, which is assumed constant:

total sites = vacant sites + occupied sites

From the experimental results and observations seen in Chapter 9, it has been assumed that N_2O is quickly desorbed from the surface of the catalyst material. This observation is based on the fact that in the work with NO/He, N_2O is seen in the outlet from the reactor almost immediately upon start-up of the reaction. Therefore, only NO and O atoms will have any significant adsorption onto the catalyst surface. It should be noted that helium is a non-adsorbing gas at room temperature. Therefore, since only NO and O atoms adsorb on the catalyst surface the concentration of occupied sites is (C_{NO*S} + C_{O*S}), and the total concentration of sites on the catalyst surface is:

$$C_t = C_v + C_{NO*S} + C_{O*S} \qquad (10.20)$$

Substituting equations (10.16) and (10.17) into equation (10.20) we have:

$$C_t = C_v + \frac{P_O \; P_{N2O} \; C_v}{K_D \; K_S} + \frac{P_O \; C_v}{K_D}$$

Solving for C_V, we get

$$C_v = \frac{C_t}{1 + P_O \; P_{N2O}/K_D \; K_S + P_O/K_D} \qquad (10.21)$$

Combining equations (10.21) and (10.18), we find that the rate law for the catalytic decomposition of NO, assuming that the adsorption of NO is the rate-limiting step is:

$$-r'_{NO} = r_{AD} = r_{N2O} = \frac{C_t k_A (P_{NO} - P_O \; P_{N2O}/K_e)}{1 + P_O \; P_{N2O}/K_D \; K_S + P_O/K_D} \qquad (10.22)$$

We now wish to sketch a plot of the initial rate as a function of the total pressure P_{TO}. Initially in a reaction, no products are present, consequently, $P_{N2O} = P_O = 0$. The initial rate is therefore given by:

$$r_{N2O} = C_t k_A P_{NOi} \qquad (10.23)$$

If we let $P_{NO} = y_{NOi} * P_{TO}$, where y_{NOi} is the initial mole fraction of NO present, then:

$$r_{N2O} = C_t k_A y_{NOi} P_{TO} \qquad (10.24)$$

Therefore we can see that $-r'_{NOi}$ = constant * function (P_{TO}) * function (y_{NOi}) and a plot of initial rate vs initial total pressure, for various values of y_{NOi}, would give a graph of the general form:

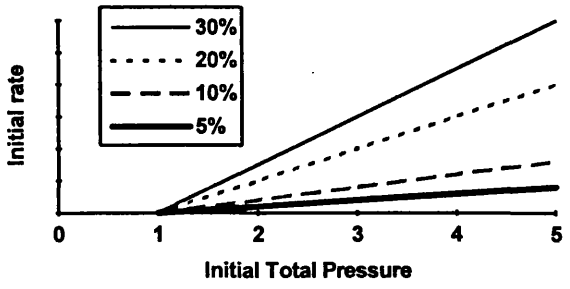

Therefore, if adsorption were the rate limiting step in the photocatalytic reaction of NO/He over TiO_2, then the data obtained would show the above relationship.

Before we examine the initial rate data from Chapter 9, we will determine the relationships for the other potential rate-limiting steps.

10.22 Is the Surface Reaction of NO Rate Limiting?

The rate of surface reaction is represented by:

$$r_S = k_S\left(C_{NO^*S} - \frac{P_{N2O}C_{O^*S}}{K_S}\right) \qquad (10.11)$$

Since we cannot readily measure the concentrations of the adsorbed species, we must utilise the adsorption and desorption steps to eliminate C_{NO^*S} and C_{O^*S} from this equation.

From the adsorption reaction rate expression in equation (10.10) and the condition that k_A is large by comparison when surface reaction is controlling, (i.e. $r_{AD}/k_A \sim 0$), we obtain a relationship for the surface concentration for adsorbed NO :

$$C_{NO^*S} = K_A \; P_{NO} \; C_v$$

In a similar manner, the surface concentration of adsorbed O can be evaluated from the desorption rate expression (10.12) together with the approximation:

$$\text{when } \frac{r_D}{k_D} \approx 0 \quad \text{then } C_{O^*S} = \frac{P_O \; C_v}{K_D}$$

Substituting for C_{O*S} and C_{NO*S} in equation (10.11) gives us:

$$r_S = k_S\left(P_{NO}K_A - \frac{P_O P_{N2O}}{K_D K_S}\right)C_v$$

$$= k_S K_A\left(P_{NO} - \frac{P_O P_{N2O}}{K_e}\right)C_v \qquad (10.25)$$

The only unmeasureable factor left to eliminate from the equation for r_S is C_V. Using equation (10.20):

$$C_t = C_V + C_{O*S} + C_{NO*S} \qquad (10.20)$$

and substituting for concentrations of the adsorbed species, C_{O*S} and C_{NO*S}, and rearranging yields:

$$C_v = \frac{C_t}{1 + P_O/K_D + K_A P_{NO}}$$

letting $K_O=1/K_D$, the final form of the rate law is:

$$-r'_{NO} = r_S = r_{N2O} = \frac{k_S C_t K_A(P_{NO} - P_{N2O}P_O/K_e}{1 + P_O K_O + K_A P_{NO}} \qquad (10.26)$$

For any initial mixture, $P_{N2O} = P_O = 0$ therefore the rate equation simplifies to:

$$r_{N2O} = \frac{k_S C_t K_A y_{NOi} P_{TO}}{1 + K_A y_{NOi} P_{TO}} \qquad (10.27)$$

Therefore, for different percentage mixtures of NO and He, a graph of initial rate vs initial total pressure will show a series of curves as indicated by the following, general form graph:

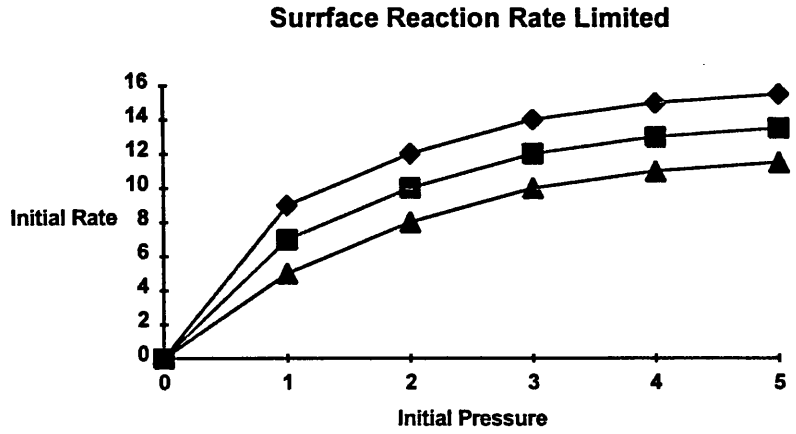

The top curve could be considered to be in the case where yNOi = 1, i.e. pure NO is added to the reactor, and the curves below indicating lower and lower percentages of NO in the feed, hence values of $y_{NOi} < 1$.

10.23 Is the Desorption of N_2O and O_3 Rate Limiting?

Finally, if we consider that the desorption of N_2O and O_3 are rate limiting then the following equations are produced:

The rate expression for the desorption of O is

$$r_D = k_D \left(C_{O^*S} - \frac{P_{O^*S}\ C_v}{K_D} \right) \qquad (10.12)$$

From the rate expression for surface reaction, (10.11), we set $r_S/k_S \sim 0$, to obtain:

$$C_{O^*S} = K_S \left(\frac{C_{NO^*S}}{P_{N2O}} \right) \qquad (10.28)$$

Similarly, for the adsorption step, (10.10), we set $r_{AD}/k_A \sim 0$ to obtain:

$$C_{NO*S} = K_A P_{NO} C_v$$

then substitute for C_{NO*S} in Equation (10.28)

$$C_{O*S} = \frac{K_A K_S P_{NO} C_v}{P_{N2O}} \qquad (10.29)$$

Combining equations (10.12) and (10.29) gives us:

$$r_D = k_D K_A K_S \left(\frac{P_{NO}}{P_{N2O}} - \frac{P_O}{K_e} \right) C_v \qquad (10.30)$$

where K_A and K_S are the adsorption and surface reaction equilibrium constants and K_e is the gas phase equilibrium constant for the reaction. To obtain an expression for C_v, we again perform a site balance:

$$C_t = C_v + C_{O*S} + C_{NO*S}$$

After substituting for the respective surface concentrations, we solve the site balance for C_v:

$$C_v = \frac{C_t}{1 + K_A K_S P_{NO} / P_{N2O} + K_A P_{NO}} \qquad (10.31)$$

Replacing C_v in equation (10.30) by equation (10.31) and multiplying the numerator and denominator by P_{N2O}, we obtain the rate expression for desorption control:

$$-r'_{NO} = r_D = r_{N2O} = \frac{k_D C_t K_S K_A (P_{NO} - P_O P_{N2O} / K_e)}{P_{N2O} + P_{NO} K_A K_S + K_A P_{N2O} P_{NO}} \qquad (10.32)$$

To determine the dependence of the initial rate on total pressure, we again set $P_{N2O} = P_O = 0$, then the initial rate law reduces to:

$$r_{N2O} = k_D C_t \qquad (10.33)$$

This relationship indicates that the initial rate of reaction is only dependent upon the total number of sites on the catalyst particles. Therefore, a mathematical relationship of this nature would lead to a graphical relationship as shown in the following general form graph;

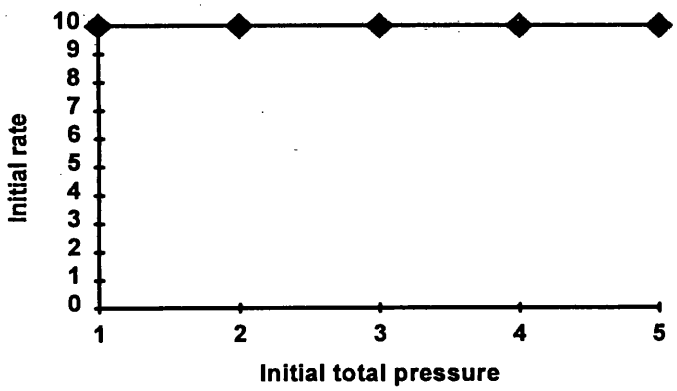

Therefore, if the desorption step were rate controlling, we would see that the initial rate would be independent of the initial pressure and also independent of the gas phase concentration of the NO. Therefore, a variation of the gas phase concentration of the NO would not result in a change in the initial rate for a system at any initial starting pressure.

10.3 Rate Limiting Factor for the Photocatalytic Reaction of NO/He over TiO_2.

From the derivations outlined in Section 10.2, the following three relationships have been determined:

If the adsorption of NO is rate limiting then:

$$r_{N2O} = C_t k_A y_{NOi} P_T \qquad (10.24)$$

If the surface reaction of NO is rate limiting then:

$$r_{N2O} = \frac{k_S C_t K_A y_{NOi} P_{TO}}{1 + K_A y_{NOi} P_{TO}} \qquad (10.27)$$

and if the desorption of N_2O and O_3 is rate limiting then:

$$r_{N2O} = k_D C_t \qquad (10.33)$$

Therefore, by considering the initial rate data in Chapter 9, it can be determined which of these three relationships is the actual rate limiting step. If we consider Figure 9.52, we can see that the initial rate of reaction varies from ~0.7 - 2.85 ppm N_2O/min/(gram catalyst) at a fixed total system pressure of 1 atmosphere, for various values of gas phase NO concentration.

The relationship derived in Section 10.23 indicates that no variation in the initial rate of reaction should be seen if the desorption step in the reaction is rate limiting. Obviously therefore, the desorption of N_2O and O_3 from the catalyst surface, as indicated by the proposed reaction system in Section 10.2, is not rate limiting.

The relationship derived in Section 10.22 indicates that a variation in total pressure, at any set value of y_{NOi}, will result in an exponential increase in the initial rate of reaction for the system, up to a maximum value. Obviously, from the data in Chapter 9, it is not possible to determine directly from Equation 10.27, as to whether the rate data in Figure 9.52 fits this relationship. Therefore, it is not directly possible to determine whether the surface reaction of NO is rate limiting or not.

The relationship derived in Section 10.21 indicates that for a variation in total system pressure, at any set value for y_{NOi}, a straight line relationship for the change in initial rate of reaction will be evident. As noted in the previous paragraph, it is again not possible to determine whether the rate of adsorption, in this case, is or is not, the rate limiting step for the photocatalytic reaction of NO.

The data available in Chapter 9, has suggested that either adsorption or surface reaction, is the rate limiting step in the photocatalytic reaction of NO on irradiated TiO_2. However, it is noted in literature (101) that approximately 75% of all heterogeneous reaction mechanisms are surface reaction limited, rather than adsorption limited. Therefore, it is probable that the photocatalytic reaction of NO on irradiated TiO_2 is surface reaction limited, under the proposed mechanism.

It is not possible to determine from the data in Chapter 9 whether the postulated rate limiting step is correct or not, however, it is possible to further examine the data to give us a further insight to the possible rate limiting step.

If we examine Figure 9.51, we see that a plot of initial reaction rate vs concentration of NO in the inlet gas, shows a possible straight line fit for the data available from 0 - 0.4 volume % concentration. If we then examine equations 10.24 and 10.27, we see that the following two general graphs are produced if simple numerical values for the constants and rate constants in these equations are used and the graphs plotted.

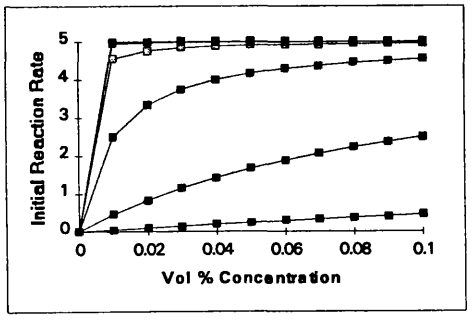

Figure 10.1. Plot of Initial Rate vs Volume % Concentration of NO for a Surface Reaction Rate Limited System.

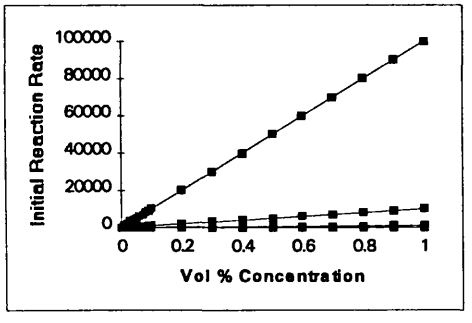

Figure 10.2. Plot of Initial Rate vs Volume % Concentration of NO for an Adsorption Rate Limited System.

In Section 10.21, and Figure 10.2, it has been shown that if the photocatalytic reaction of NO on TiO_2 was adsorption rate limited then a straight line relationship would be seen between the concentration of the NO in the gas phase, y_{NOi} and the initial reaction

rate for the system. If we examine Figure 9.51 then we can see that the experimental data of Chapter 9 indicates that the adsorption step could be the rate limiting factor.

If we then examine Section 10.22, we can see that for the photocatalytic reaction of NO on TiO_2, if the surface reaction was the rate limiting step, then an exponential relationship between the gas phase concentration of the NO and the initial reaction rate would be seen. Therefore, if we consider the experimental data from Chapter 9 shown in Figure 9.51, the straight line relationship seen in this figure would suggest that the surface reaction is not rate limiting, since the relationship is not exponential in nature. However, if we examine Figure 10.2, then we can see that depending on the numerical values for the various rate constants in equation 10.27, a straight line relationship can be seen for the NO/TiO_2 system at low values of y_{NOi}. Therefore, it is possible that the reaction of NO on TiO_2 is surface reaction rate limited.

From the observations made in the previous two paragraphs, it is again impossible to determine whether the photocatalytic reaction of NO on TiO_2 is adsorption or surface reaction rate limited. However, further work at various system pressures, or at a much wider range of y_{NOi} values, would be able to confirm which of these two possible reaction steps is the rate limiting factor.

10.4 Hougen-Watson Analysis of the Kinetic Data.

The reaction pathway show previously in Section 10.2, has been examined in Section 10.3 in order to try and determine the rate-limiting step for the reaction. However, due to the nature of the available data it has not been possible to determine the nature of the rate-limiting step, the two potential steps being; (i) Surface reaction rate limited, or (ii) Adsorption rate limited.

Use of the Hougen-Watson kinetic approach for the analysis of the data, may however, yield more information.

If we first examine the nature of the three rate-limiting equations from the previous section then we have:

(i) Adsorption Rate Limited System:

$$r_{N2O} = C_t k_A y_{NOi} P_{TO} \qquad (10.24)$$

(ii) Surface Reaction Rate Limited System:

$$r_{N2O} = \frac{k_S C_t K_A y_{NOi} P_{TO}}{1 + K_A y_{NOi} P_{TO}} \qquad (10.27)$$

(iii) Desorption Rate Limited System:

$$r_{N2O} = k_D C_t \qquad (10.33)$$

We can rearrange the previous three equations to give relationships of the general form, y = mx + c:

(1) Adsorption Rate Limited System:

$$\frac{r_{N2O}}{P_{TO}} = C_t k_A y_{NOi} \qquad (10.34)$$

(2) Surface Reaction Rate Limited System:

$$\frac{r_{N2O}}{k_S C_t K_A P_{TO}} = y_{NOi} + \frac{1}{K_A P_{TO}} \qquad (10.35)$$

(3) Desorption Rate Limited System:

$$r_{N2O} = k_D C_t \qquad (10.33)$$

If we now plot r_{N2O} versus y_{NOi} then this gives us Figure 10.1.

We can see from the form of the three equations, 10.33, 10.34 and 10.35 that 10.35 is the best approximation to the form of the data. Hence, this gives further weight to the

conclusion that the surface reaction step, is the rate-limiting step, for the photocatalytic reaction of NO over illuminated titanium dioxide.

10.5 Physical Modelling of the Reactor System.

As was seen in Section 9.56, Chapter 9, the height of the catalyst bed in the reactor effects the degree of reaction of the NO and hence the amount of N_2O seen in the outlet from the reactor.

Also, as seen in Section 9.53, Chapter 9, the flowrate of the reaction gas through the reactor system significantly effects the amount of N_2O seen in the outlet from the photocatalytic reactor.

The two observations noted in the preceding two paragraphs allow some simple modelling of the reactor system to be undertaken.

10.51 Basic Model.

If we consider the photocatalytic reactor to be a fixed bed reactor, then the following design equation is commonly used, if we consider the simplistic situation of negligible pressure drop across the reactor and no catalyst decay.

$$F_{NOi} \frac{dX}{dW} = -r_{NO} \qquad (10.36)$$

At steady state conditions, the rate of NO disappearance is equal to the rate of N_2O appearance, therefore:

$$F_{NOi} \frac{dX}{dW} = r_{N2O} \qquad (10.37)$$

Upon integration, as dW --> 0, Equation 10.37 yields:

$$W = F_{NOi} \int_0^X \frac{dX}{r_{N2O}} \qquad (10.38)$$

If the experimental data available from Chapter 9 had been such that a rate limiting step could have been determined in Section 10.2, then the reactor equation 10.38 would have allowed an estimate of the mass of catalyst required for a set conversion of NO to N_2O to be determined. However, due to the uncertainty in the rate limiting step an estimate of the percent conversion at various reactor conditions is not possible.

10.6 Is the Measured Reaction Rate the Actual Reaction Rate?

In the previous sections, we have only considered that the limiting steps for reaction are the rate of adsorption of reactant, rate of surface reaction and the rate of desorption of products. We have not considered if mass transfer is a limiting step for the reaction, whether mass transfer within a porous system or bulk mass transfer within the reactant gas mixture.

Based on previously discussed work in this thesis, see Section 7.3, it was shown that the catalysts used within this work were non-porous, thus mass transfer limitations due to porous diffusion limitations will not occur in this work. Therefore, the only type of mass transfer we shall consider is that due to *external resistance*, the diffusion of reactants or products between the bulk gas and the external surface of the catalyst.

Most of the classic models for external resistance to mass transfer, are based around the flow past a single particle. Reaction is considered to take place only on the catalyst surface and not in the gas surrounding it, this being the accepted case where photocatalytic reactions are concerned. The fluid velocity in the vicinity of the catalyst particle will vary with the position around the particle. The hydrodynamic boundary layer is usually defined as the distance from the catalyst particle to where the gas velocity is 99% of the bulk velocity U_0. Similarly, the mass transfer boundary layer thickness, δ, is defined as the distance from the catalyst particle at which point the concentration of the diffusing species reaches 99% of the bulk concentration.

A representation of the boundary layer and the concentration profile around a catalyst particle is shown in Figure 10.2. As can been seen from the figure, the change in concentration from C_{A0} to C_{AS} takes place in a very narrow fluid layer next to the surface of the catalyst particle.

The classical approach for modelling the diffusion to the surface of a catalyst particle, described in the previous paragraphs, yields a relationship called the *Frössling correlation*, as shown in Equation 10.39:

$$Sh = 2 + 0.6\,\mathrm{Re}^{1/2} Sc^{1/3} \qquad (10.39)$$

The Sherwood, Reynolds and Schmidt numbers are detailed as:

$$Sh = \frac{k_c d_p}{D_{AB}} = \frac{(m/s)(m)}{m^2/s} \qquad \text{dimensionless (10.40)}$$

$$Sc = \frac{\nu}{D_{AB}} = \frac{m^2/s}{m^2/s} \qquad \text{dimensionless (10.41)}$$

$$\mathrm{Re} = \frac{U \rho d_p}{\mu} = \frac{(m/s)(Kg/m^3)(m)}{Kg/m.s} \qquad \text{dimensionless (10.42)}$$

We will now use this correlation to estimate whether the initial rate data discussed in the previous sections of this chapter is true rate data, or the product of mass transfer limitations on the photocatalytic reactions.

If we use the physical data for the NO/N_2 system detailed in Section 7.6, an average gas velocity of 0.01m/s, an average particle size of 200μm and an average diffusivity for NO of 10E-5m^2/s, then this gives us a value for the Schmidt Number of ~2.26. Substituting this value into equation 10.40 yields a value for the mass transfer coefficient of
~2.26E^{-3}m/s.

From this value it is still unclear as to whether the system is, or is not, mass transfer limited. Unfortunately, further data relating the initial reaction rate to the flow rate in the NO/He system, is not available since this would allow a confirmation to be obtained.

Nomenclature:

r_A = Rate of generation of species A per unit volume (gmoles A/sec*dm^3)
$-r'_A$ = Rate of disappearance of species A per mass of catalyst (gmol/g*s)
k = Specific reaction rate (units vary)
P_i = Partial pressure of species i (atm)
Cv = Concentration of vacant reaction sites on the catalyst surface (mol/g(catalyst))
K_A = Adsorption equilibrium constant for reaction A (units vary)
F_A = Molar flowrate of species A (gmoles/sec)
X = Conversion of key reactant, A.
W = Weight of Catalyst (grams)
d_p = Diameter of a catalyst particle (m)
D_{AB} = Gas-phase diffusivity (m^2/s)
v = Kinetic viscosity (m^2/s)
U = Free stream velocity (m/s)
ρ = Fluid density (Kg/m^3)
μ = Viscosity (Kg/m.s)

CHAPTER 11.

11.0 THESIS CONCLUSIONS AND SUGGESTIONS FOR FURTHER WORK.

11.1 Objectives of the Project.

The purpose of this research project was to develop the basis for a novel catalytic process for the abatement of nitrogen oxides (NO_X). The abatement process was achieved by light-induced reactions using three photocatalysts: titanium dioxide, size modified titanium dioxide and iron doped titanium dioxide. The advantages of using an annular fluidised gas/solid reactor were to be exploited. However, this was found to be impractical, due to the kinetics of the reaction and the experiments were finally carried out in an annular fixed bed reactor. The surface chemistry and reaction kinetics of the process were studied to allow basic modelling of the reactor system to be achieved.

11.2 The Basis of Photocatalysis.

Photocatalytic reactions taking place on n-type semiconductor materials are based on the following phenomenon. A photon of electromagnetic radiation, whose energy is equal to or greater than the band gap for the n-type material, excites an electron from the valence band to the conductance band, thus leaving a positive hole in the valence band. In the presence of electrophilic compounds, the solid surface is covered by negative adsorbed species A^-. Therefore, the photoproduced hole is attracted to the surface by the electrical field thus created. Under these conditions the semiconductor becomes capable of separating the photoproduced charges and can behave as a photocatalyst. Maintenance of the electrical neutrality may be achieved either by direct charge recombination of the hole

and electron or by an equilibrium between the holes reacting with oxidizable negative species and the electrons captured by reducible species.

11.3 Previous Work.

Previous work in the area investigated in this thesis is discussed in Chapter 5, under four main headings, (i) Photolysis of NO_X and Other Gases, Relevant to this Area of Research; (ii) General Photocatalysis; (iii) Action of NO_X on Illuminated Semiconductors; (iv) Photocatalysts other than Titanium Dioxide.

These categories are further subdivided within these sections to give a substantial outline of previous research work in these areas.

11.4 Non-Catalytic Experimental Work.

The non-catalytic experimental work described in Chapter 7, has shown the following points:-

11.41. The inlet and expected outlet gases for the reactor systems to be examined in later chapters, can be analysed for using gas chromatography and the conditions for this analysis have been determined.

11.42. Experimental work has been undertaken to produce catalysts with physical properties which have advantages for use in a fluidised or fixed bed reactor systems. Both physical and chemical modifications of Degussa P-25 titanium dioxide have been undertaken.

11.43. Surface areas for all catalysts to be used in the reactor systems described in this work have been determined by nitrogen adsorption techniques (BET).

11.44. Nitrogen gas adsorption isotherms have been determined for Degussa P-25, SM Degussa P-26 and Fe^{3+} Doped Degussa P-25. All of these isotherms have shown that the materials are of a non-porous nature, therefore pore diffusion effects need not be considered in reaction pathway modelling outlined in Chapter 10.

11.45. X-ray diffraction data for SM Degussa P-25 manufacture at different temperatures showed that heating of the initial Degussa P-25 above 600°C resulted in a phase change taking place within the original material. Therefore, it was possible to set the preparation temperature such that only the physical properties of the Degussa P-25 changed and the crystalline structure remained the same as the original material.

11.46. Determination of the Geldart Group classification and minimum fluidisation velocity of several potential photocatalysts and support materials were undertaken. The results obtained allowed some of the operating parameters for the photocatalytic reactor systems examined in Chapter 9 to be set.

11.47. Literature correlations for the fluidising properties of some particulate materials, were investigated for their applicability to the catalysts and support materials used in later chapters. It was shown that the fluidising properties of Degussa P-25 were not possible to estimate using the correlations considered, however, the size modified (SM) materials did fit the correlations considerably better.

11.48. Degree of attrition was examined for several of the potential catalyst materials to be used in later work. It was shown that the size modified (SM) materials manufactured by myself, were significantly more resistant to attrition than the original Degussa P-25 material.

11.49. The physical nature of Degussa P-25, SM Degussa P-25 and Fe^{3+} Doped Degussa P-25 was examined using electron microscopy. These observations showed the primary particles of Degussa P-25 and their appearance when combined to form SM Degussa P-25 and Fe^{3+} Doped Degussa P-25.

11.5 Photolytic Experimental Work.

The photolysis experimental work described in Chapter 8, has shown the following points:-

11.51. Nitrogen, oxygen and nitric oxide do not undergo photolysis under UV irradiation from an 8 watt black-light-blue in an annular flow reactor.

11.52. Nitrogen dioxide undergoes photolysis when irradiated by an 8 watt black-light-blue in an annular flow reactor. The photolysis yields a mixture of NO_2, NO and O_3 as product gases, also when O_2 is present in the inlet gas to the reactor N_2O may be seen in the outlet.

11.53. The production of O_3 by photolysis of NO_2 has been shown to be dependant on the flowrate at which the gas is introduced into the reactor, this results from the increased residence time within the reactor at lower flowrates.

11.54. The production of O_3 from the photolysis of NO_2, has been seen to be due to the irradiation by UV light of the NO_2 and has also been shown to be dependant in some way to the temperature at which the reactions occur.

11.55. The production of N_2O from the photolysis of NO_2 was not able to be confirmed, as any N_2O was at the limit of detection of the analysis equipment used and hence the results were unreliable.

11.6 Photocatalytic Experimental Work.

The photocatalysis experimental work described in Chapter 9, has shown the following points:-

11.601. Photocatalysis reactions of NOx in a fluidised bed reactor system were not observed. It was assumed that this was due, in the main, to the short residence times of the reactant gases in the reactor when flows, large enough to fluidise the catalyst, were used.

For $NO_2 + N_2$ reacting on UV irradiated titanium dioxide:

11.611. NO_2 reacts on a UV irradiated TiO_2 catalyst surface to produce N_2O and O_3 in the gas phase. NO is presumably produced but it was not possible to detect any due to the analysis system used.

11.612. In a system containing $NO_2 + N_2$ bulk, N_2O was seen in the exit stream from the reactor first, with O_3 seen second. When an oxygen purge was used or residual oxygen was present on the catalyst surface then O_3 was seen first in the reactor exit stream followed by N_2O.

11.613. The photocatalytic reaction of NO_2 to give $N_2O + O_3$ was seen to be erratic and depends on the pre-treatment of the catalyst surface, i.e. had the catalyst been purged for significant periods of time and was residual O_2 present on the catalyst surface. It was therefore impossible to give any definite correlations between the degree of reaction and quantitative parameters such as flowrate, bed height, UV intensity etc.

11.614. Qualitative results for the photocatalytic reaction of NO_2 show that; an increase in the flowrate of the inlet gases gives a decrease in the degree of photocatalytic reaction seen; the photocatalytic reaction was confirmed as UV-light initiated, since when the UV source was turned off the photocatalytic reaction was seen to stop; a relationship between the temperature of the reactor and the degree of photocatalytic reaction seen was noted.

11.615. Postulated reaction mechanisms for the photocatalytic reaction of NO_2 on irradiated titanium dioxide have been suggested.

For $NO + N_2$ reacting on UV irradiated titanium dioxide:

11.621. The system of nitric oxide and nitrogen as the inlet gas to a photocatalytic system was not investigated, due to the fact that it would have been impossible to determine if any nitrogen was formed from the NO itself.

For NO_2 + helium reacting on UV irradiated titanium dioxide:

11.631. NO_2 reacts on a UV irradiated TiO_2 catalyst surface to produce O_3 in the gas phase when helium was present as the bulk inlet gas. No N_2 or O_2 was detected as outlet gases from the reactor.

11.632. When helium was used as the bulk gas with NO_2, it was seen that only O_3 was seen in the outlet from the reactor, as compared with using nitrogen as the bulk gas when both N_2O and O_3 were observed in the reactor outlet.

11.633. An increase in inlet gas flowrate resulted in a reduction in the levels of O_3 in the outlet from the reactor.

11.634. The reaction of NO_2 on irradiated TiO_2 was shown to be photocatalytic in nature, due to the fact that when the UV source was switched off, the reaction was seen to stop.

11.635. Increasing the intensity of the incident UV light used in the reactor in which the photocatalytic reaction of NO_2 + helium was performed, showed that an increase in the outlet concentration of O_3 resulted.

11.636. A relationship between the degree of photocatalytic reaction seen at the outlet from the reactor and the temperature of the reactor was seen, however it was not possible to quantify this relationship with the experimental equipment available.

11.637. Postulated reaction mechanisms for the reaction of NO_2 + helium on irradiated TiO_2 are presented.

For NO + helium reacting on UV irradiated titanium dioxide:

11.641. NO reacts on a UV irradiated TiO_2 catalyst surface to produce N_2O and O_3 in the gas phase.

11.642. An increase in the flowrate of the reaction gas into the reactor resulted in a decrease in the degree of photocatalytic reaction observed.

11.643. The reaction of NO + helium was shown to photocatalytic due to the fact that upon switching off of the UV light source, the reaction was seen to stop.

11.644. The photocatalytic reaction of NO + helium was seen to have a temperature dependence, resulting in an increased temperature leading to an increased degree of photocatalytic reaction being observed.

11.645. It was seen that increasing the depth of the photocatalyst bed in the reactor, resulted in a proportional increase in the degree of photocatalytic reaction seen across the reactor.

11.646. Postulated mechanisms for the photocatalytic reaction of NO + helium on irradiated TiO_2 were put forward.

For NO + helium reacting on UV irradiated titanium dioxide, miscellaneous experimental work:

11.651. An examination of several photocatalytic materials was undertaken. It was determined that Degussa P-25 was the best photocatalyst material from those examined in this work.

11.652. The effect of NO concentration in the photocatalytic system, with helium as the bulk gas, was examined. It was seen that a first order relationship between NO concentration and the rate of N_2O production existed.

11.7 Kinetic/Mechanistic Modelling Work.

A Langmuir/Hinshelwood and Hougen/Watson analysis of the available rate data inferred that the rate limiting step for the photocatalytic reaction of nitric oxide on the surface of illuminated titanium dioxide, is the rate of reaction at the surface of the photocatalyst and not any mass transfer limitations.

Analysis of the available rate data using the *Frössling Correlation* was not conclusive in determining whether the rate data obtained was, or was not, mass transfer limited rate data or reaction rate data.

11.8 Suggestions for Future Work.

Numerous areas of research still remain to be covered following this initial thesis on the photocatalytic abatement of NOx.

These areas are outlined as follows;

Detailed chemistry questions:

11.801. Conclusive confirmation of the rate limiting step in the photocatalytic reactions.

11.802. Determination of the effect of catalyst crystalline composition on the degree and nature of reaction seen on the surface.

11.803. Determination of any enhancement in the rate of reaction or the nature of the reaction by doping of the catalyst with other metal ions.

11.804. Examination of the effects of using both band-gap and supra band gap illumination on the relative percentages of products seen from the reaction.

Chemical engineering questions:

11.811. Determination of the degree of penetration of UV light through a stationary catalyst bed and optimisation of the thickness of the catalyst bed.

11.812. Determination of the optimum size of catalyst particle for a practical engineering application.

11.813. Determination of the mass transfer and reaction rate limited regimes for the reaction of NO/He over TiO_2.

11.814. Modelling of the reactor system in order to be able to scale up the reactor system and estimate the commercial practicality of the system.

REFERENCES.

1. Daroux, M., Klvana, D., Duran, M., and Bideau, M. (1985). Photocatalytic Oxidation of Ethane over TiO_2. *Can. J.Chem. Eng.* 63, 668 - 673.

2. Geldart, D. (1973). Types of Gas Fluidisation. *J.Powder.Tech.* 7, 285 - 292.

3. Courbon, H. and Pichat, P. (1984). Room temperature interaction of NO with UV illuminated Titanium Dioxide. *J.Chem.Soc., Faraday Trans.* 80, 3175 - 3185.

4. Pichat, P., Herrmann, J.M., Disdier. J., and Mozzanega, M. (1979). Photocatalytic Oxidation of Propene Over Various Oxides at 320K. *J.Phys.Chem.* 83. Vol 24. 3122 - 3126.

5. Cunningham, J., Kelly, J.J., and Penny, A.L. (1971). Reactions Involving Electron Transfer at Semiconductor Surfaces. *J.Phys.Chem.* 75. No.5. 617 - 625.

6. Esplugas, S., Vincente, M. and Prat, C. (1989). The Importance of Mounting the Lamp Centrally in an Annular Photoreactor. *Anales De Quimica.* 85. 152 - 154.

7. Pichat, P., Herrmann, J., Courbon, J., Disdier, J. and Mozzanega, M. (1982). Photocatalytic Oxidation of Various Compounds over TiO_2 and other Semiconductor Oxides; Mechanistic Considerations. *Can.J.Chem.Eng.* 60. 27 - 32.

8. Whitaker, S. and Cassano, A.E. (1986). Concepts and Design of Chemical Reactors. *Chem.Eng: Concepts and Reviews.* 3. Chapter 8.

9. Tanaka, K. and Blyholder, G. (1971). Photocatalytic Reactions on Semiconductor Surfaces: 1. Decomposition of Nitrous Oxide on Zinc Oxide. *J.Phys.Chem.* 75. 1037 - 1043.

10. Pichat, P., Herrmann, J.M., Jenny, B. et al. (1985). Pt/TiO2 Catalysts. Characterisation and use in Photocatalytic reactions. *Adv.Catal.Proc. Natl.Symp. Catal.* 7th Year. 741 - 749.

11. Herrmann, J-M., Disdier, J. and Pichat, P. (1984). Effect of Chromium Doping on the Electrical and Catalytic Properties of Powered Titania under UV and Visible Illumination. *Chemical Physics Letters.* 108. 618 - 622.

12. Rizzuti, L. and Yue, P.L. (1983). The Measurement of Light Transmission through an Irradiated Fluidised Bed. *Chem.Eng.Sci.* 38. 1241 - 1249.

13. Yue, P.L., Khan, F. and Rizzuti, L. (1983). Photocatalytic Ammonia Synthesis in a Fluidised Bed Reactor. *Chem.Eng.Sci.* 38. 1893 - 1900.

14. Pitts, J.N., Sharp, J.H. and Chan, S.I. (1964). Effects of Wavelength and Temperature on Primary Processes in the Photolysis of Nitrogen Dioxide. *J.Chem.Phys.* 42. 3655 - 3662.

15. Calvert, J.G. and Pitts, J.N. The Interaction of Light with Simple Molecules. The Oxides of Nitrogen. *Photochemistry.* Chapter 3. 209 - 222.

16. Daroux, M., Parent, Y. and Klvana, D.A. (1980). New Reactor for the Study of Photocatalytic Reactions. *Chem.Eng. Commun.* 4. 501 - 506.

17. Schiavello, M., Rizzuti, L., Bickley, R. and Yue, P.L. (1984). Photoassisted Dinitrogen Fixation over Titania Crystals in a Flow Reactor. *8th.Int.Cong. Catal.* 3. 383 - 394.

18. United Kingdom Atomic Energy Authority. Trace Gases and there Relative Contribution to the Greenhouse Effect. AERE-R13716

19. Her Majesty's Inspectorate of Pollution. Nitric Acid Works (Manufacture of nitric acid). BPM 24/87

20. Yacono, C.X.R. University of London.Umf correlations. PhD Thesis, (1975)

21. Davidson, J.F. and Harrison, D. Umf correlations.Fluidised Particles. (1963)

22. Leva, M.Umf correlations.Fluidisation. (1959)

23. Wen, C.Y. and Yu, Y.H.Umf correlations.AIChE. 12. 610 (1966)

24. Grace, J.R. (1971). An evaluation of models for fluidised bed reactors. *AIChE Symp. Ser.* 67. 159 - 167.

25. Grace, J.R. (1984). Generalised models for isothermal fluidised bed reactors. *Rec. Adv. Eng. Anal. of Chem. React. Sys.* Ed. Doraiswamy.

26. Geldart, D.Chapter 11. Fluidised beds as chemical reactors.Gas Fluidisation Technology. (1986)

27. Kunii, D. and Levenspiel, O.Three-phase bubbling bed model. Fluidisation Engineering. (1969)

28. Fryer, C. and Potter, O.E. Counter-current backmixing model for fluidised bed catalytic reactors; applicability of simplified solutions. *Ind.Eng.Chem. Fund.* 11. 338 - 344.

29. Hall, T.C. Jr and Blacet, F.E. (1952). Separation of the Absorption Spectra of NO2 and N_2O_4 in the range 2400 - 5000A. *J. Chem. Phys.* 20. (11). 1745 - 1749.

30. Pitts, J.N. Jr., Sharp, J.H., and Chan, S.I. (1963). Primary Process in the Photolysis of Nitrogen Dioxide at 4047A and a Spectroscopic-Photochemical Determination of the Dissociation Energy. *J. Chem. Phys.* 238 - 239.

31. Zelikoff, M. and Aschenbrand, L.M. (1954). Vacuum Ultraviolet Photochemistry, Part 1 and Part 2. Nitrous Oxide at 1470A and 1849A. *J. Chem. Phys.* 22. (10). 1680 - 1687.

32. McEwan, M.J. and Philips, L.F. Chapters 2 and 7. Chemistry of the Atmosphere

33. Stern, A.C., Wohlers, H.C., Boubel, R.W., and Lowry, W.P.Chapter 8. The Chemistry of Air.Fundamentals of Air Pollution. 92 - 95.

34. Campbell, I.M.Chapter 8. Basic Photochemical Considerations.Energy and The Atmosphere. 214 - 236

35. Seinfeld, J.H.Chapter 4. Air Pollution Chemistry.Air Pollution. 142 - 159.

36. Stephens, E.R., Hanst, P.L., Doerr, R.C., and Scott, W.E. (1956). Reactions of Nitrogen Dioxide and Organic Compounds in Air. *Ind. Eng. Chem.* 48. (9). 1498 - 1504.

37. Seinfeld, J.H.Air Pollution Chemistry.Lectures in Atmospheric Chemistry. AIChE Monograph Series 76. (12) (1980)

38. Stern, A.C.Air pollution Chemistry.Air Pollution. Third Edition. (Air pollutants, Their Transformation and Transport). Chapter 6.

39. Cant, N.W. and Cole, J.R. (1992). Photocatalysis of the Reaction between Ammonia and Nitric Oxide on TiO_2 Surfaces. *J. Catalysis.* 134. 317 - 330.

40. Costanza, V. and Seinfeld, J.H. (1981). Stochastic sensitivity analysis in chemical kinetics. *J. Chem. Phys.* 74 (7) 3854 - 3855.

41. Ford, H.W. and Jaffe, S. (1963). Photolysis of Nitrogen Dioxide at 3660 and 4047Å at 25°C. *J. Chem. Phys.* 38 (12) 2935 - 2942.

42. Khan, F., Yue, P.L., Rizzuti, L., Augugilaro, V. and Brucato, A. (1983). Photoassisted Water Cleavage and Nitrogen Fixation over Titanium-Exchanged Zeolites. *Ind. Eng. Chem. Res. Dev.* 22. 238 - 241.

43. Harrison, B, Wyatt, M. and Gough, K.G.Catalysis of Reactions Involving the Reduction or Decomposition of Nitrogen Oxides.Catalysis. Chapter 4.

44. Srnak, T.Z., Dumesic, J.A., Clausen, B.S., Törnqvist, E. and Topsøe, N.-Y. (1992). Temperature-Programmed Desorption/Reaction and in Situ Spectroscopic Studies of Vanadia/Titania for Catalytic Reduction of Nitric Oxide. *J. Catalysis.* 135. 246 - 262.

45. Toering, W. Nitrogen Oxides from Nitric Acid Production. (NOx formation and abatement possibilities). Air Pollution by Nitrogen Oxides. 671 - 686.

46. Prasad, R., Kennedy, L.A. and Ruckenstein, E. (1984). Catalytic Combustion. *Catal. Rev.-Sci. Eng.* 26(1). 1 - 58.

47. Thermal Syndicate Ltd. P.O.Box No 6, Wallsend, Northumberland. NE28 6DG. Spectrosil®. Synthetic Vitreous Silica. Leaflet TD8.

48. De Bernardez, E.R., Clariá, M.A. and Cassano, A.E.Analysis and Design of Photoreactors.Reactor Design. Chapter 13.

49. Romero, R.L., Alfano, O.M., Marchetti, J.L. and Cassano, A.E. (1983). Modelling and Parametric Sensitivity of an Annular Photoreactor with Complex Kinetics. *Chem. Eng. Sci.* 38 (9). 1593 - 1605.

50. Irazoqui, H.A., Cerdá, J. and Cassano, A.E. (1973). Radiation Profiles in an Empty Annular Photoreactor with a Source of Finite Spatial Dimensions. *AIChE Journal.* 19 (3). 460 - 467.

51. Hill, F.B. and Felder, R.M. (1965). Effects of Mixing on Chain Reactions in Isothermal Photoreactors. *AIChE.* 11. (5) 873 - 885.

52. Krishna, M.S. (1972). Transfer Rates at the Inner Wall of Annular Fluidised Beds. *Indian J. Tech.* 10. 163 - 165.

53. Kang, Y., Yoo, Y.T. and Kim, S.D. (1981). Gas Mixing in an Annular Fluidised Bed. *J. Korean Inst. Chem. Eng.* 19. (4). 291 - 302.

54. Cassano, A.E., Silveston, P.L. and Smith, J.M. (1967). Photochemical Reaction Engineering. *Industrial Eng. Chem.* 59. (1) 18 - 38.

55. Kashuri, K and Laddha, G.S. (1982). Residence Time Distribution in Annular Packed and Fluidised Beds. *Indian J. Tech.* 20. 438 - 440.

56. Stramigioli, C., Santarelli, F. and Foraboschi, F.P. (1977). Photosensitised Reactions in an Annular Continuous Photoreactor. *Appl. Sci. Res.* 33. 23 - 44.

57. Funayama, H., Sugawara, T. and the lated Ohashi, H.Direct Determination of Absolute Light Intensity Profiles in Heterogeneous Photoreactors.World Congress III of Chemical Engineering, Tokyo, 223 - 226. 1986.

58. Rizzuti, L and Yue, P.L. (1983). The Measurement of Light Transmission Through an Irradiated Fluidised Bed. *Chem. Eng. Sci.* 38. (8) 1241 - 1249.

59. Grace, J.R. An Evaluation of Models for Fluidised Bed Reactors. *AIChE Symposium Series.* 116. Vol. 67. 159 - 167.

60. Geldart, D. (1973). Types of Gas Fluidisation. *Powder Technology.* 7. 285 - 292.

61. De Bernardez, E.R. and Cassano, A.E. (1986). Methodology for an Optical Design of a Photoreactor. Application to Methane Chloro Derivatives Production. *Ind. Eng. Chem. Process Des. Dev.* 25. 601 - 612.

62. Yokota, T., Takahata, Y., Nanjo, H. and Takahashi, K. (1989). Estimation of Light Intensity in a Solid-Liquid Photoreaction System. *J. Chem. Eng. Japan.* 22. (5) 537 - 542.

63. De Bernardez, E.R. and Cassano, A.E. (1985). A Priori Design of a Continuous Annular Photochemical Reactor: Experimental Validation for Simple Reactions. *J. Photochemistry.* 30. 285 - 301.

64. Kirk Othmer Nitric Acid. Volume 15. Nitric Acid.

65. Davis, A.P. and Hao, O.J. (1991). Notes: Reactor Dynamics in the Evaluation of Photocatalytic Oxidation Kinetics. *J. Catalysis.* 131. 285 - 288.

66. MacConnachie, P.W.J. Private Communication.

67. Busby, J.A., Knapton, A.G. and Budd, A.E.R. Catalytic Processes in Nitric Acid Manufacture. The Fertiliser Society. Proceedings No. 169. (1978)

68. Reichmann, M.G. and Bell, A.T. (1987). The Influence of Preparation Chemistry on the Phase Distribution of Silica-Supported Titania. *Applied Catalysis.* 32. 315 - 326.

69. Formenti, M., Juillet, F., Meriadeau, P., Teichner, S.J. and Vergnon, P. (1972). Preparation in a Hydrogen-Oxygen Flame of Ultrafine Metal Oxide Particles. Oxidative Properties Toward Hydrocarbons in the Presence of Ultraviolet Radiation. *J. Colloid and Interface Science.* 39. (1) 79 - 89.

70. Kirkbir, F. and Komiyama, H. (1986). Preparation of Porous, Amorphous, and Fine TiO_2 Particles by Chemical Vapour Deposition. *World Congress III of Chemical Engineering, Tokyo. New Material Processing.* 5b-304. 361 - 364.

71. AERE Harwell. Trace Gases and Their Relative Contribution to the Greenhouse Effect. HMSO AERE R13716.

72. Macdonald, E.Environmental Control in the Oil Industry.Environmental Protection Bulletin 007.

73. Environmental Data Services Ltd.Global Warming Policy Gets into Gear.ENDS. Report 184. May 1990.

74. Rhoads, T.W., Marks, J.R. and Siebert, P.C. (1990). Overview of Industrial Source Control for Nitrogen Oxides. *Environmental Progress.* 9 (2). 126 - 130.

75. Her Majesty's Inspectorate of Pollution.Nitric Acid Works (Manufacture of nitric acid).BPM 24, (1987)

76. United Nations Environment Programme. The State of the World Environment. 1989. UNEP/GC.15/7/Add.2.

77. Thorne, L.T. and Woods, I.T. (1991). Considerations in Using Cost Benefit Analysis to Identify Strategies to Reduce SO_2 and NOx. *Environmental Protection Bulletin 014.*

78. Ford, H.W., Doyle, G.J. and Endow, N. (1956). Kinetics of Photolysis of Low Concentrations of Nitrogen Dioxide in Air. *Advances in Chemistry Series.* "Ozone Chemistry and Technology".

79. Hargreaves, G.B.Improving the Environment - The Installation of NOx Abatement Equipment in the Sevenside No 2 and 3 Nitric Acis Plants.PhD Thesis for the IChemE.

80. Stanley-Wood, N.G. and Johansson, M.E. (1986). Variation of adsorption forces with degree of compaction. *Acta Pharm. Suec.* 23. 271 - 278.

81. Matheson Gas Products.Various sections.Book - "Matheson Gas Data Book".

82. Courbon, H., Formenti, M. and Pichat, P. (1977). Study of Oxygen Isotopic Exchange over Ultraviolet Irradiated Anatase Samples and Comparison with the Photooxidation of Isobutane into Acetone. *J. Phys. Chem.* 81. (6) 550 - 554.

83. Ait Ichou, I., Formenti, M. and Teicher, S.J. (1983). Reverse Spillover of Hydrogen Adsorbed Species in Dehydrogenation Photocatalysis on Pt/TiO_2 Catalysts. *Elsevier Science Publications B.V., Amsterdam.* "Spillover of Adsorbed Species". 63 - 75.

84. Ileperuma, O.A., Tennakone, K. and Dissanayake, W.D.D.P. (1990). Photocatalytic Behaviour of Metal doped Titanium Dioxide. Studies on the Photochemical Synthesis of Ammonia on Mg/TiO_2 Catalyst Systems. *Applied Catalysis.* 62. L1 - L5.

85. Iseda, K. (1990). Oxygen effect on Ethylene formation by photocatalytic dehydration reaction of ethanol over some titanium dioxide photocatalysts. *Chemistry Express.* 5. (10) 729 - 732.

86. Lee, T.J. and Kim, Y.G. (1985). Experimental Study of Characteristics of Pt/TiO_2 Catalyst. *Chem. Eng. Commun.* 34. 277 - 293.

87. Dibble, L.A. Gas-Solid Heterogeneous Photocatalytic Oxidation of Trichloroethylene by Near Ultraviolet Illuminated TiO_2. PhD Thesis. Arizona State University. 1989.

88. Grace. J.R. (1981). Fluidised Bed Reactor Modelling. An Overview. *ACS Symposium Series.* No 168. Chemical Reactors.

89. Bickley, R.I. et al. (1991). A Structural Investigation of Titanium Dioxide Catalysts. *J. Solid State Chem.* 92. 178 - 190.

90. Baba, S. Photocatalysis of Organic Materials. MPhil Thesis, 1991. University of Bath.

91. Coulson, J.M. and Richardson, J.F.Chapter 7. Sorption Processes.Chemical Engineering. Volume 3. 2nd Edition.

92. Ollis, D.F. and Al-Ekabi, H. General Publication on Photocatalysis. Photocatalytic Purification and Treatment of Water and Air. Conference Proceedings 1992.

93. Valladares, J.E. and Bolton, J.R. (1992). Relationship for quantum yeild vs TiO_2 density. *Photocatalytic Purification and Treatment of Water and Air.* Conference Proceedings.

94. T-Raissi, A. and Muradov, N.Z. (1992). Nitroglycerin destruction with deposited TiO_2 films. *Photocatalytic Purification and Treatment of Water and Air.* Conference Proceedings.

95. Al-Ekabi, H. and Ollis, D.F. (Editors). A specific conference on Photocatalysis. *Photocatalytic Purification and Treatment of Water and Air.* Conference Proceedings.

96. White, S. Chemistry of NOx Photocatalysis on Titanium Dioxide. *Private Communications.* Co-operative research with Bradford University.

97. Coast Air UV Systems Ltd. UV source output data. Coast Air Company Information.

98. Fox, M.A. (1992). The role of hydroxyl radicals in the photocatalysed detoxification of organic pollutants. *Photocatalytic Purification and Treatment of Water and Air.* Conference Proceedings.

99. Matthews, R.W. (1992). Photocatalysis in Water Purification: Possibilities, Problems and Prospects. *Photocatalytic Purification and Treatment of Water and Air.* Conference Proceedings.

100. Heller, A., Nair, M., Davidson, L. et al. (1992). Photoassisted Oxidation of Oil and Organic Spills on Water. *Photocatalytic Purification and Treatment of Water and Air.* Conference Proceedings.

101. Fogler, H. Scott. Reactor and reaction modelling and kinetics. *Elements of Chemical Reaction Engineering.*

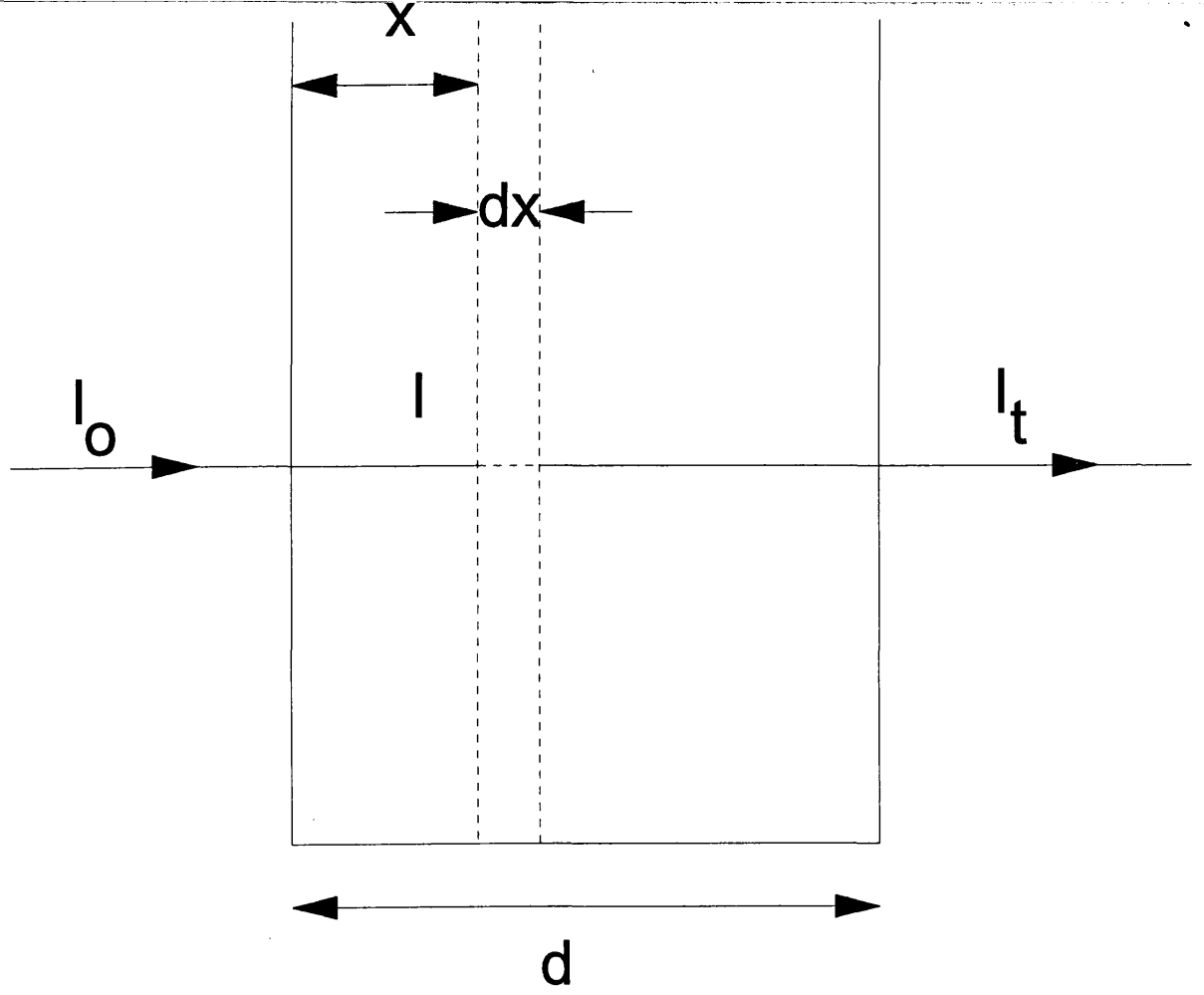

Figure 2.1 The change in intensity, I, with optical path, x.

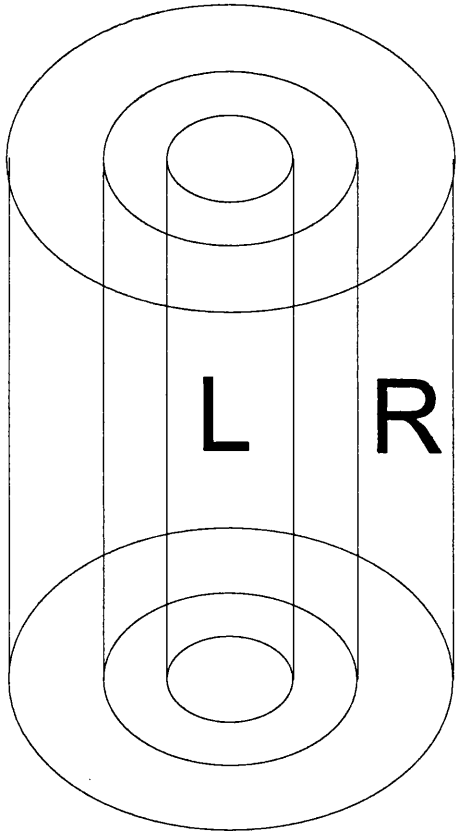

FIGURE 2.2 AN ANNULAR PHOTOREACTOR.

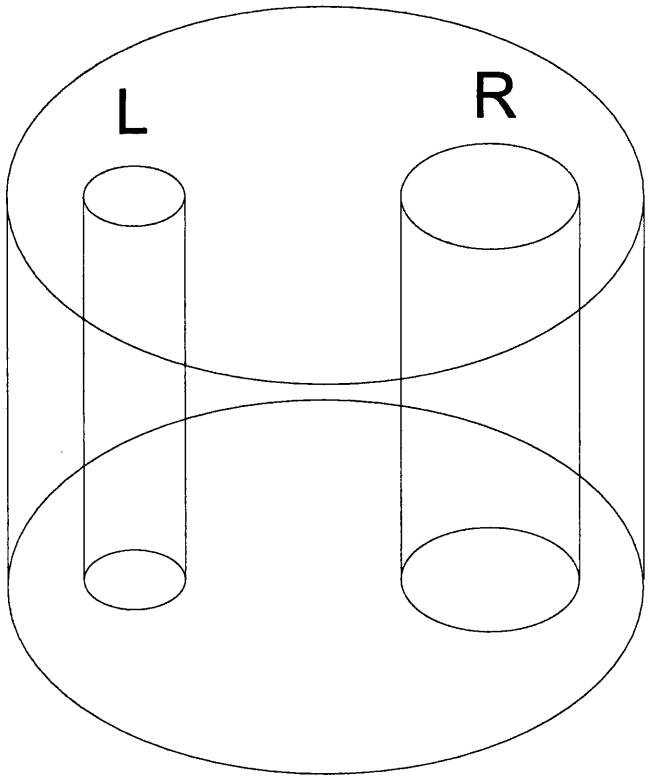

Figure 2.3 Cylindrical reactor with elliptical reflector.

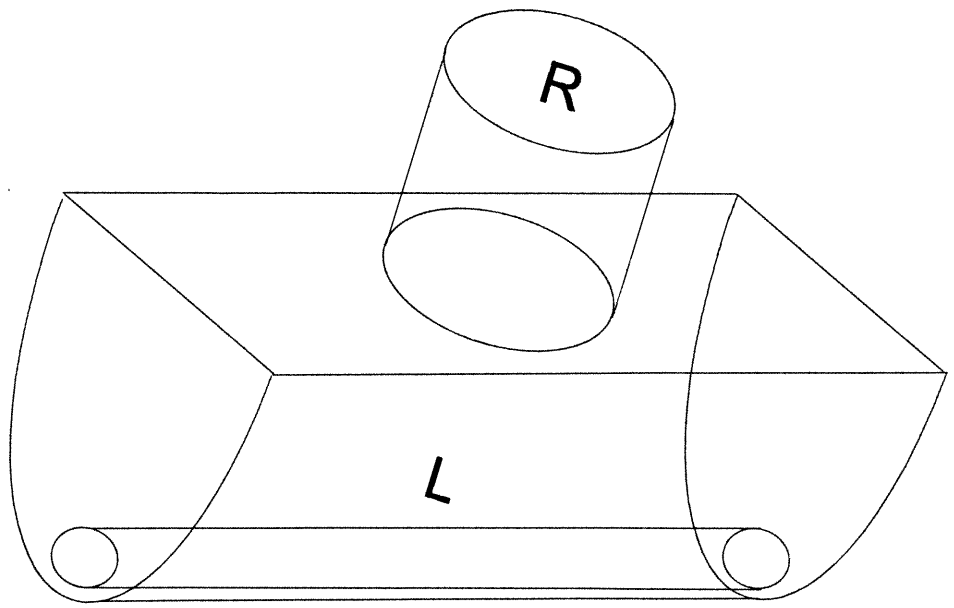

Figure 2.4 Cylindrical reactor irradiated from the bottom.

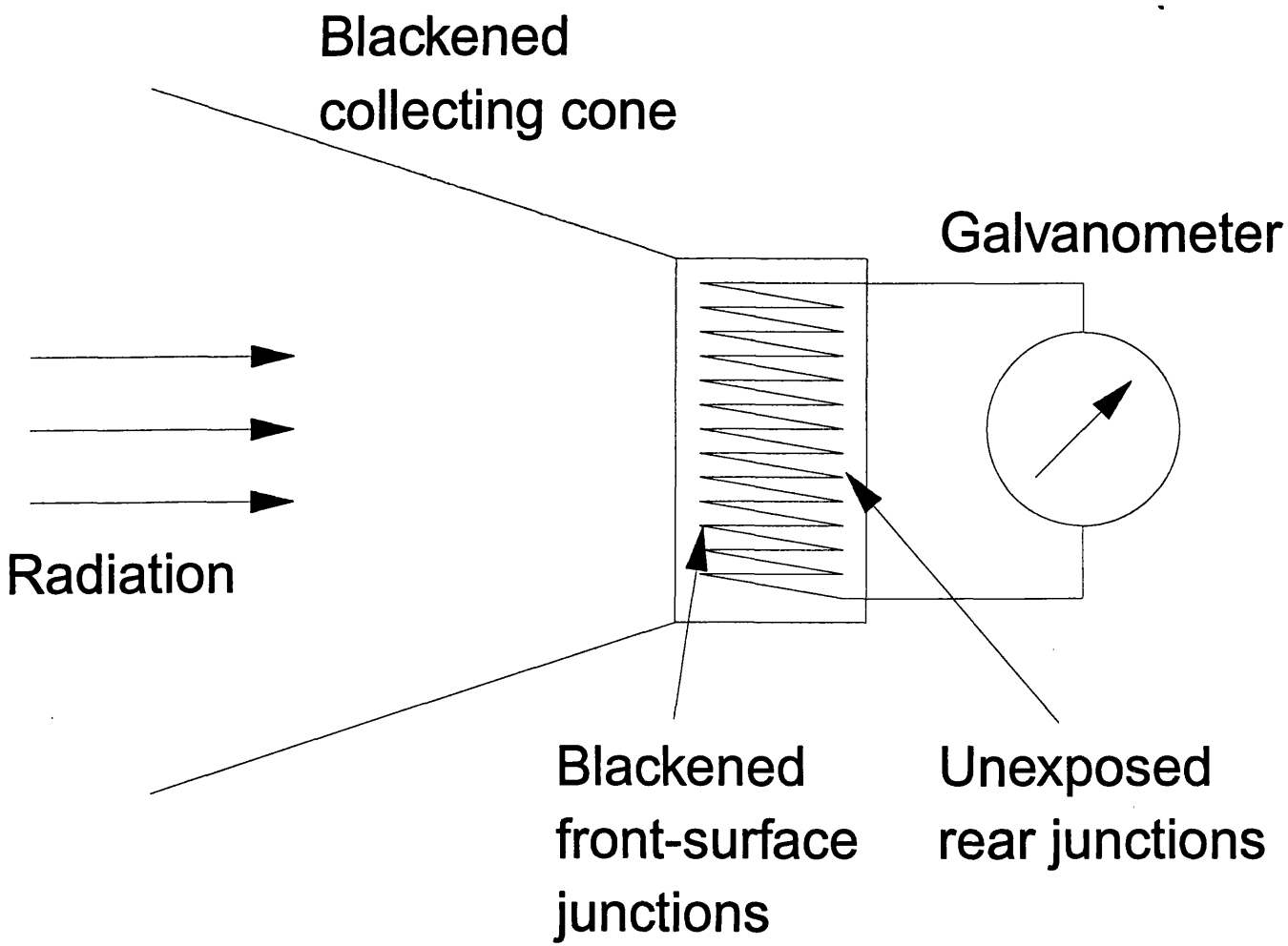

Figure 2.5 A Thermopile

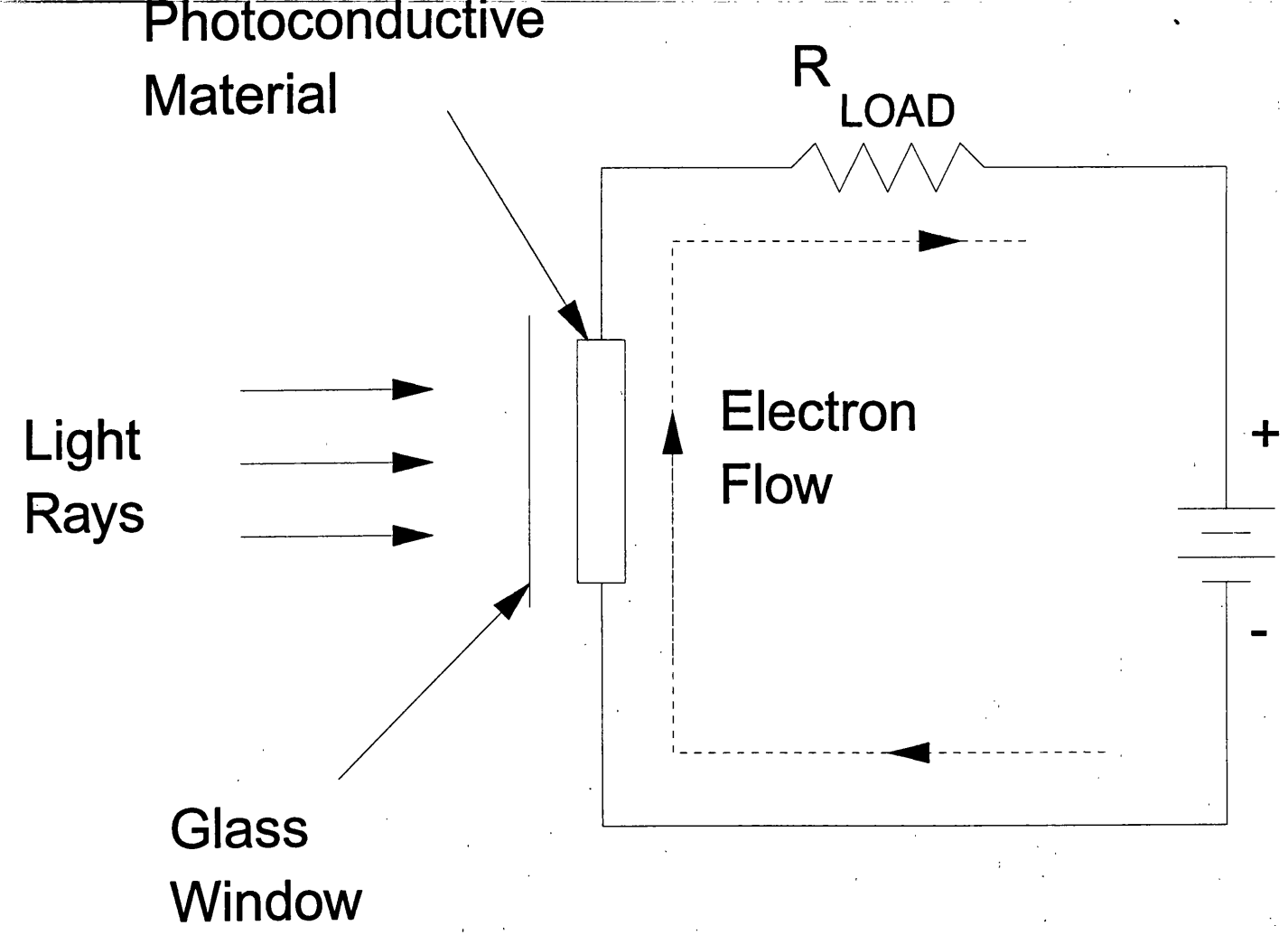

Figure 2.6 A Photoconduction Cell

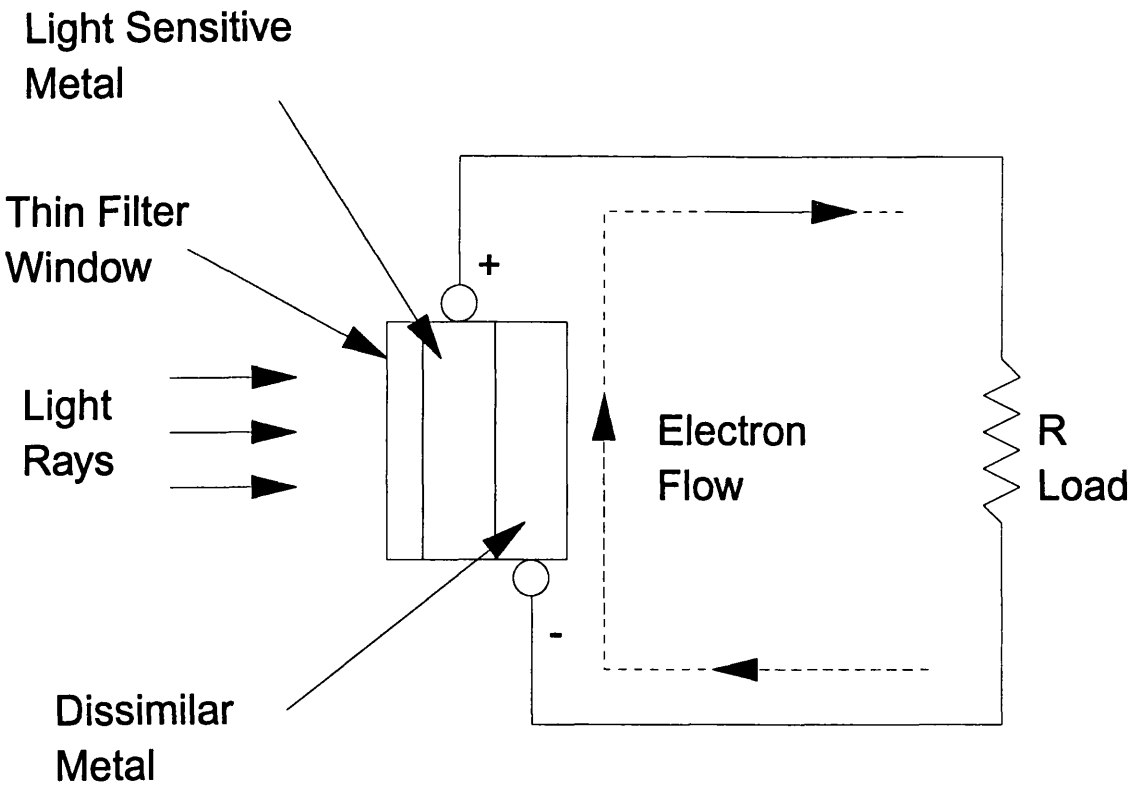

Figure 2.7 A Photovoltaic Cell

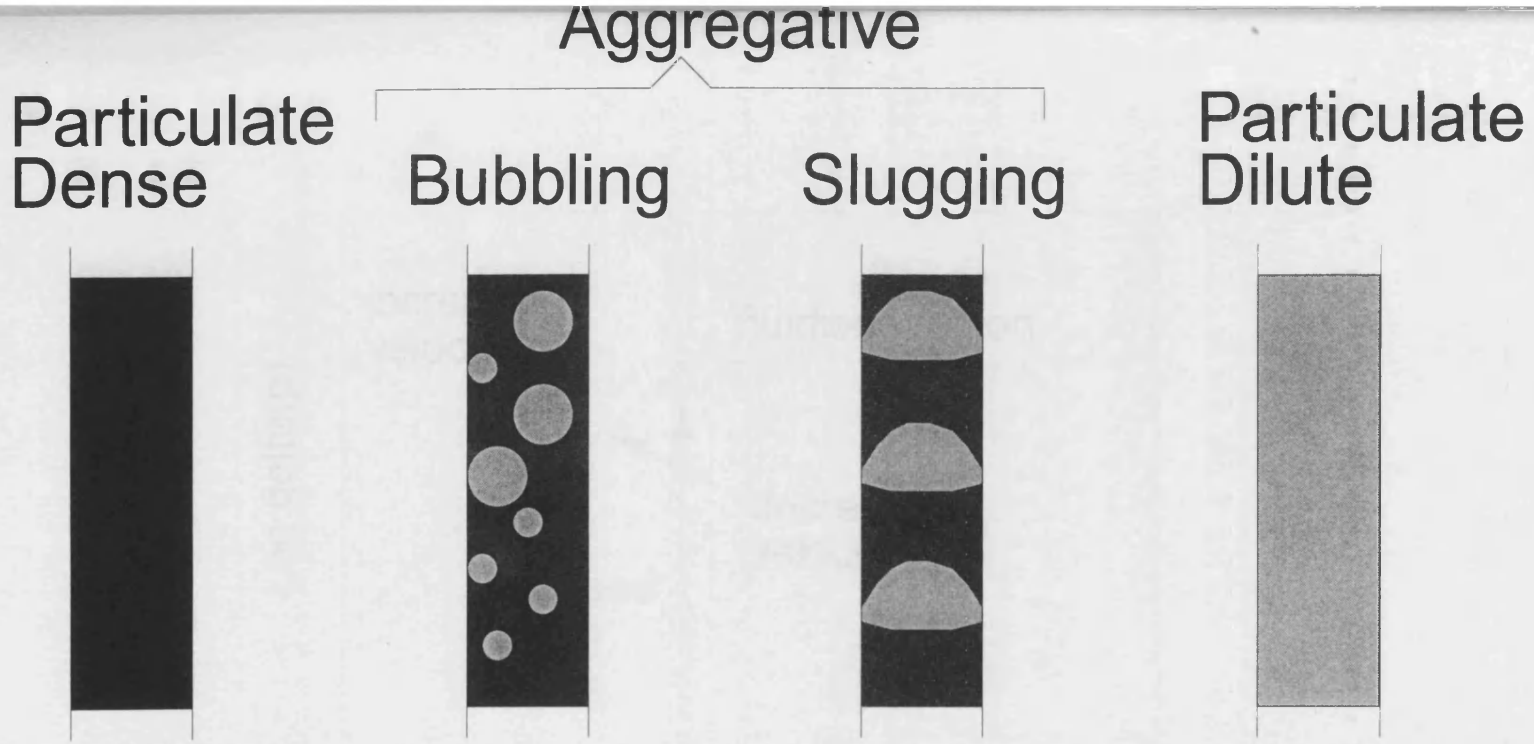

Figure 3.1 Concentrations in fluid-solid systems.

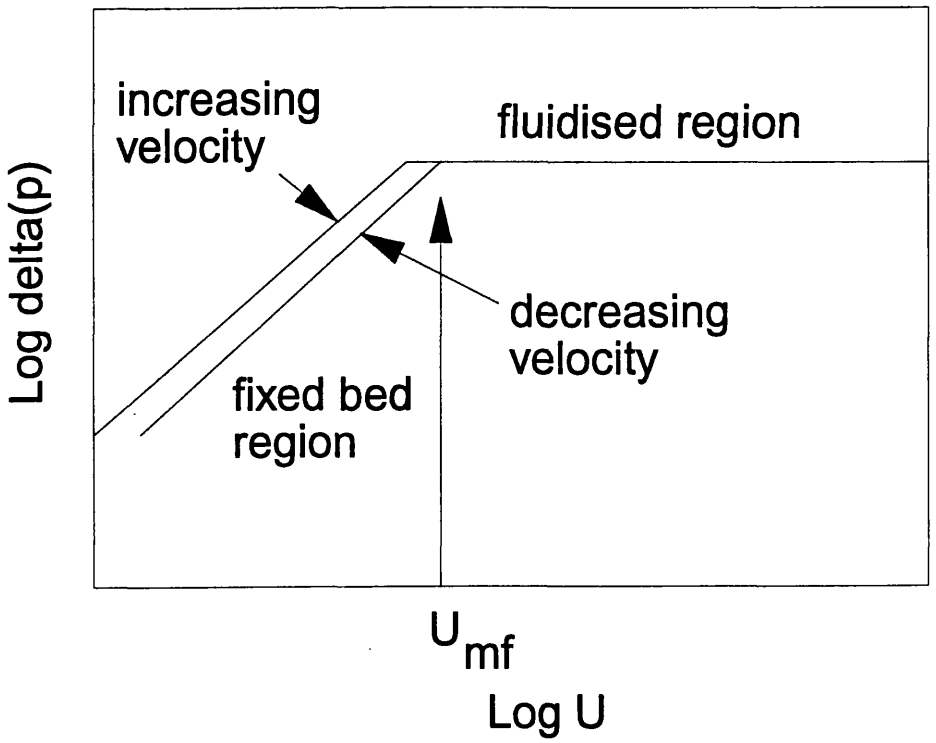

Figure 3.2 Ideal pressure drop vs velocity curve.

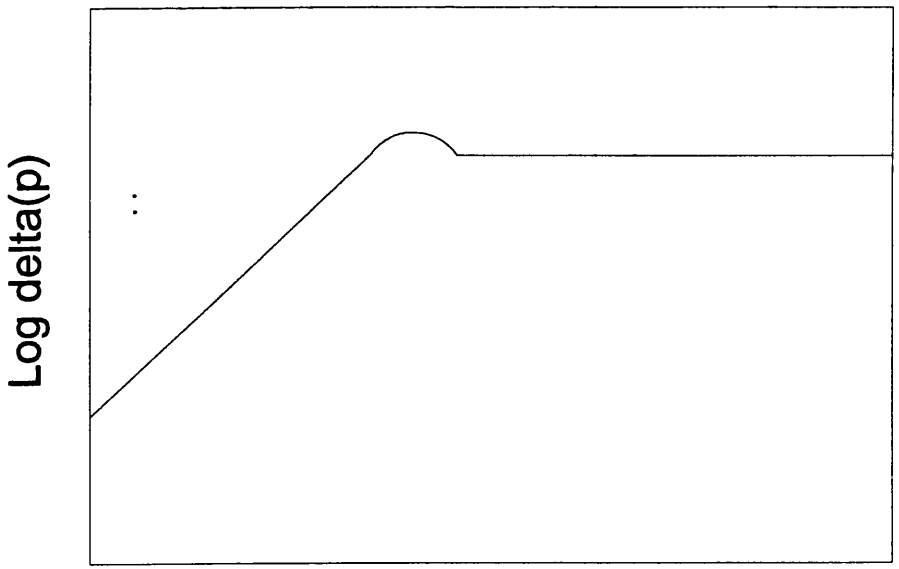

Figure 3.3 Effect of particle interlocking on pressure drop.

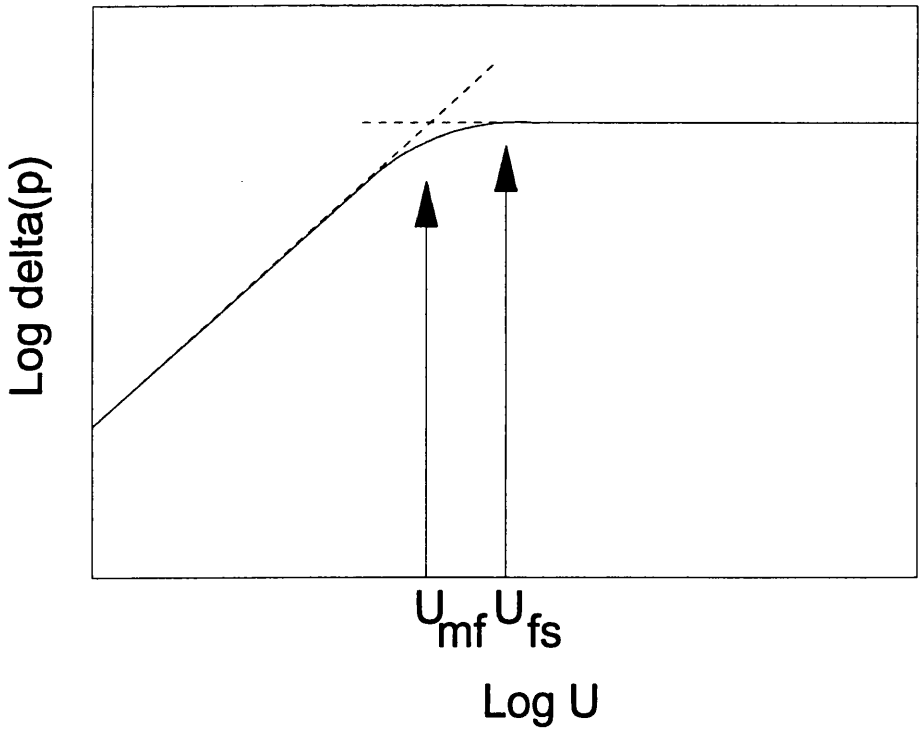

Figure 3.4 Effect of the presence of non-fluidised regions in the bed.

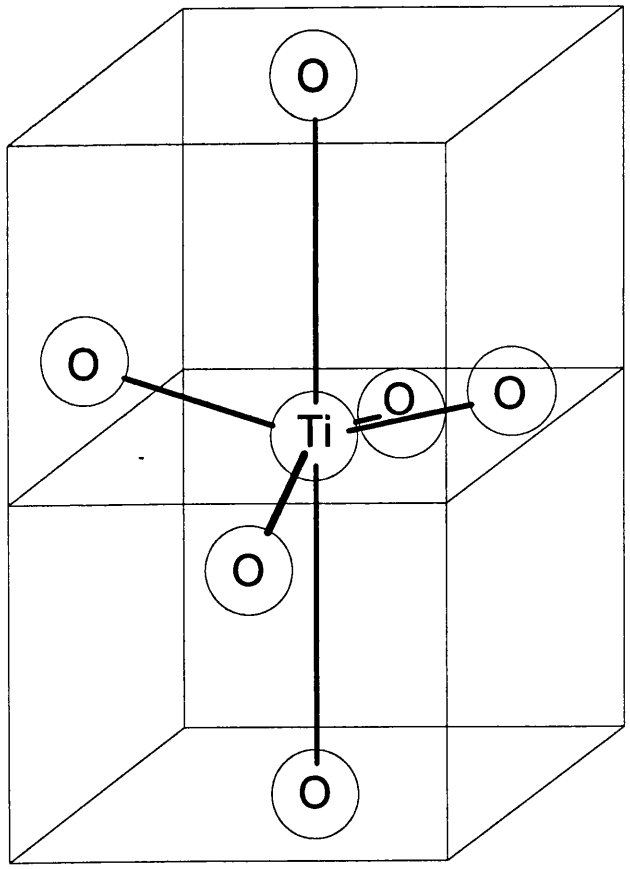

Figure 4.1. The Unit Cell Structure of Anatase.

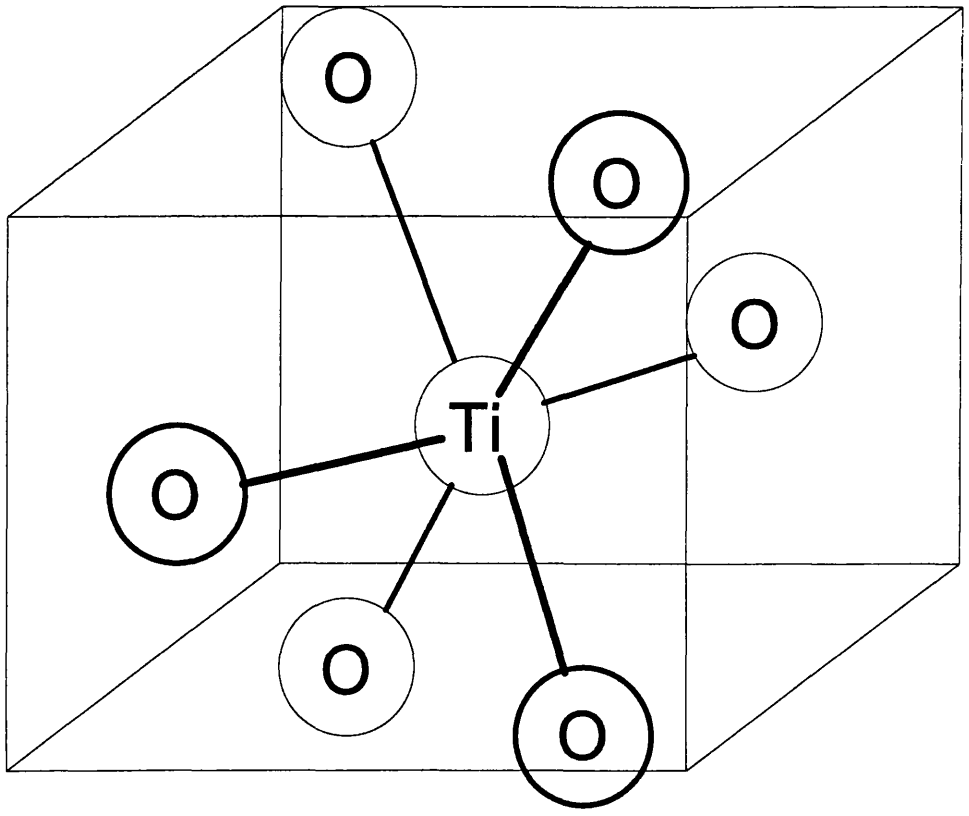

Figure 4.2. The Unit Cell Structure of Rutile.

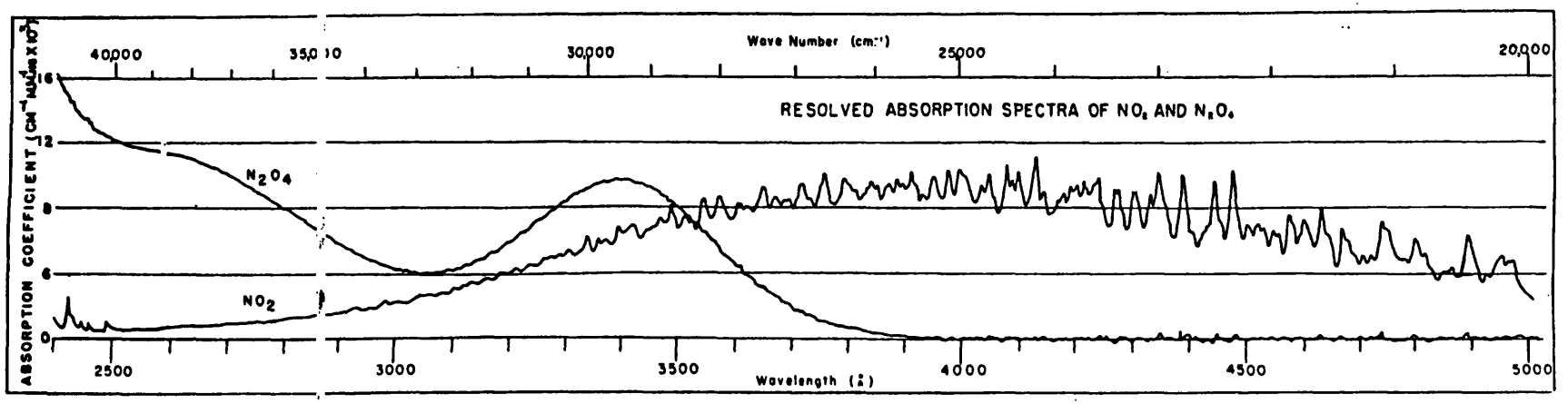

Figure 5.1 Absorption coefficients of NO_2 and N_2O_4 vs wavelength and wavenumber, measured at 25°C. (reproduced from reference 15 and 29)

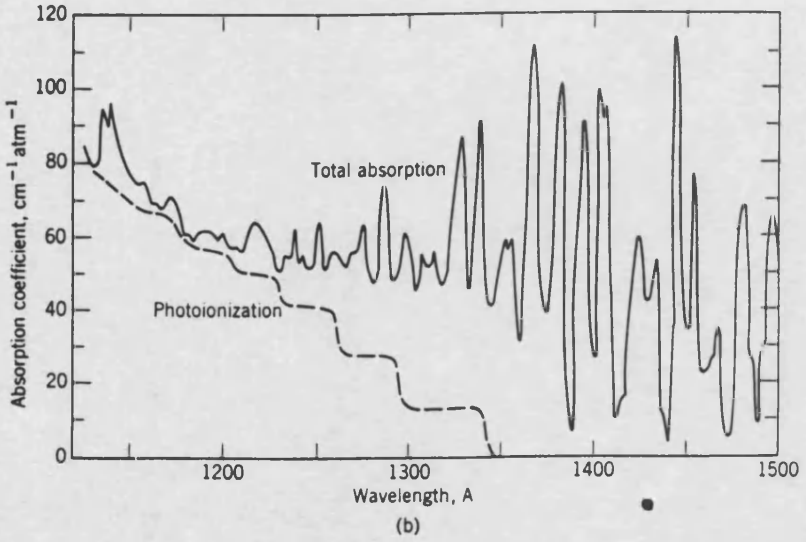

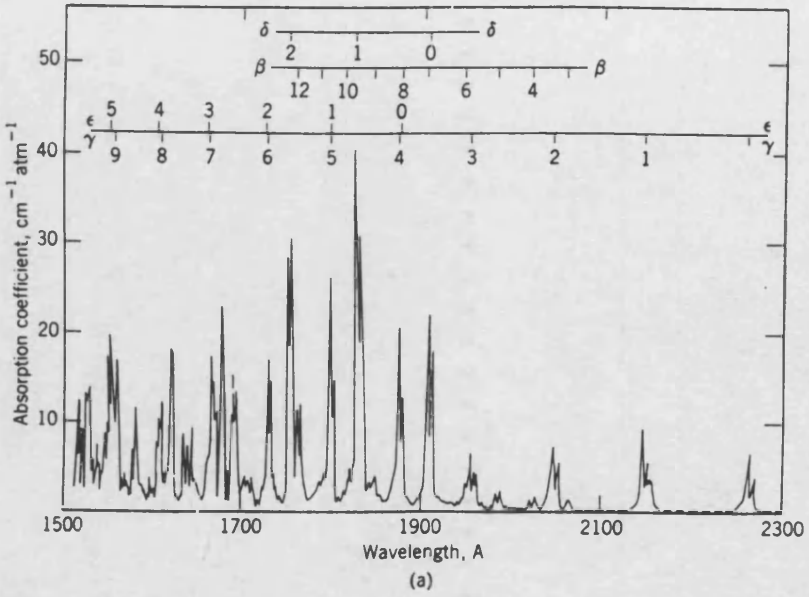

Figure 5.2 Absorption coefficients for NO vs wavelength (reproduced from reference 15)

Temperature (°C)	Φ_{O_2} 3660 Å	4047 Å	4358 Å[a]
23	0.95	0.36	(0.005)
23	0.92	0.35	(0.005)
71	1.02	0.41	(0.012)
71	0.95	0.42	(0.014)
133	0.99	0.50	(0.018)
133	0.97	0.52	(0.018)
223	1.00	0.70	(0.035)
223	b	0.71	(0.030)
293	b	0.90	b
293	b	0.92	b

Figure 5.3 Quantum yields of oxygen as a function of temperature at several wavelengths.
(reproduced from reference 14)

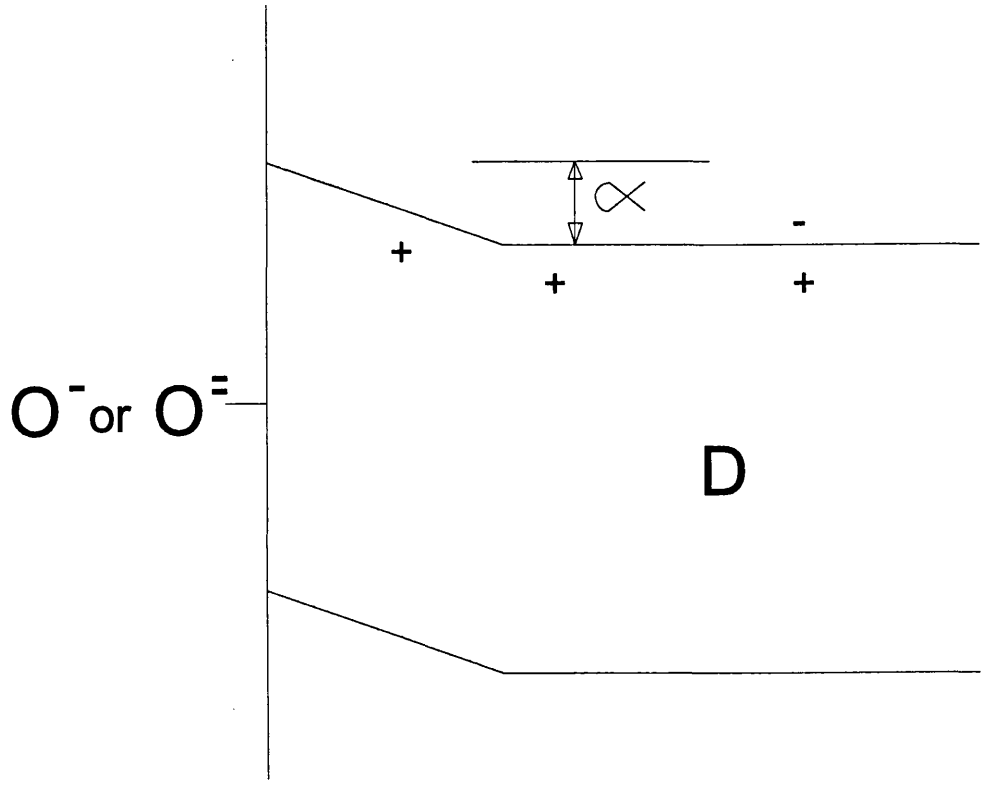

Figure 5.4a. Tanaka.[9] N_2O model for dark conditions.

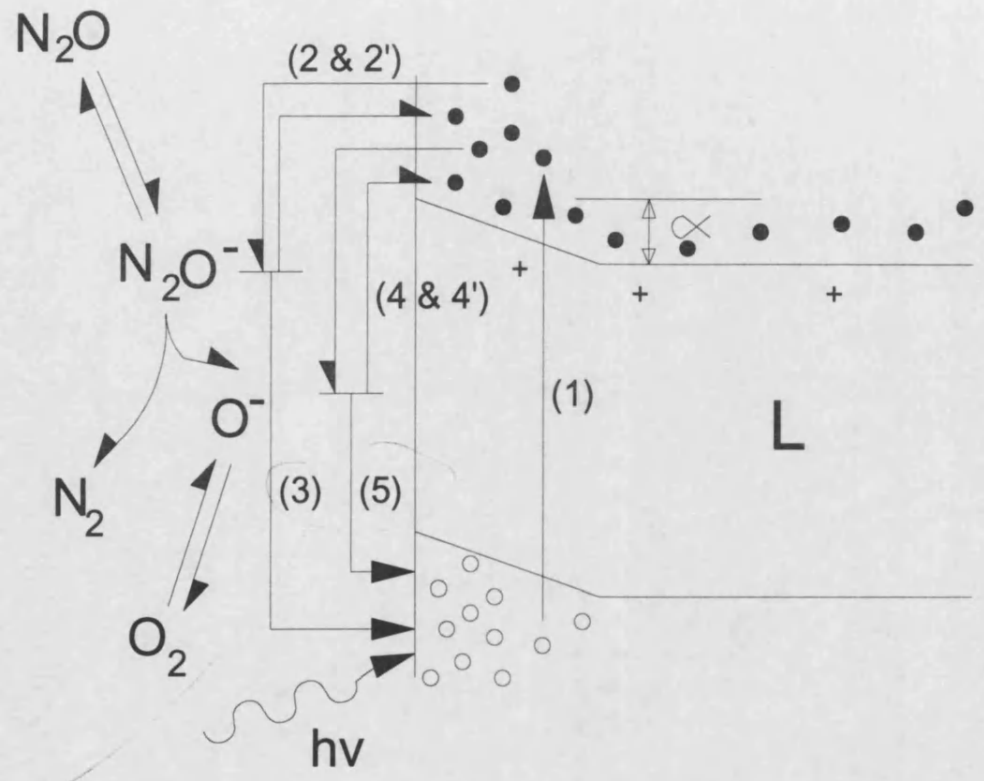

Figure 5.4b. Tanaka[9] N_2O rate model, under illumination.

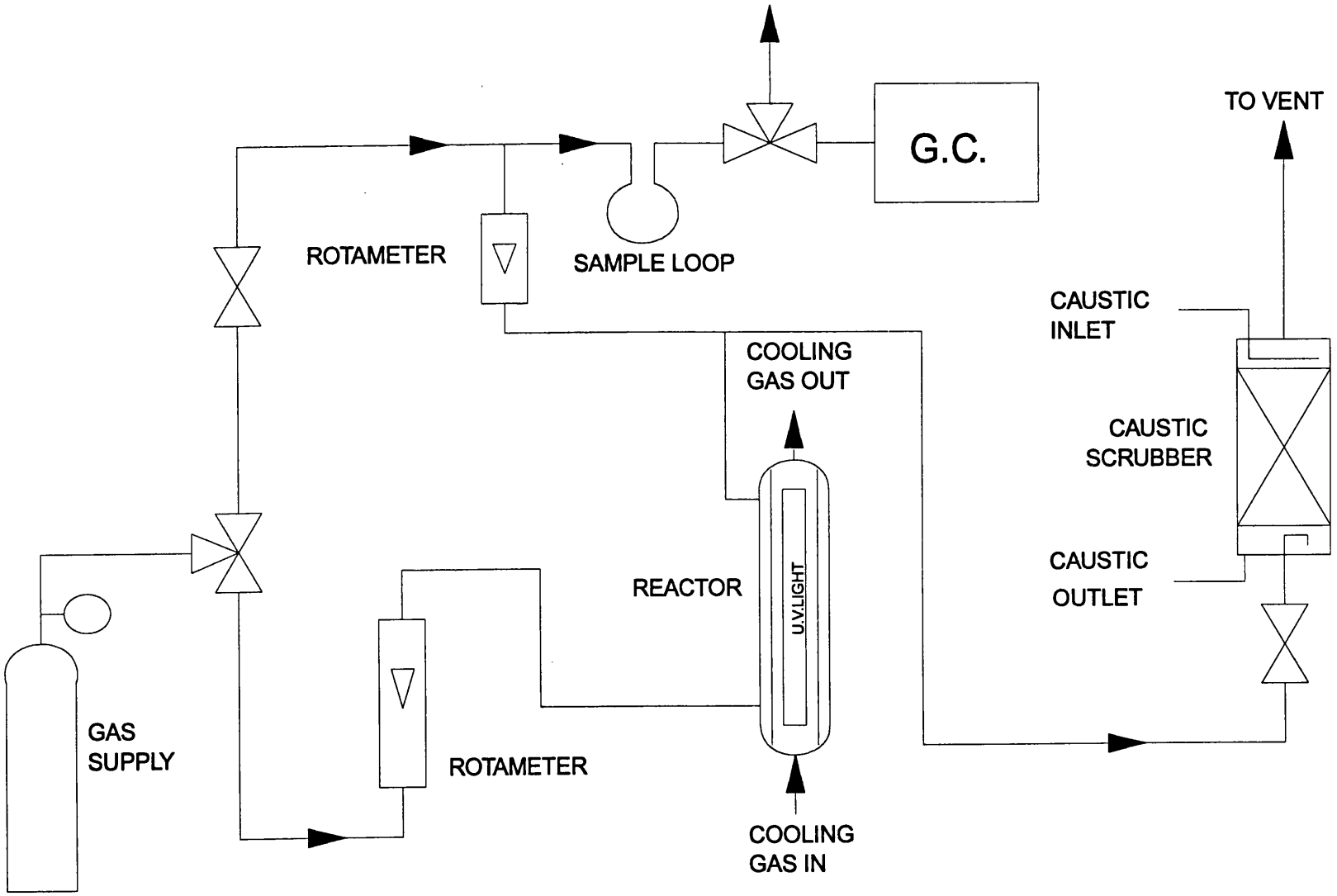

Figure 6.1. Layout of the experimental rig.

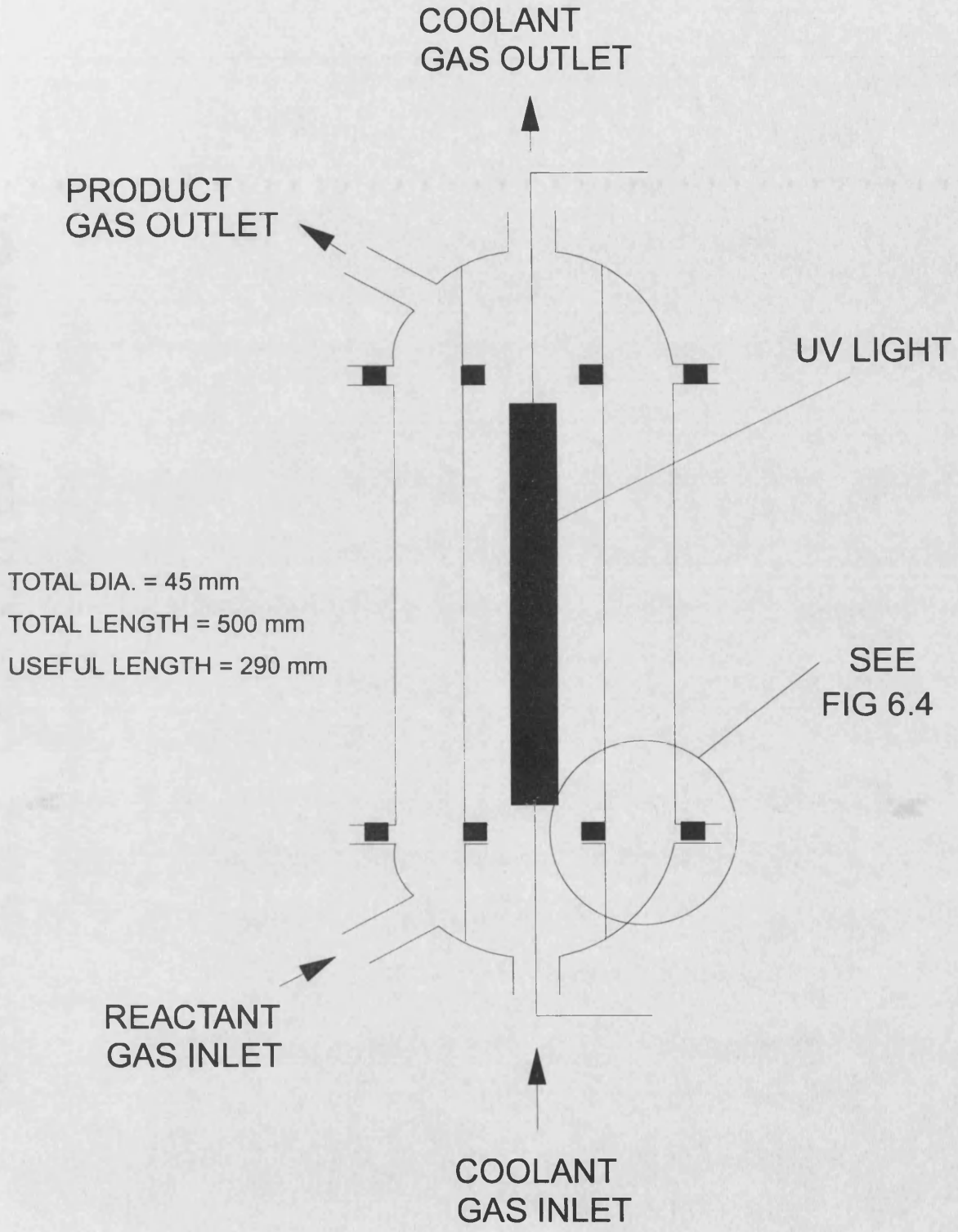

FIGURE 6.2. PHOTOCATALYTIC REACTOR

Absolute Spectral Power
8 Watt Black-Light-Blue

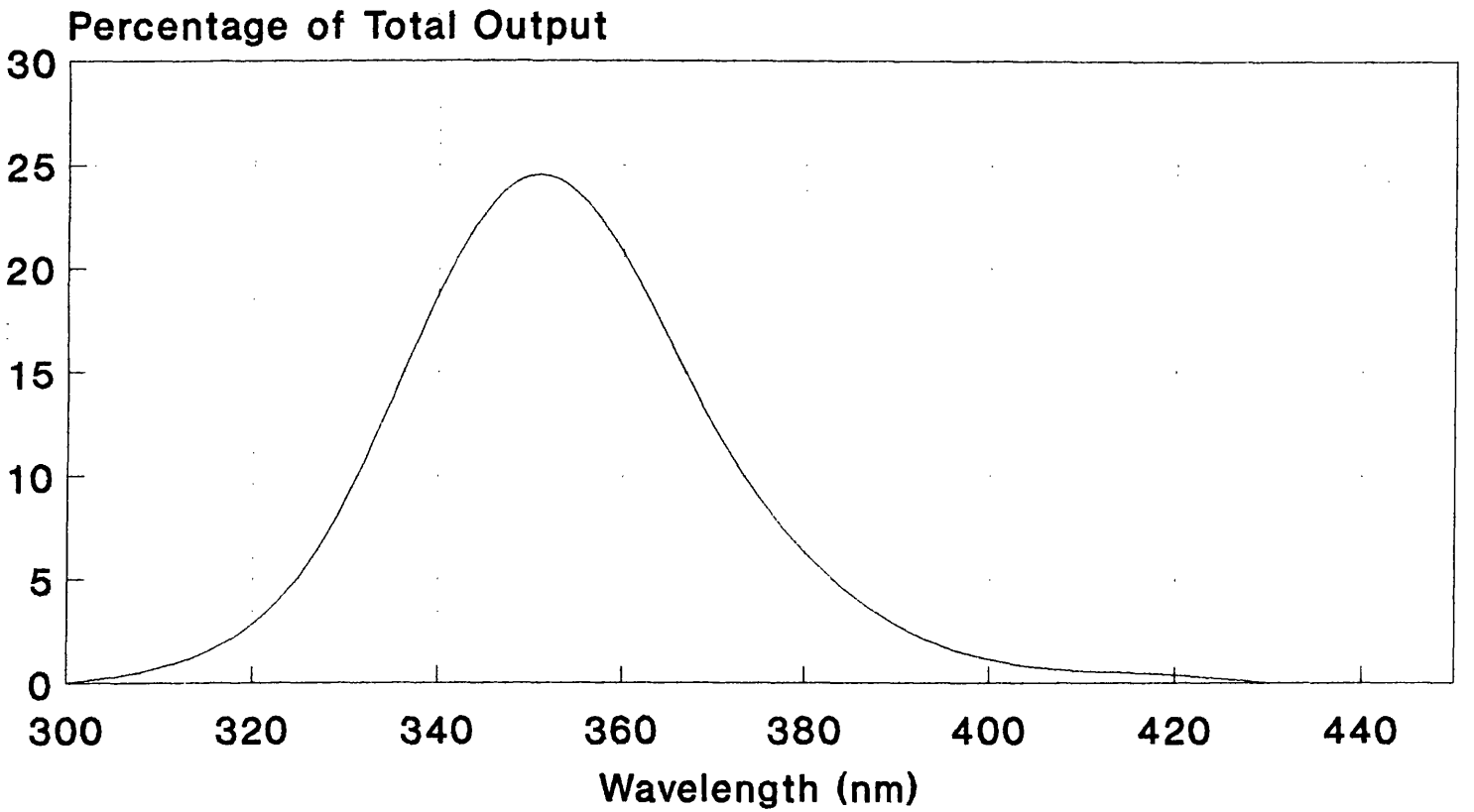

UV Power Output = 0.8 watts
Useful UV Output = 0.56 watts

Figure 6.3

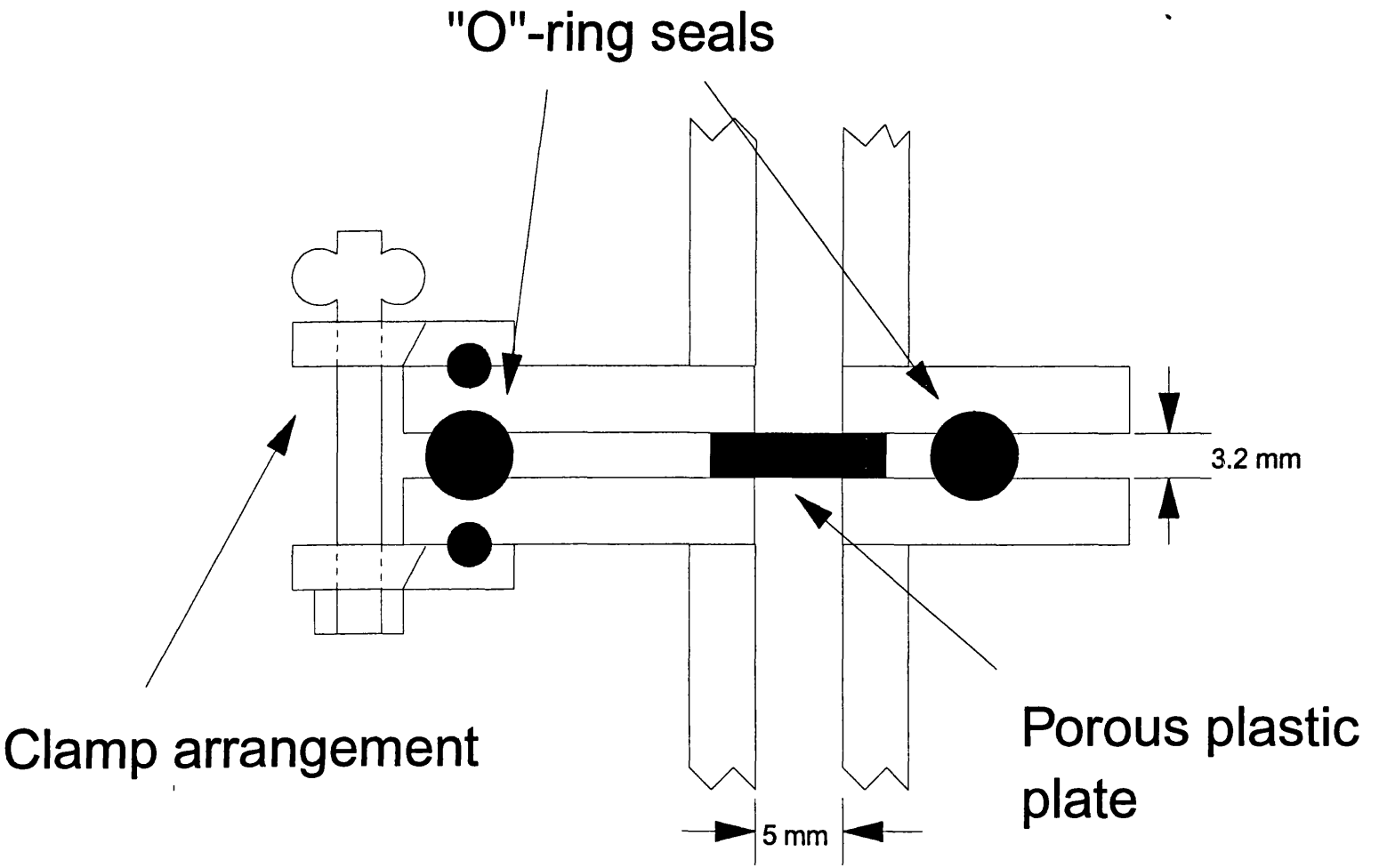

FIGURE 6.4. REACTOR SEAL DETAIL

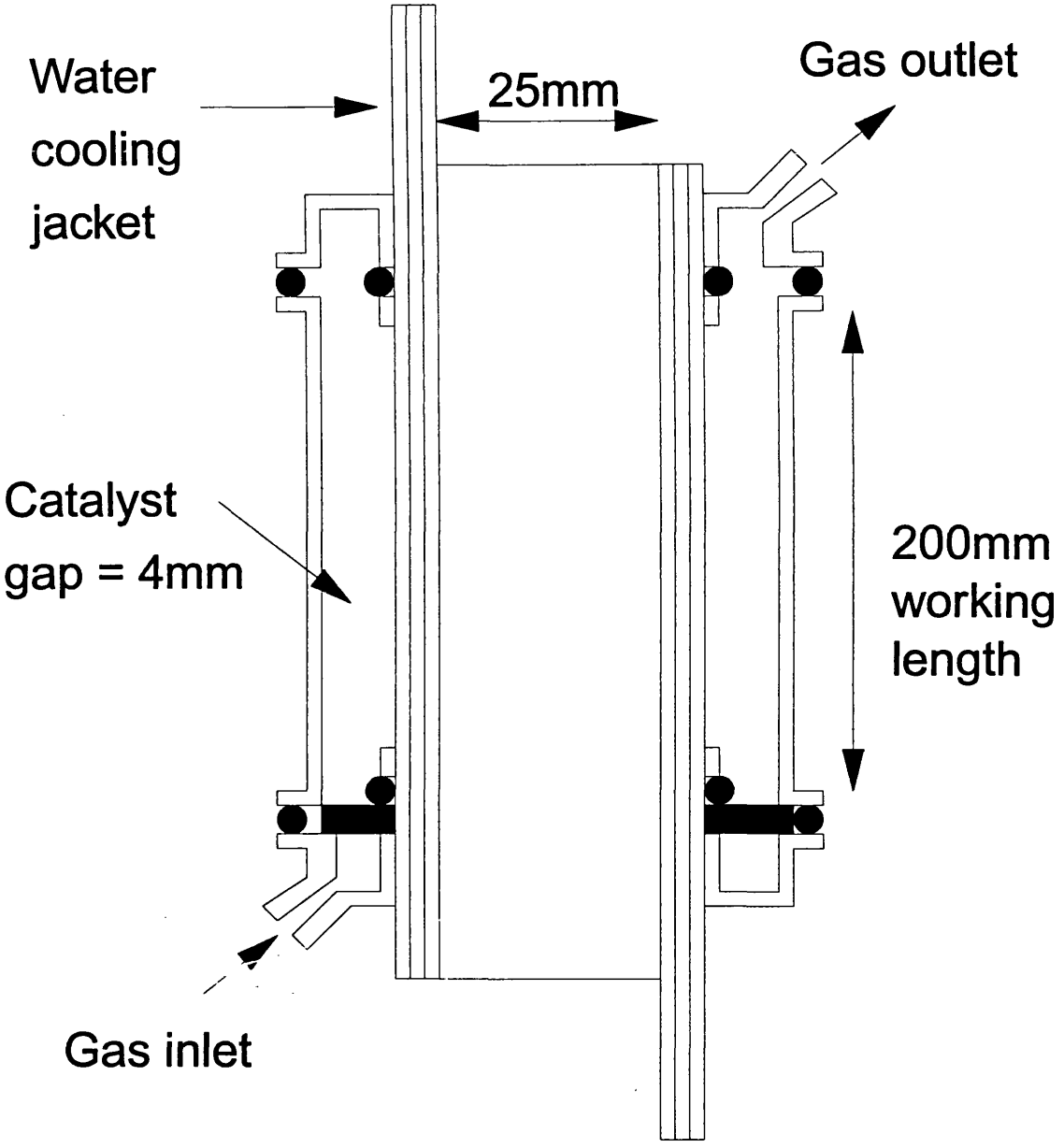

Figure 6.5 Photocatalytic reactor (250 watt version)

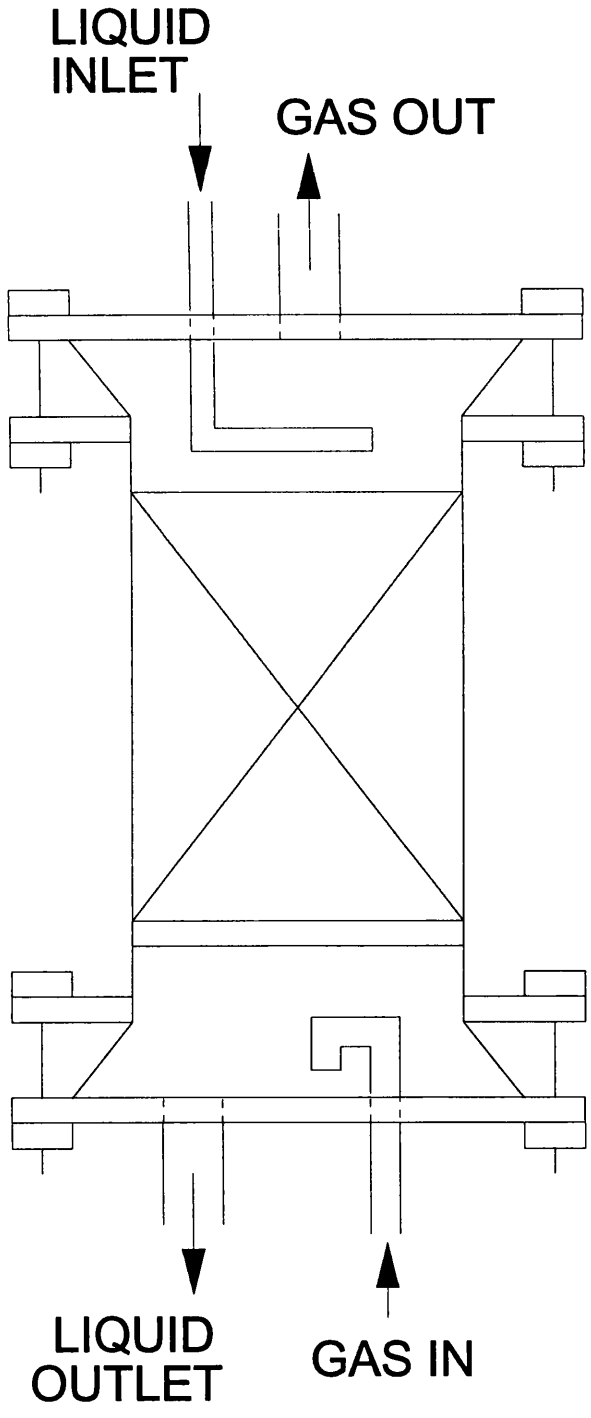

FIGURE 6.6. CAUSTIC SCRUBBER

Absolute Spectral Power
250 Watt Medium Pressure Mercury

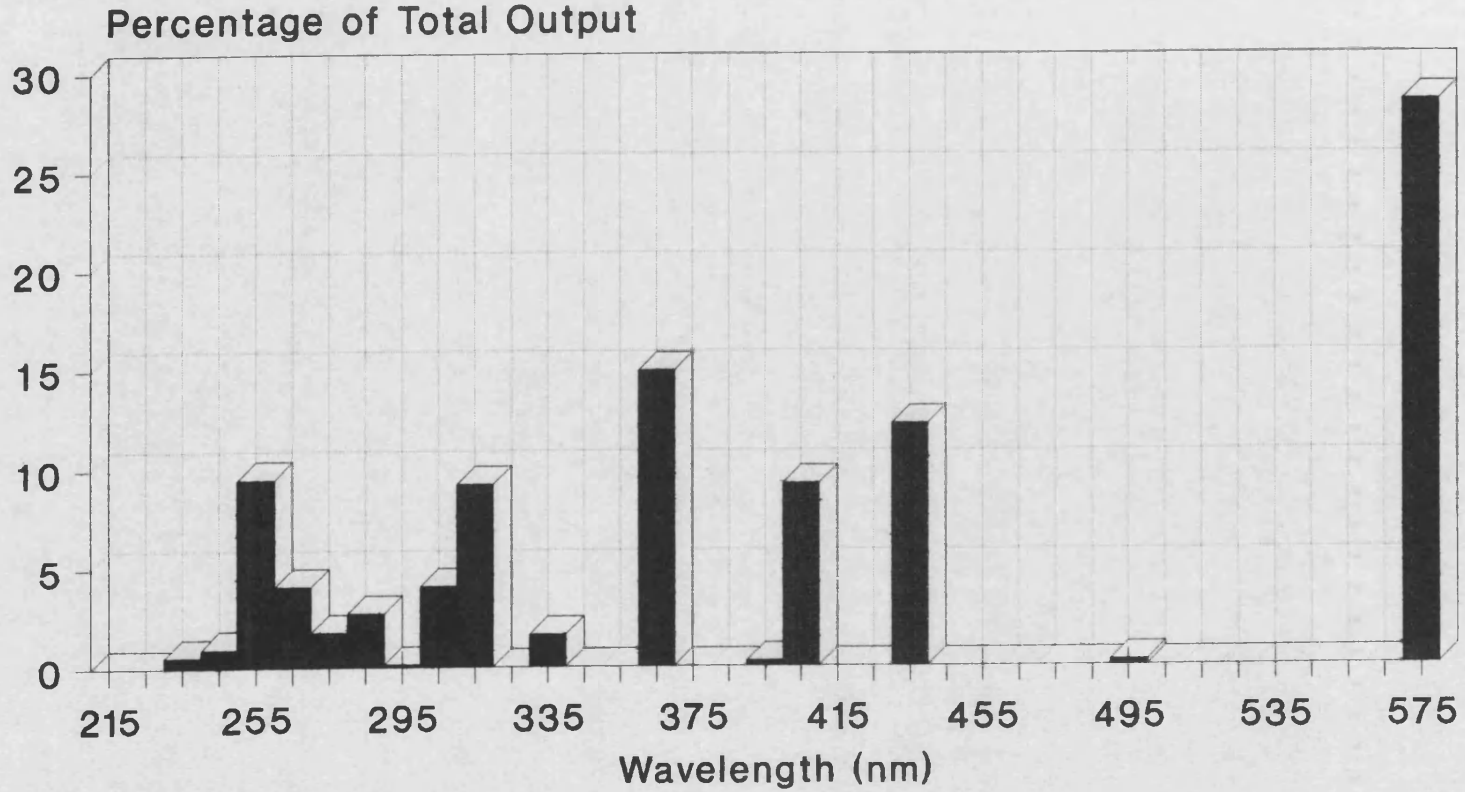

UV Power Output = 20 watts
Useful UV Output = 9.0 watts

Figure 6.7

Plot of BET Equation for Degussa P-25.

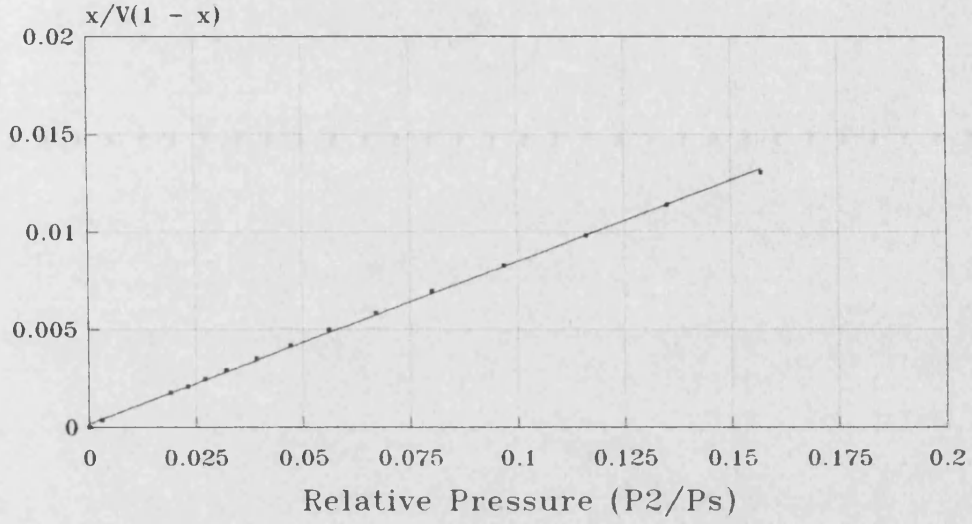

Surface area = 53.02 m2/g

Figure 7.1

Plot of BET Equation for Size Modified Degussa P-25.

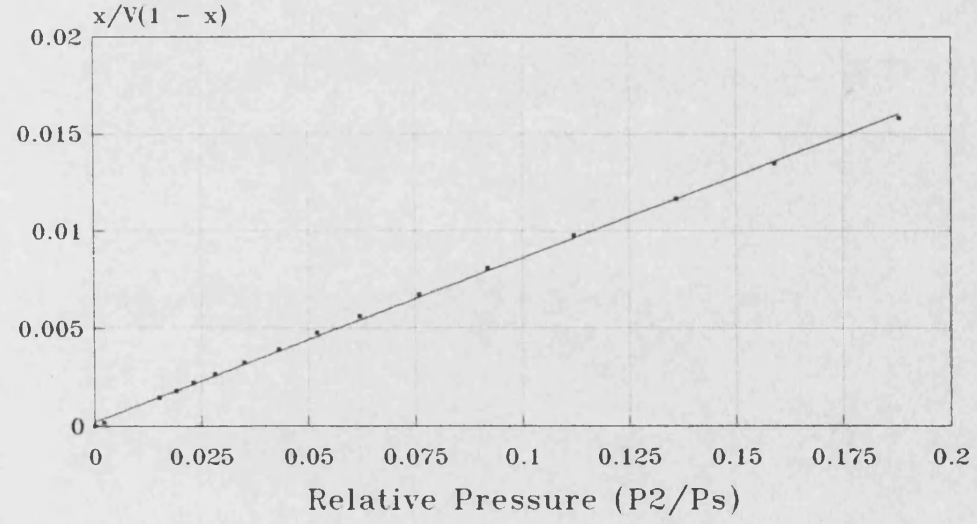

Surface Area = 52.10 m2.g

Figure 7.2

Adsorption Isotherm for
Degussa P-25.

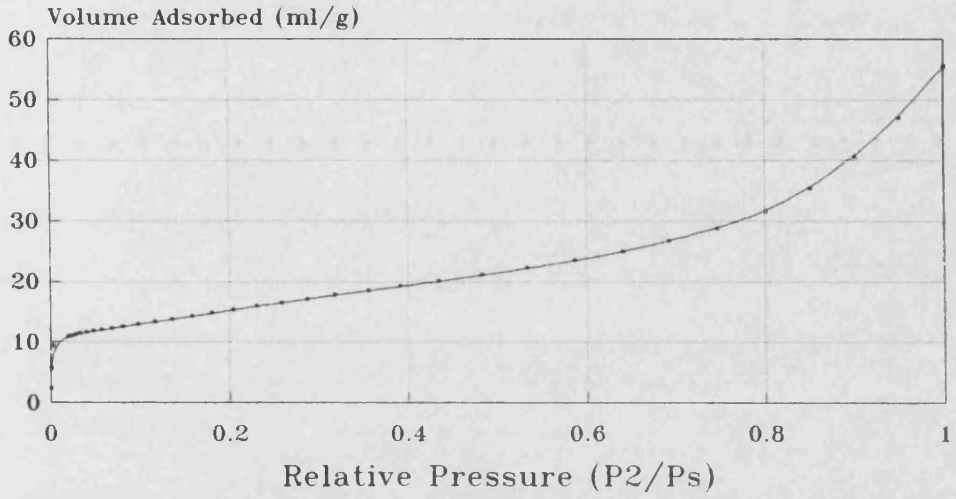

Figure 7.3

Adsorption Isotherm for
Size Modified Degussa P-25.

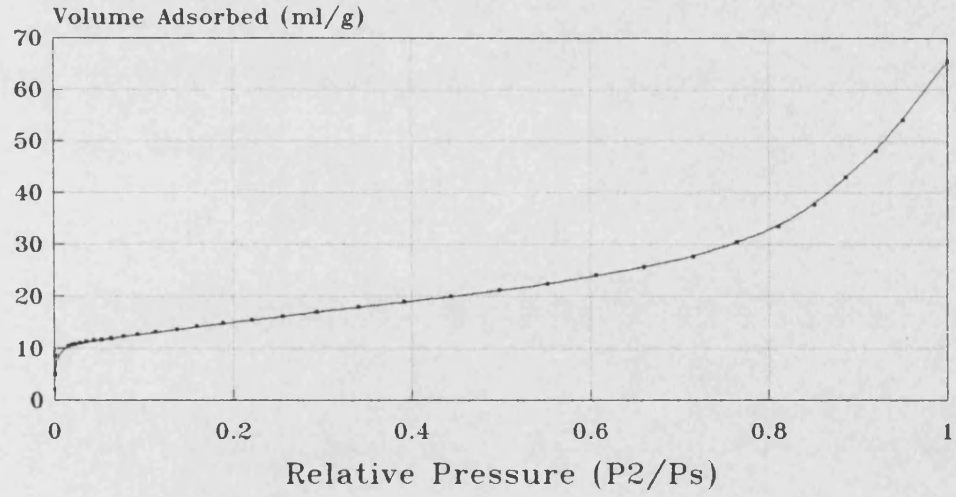

Figure 7.4

X-Ray Diffraction Data for TiO2 from SCM.

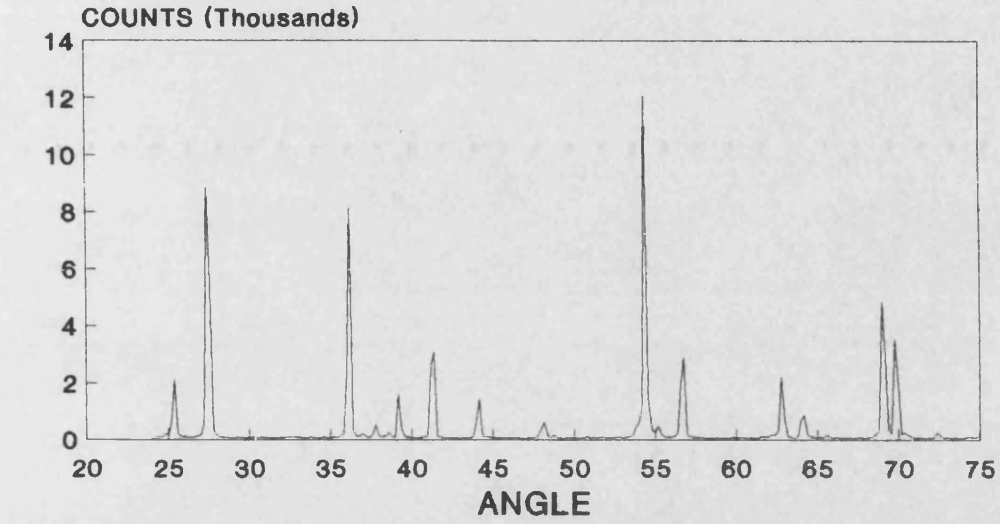

Anatase:Rutile Ratio = 23:77

Figure 7.5

X-Ray Diffraction Data for TiO2 from Tioxide

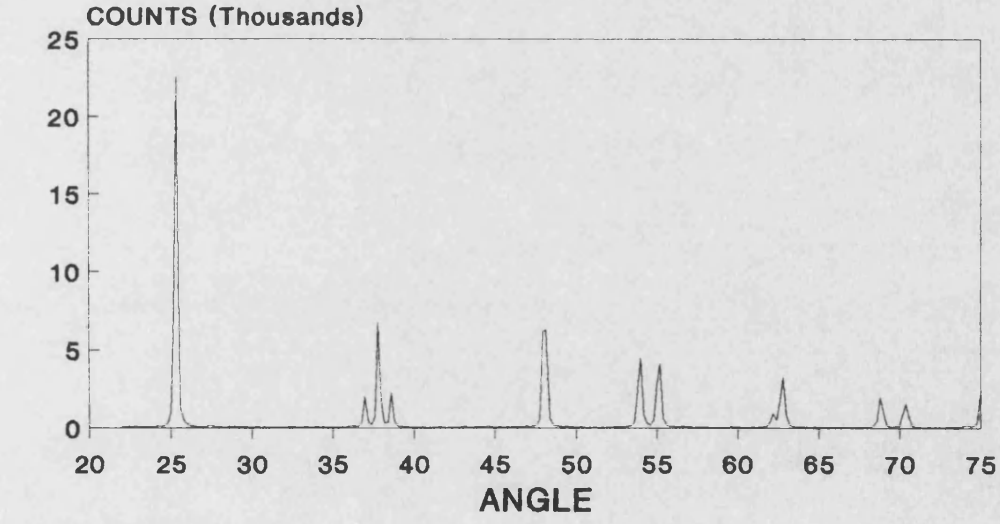

Anatase:Rutile Ratio = 99:1

Figure 7.6

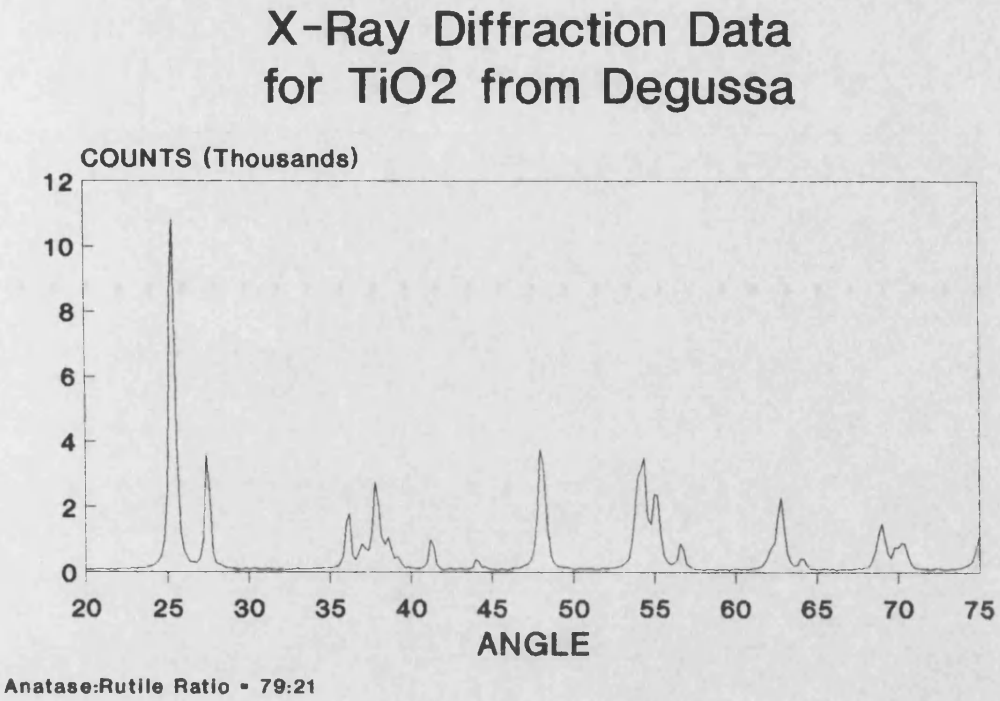

Figure 7.7

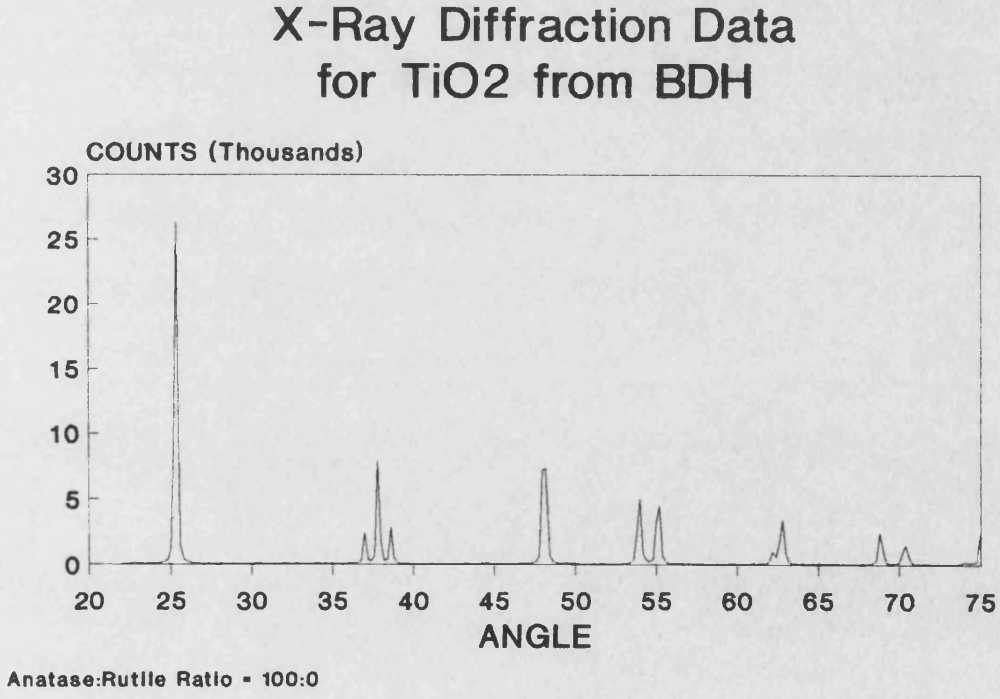

Figure 7.8

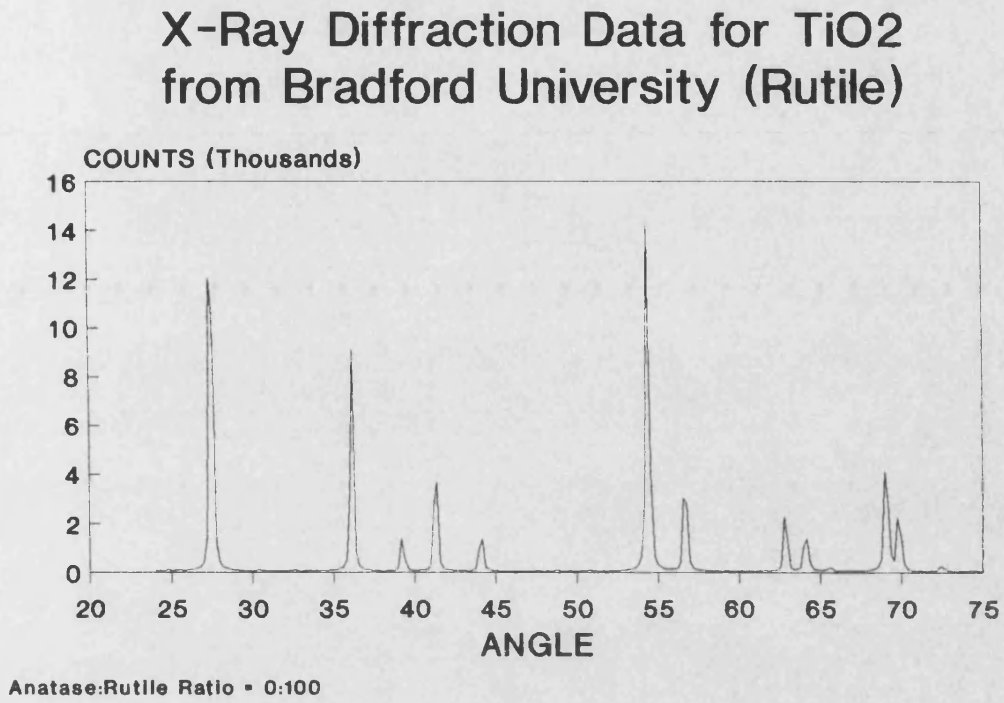
X-Ray Diffraction Data for TiO2
from Bradford University (Rutile)
COUNTS (Thousands)
16
14
12
10
8
6
4
2
0
20
25
30
35
40
45
50
55
60
65
70
75
ANGLE
Anatase:Rutile Ratio = 0:100

Figure 7.9

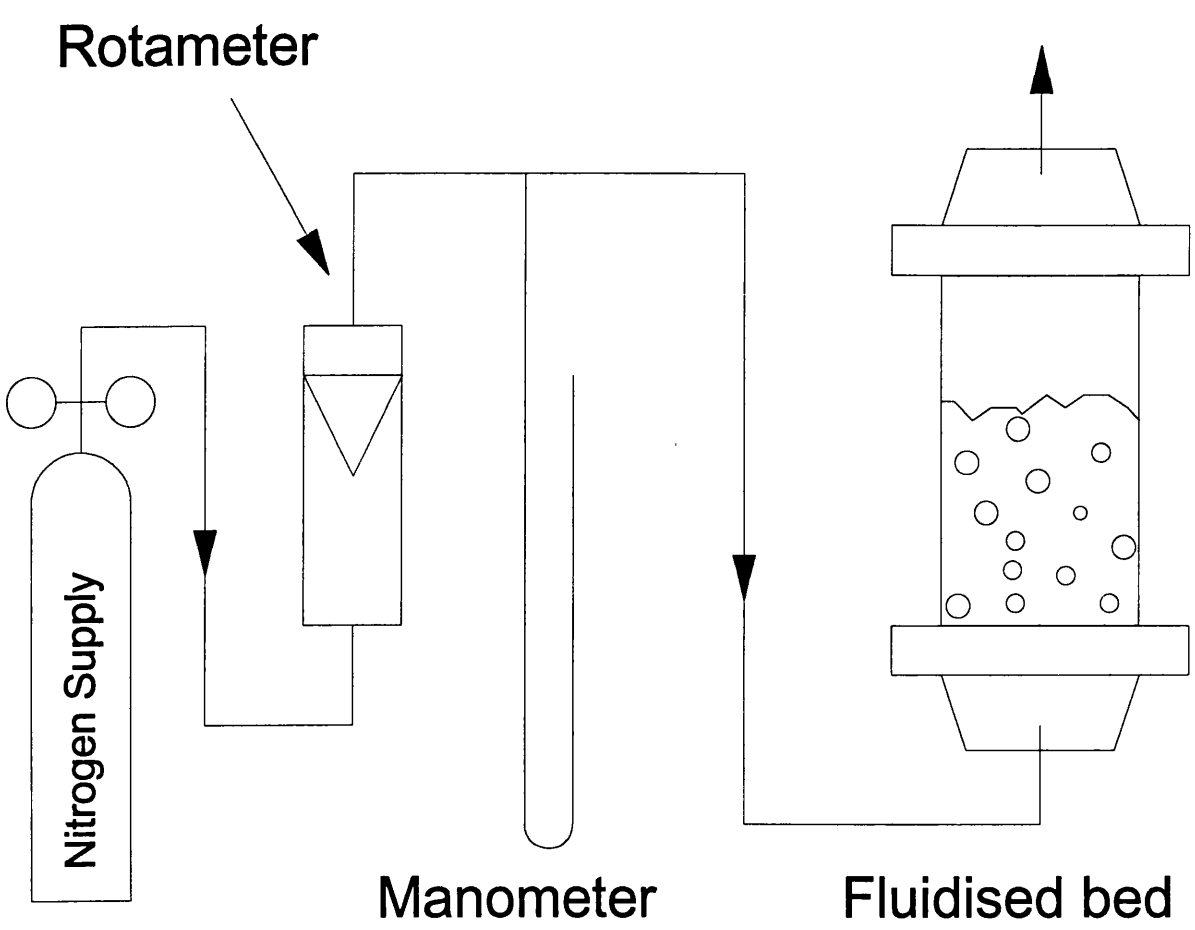

Figure 7.10. A Flat-Fluidised Bed
for Determining Fluidising Properties.

Pressure Drop Curve
For the Porous Distribution Plate

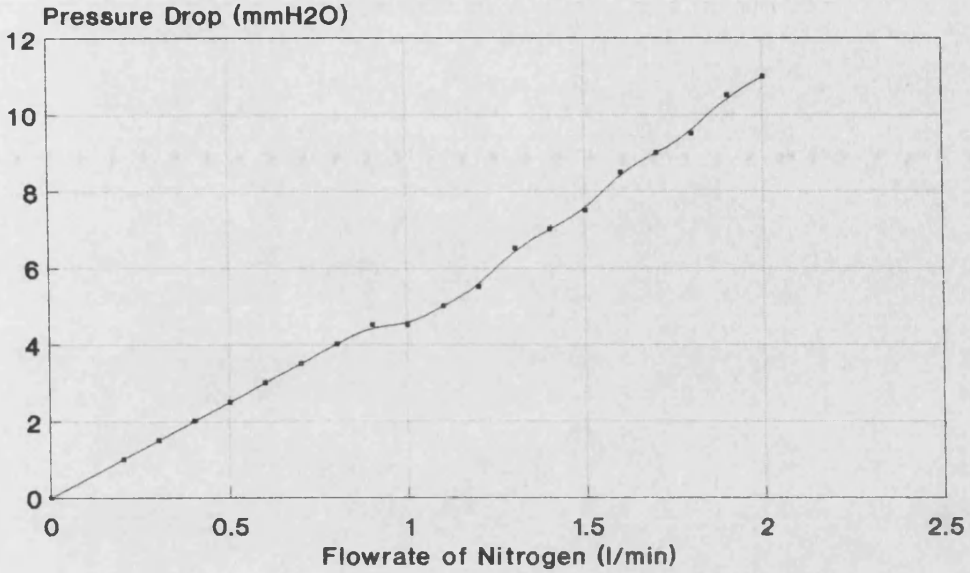

Figure 7.11

Pressure Drop Curve
TiO2 from Tioxide

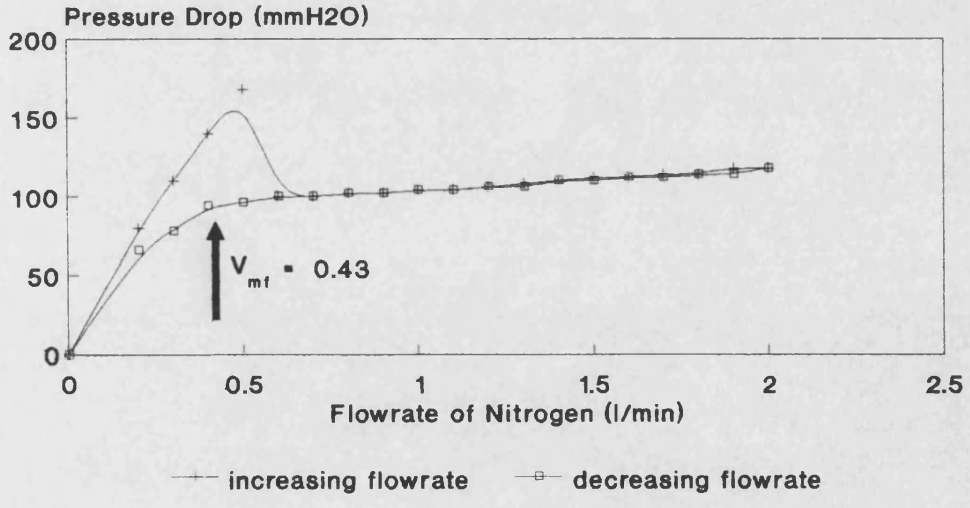

Figure 7.12.

Initial bed height of 145 mm
Particle size 180 - 150 microns

Pressure Drop Curve
TiO2 from Tioxide

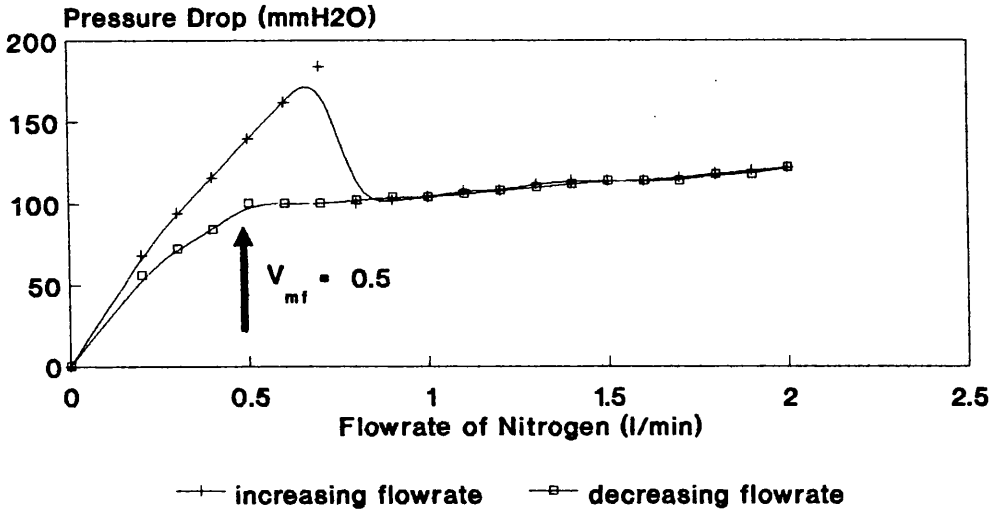

Figure 7.13

Initial bed height of 146 mm
Particle size 212 - 180 microns

Pressure Drop Curve
TiO2 from Tioxide

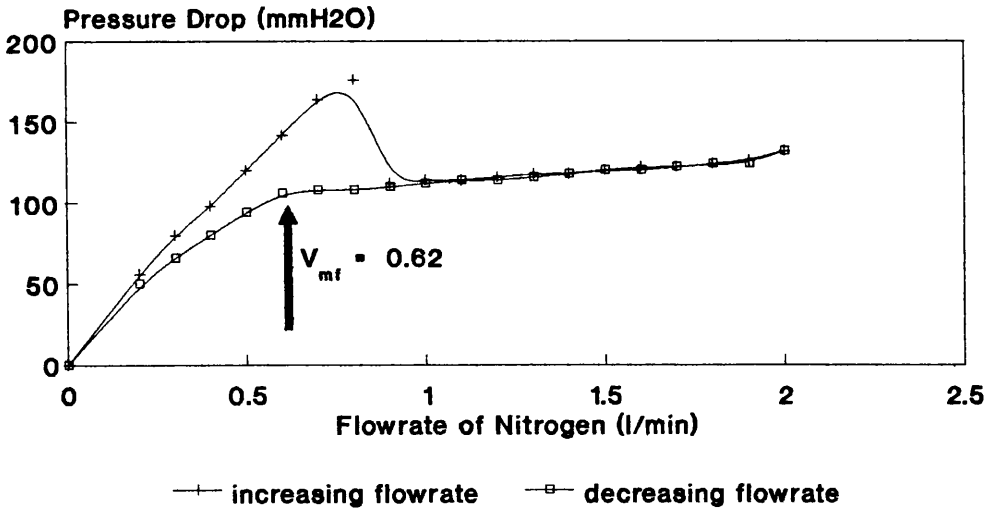

Figure 7.14

Initial bed height of 148 mm
Particle size 250 - 212 microns

Pressure Drop Curve For Degussa P-25

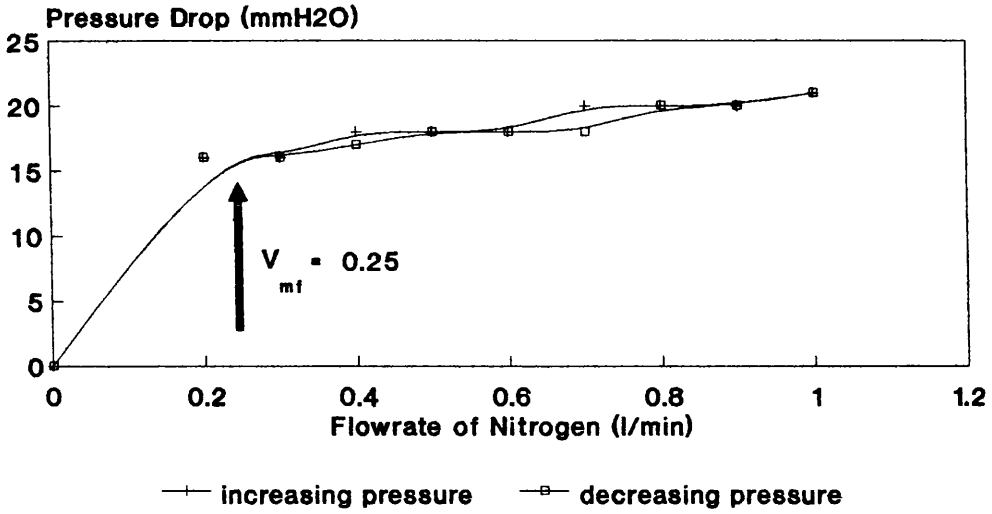

Figure 7.15

Initial bed height of 146 mm
Particle size 250 - 150 microns

Pressure Drop Curve for Gamma Alumina

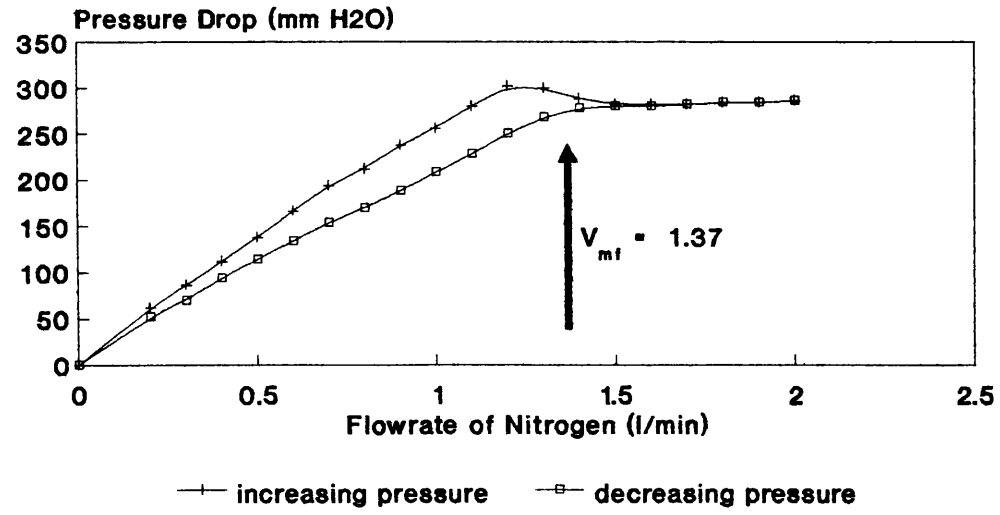

Figure 7.16

Initial bed height 147 mm
particle size 250 - 150 microns

Pressure Drop Curve for Size Modified Degussa P-25

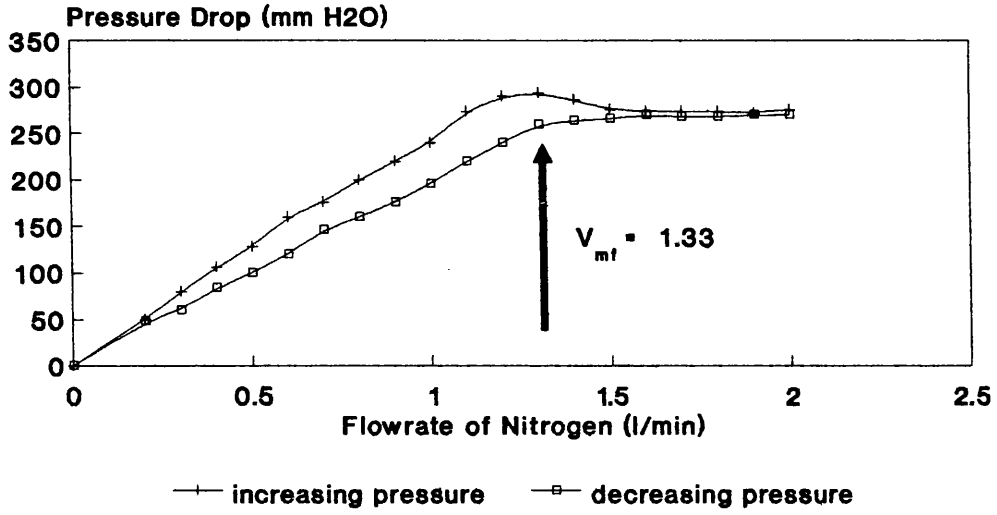

Figure 7.17

Initial bed height 150 mm
particle size 250 - 150 microns

Pressure Drop Curve for Size Modified P-25 + 1/2 % Fe3+

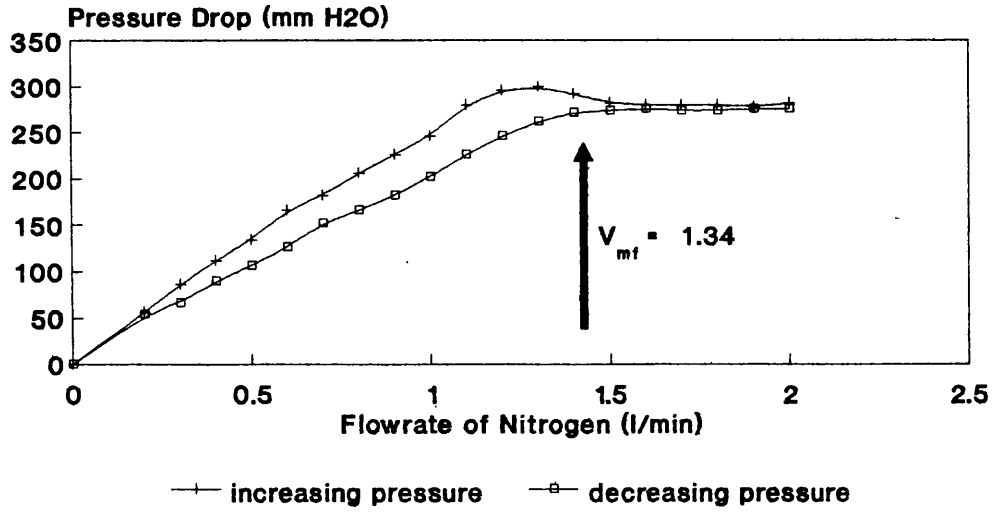

Figure 7.18

Initial bed height 151 mm
particle size 250 - 150 microns

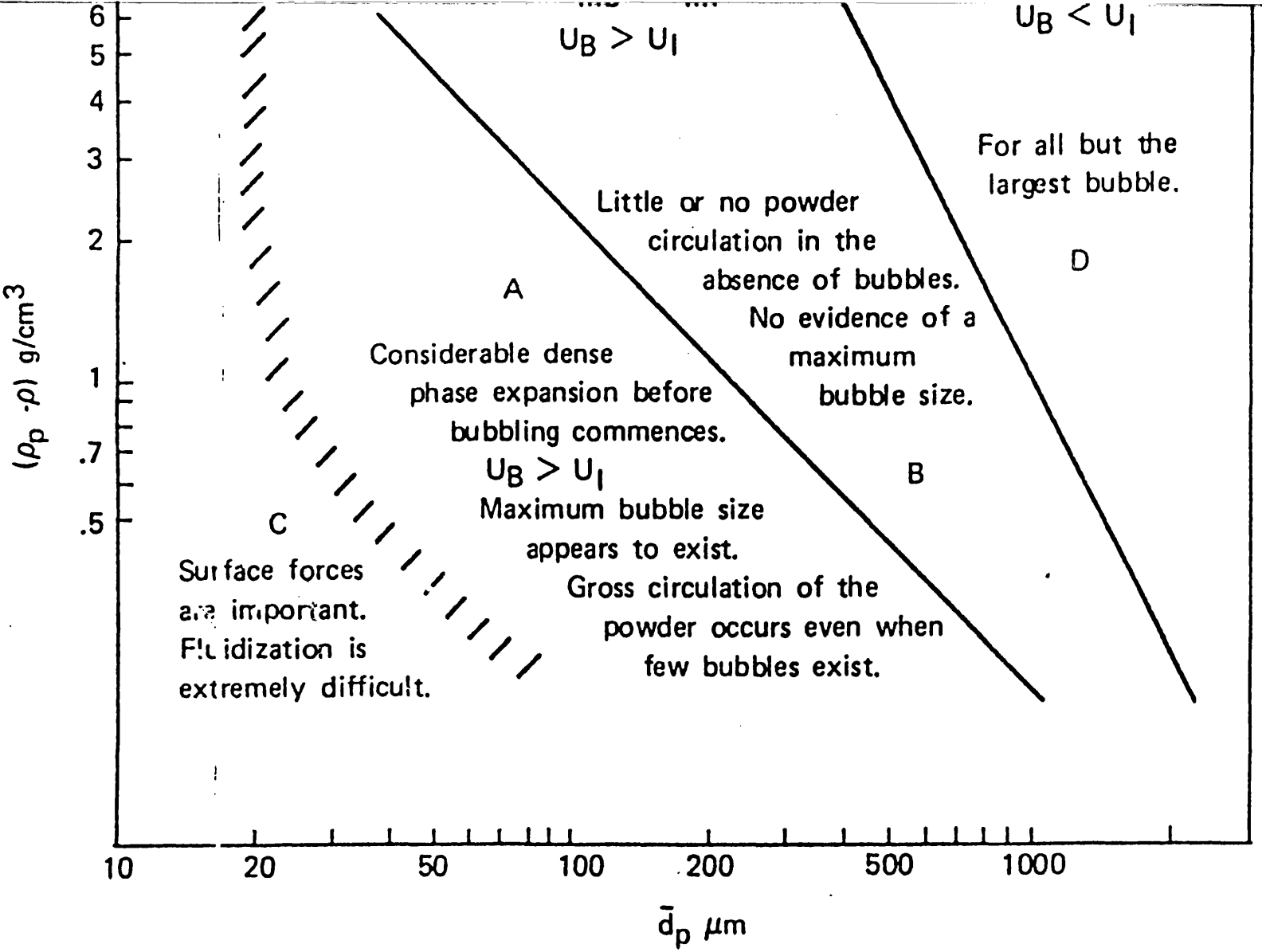

Figure 7·19 Geldart's particle classification diagram.

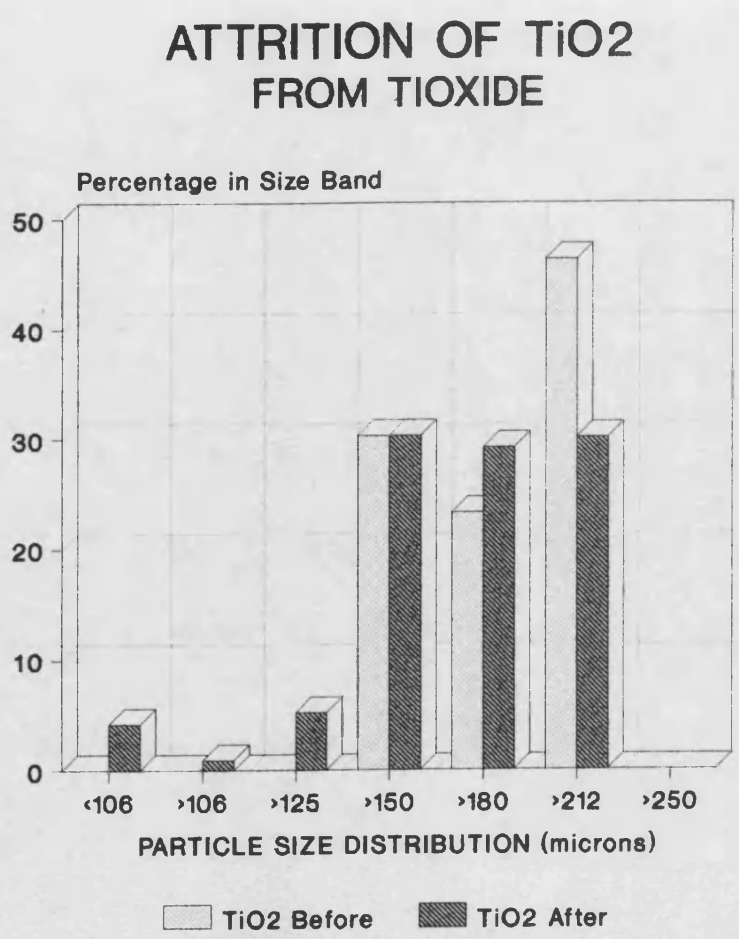

Figure 7.20

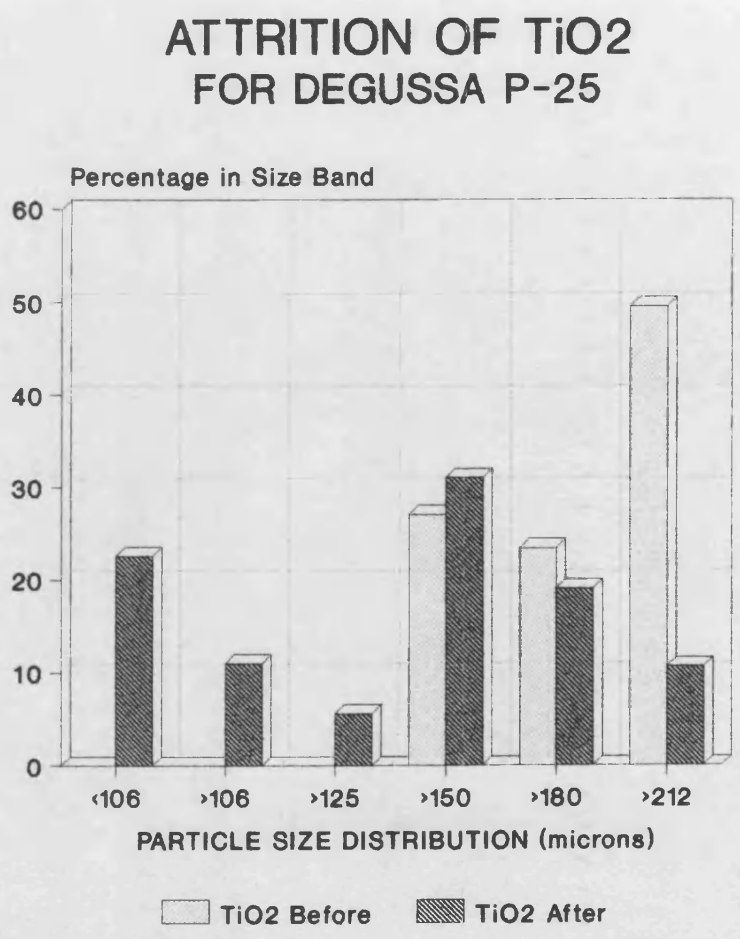

Figure 7.21

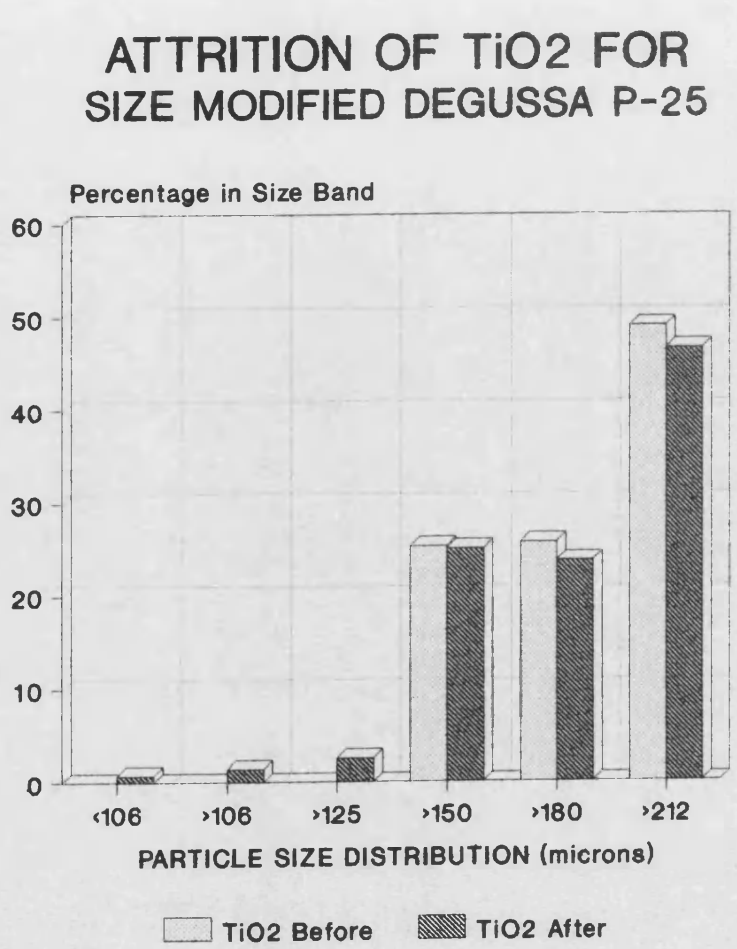
ATTRITION OF TiO2 FOR
SIZE MODIFIED DEGUSSA P-25
Percentage in Size Band
60
50
40
30
20
10
0
<106
>106
>125
>150
>180
>212
PARTICLE SIZE DISTRIBUTION (microns)
TiO2 Before
TiO2 After

Figure 7.22

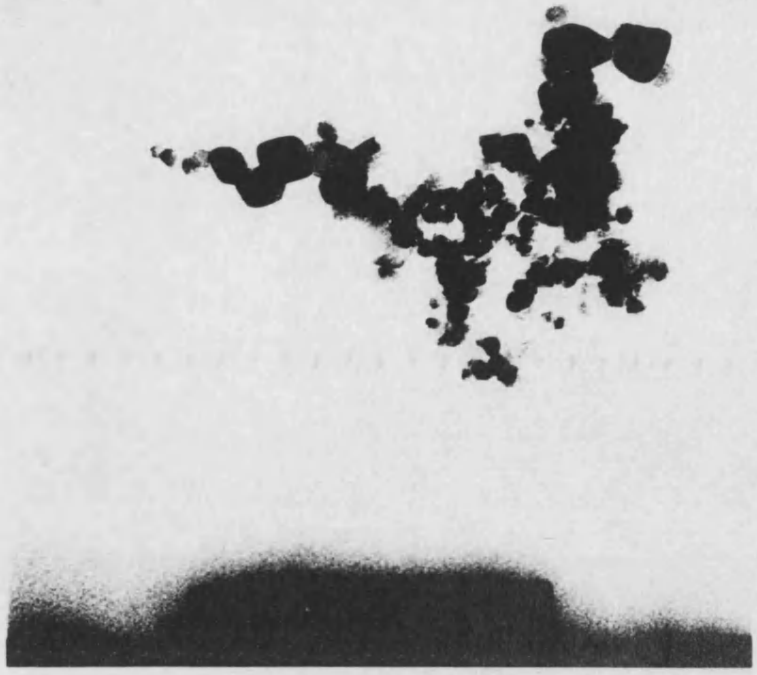

Figure 7.23. Degussa P-25 primary particles by TEM.

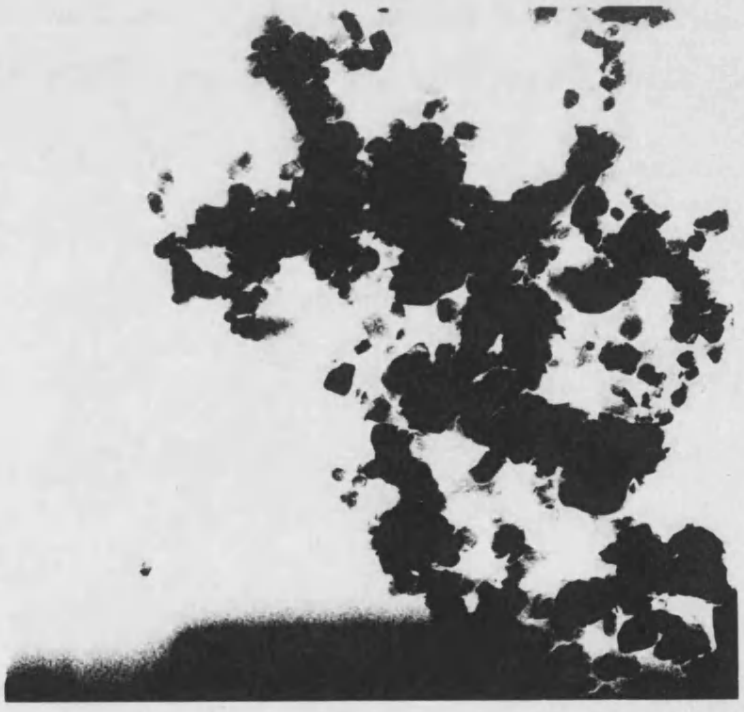

Figure 7.24. Degussa P-25 primary particles by TEM.

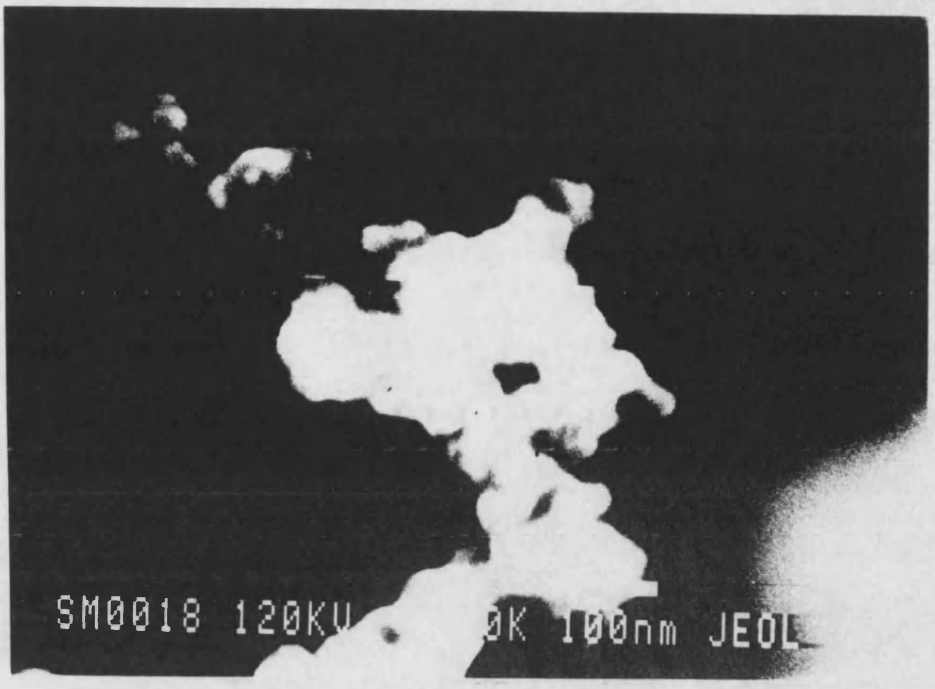

Figure 7.25. Degussa P-25 primary particles by SEM.

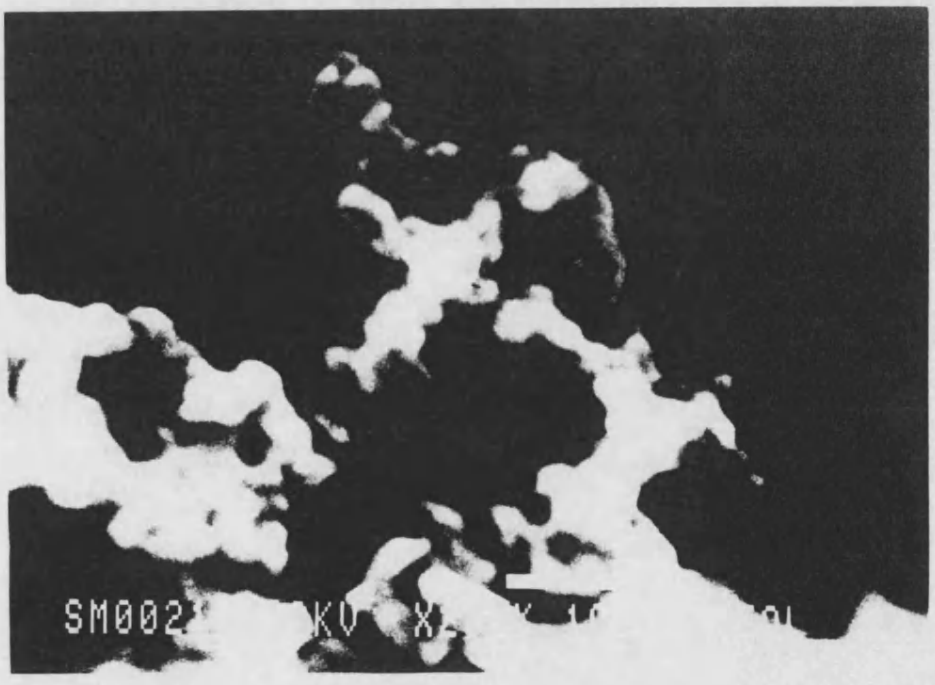

Figure 7.26. Degussa P-25 primary particles by SEM.

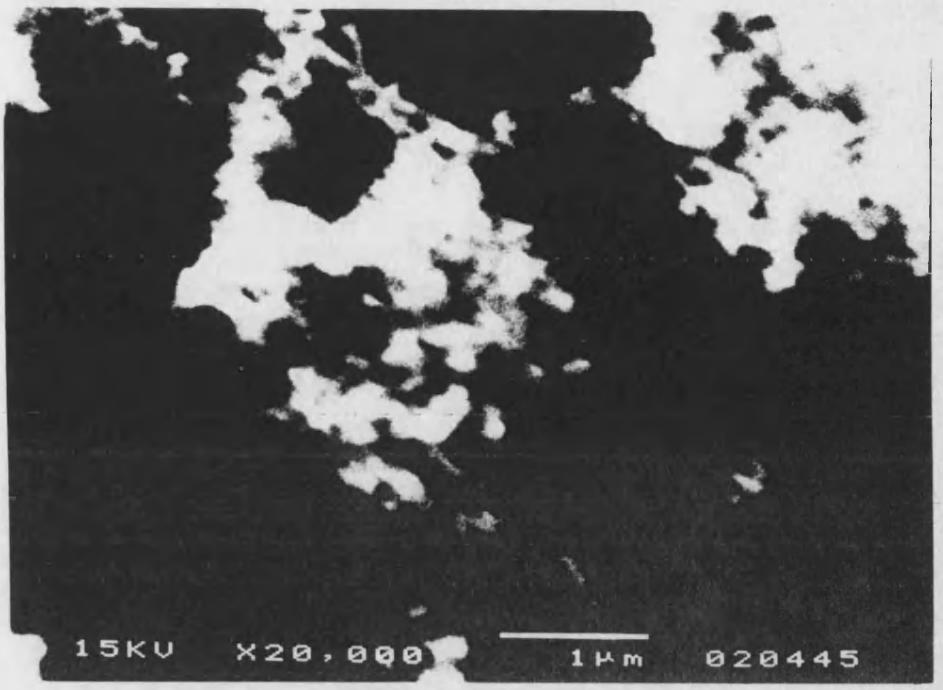

Figure 7.27. Degussa P-25, surface view of agglomerates by SEM.

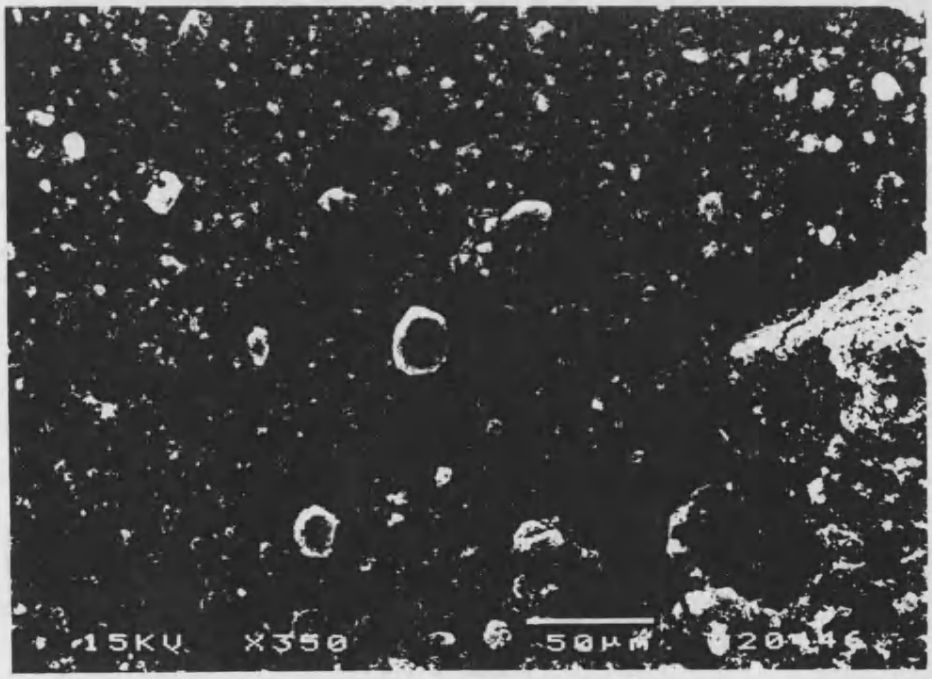

Figure 7.28. Degussa P-25, view of agglomerated particles by SEM.

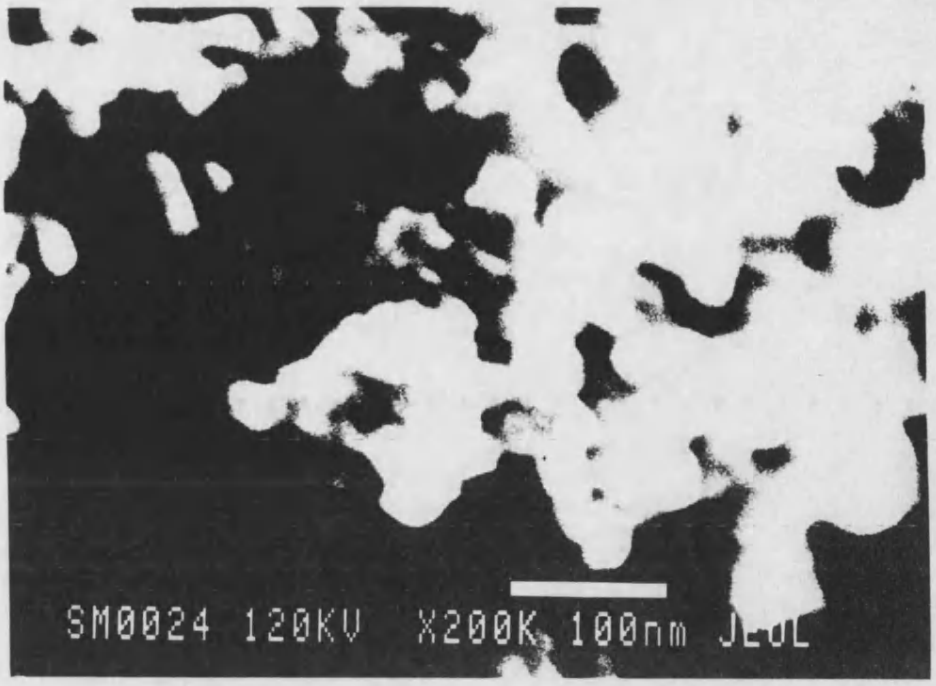

Figure 7.29. Size Modified Degussa P-25, surface view of particles by SEM.

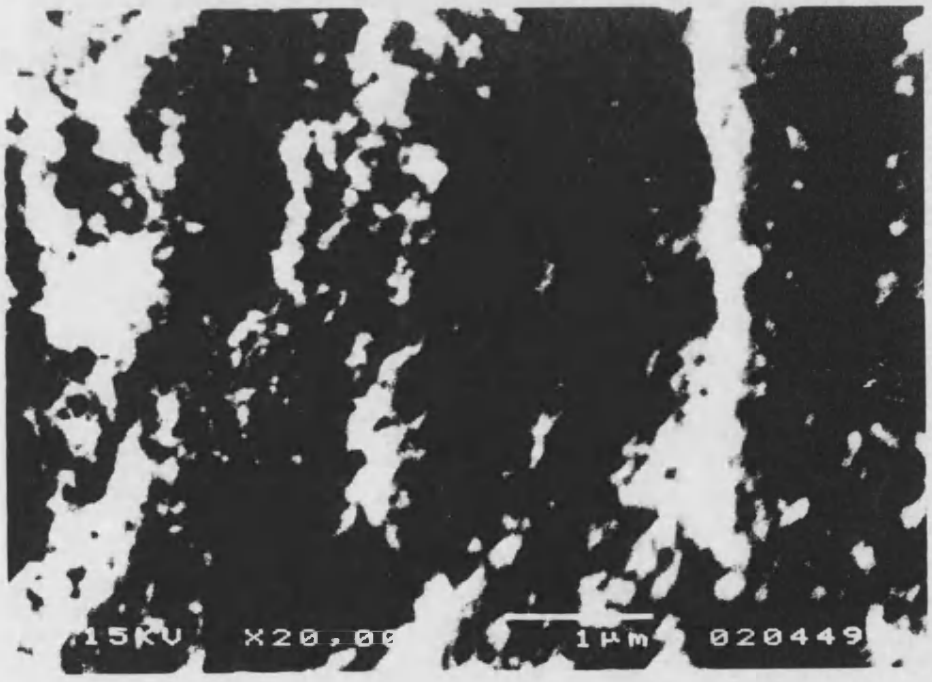

Figure 7.30. Size Modified Degussa P-25, edge view of particles by SEM.

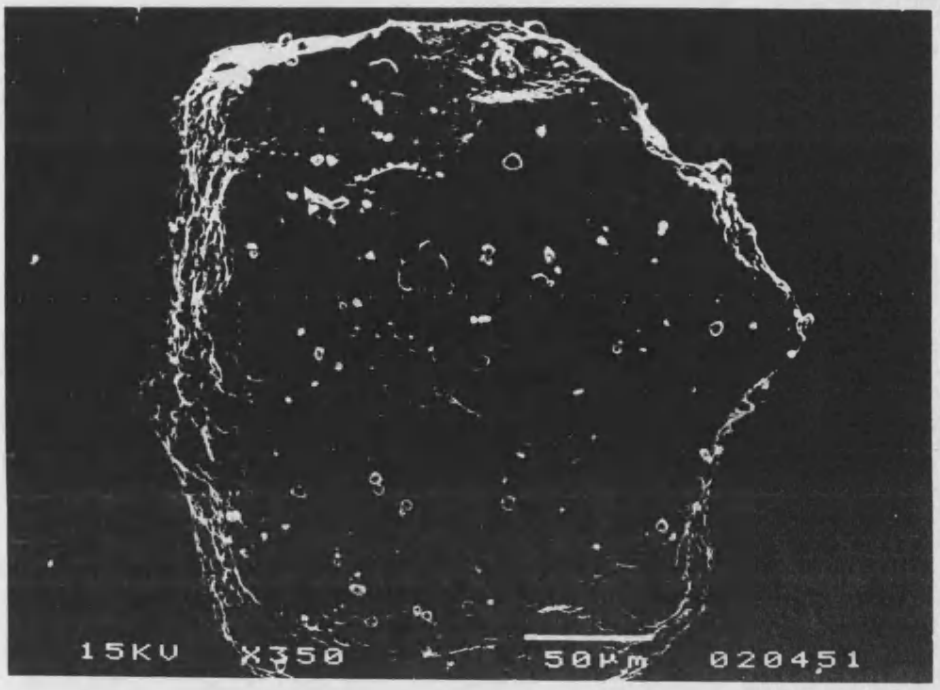

Figure 7.31. Size Modified Degussa P-25, view of particles by SEM.

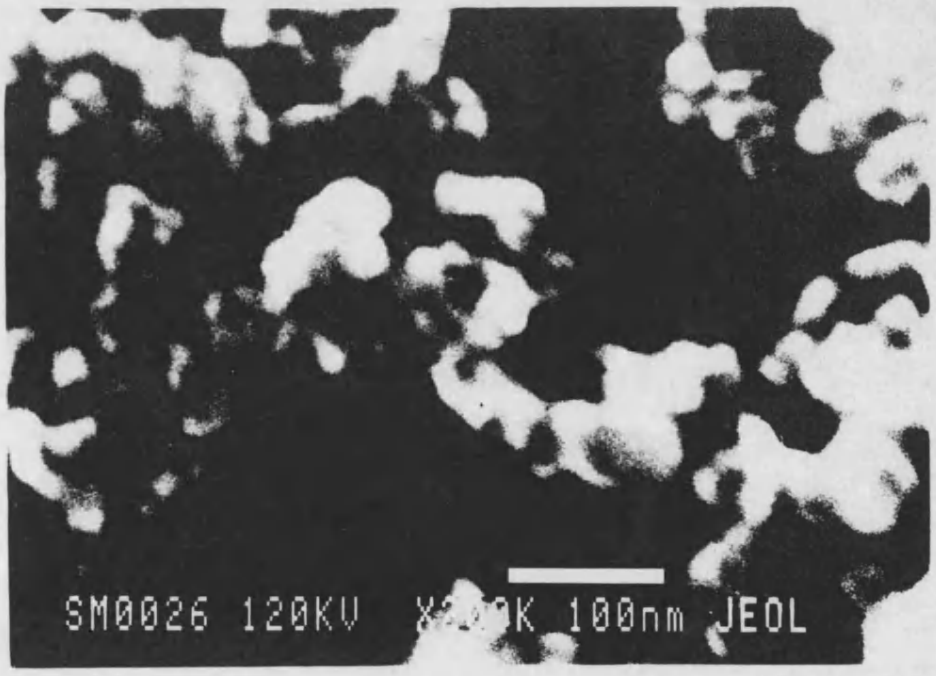

Figure 7.32. Iron-Doped Degussa P-25, surface view of particles by SEM.

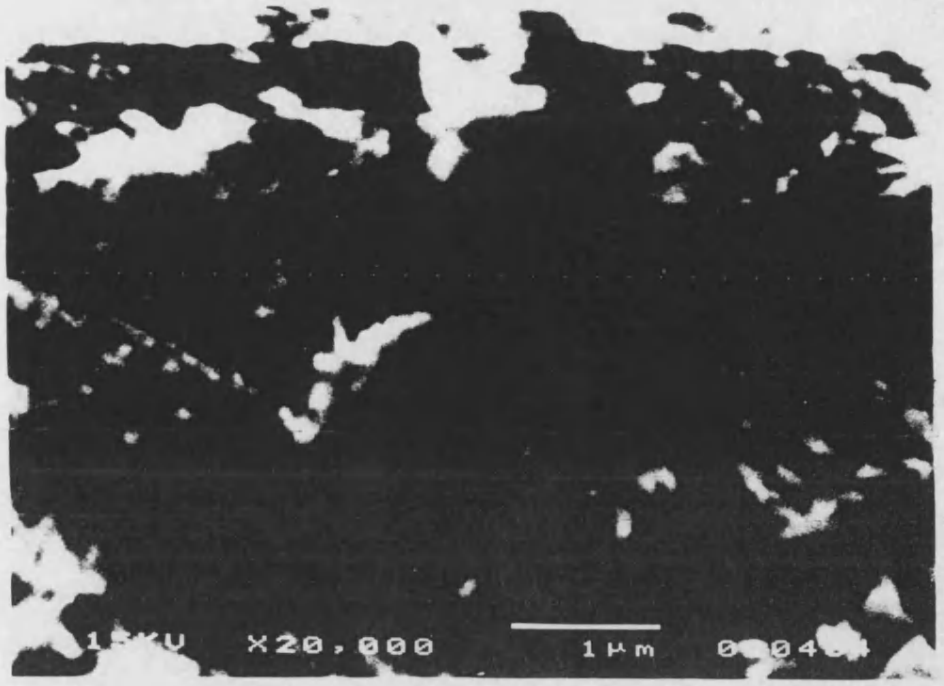

Figure 7.33. Iron-Doped Degussa P-25, edge view of particles by SEM.

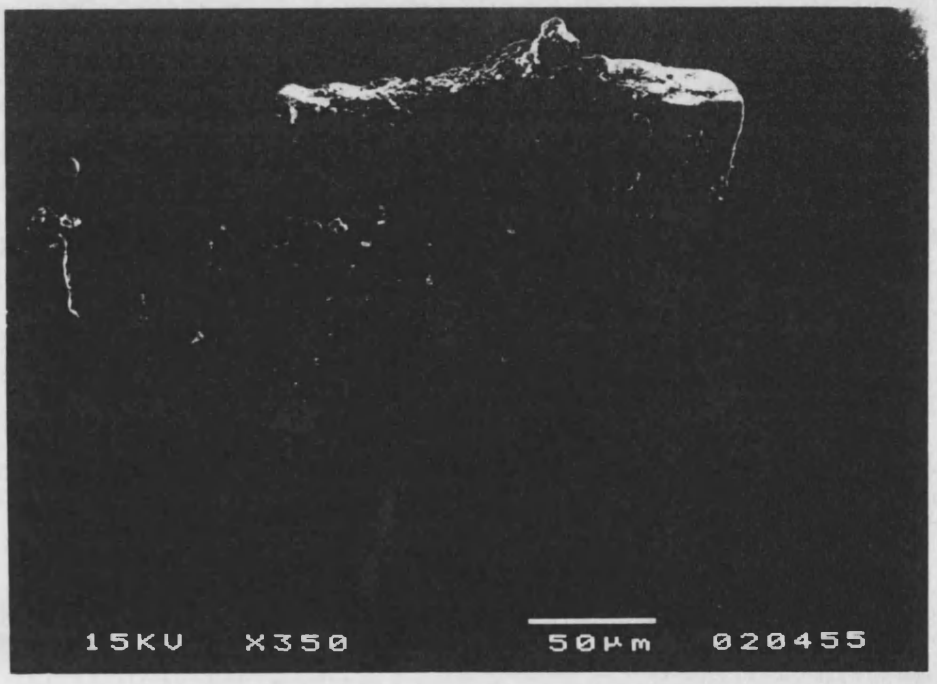

Figure 7.34. Iron-Doped Degussa P-25, view of particles by SEM.

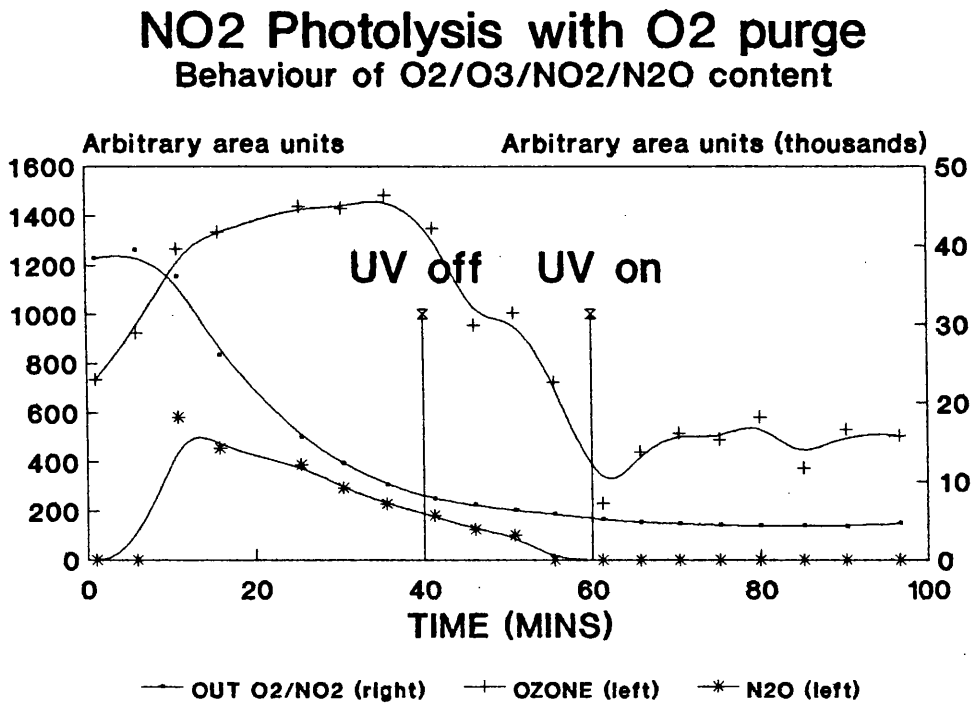

Figure 8.1

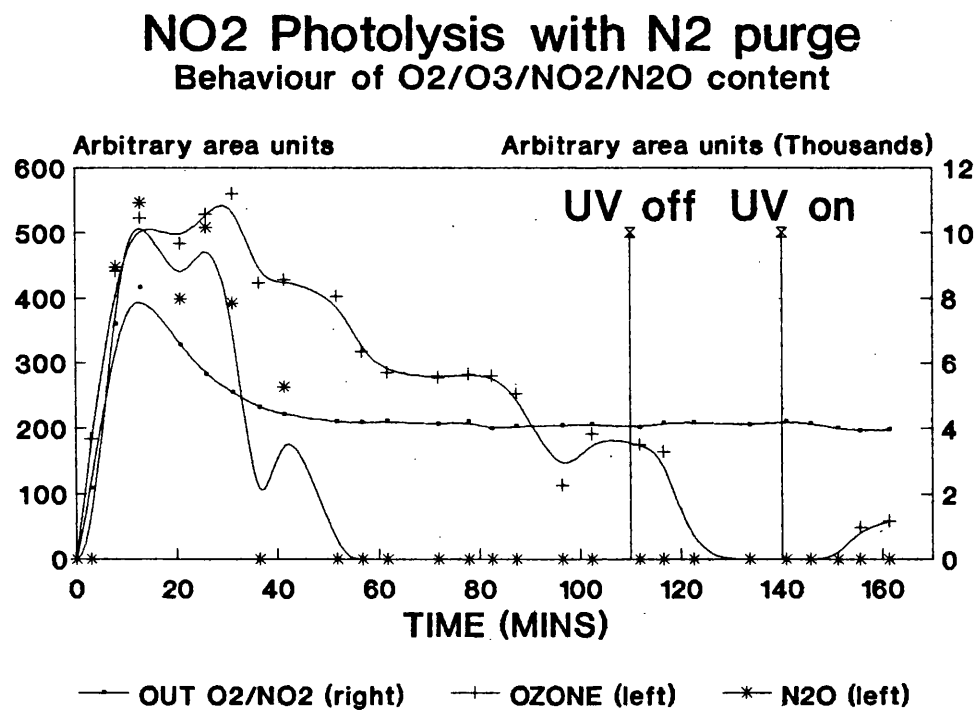

Figure 8.2

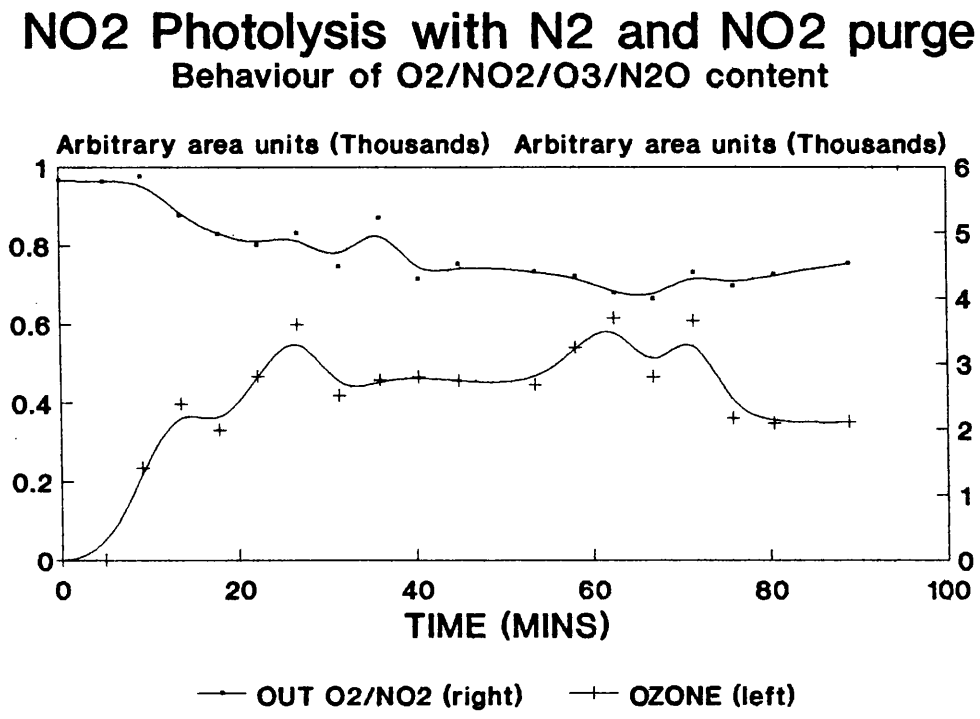

Figure 8.3

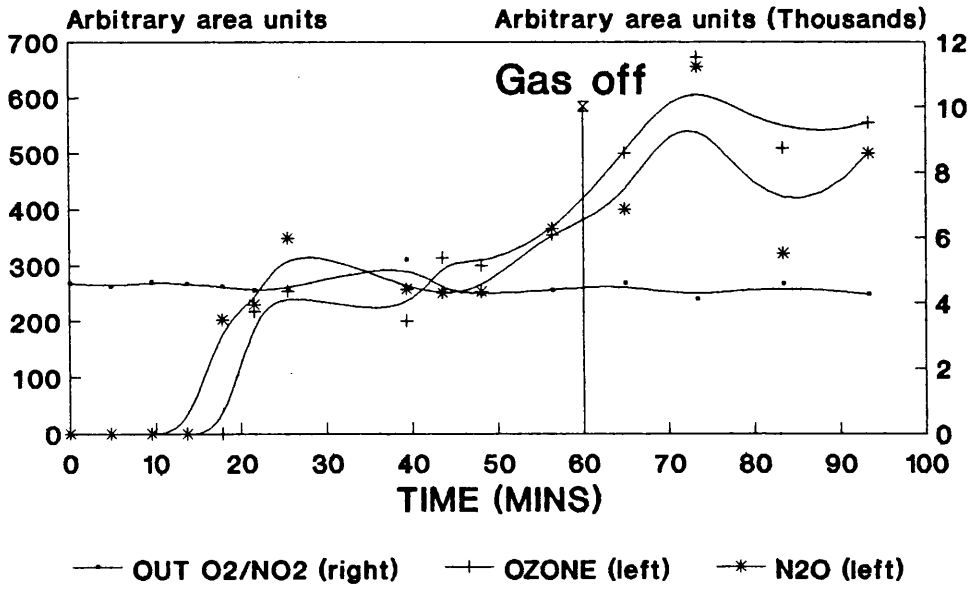

Figure 8.4

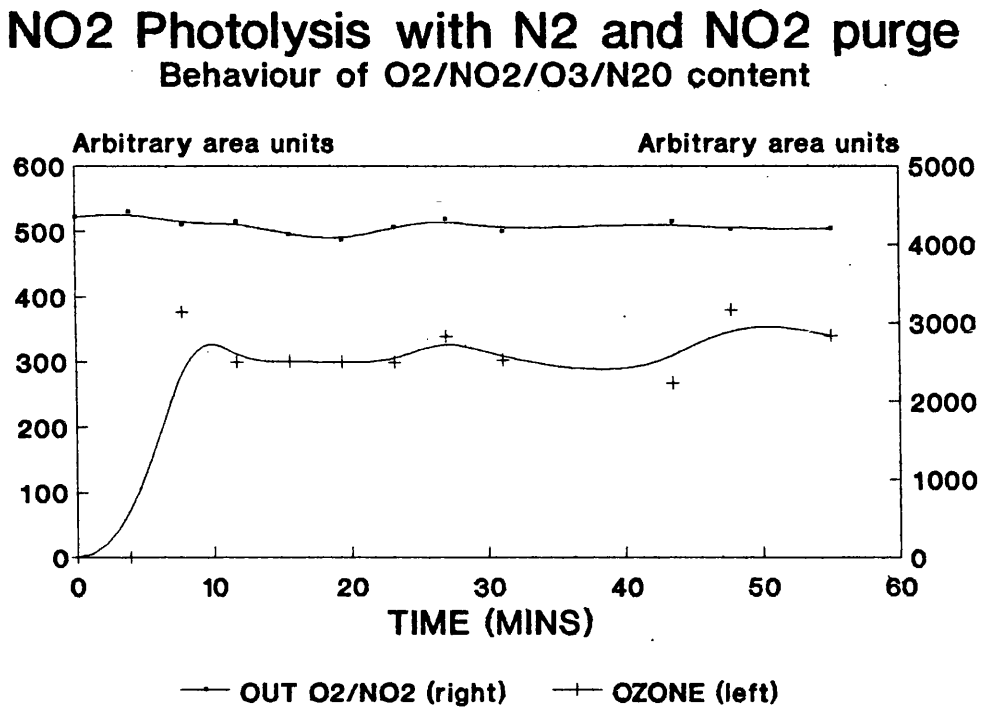

Figure 8.5

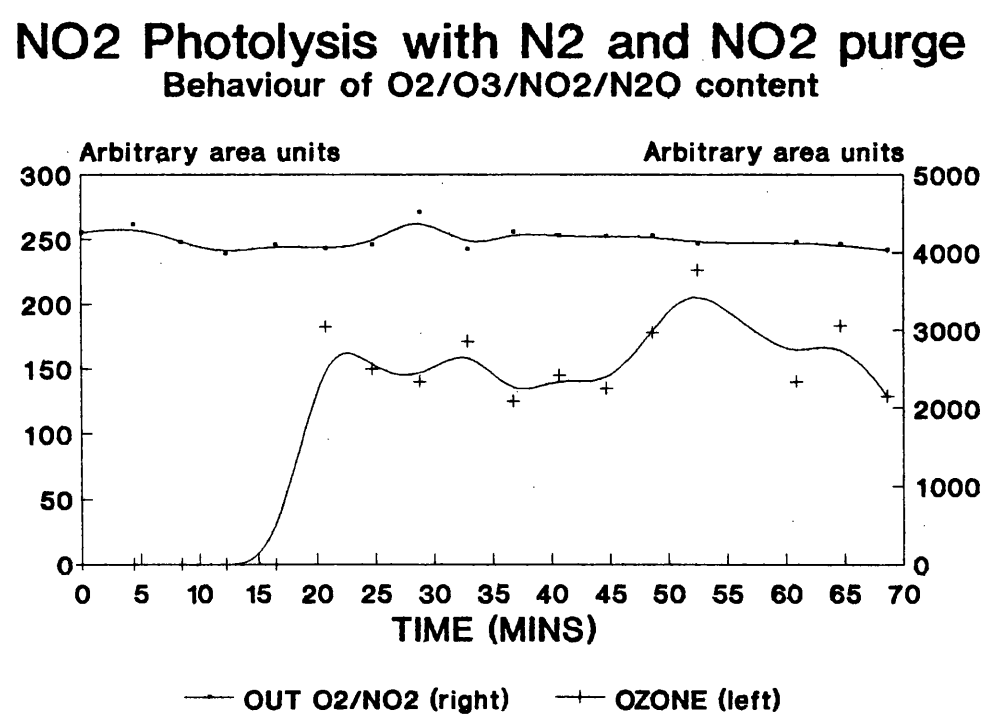

Figure 8.6

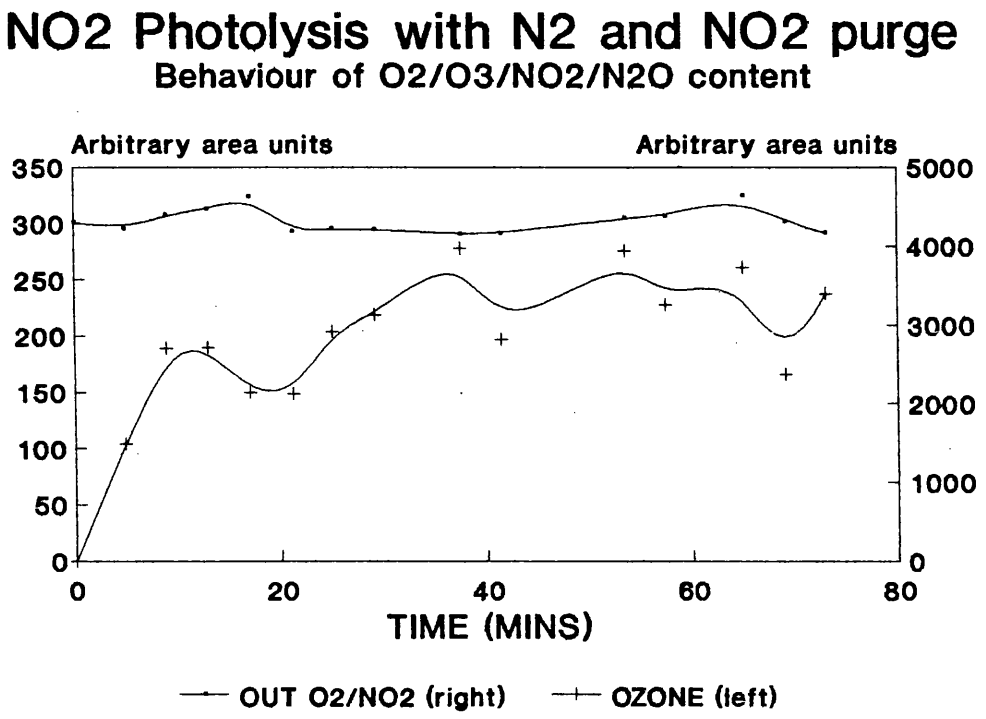

Figure 8.8

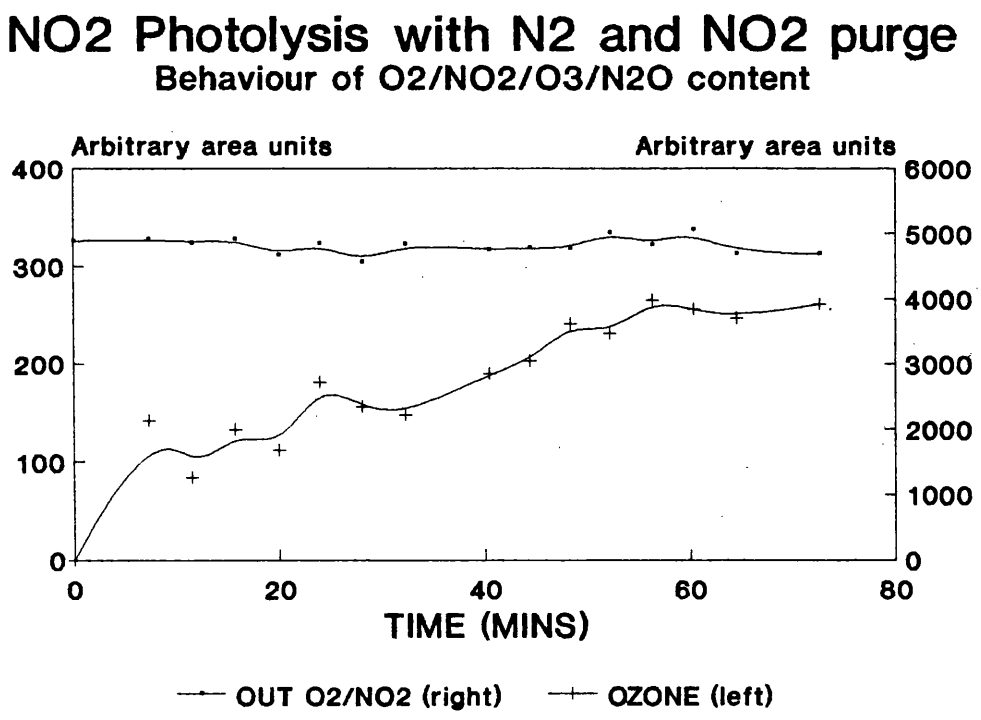

Figure 8.9

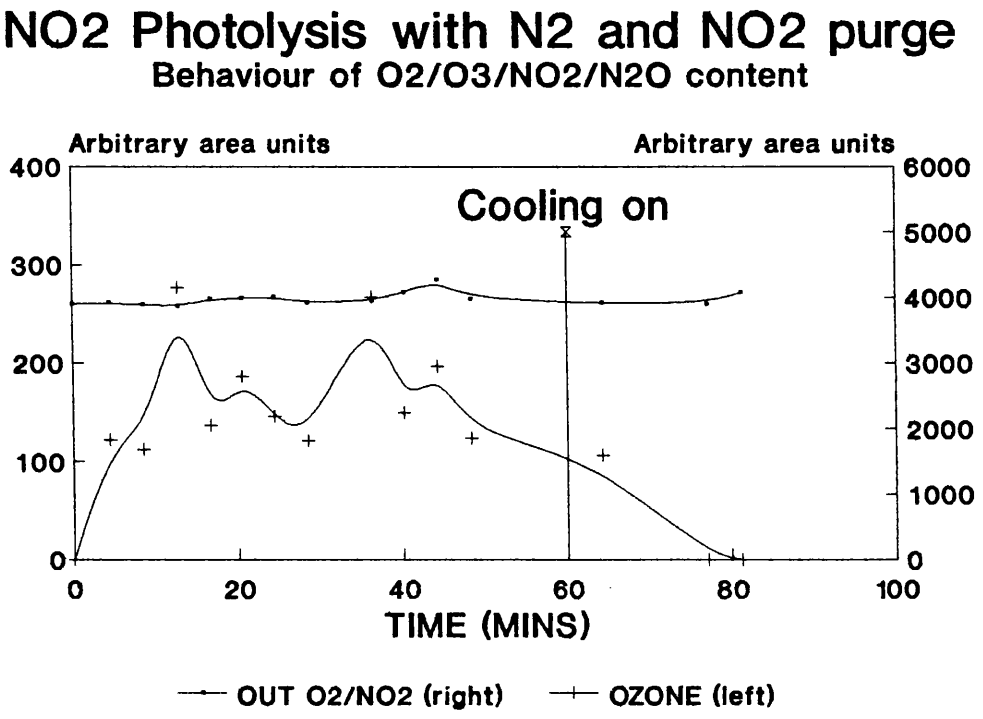

Figure 8.10

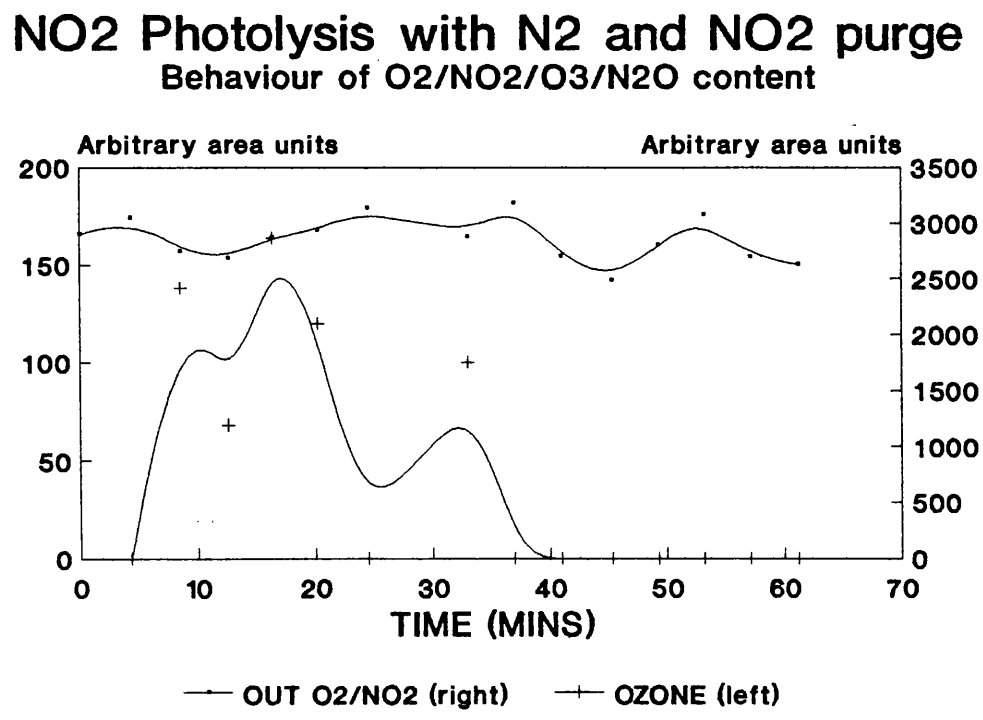

Figure 8.11

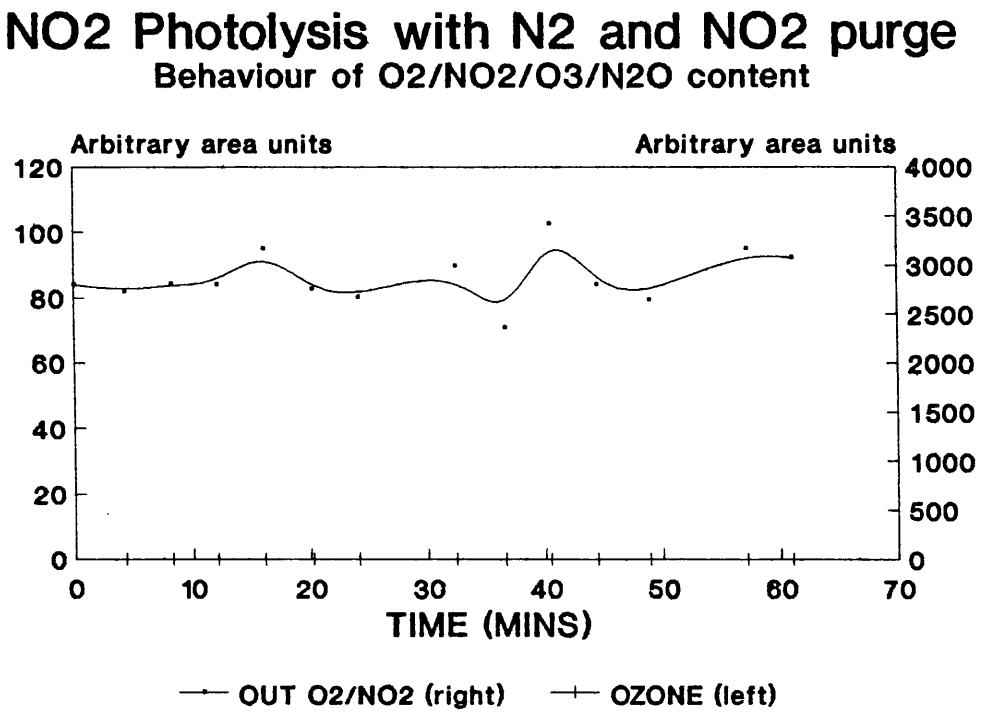

Figure 8.12

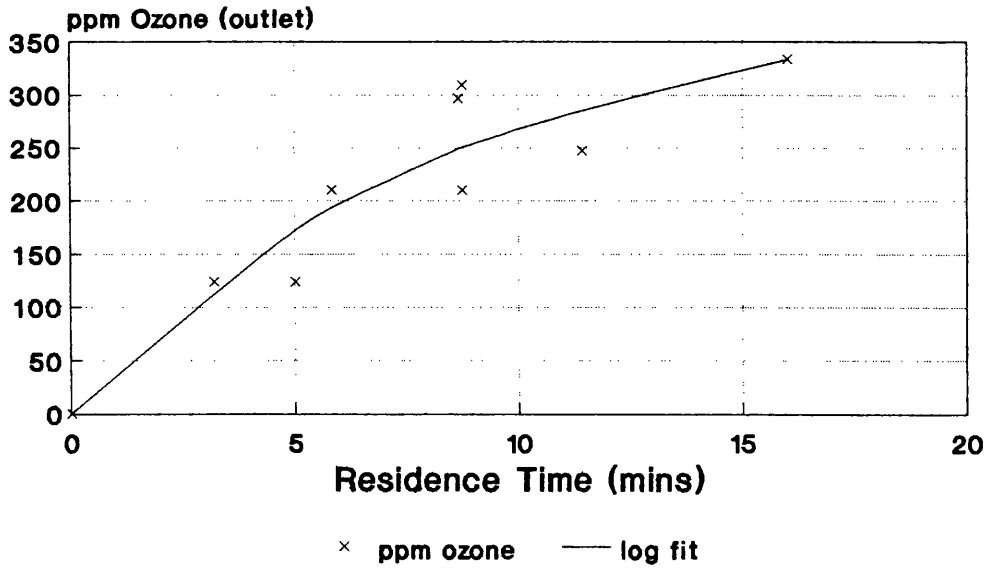

Figure 8.13

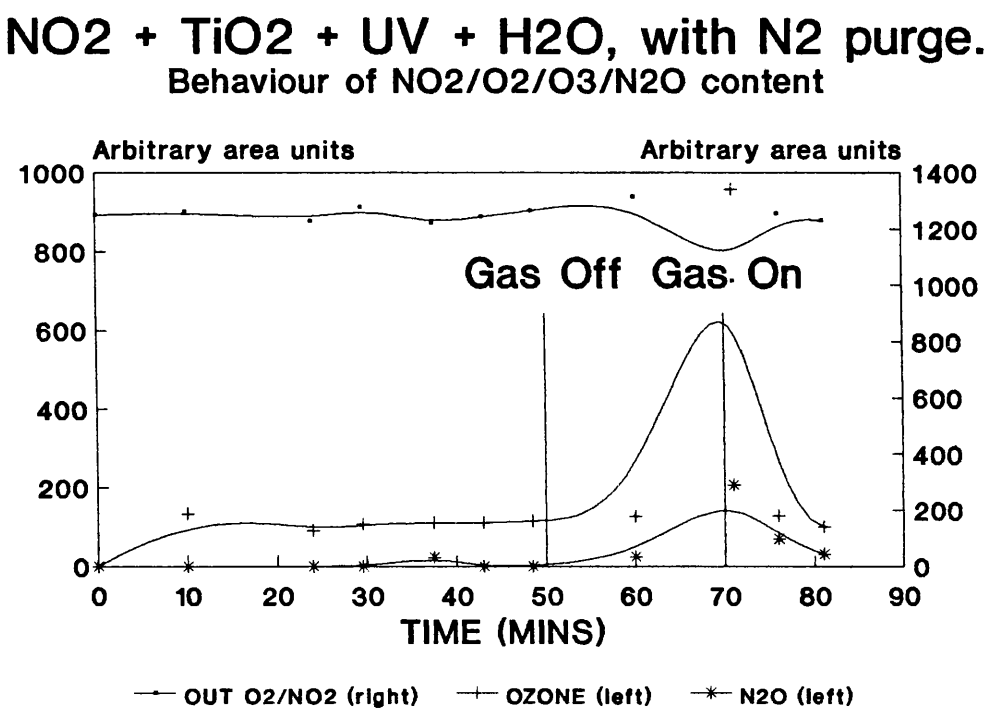

Figure 9.1

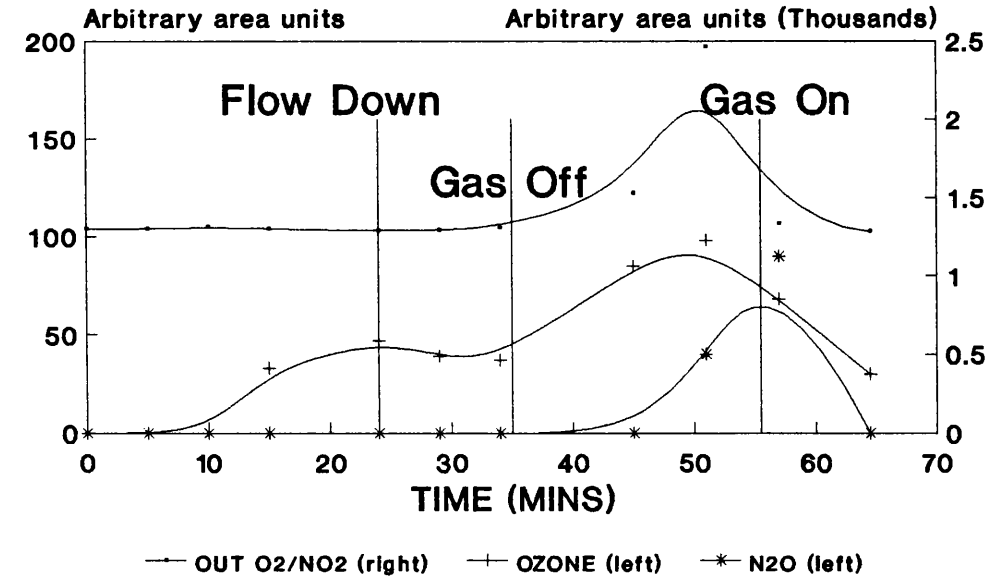

Figure 9.2

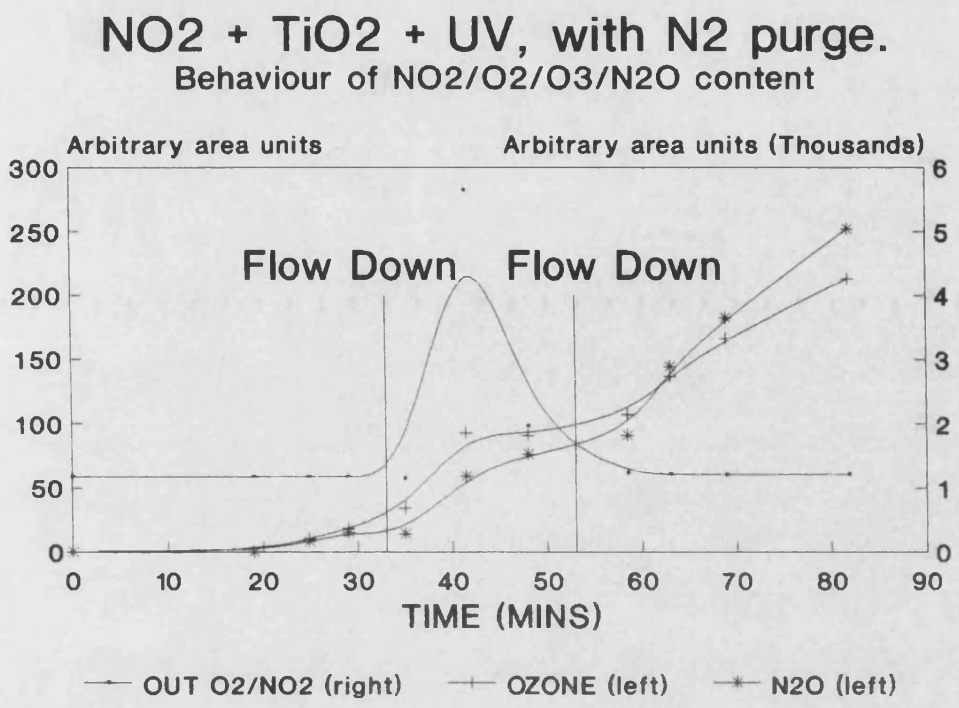

Figure 9.3

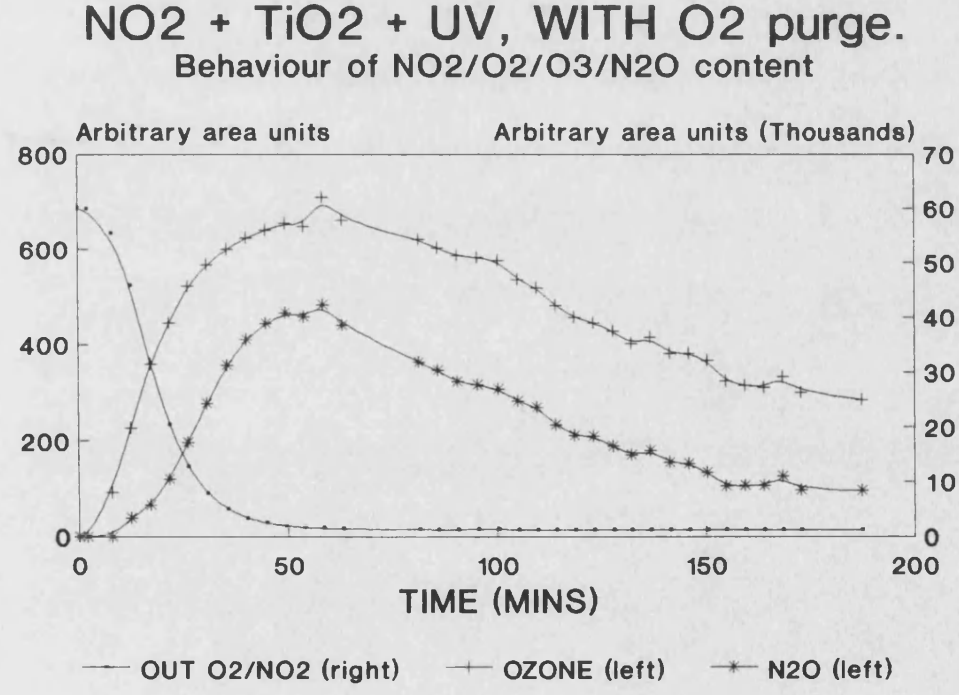

Figure 9.4

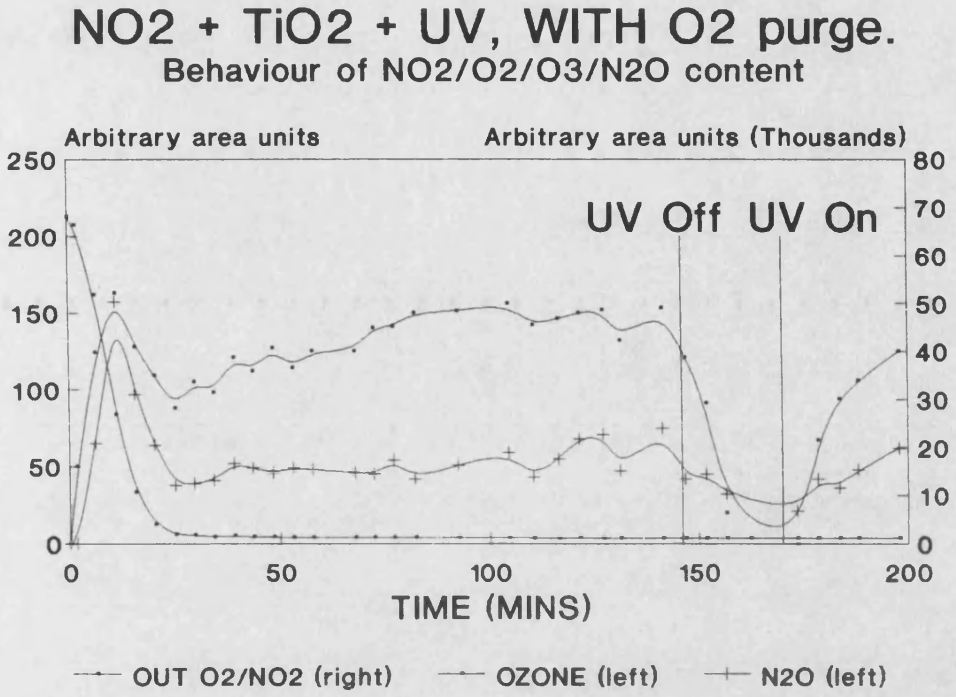

Figure 9.5

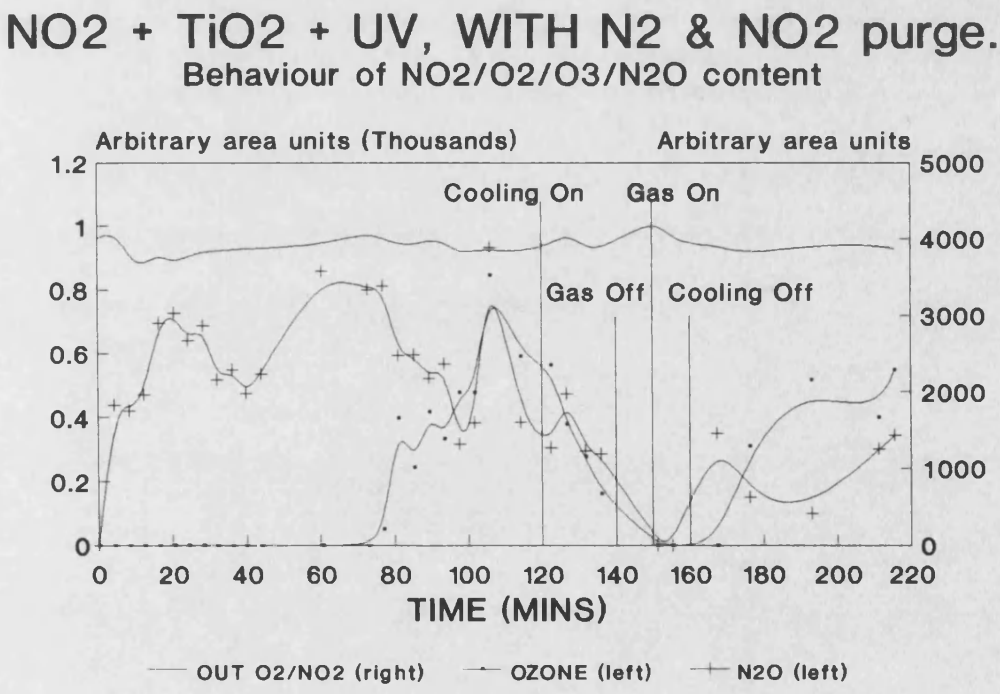

Figure 9.6

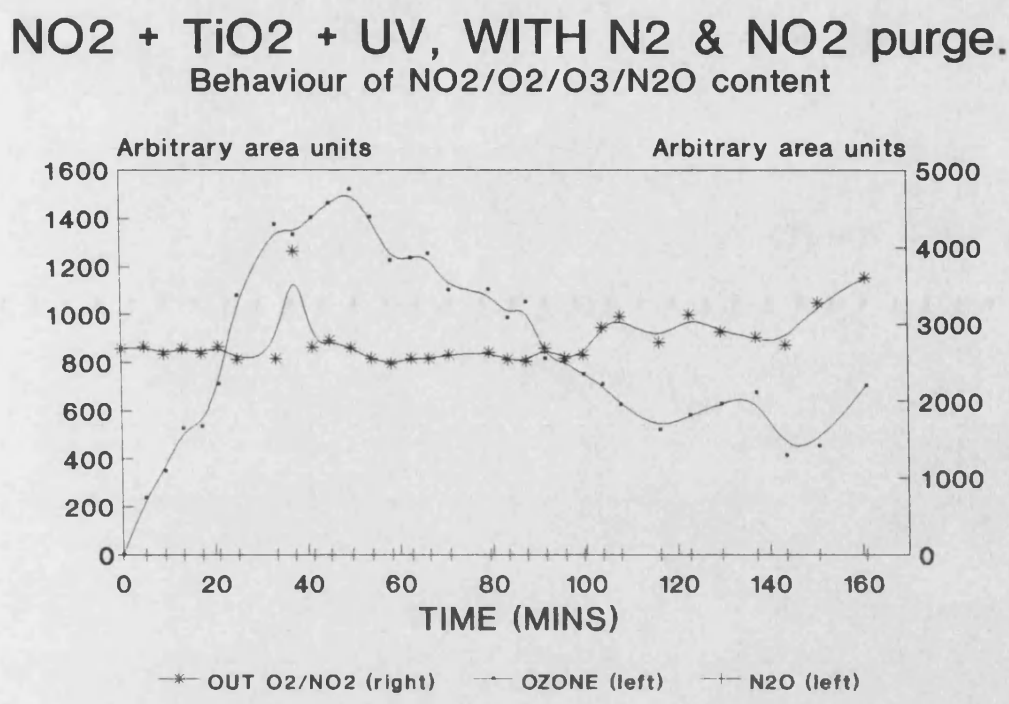

Figure 9.7

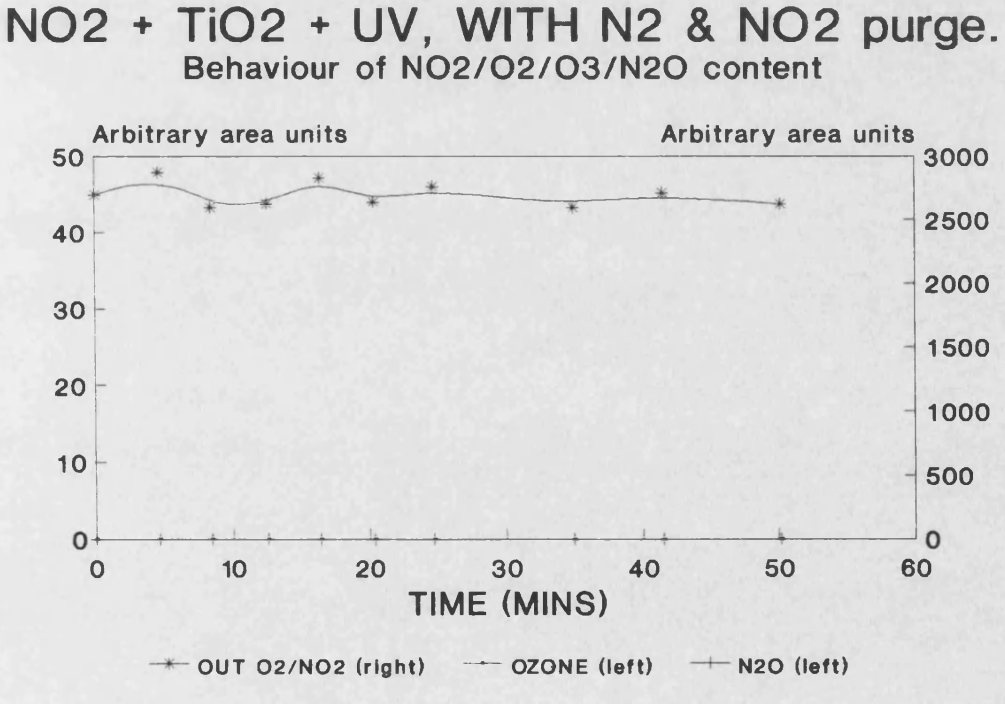

Figure 9.8

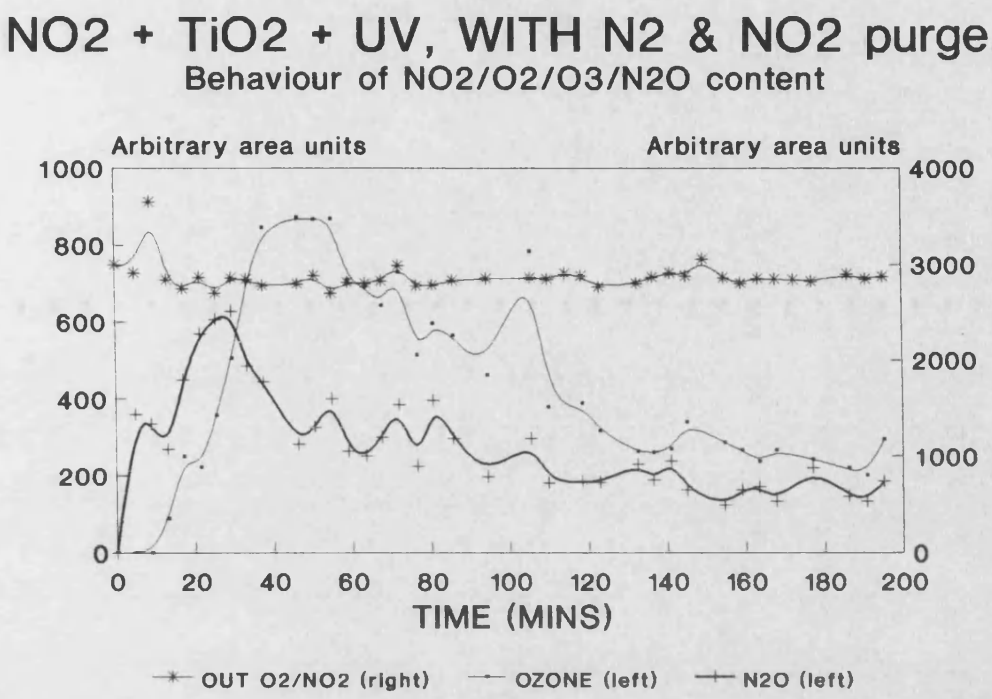

Figure 9.9

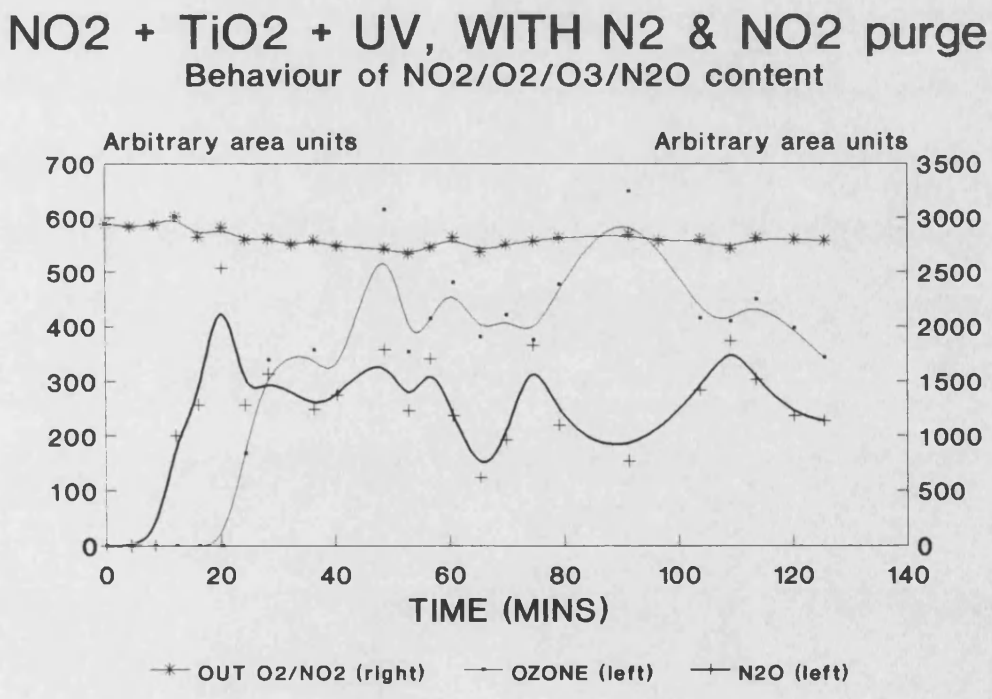

Figure 9.10

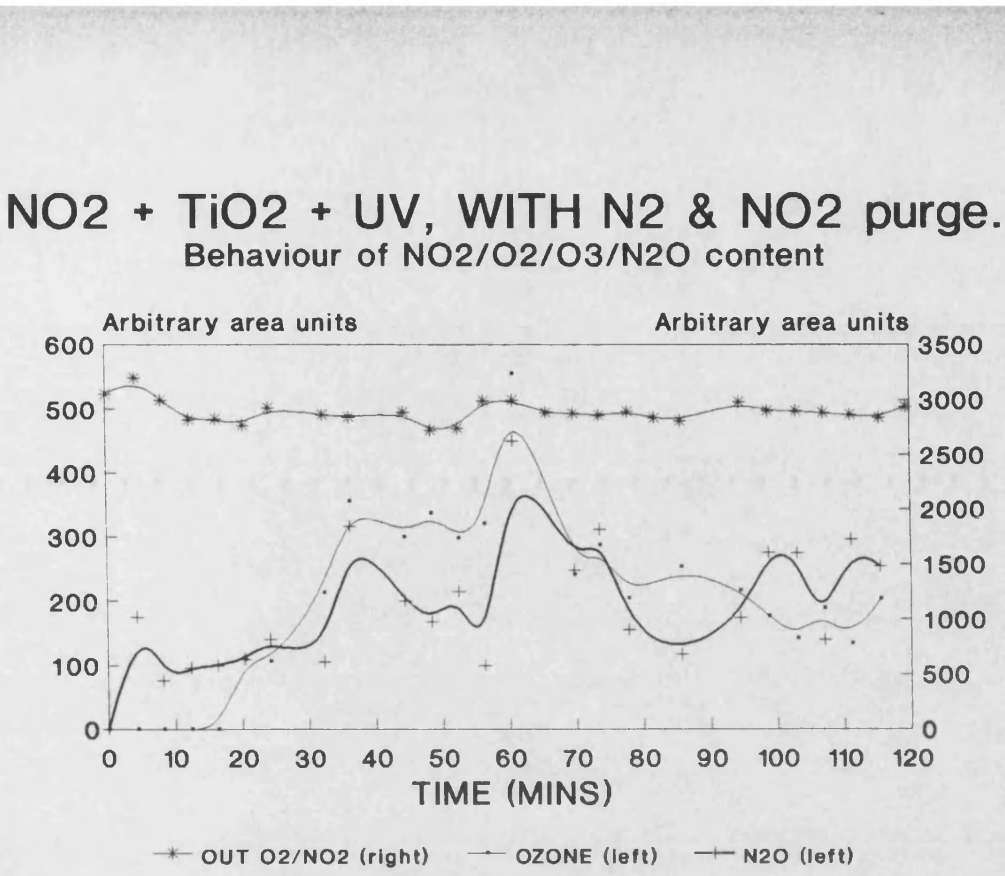
NO2 + TiO2 + UV, WITH N2 & NO2 purge.
Behaviour of NO2/O2/O3/N2O content
Arbitrary area units
Arbitrary area units
600
500
400
300
200
100
0
3500
3000
2500
2000
1500
1000
500
0
0 10 20 30 40 50 60 70 80 90 100 110 120
TIME (MINS)
OUT O2/NO2 (right)
OZONE (left)
N2O (left)

Figure 9.11

NO2 photocatalysis vs Residence Time with N2 bulk

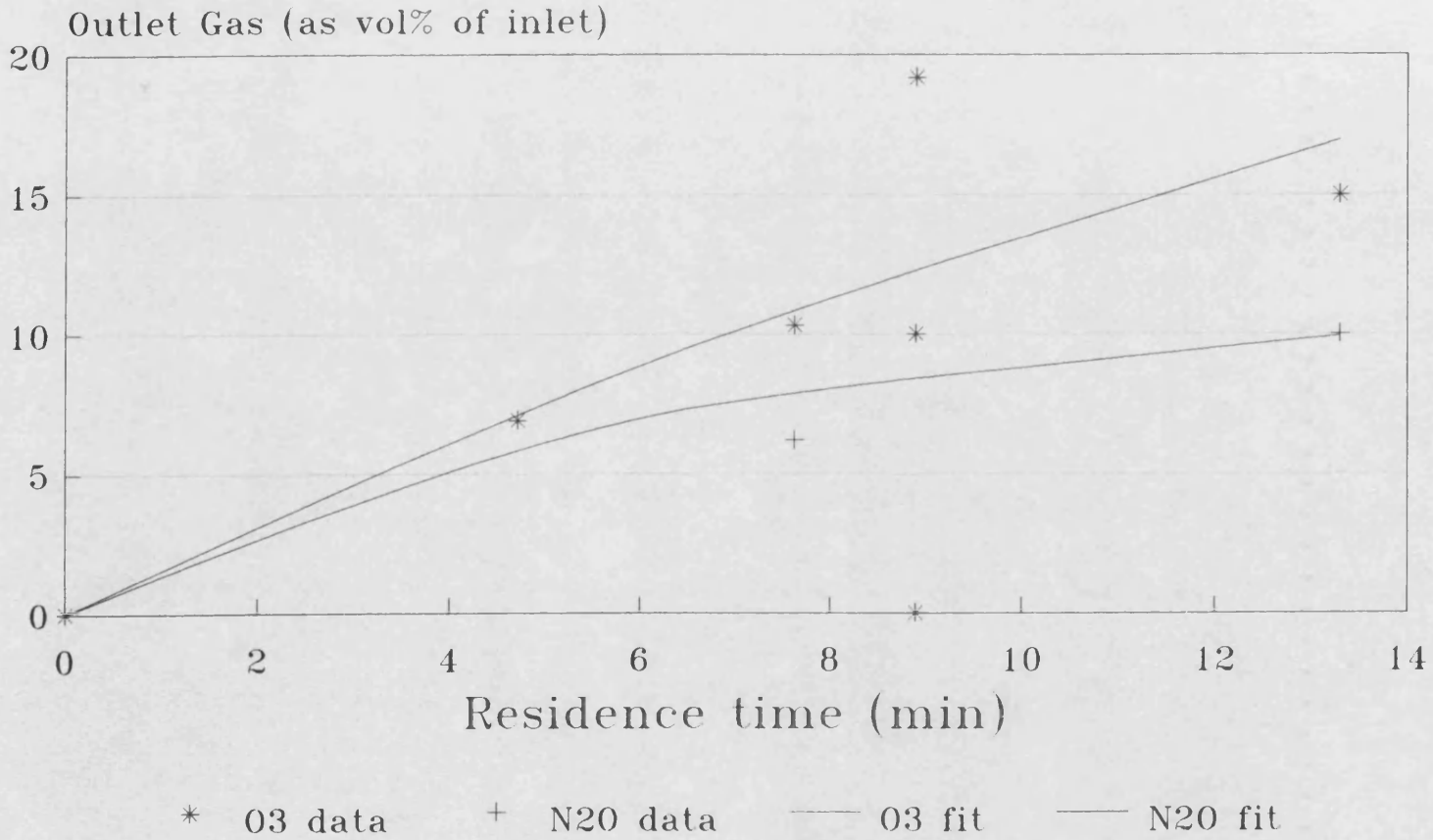

Figure 9.12

NO2 + TiO2 + UV, WITH N2 & NO2 purge.

Behaviour O3/N2O & Temperature

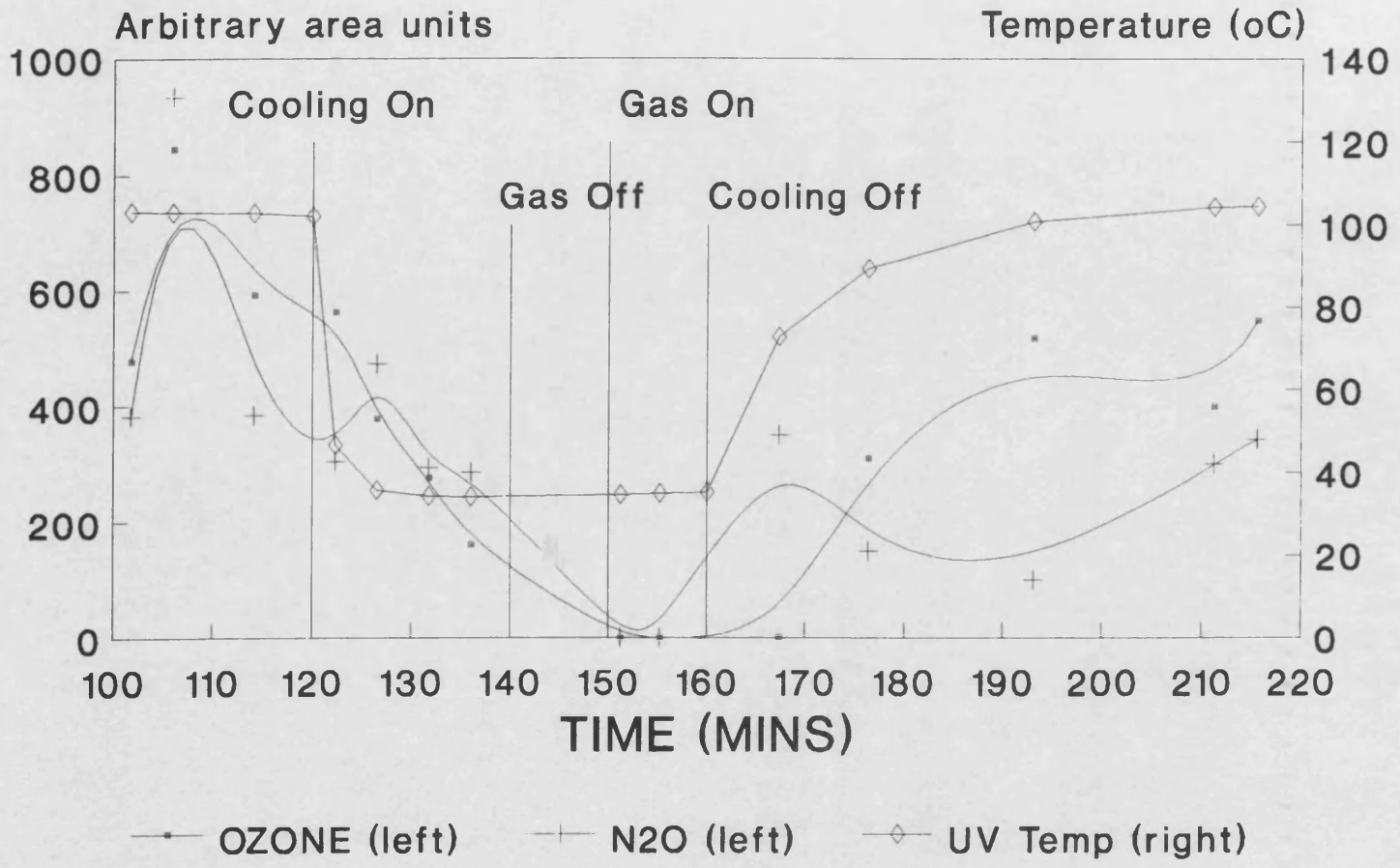

Figure 9.13

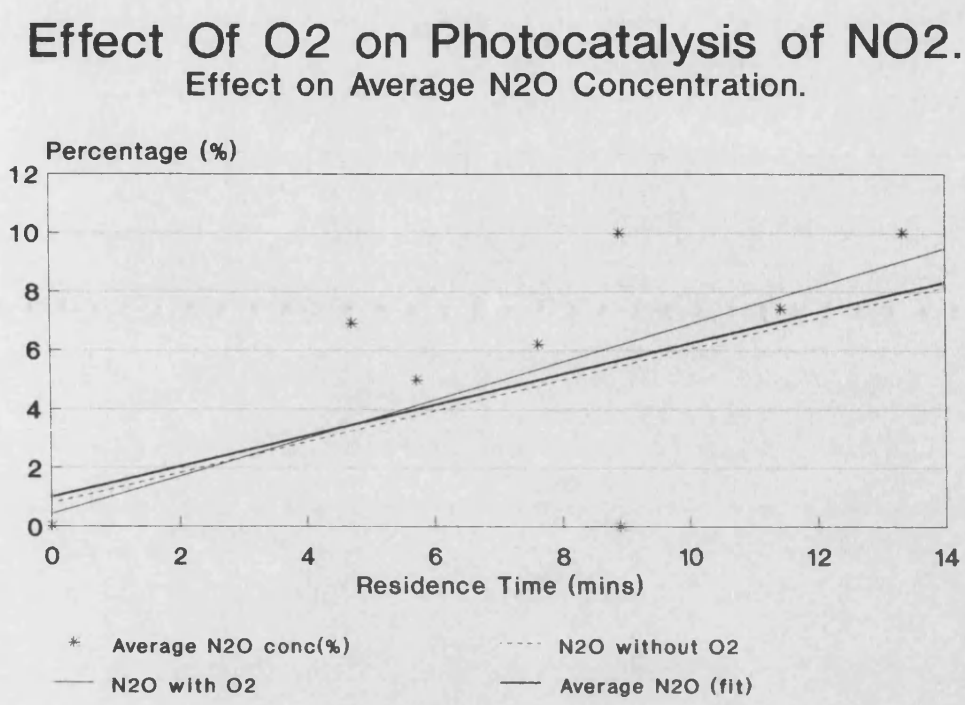

Figure 9.14

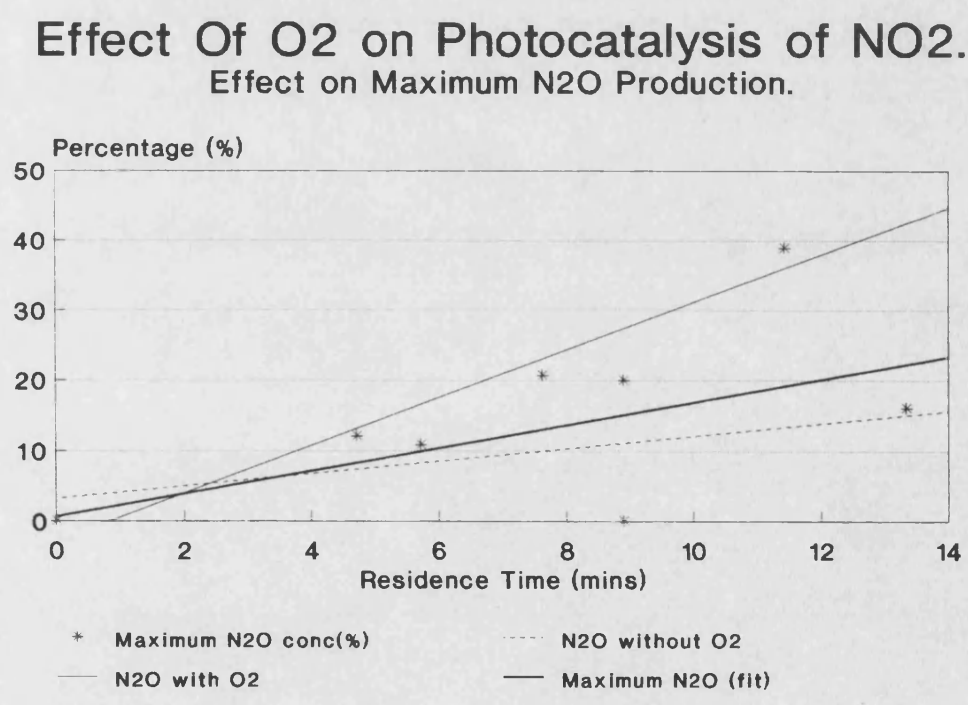

Figure 9.15

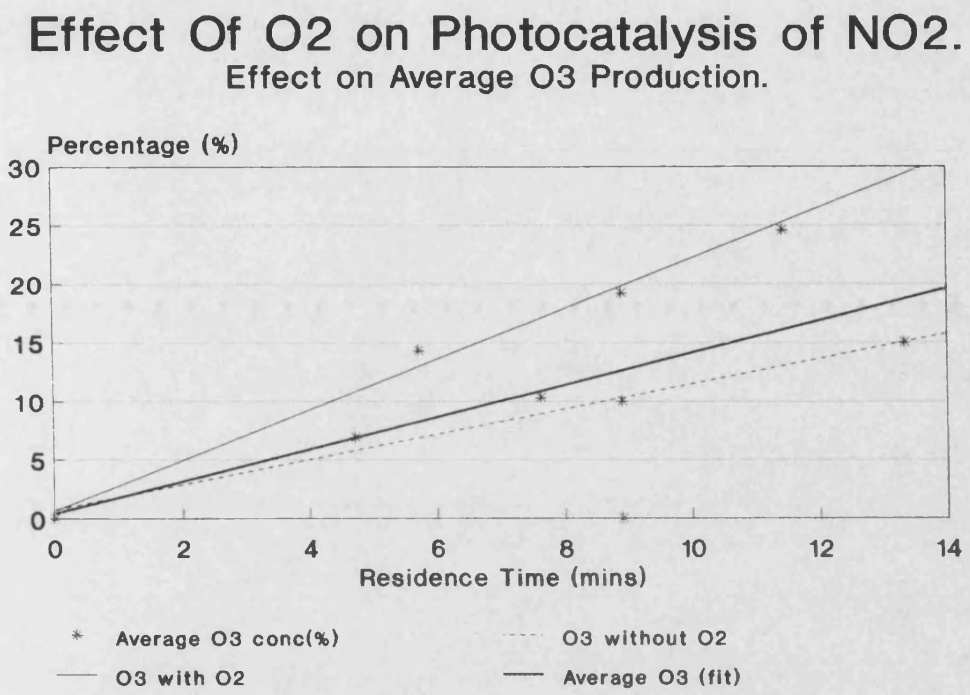

Figure 9.16

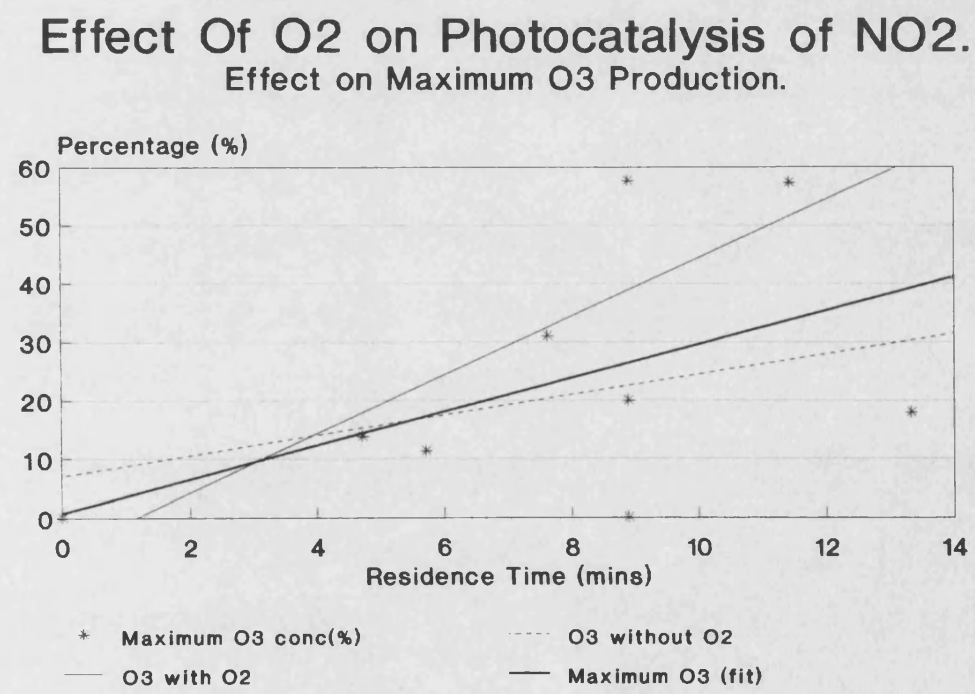

Figure 9.17

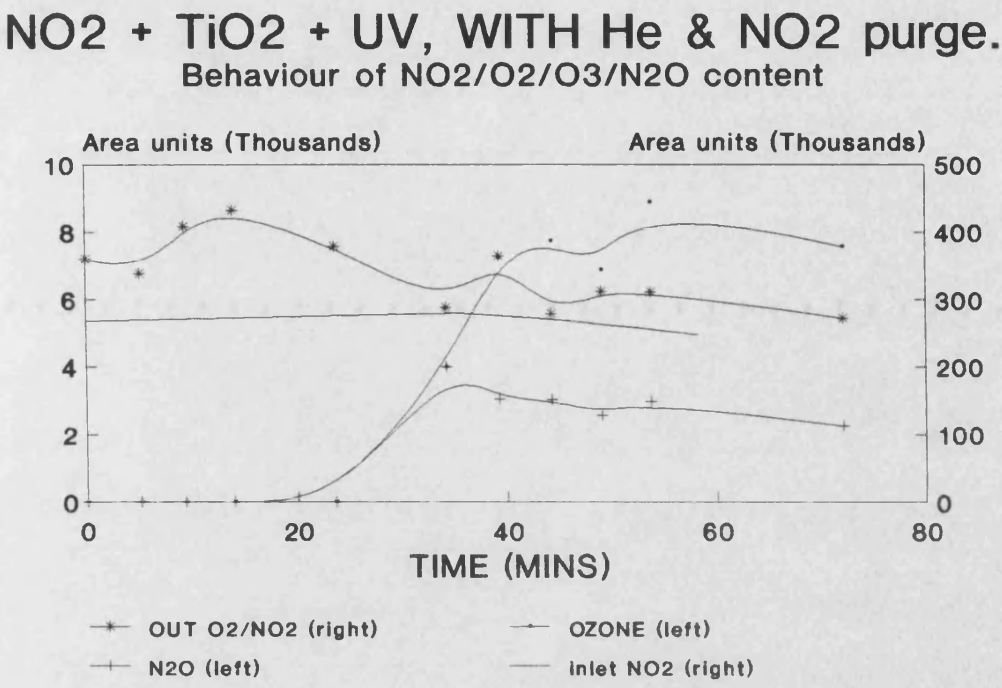

Figure 9.18

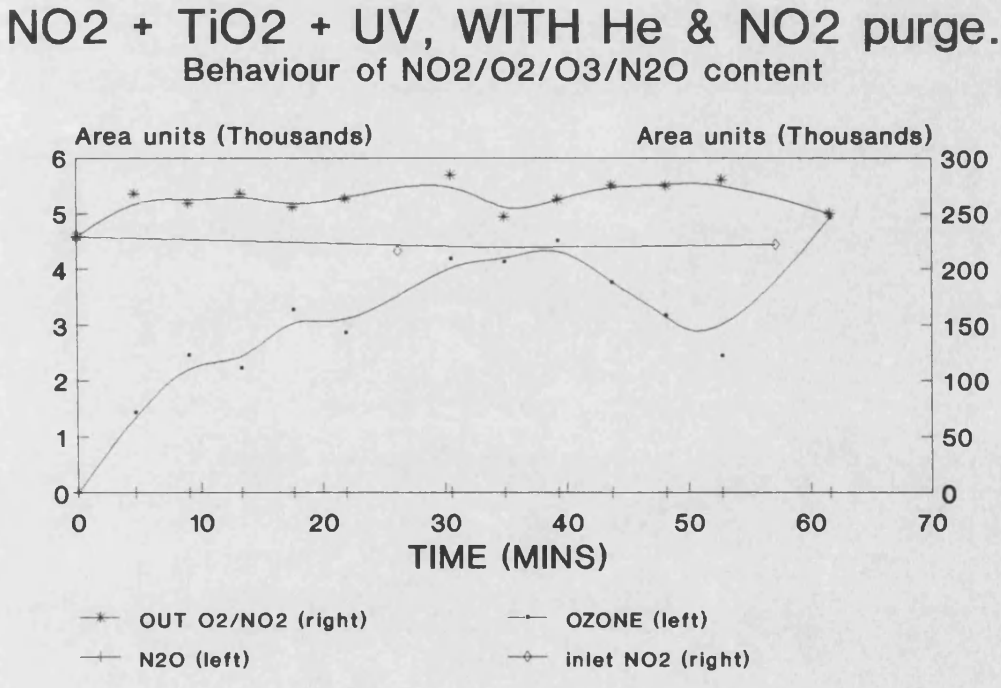

Figure 9.19

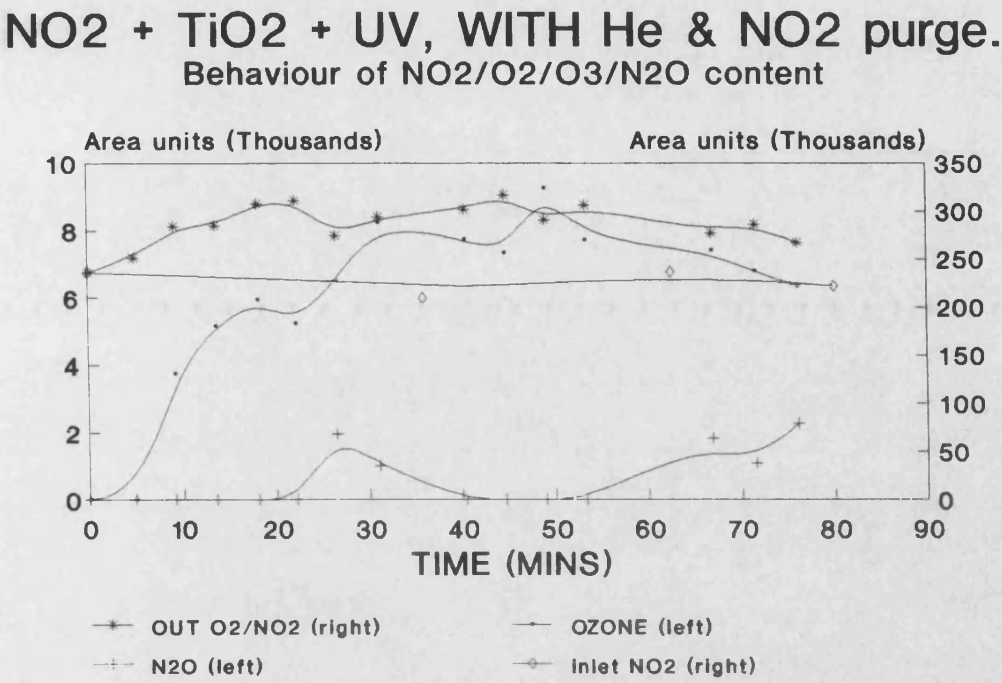

Figure 9.20

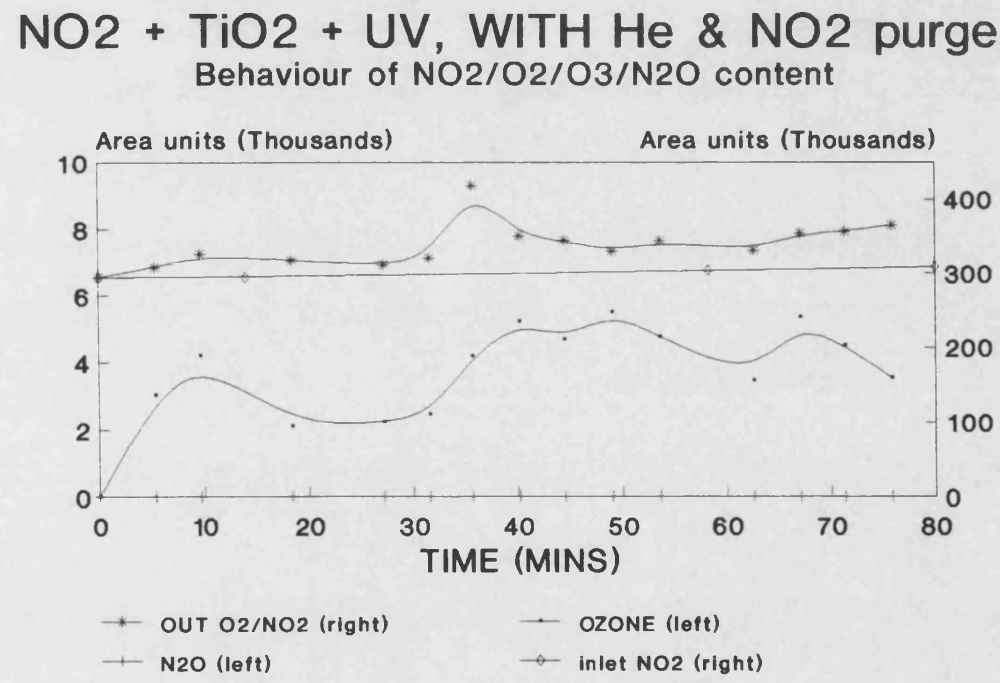

Figure 9.21

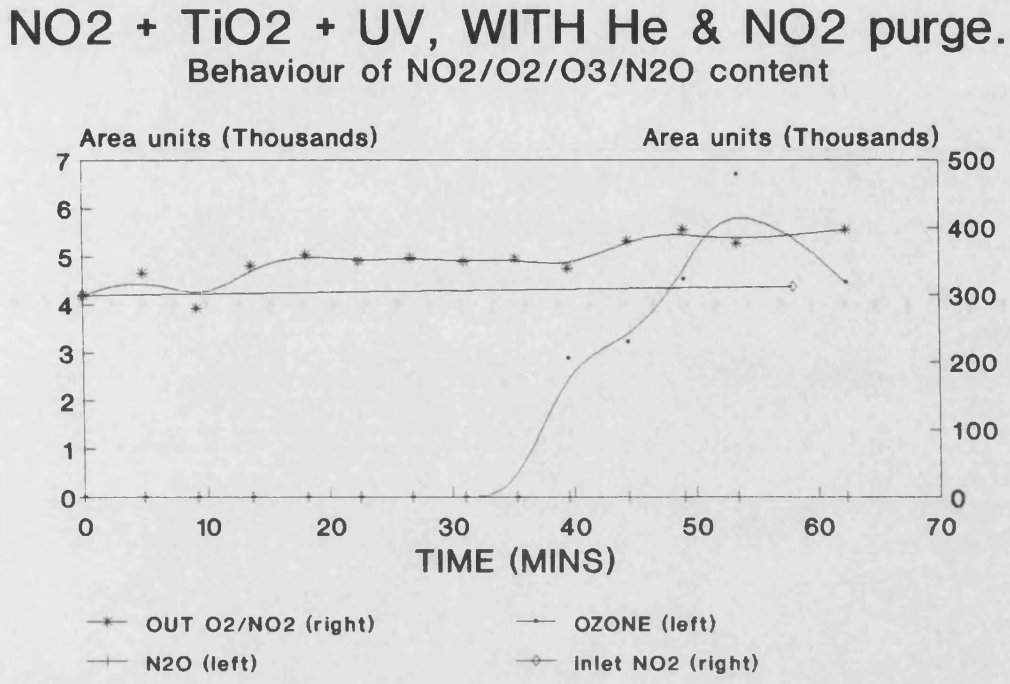

Figure 9.22

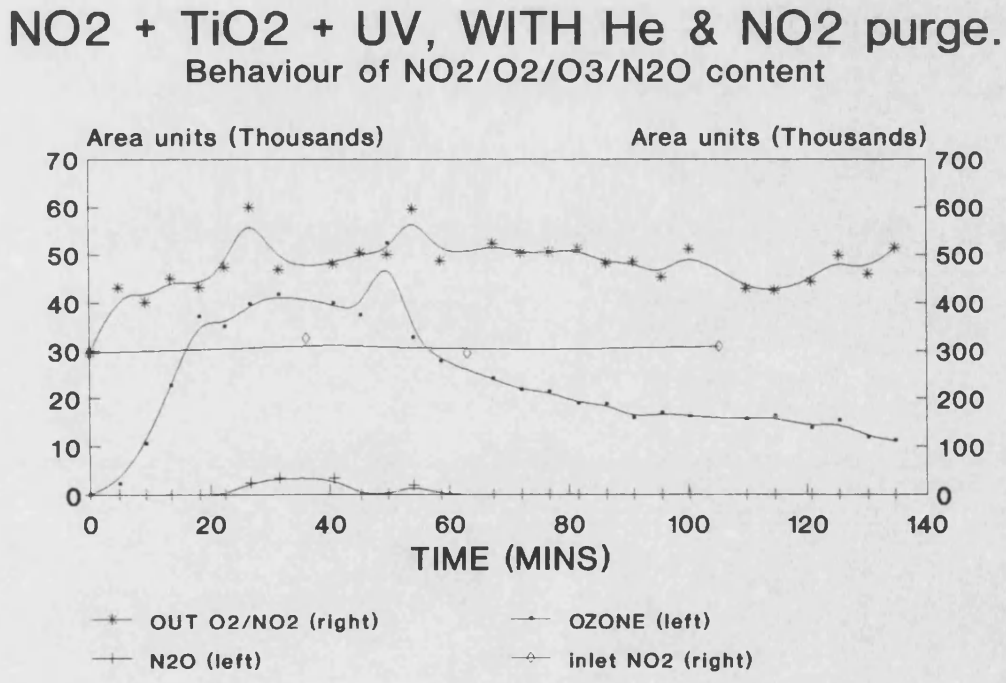

Figure 9.23

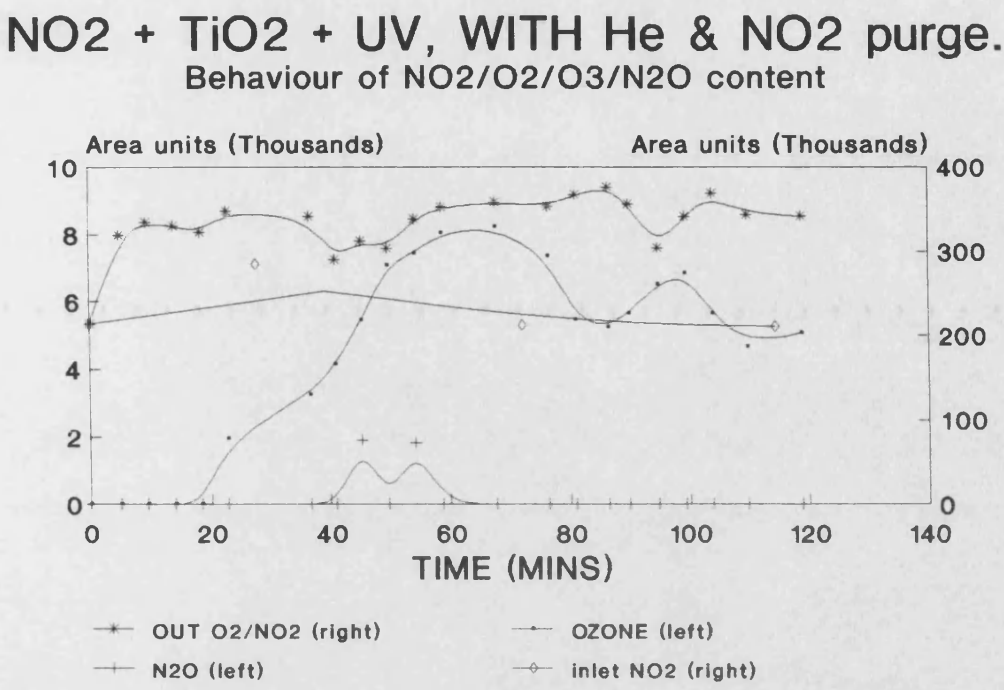

Figure 9.24

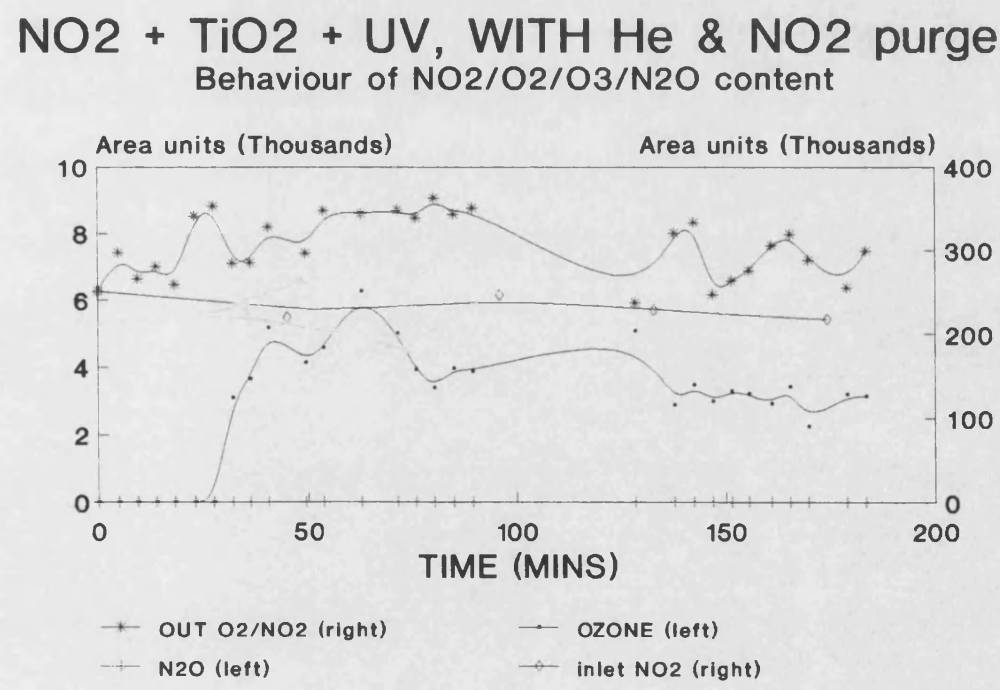

Figure 9.25

Time vs Concentration Graph for the Photocatalysis of NO2 (8 Watt Reactor)

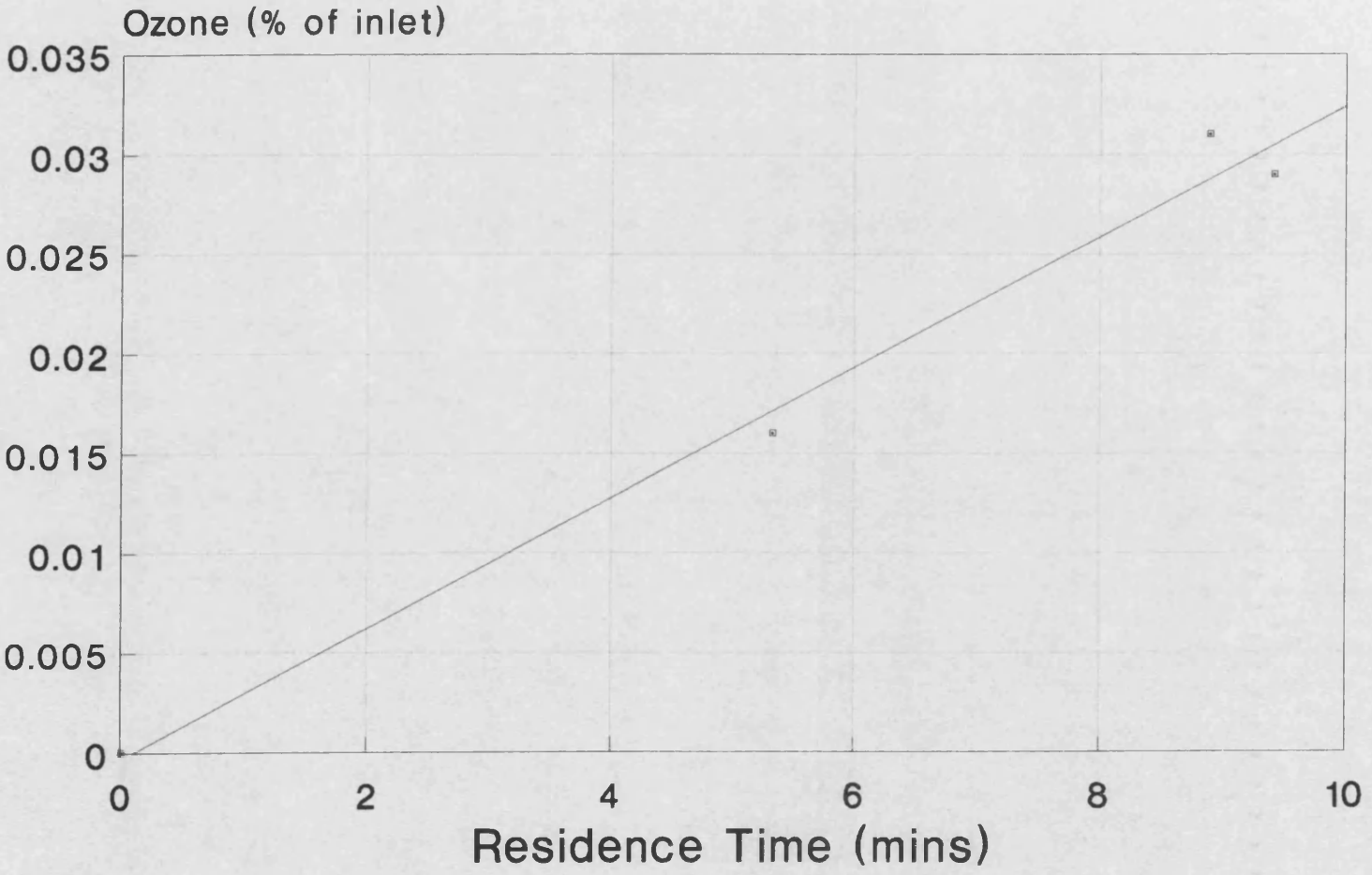

Figure 9.26

Time vs Concentration Graph for the Photocatalysis of NO2 (250 Watt Reactor)

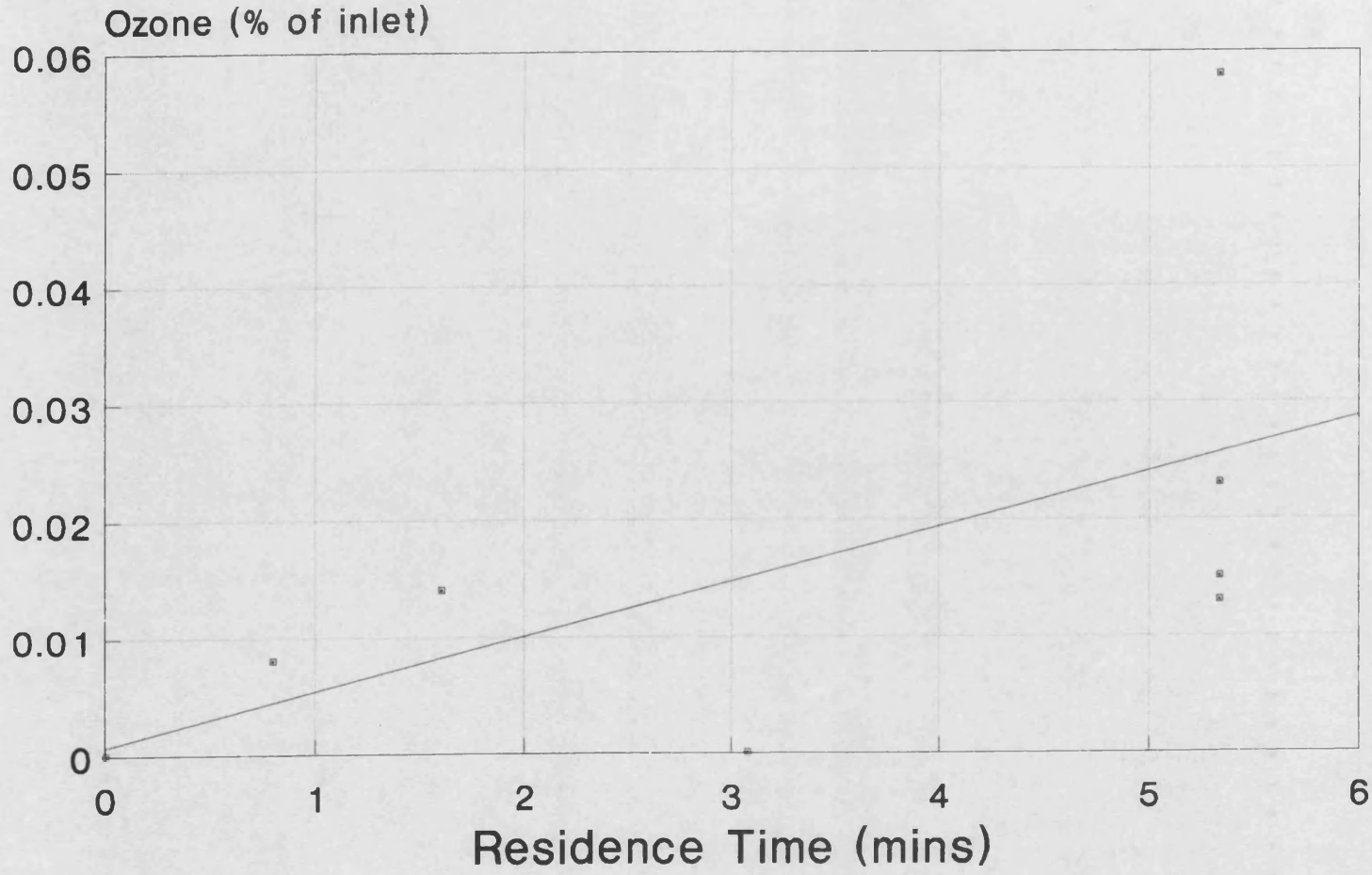

Figure 9.27

Absolute Spectral Power
8 Watt Black-Light-Blue

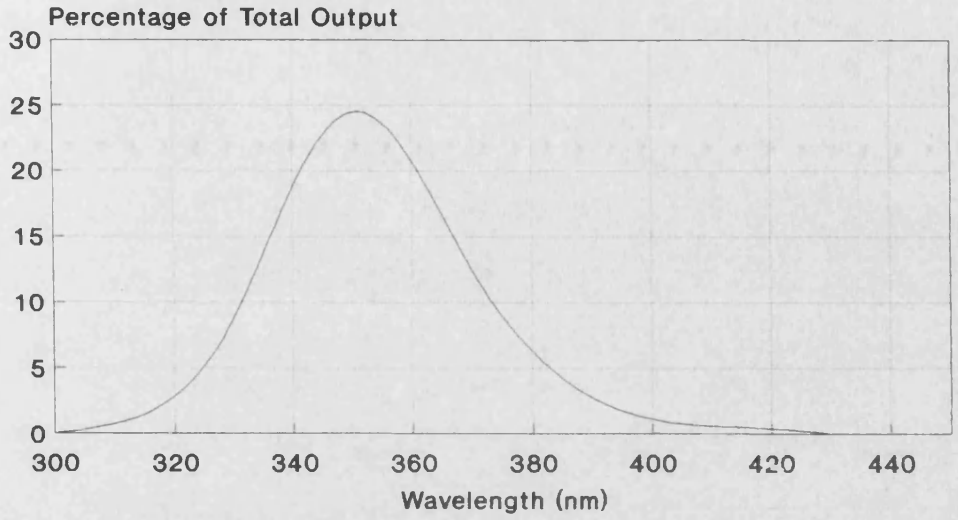

UV Power Output = 0.8 watts
Useful UV Output = 0.56 watts

Figure 9.28

Absolute Spectral Power
250 Watt Medium Pressure Mercury

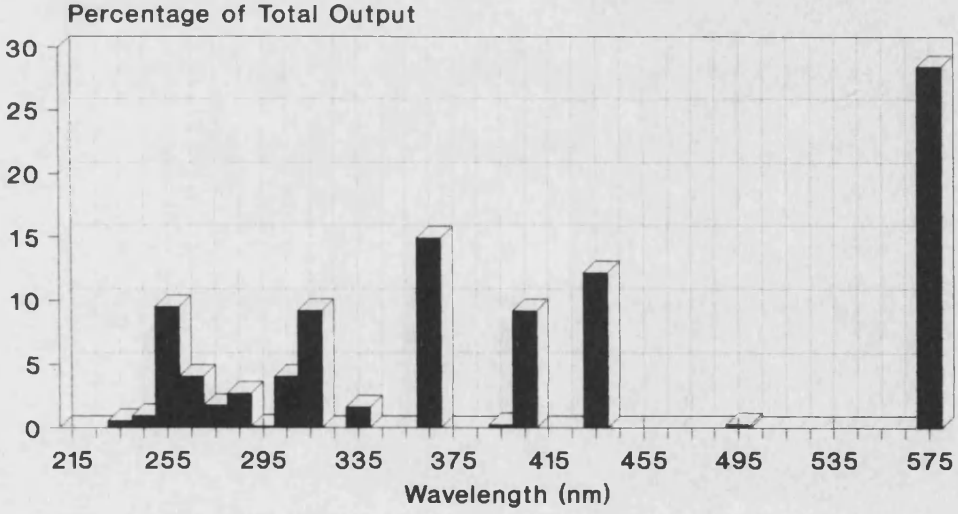

UV Power Output = 20 watts
Useful UV Output = 9.0 watts

Figure 9.29

Relationship Between UV Intensity and Degree of Photocatalytic Reaction.

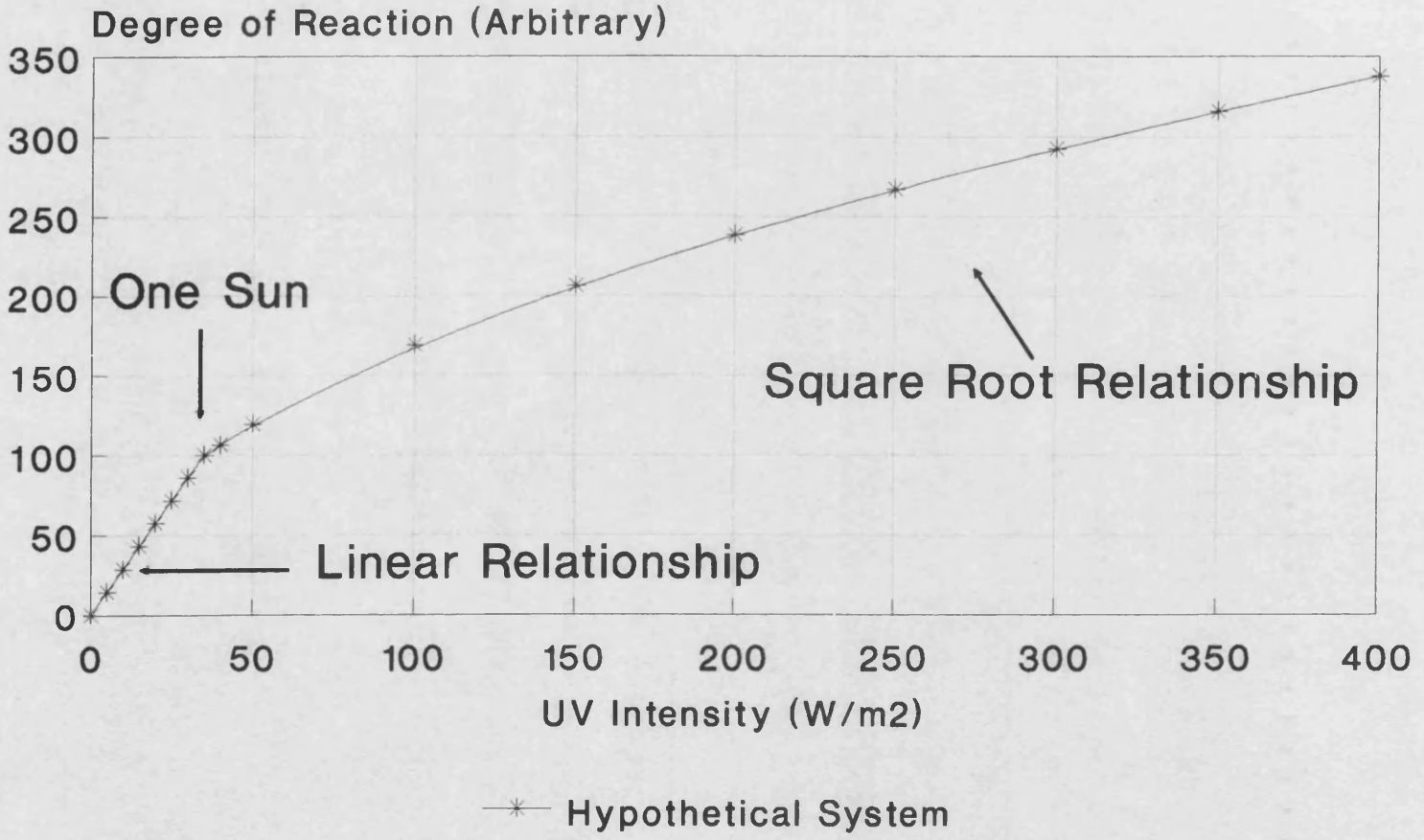

Figure 9.30

NO_2 + TiO_2 + UV, WITH He & NO_2 purge.

Behaviour of O_3 Production & Temperature

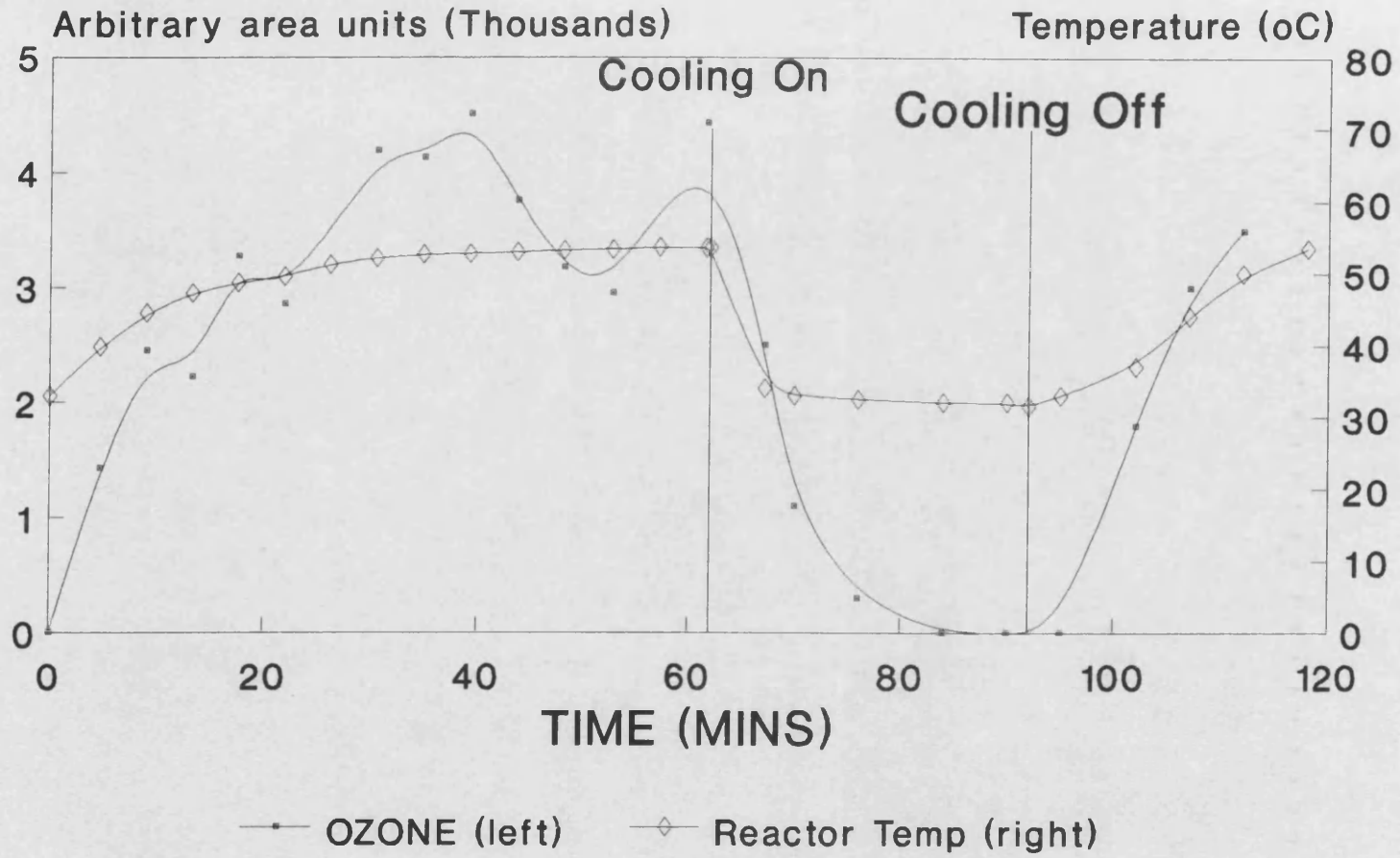

Figure 9.31

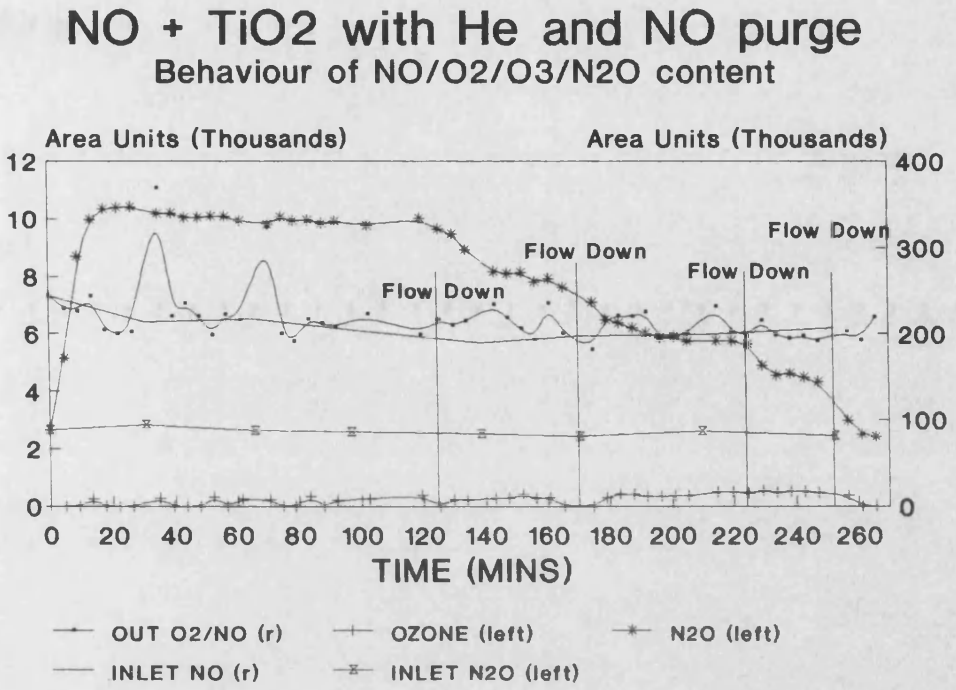

Figure 9.32

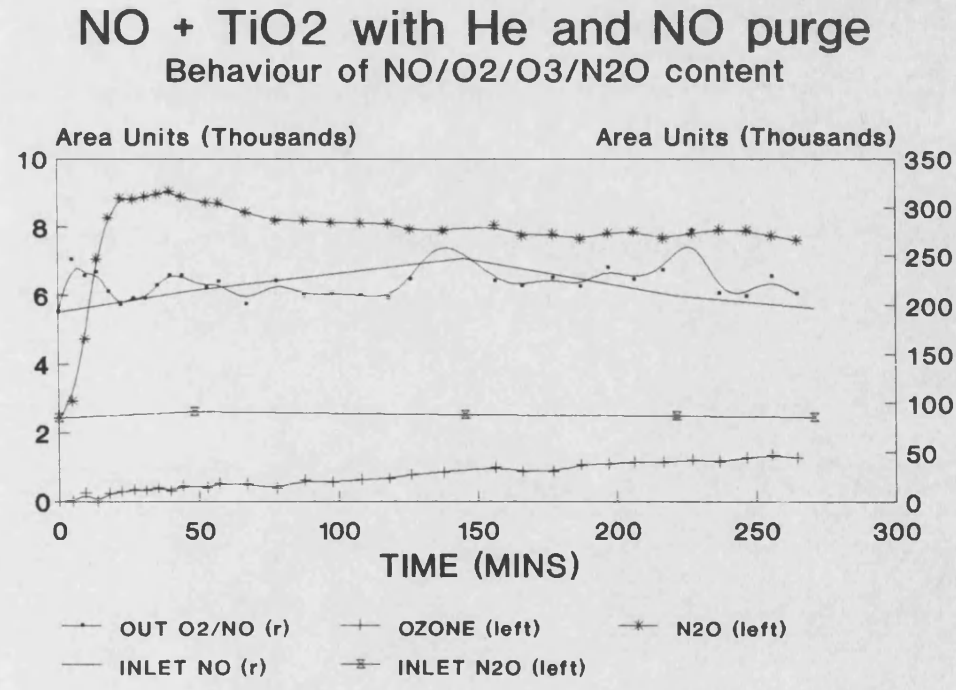

Figure 9.33

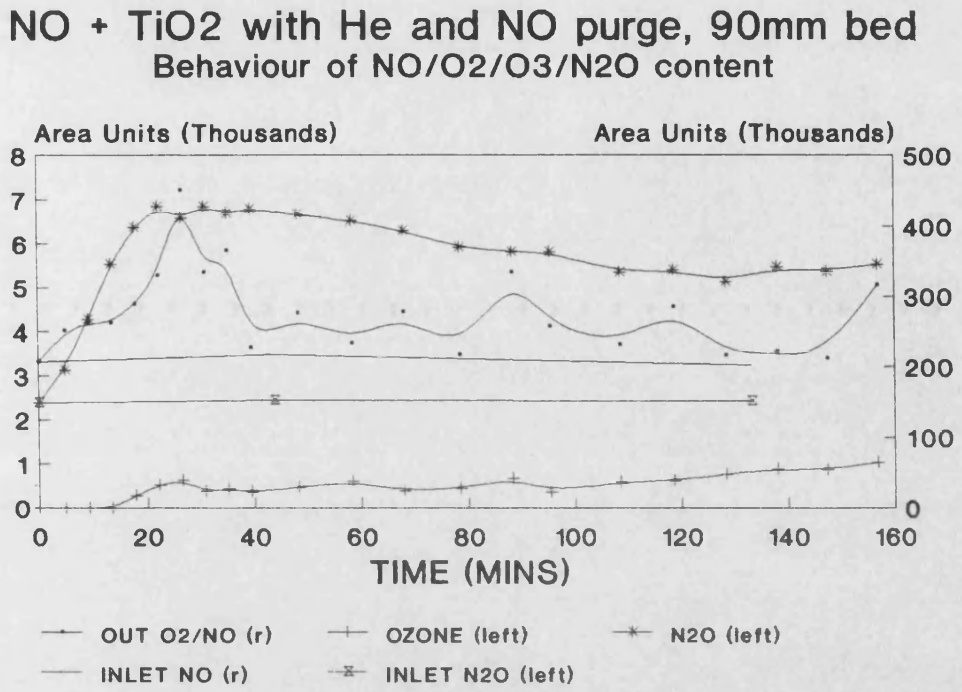

Figure 9.34

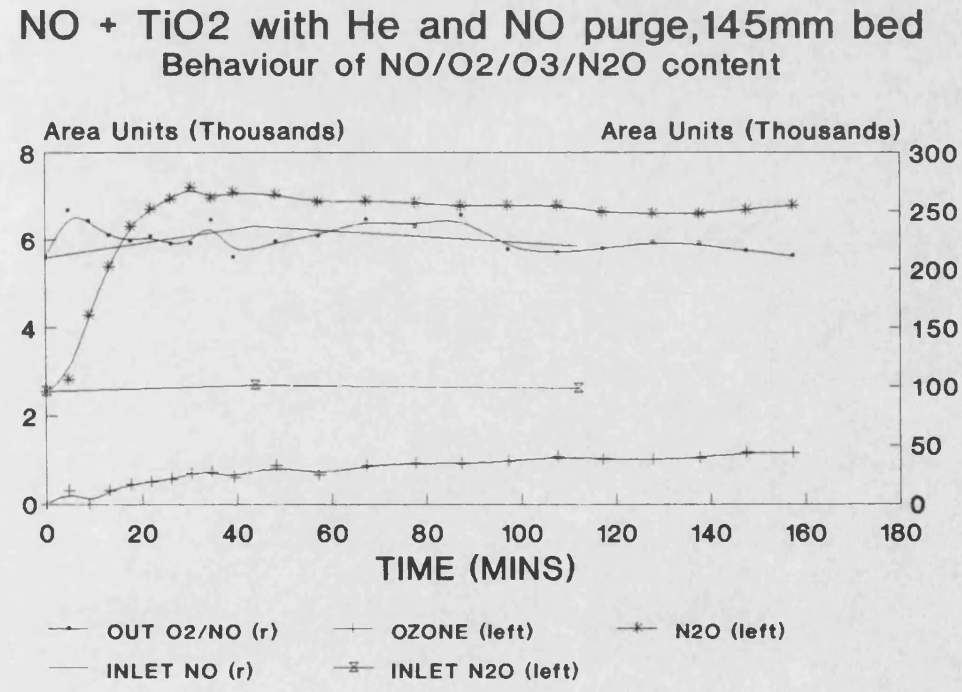

Figure 9.35

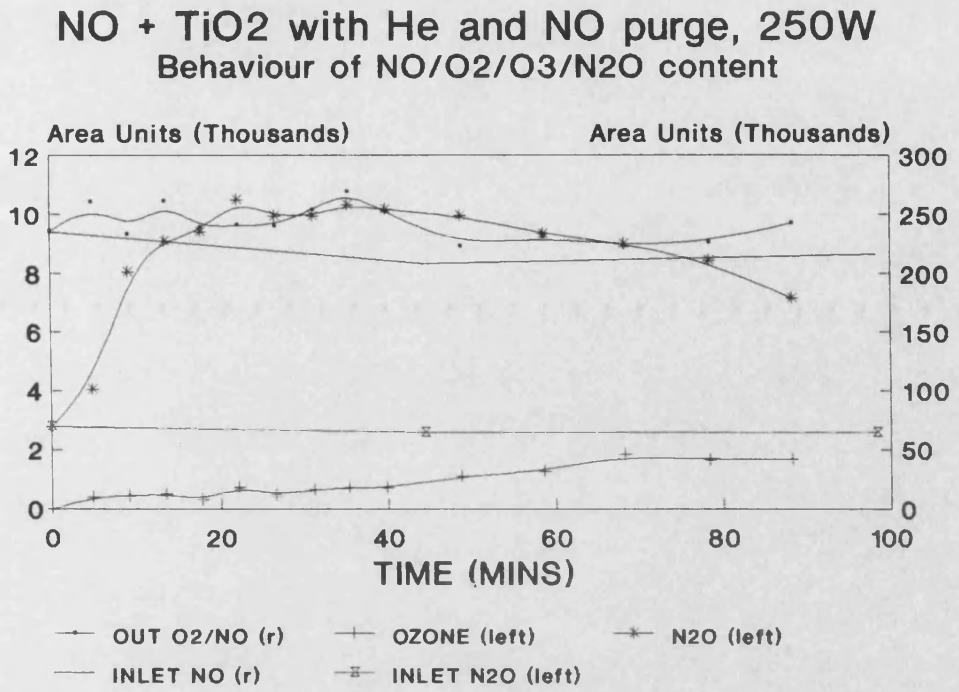

Figure 9.36

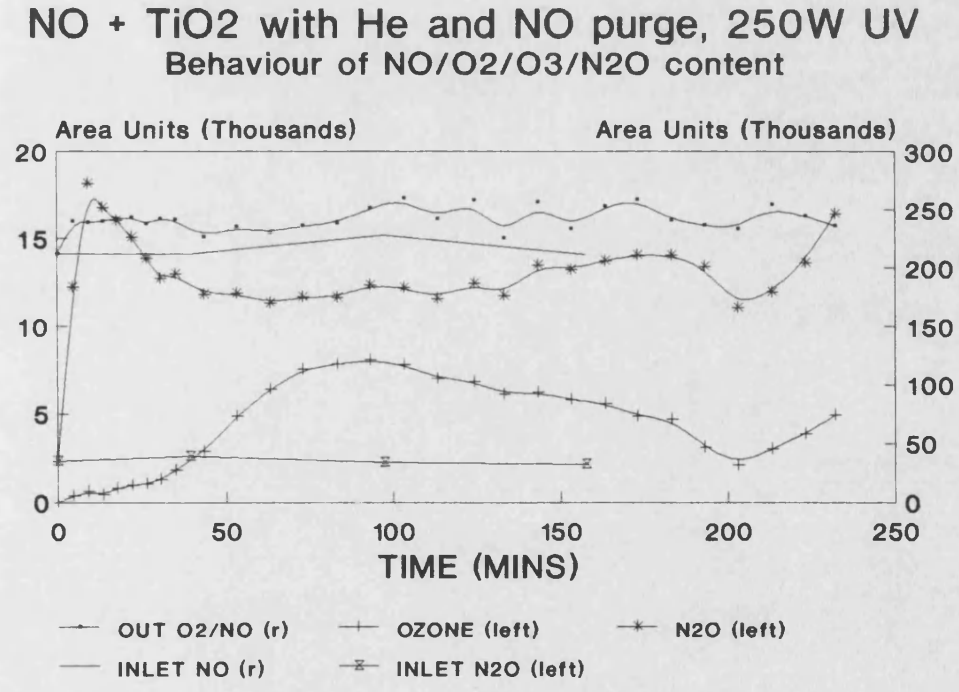

Figure 9.37

Time vs Concetration Graph for the Photocatalysis of NO (8 Watt Reactor)

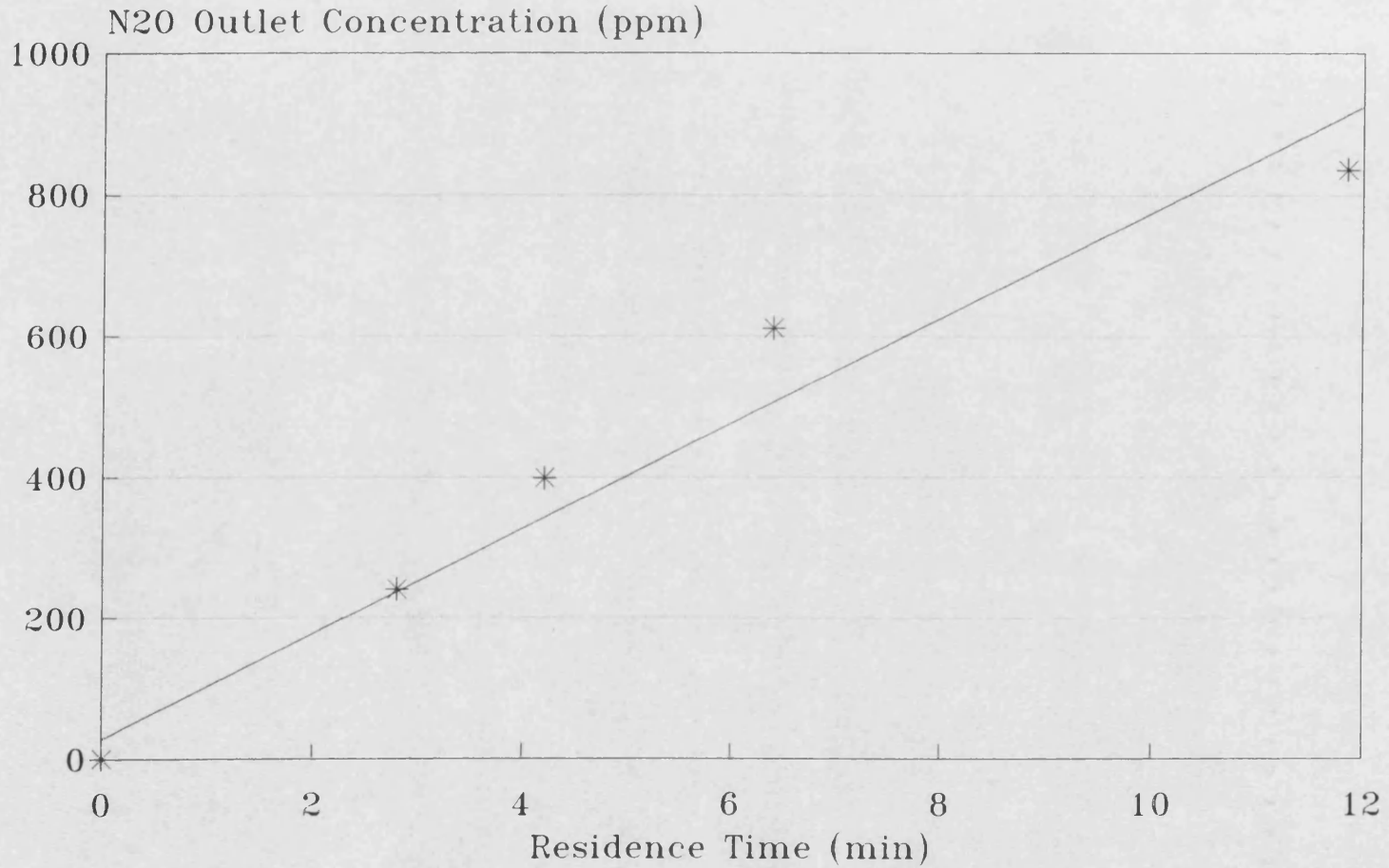

Figure 9.38

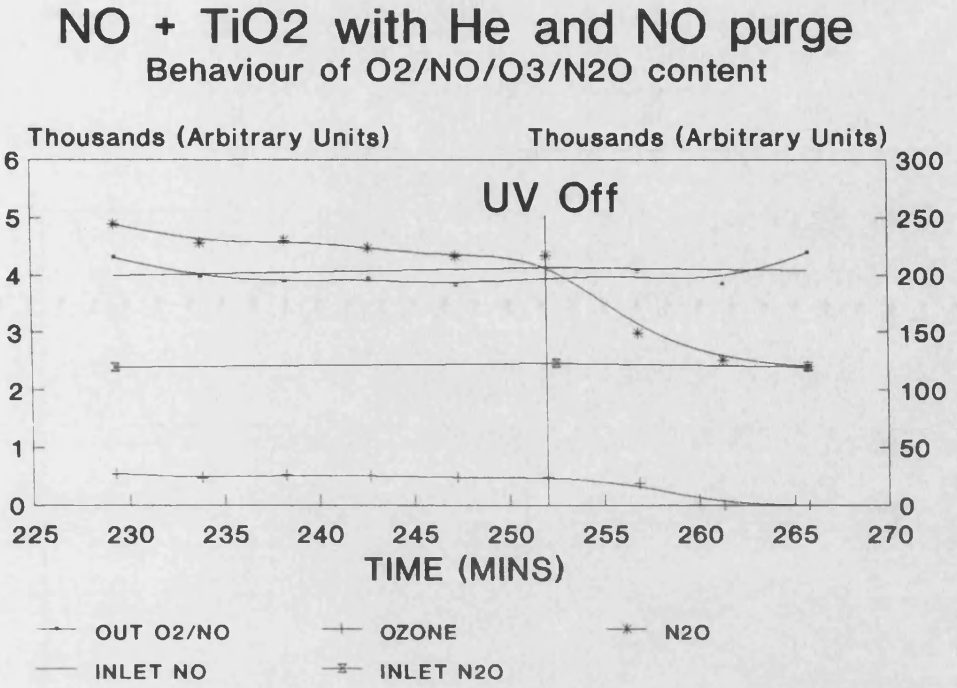

Figure 9.39

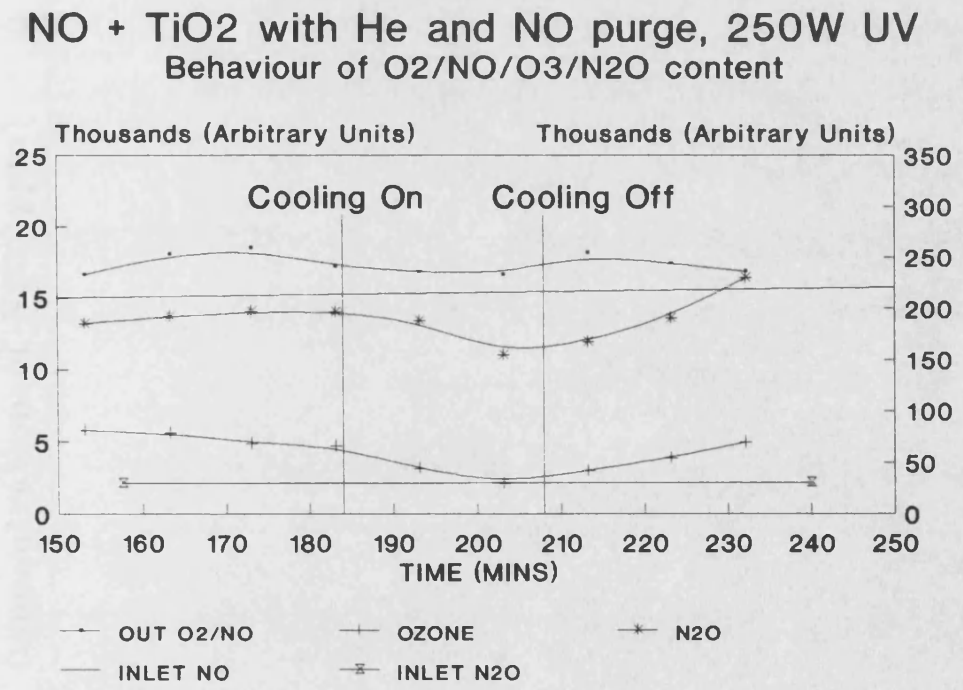

Figure 9.40

Bed Length vs Conversion for the Photocatalytic Reaction of NO/He.

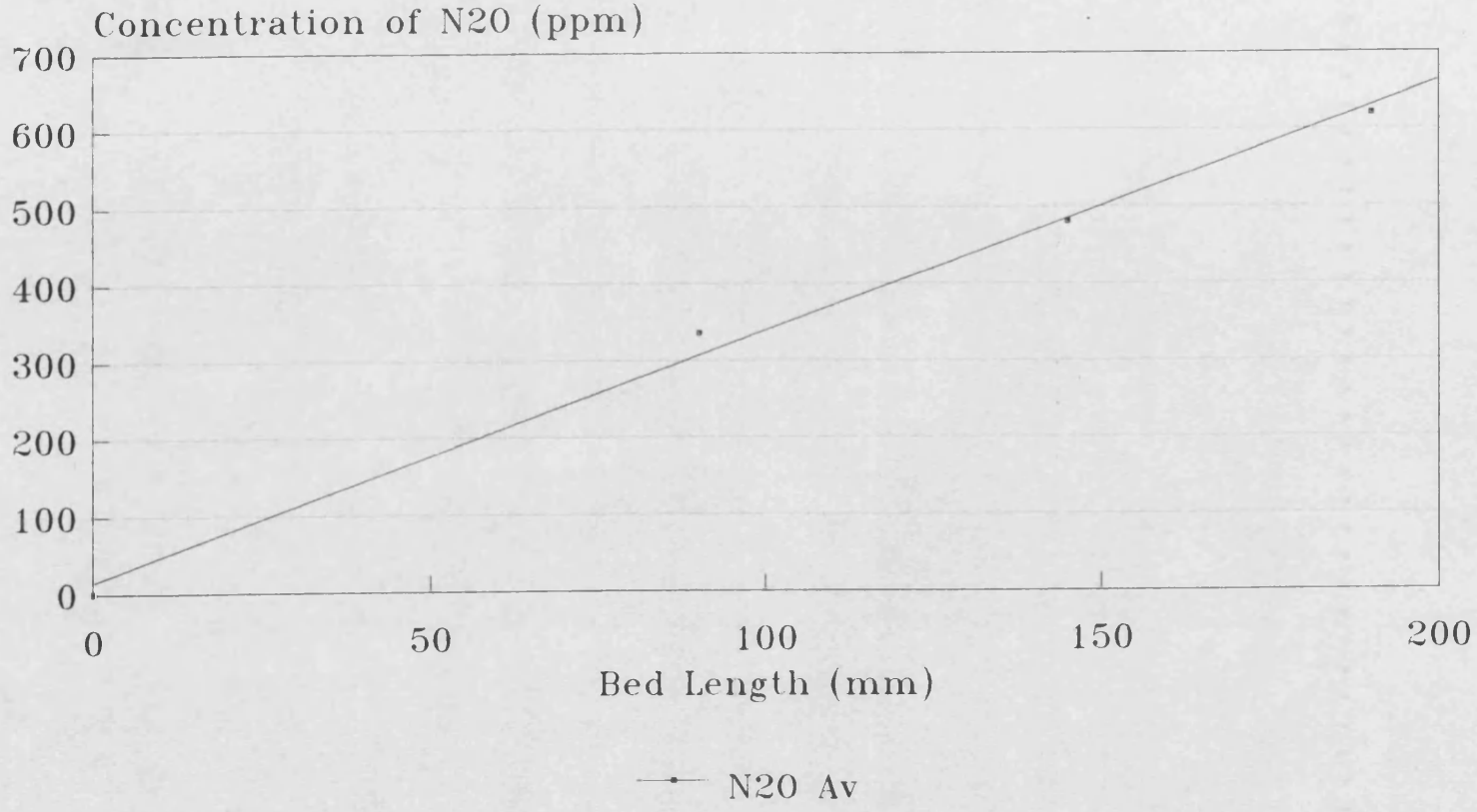

Residence Time = 11.5min

Figure 9.41

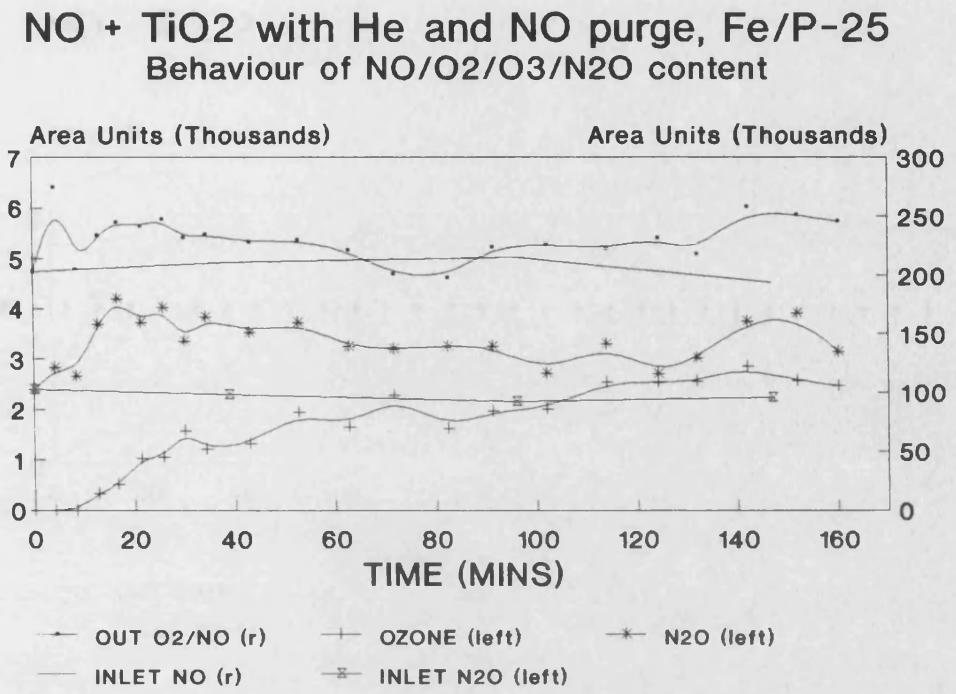

Figure 9.42

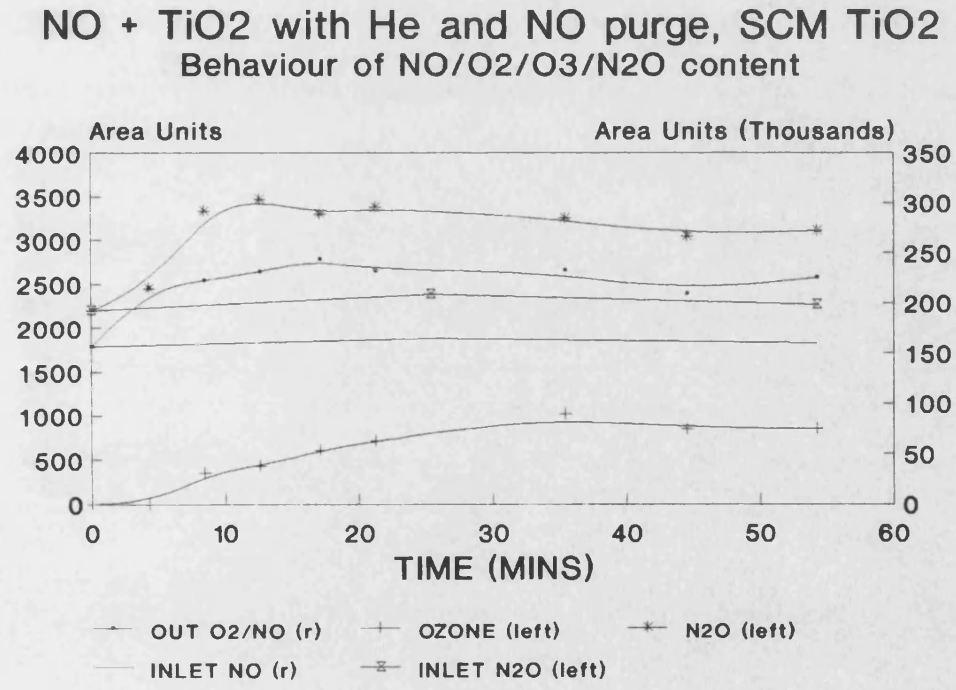

Figure 9.43

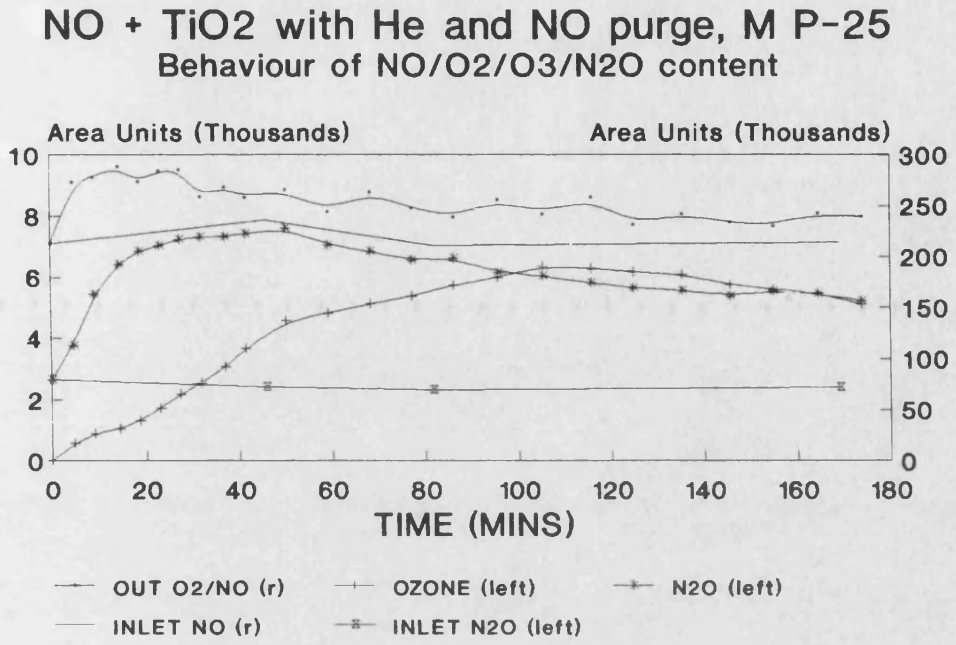

Figure 9.44

Particle size 150 -› 250 microns

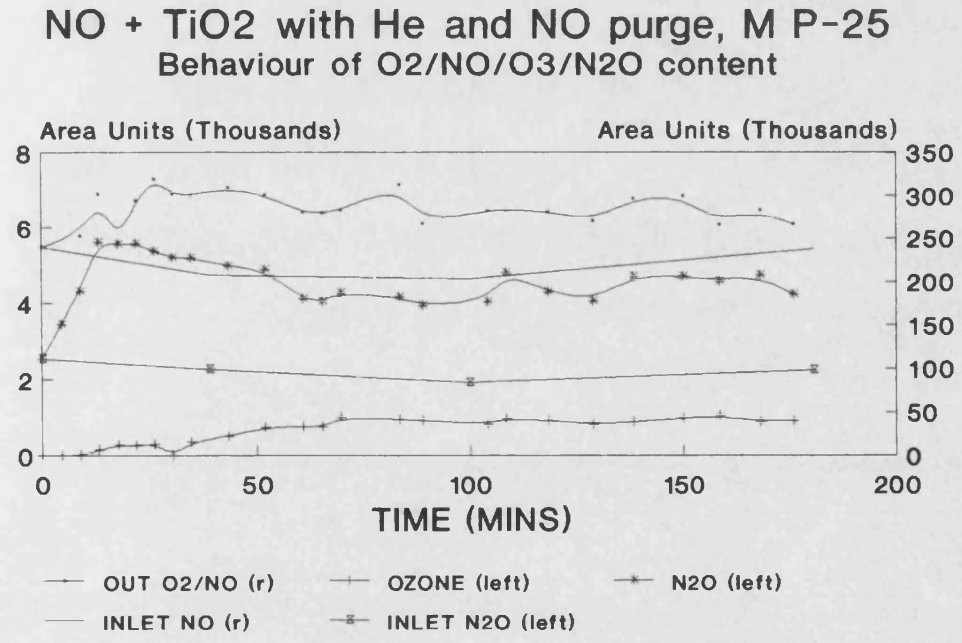

Figure 9.45

Particle size 75 -› 150 microns

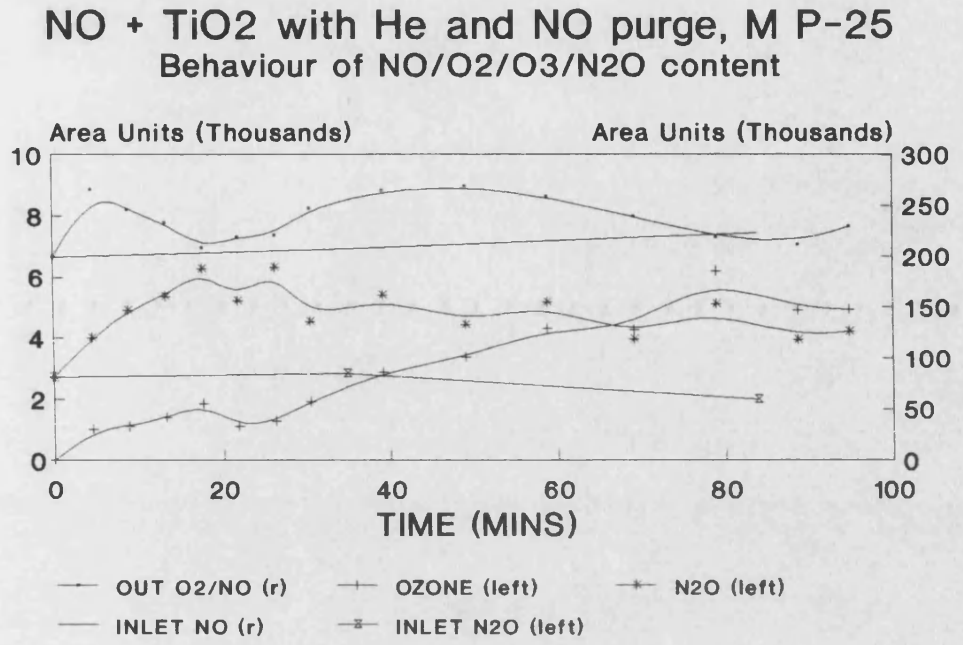

Figure 9.46

Particle size < 75 microns

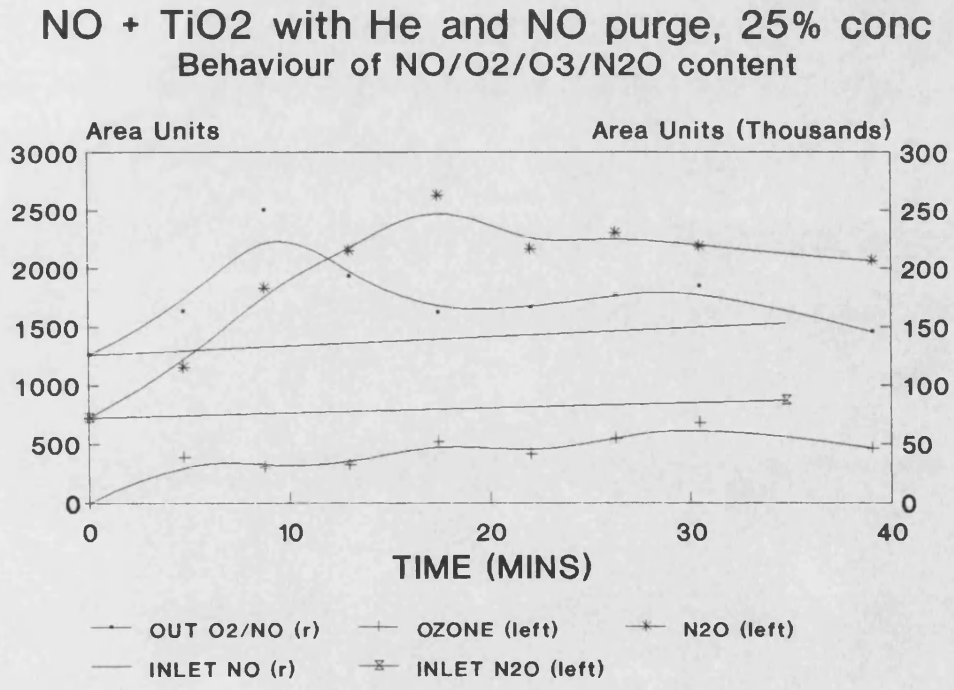

Figure 9.47

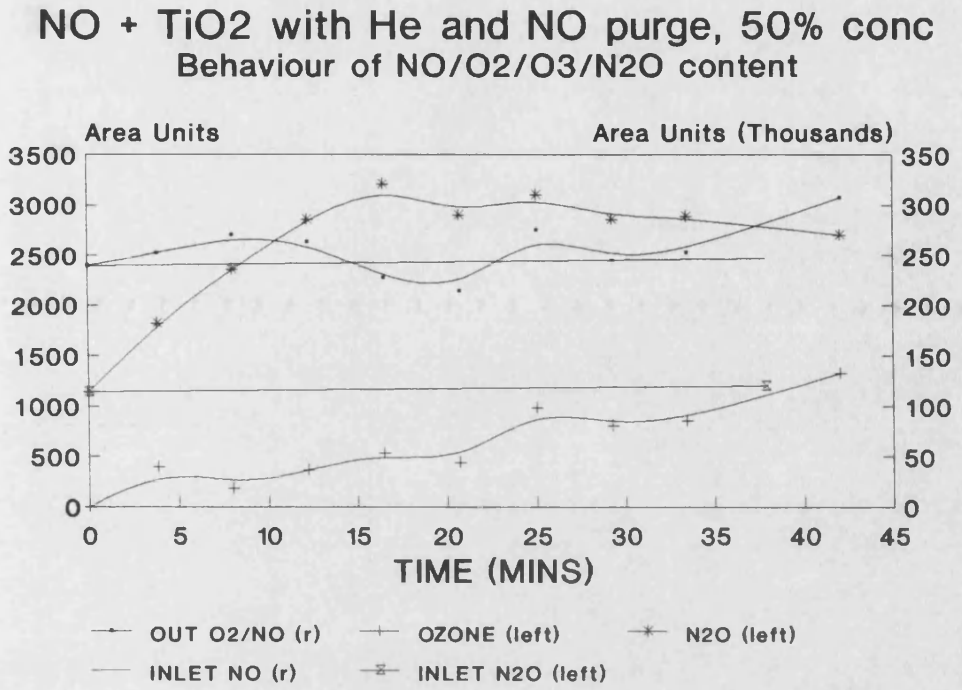

Figure 9.48

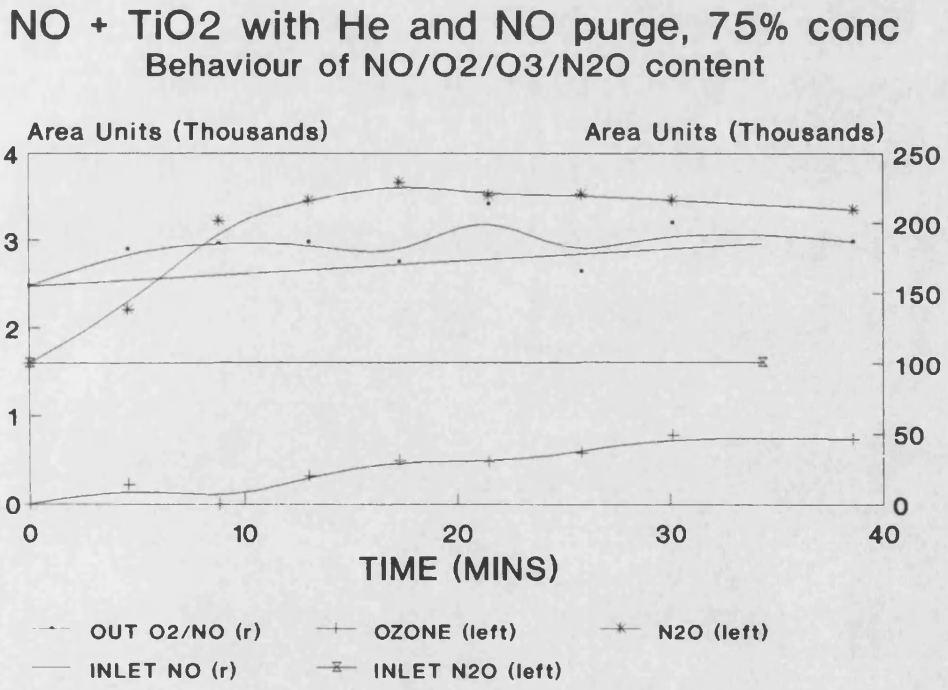

Figure 9.49

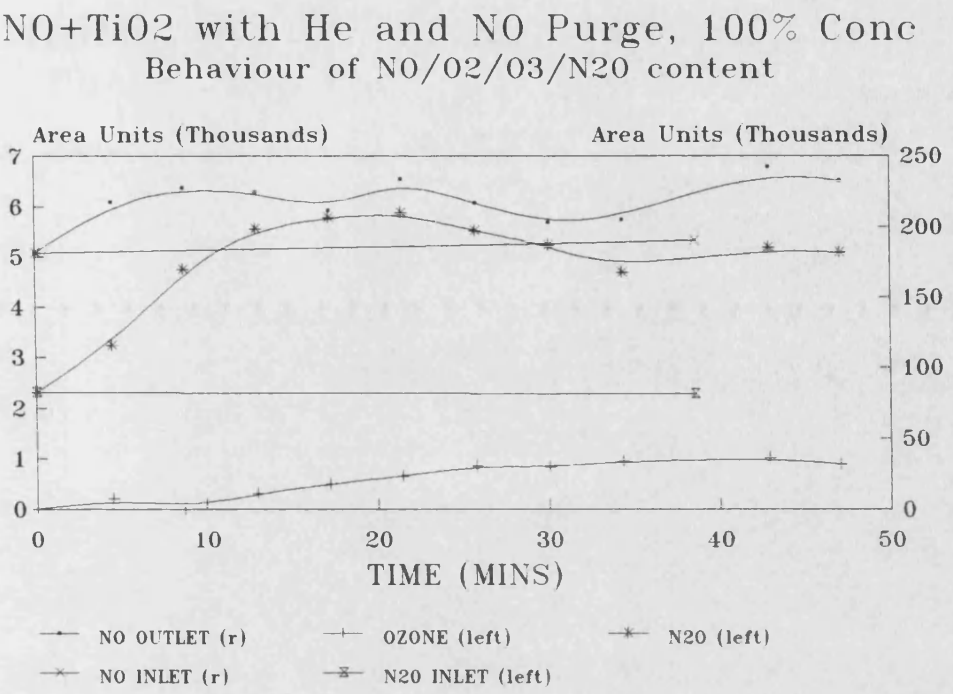

Figure 9.50

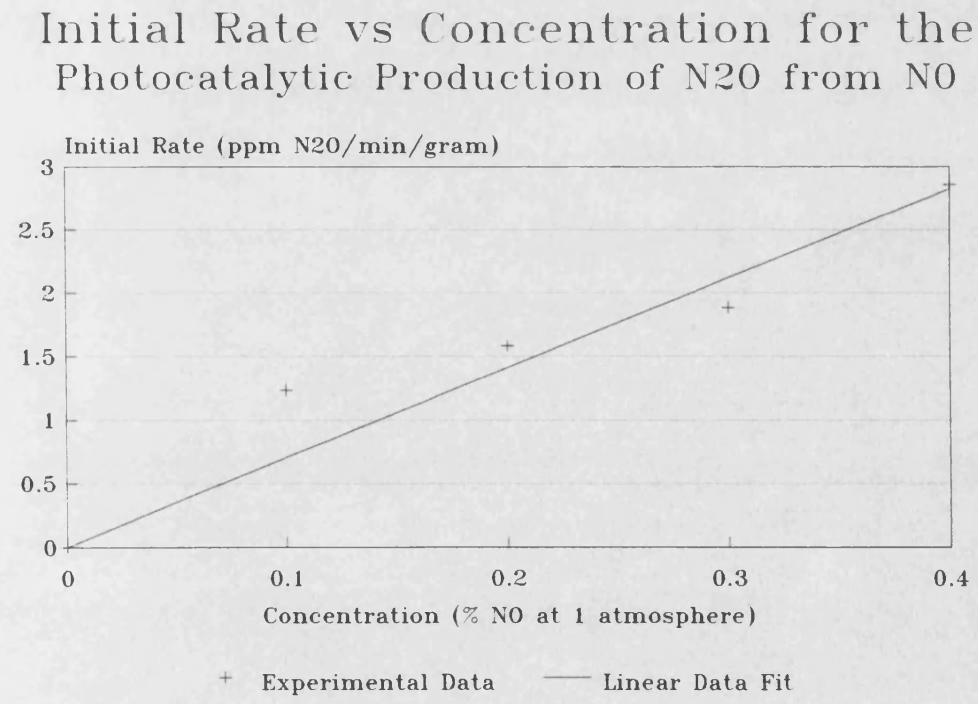

Figure 9.51

Initial Rate vs Total Pressure for the Photocatalytic Production of N20 from N0

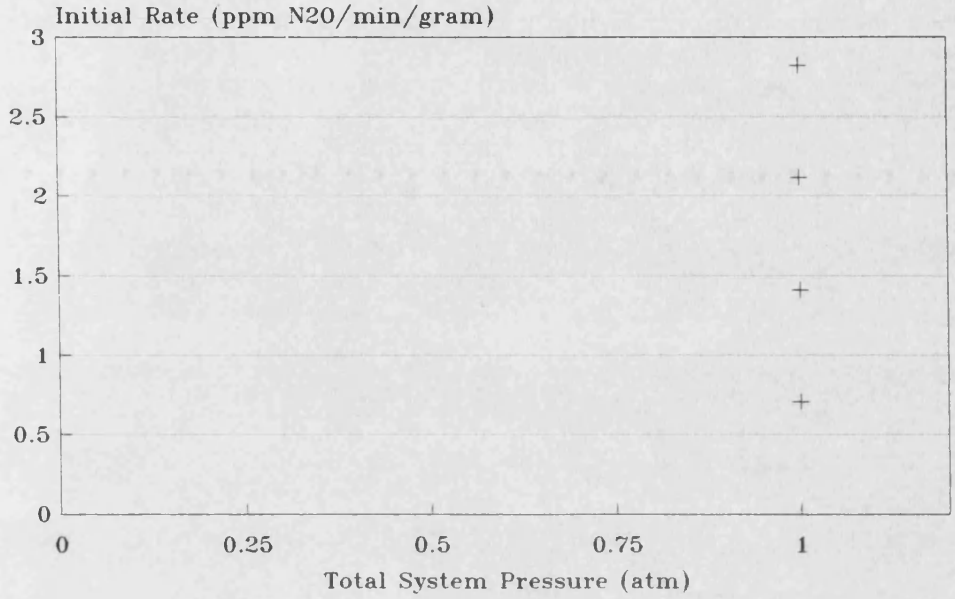

Figure 9.52

Initial Rate vs Concentration for the Photocatalytic Production of N20 from N0

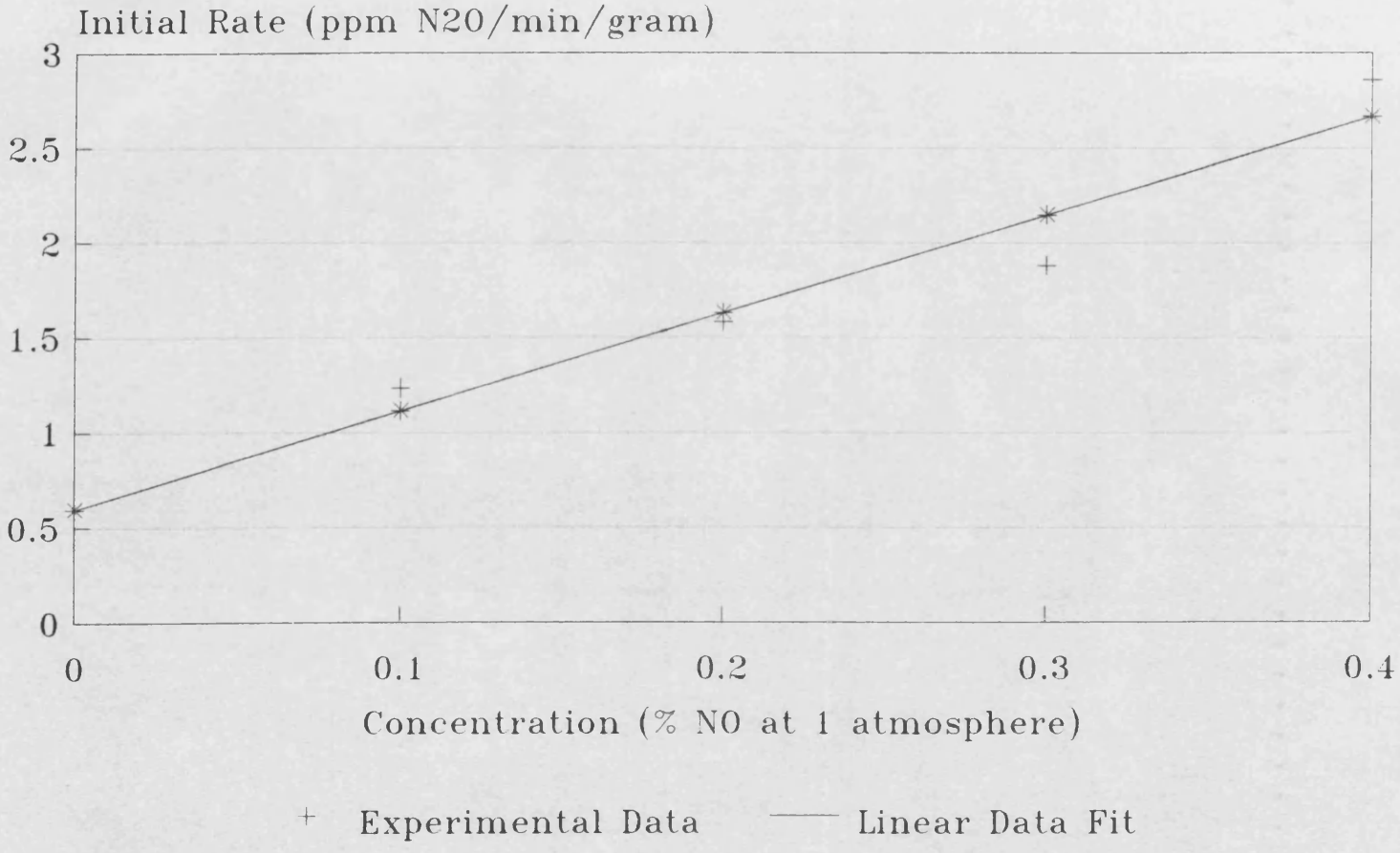

Figure 10.1

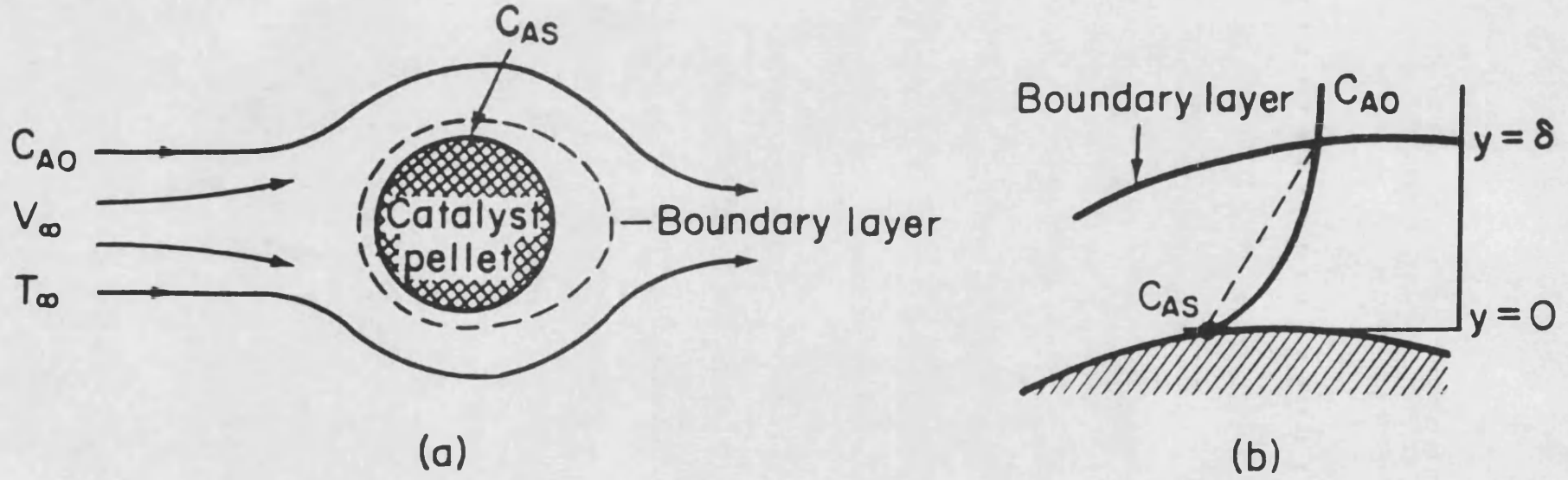

Figure 10.2 Boundary layer around the surface of a catalyst pellet.